



**ADVERTIMENT.** L'accés als continguts d'aquesta tesi queda condicionat a l'acceptació de les condicions d'ús establertes per la següent llicència Creative Commons:  <https://creativecommons.org/licenses/?lang=ca>

**ADVERTENCIA.** El acceso a los contenidos de esta tesis queda condicionado a la aceptación de las condiciones de uso establecidas por la siguiente licencia Creative Commons:  <https://creativecommons.org/licenses/?lang=es>

**WARNING.** The access to the contents of this doctoral thesis it is limited to the acceptance of the use conditions set by the following Creative Commons license:  <https://creativecommons.org/licenses/?lang=en>

# UAB

Universitat Autònoma de Barcelona

## NOVEL EXPERIMENTAL MODELS TO STUDY AMYOTROPHIC LATERAL SCLEROSIS AND FRONTOTEMPORAL DEMENTIA

Presented by

**Joana Garcia Garcia**

### ACADEMIC DISSERTATION

To obtain the degree of PhD in Neuroscience by the  
Universitat Autònoma de Barcelona

October 2024

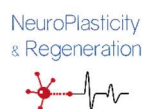
Thesis supervisor

**Dr. Rubèn López Vales**

Academic tutor

**Dr. Xavier Navarro Acebes**

Group of Neuroplasticity and Regeneration,  
Institut de Neurociències





This study was funded by:

---

- The project PDC2021-121791-I00 “Neuroresolving therapeutics for Spinal Cord Injury” from Ministerio de Ciencia, Innovación y Universidades of Spain to Rubèn López Vales (2021-2024).
- The project PID2020-120267RB-I00 “Papel de la interleucina-38 en lesiones y enfermedades del sistema nervioso central” from Ministerio de Ciencia, Innovación y Universidades of Spain to Rubèn López Vales (2021-2024).
- The project HR17-00777 “Activation of the resolution programs of inflammation as a novel therapeutic approach for the treatment of amyotrophic lateral sclerosis” from Health Research Program of Fundació La Caixa to Rubèn López Vales (2018-2022).
- A 4-year PhD fellowship (Call 2020) from Fundació Tatiana Pérez Guzmán el Bueno to Joana Garcia Garcia.
- A travel grant from Fundació Tatiana Pérez Guzmán el Bueno to Joana Garcia Garcia to perform a research stay at Mancuso Lab in VIB-UAntwerpen Center for Molecular Neurology (Antwerp, Belgium).



## Table of contents

---

I.	Abstract.....	1
II.	Abbreviations .....	5
III.	Introduction.....	11
	1. Amyotrophic lateral sclerosis - Frontotemporal dementia spectrum disorder.....	13
	1.1. ALS/FTD genetics .....	15
	2. Amyotrophic lateral sclerosis.....	18
	2.1 ALS pathophysiology .....	18
	2.2. ALS experimental models .....	29
	2.3. ALS treatment.....	32
	3. Microglia in ALS .....	34
	3.1. Microglia generalities.....	34
	3.2. Microglia in ALS pathogenesis.....	36
	3.3. Modelling human microglia <i>in vitro</i> and <i>in vivo</i> .....	40
	4. C9orf72 ALS/FTD .....	47
	4.1. C9orf72 gene, protein, and function.....	48
	4.2. C9orf72 pathogenesis.....	49
IV.	Hypothesis and objectives .....	55
V.	Material and methods .....	59
VI.	Results.....	79
	Chapter 1. ALS-linked SOD1 <sup>G93A</sup> mutation disrupts microglial functions in a cell-autonomous manner in human ESC-derived microglia <i>in vitro</i> .....	81
	Chapter 2. Xenotransplantation of human microglia into the mouse spinal cord .....	97
	Chapter 3. Phenotypic characterization of a novel C9orf72 G4C2 HRE knock-in mouse model .....	107
VII.	Discussion.....	127
VIII.	Conclusions.....	153
IX.	References.....	157



# I. Abstract

---





Amyotrophic lateral sclerosis (ALS) and frontotemporal dementia (FTD) are neurodegenerative diseases that represents two ends of a continuous disease spectrum, sharing key pathological and genetic features, despite manifesting primarily as motor symptoms in ALS and behavioural symptoms in FTD. A proper understanding of their pathogenic mechanisms is crucial for developing new therapeutic approaches. However, a significant barrier to progress in this field is the poor translation of findings from animal models to clinical applications, particularly evident in the failure of many ALS clinical trials. This gap can be attributed, in part, to limitations in current experimental models.

In this PhD thesis, we first faced mouse microglia limitations due to species-specific differences. Shifting toward more human-based biomedical research, we edited a human embryonic stem cell (ESC) line to introduce the ALS-causing SOD1<sup>G93A</sup> mutation by Clustered Regularly Interspaced Short Palindromic Repeats (CRISPR)/Cas9 technology. Our aim was to investigate whether the mutant SOD1 directly impacts distinct microglial functions in human ESC-derived *microglia in vitro*. We found that SOD1<sup>G93A</sup> mutation altered the cytokine profile at baseline conditions, heightened the microglial response to a pro-inflammatory stimulus, moderately impaired phagocytic function, caused metabolic changes in unstimulated conditions, and adapted differently their metabolism in response to lipopolysaccharide (LPS) when compared to control microglia.

In the recent years, the development of chimeric mouse models with human microglia has emerged as a promising tool for better understanding microglial biology, since human microglia engrafted in the mouse central nervous system (CNS) mimic more closely the primary human microglial transcriptome compared to *in vitro* microglia. While most of studies xenotransplanted human microglia into the brain, thus we opted for transplantation into the neonatal mouse spinal cord as this is more relevant in the ALS field. We found that administration of 50,000 microglial progenitors (MPs) into the caudal spinal cord region of neonatal Rag2<sup>-/-</sup> IL2 $\gamma$ <sup>-/-</sup> hCSF1<sup>KI</sup> mice resulted in robust human microglia (CD45<sup>+</sup> P2RY12<sup>+</sup>) colonization throughout all the spinal cord, from cervical to sacral, at least up to 10 months post-transplantation. Focusing on the lumbar spinal cord, we found that the

human microglial chimerism increased over the time and reached higher colonization in the white matter than in grey matter.

In the last chapter of this PhD thesis, we characterized phenotypically a newly generated *C9orf72* mouse model, knock-in for 30 GGGGCC (G4C2) repeats in the mouse *C9orf72* gene. Although *C9ORF72* mutations are the most common genetic cause of ALS and FTD, existing mouse models have failed to fully recapitulate the ALS motor symptoms or FTD behavioural features. We found that, after 18 months of follow up, our *C9orf72* mouse model did not develop ALS-like motor deficits. In contrast, aged homozygous *C9orf72* mice acquired some FTD-related behavioural deficits, including depressive-like behaviour and memory decline.

In summary, this doctoral thesis characterized distinct novel experimental approaches to advance the investigation in the ALS and FTD field. These findings provide valuable insights that may help to better understand the pathogenic mechanisms involved in these diseases, which ultimately could facilitate the development of new therapeutical strategies of these neurodegenerative diseases.

## II. Abbreviations

---



<b>AAV:</b> Adeno-associated viral vector	<b>CSF:</b> Cerebrospinal fluid
<b>AD:</b> Alzheimer's disease	<b>CSF1:</b> Colony stimulating factor 1
<b>ADAP:</b> Adhesion and degranulation-promoting adapter protein	<b>CSF1R:</b> CSF1 receptor
<b>AIF:</b> Apoptosis inducing factor	<b>CX3CR1:</b> C-X3-C motif chemokine receptor 1
<b>ALS:</b> Amyotrophic lateral sclerosis	<b>DAM:</b> Disease-associated microglia
<b>ALSbi:</b> ALS with behavioural impairment	<b>DDP4:</b> Dipeptidyl peptidase 4
<b>ALScbi:</b> ALS with cognitive and behavioural impairment	<b>DMEM/F12:</b> Dulbecco's Modified Eagle Medium/Ham's F-12
<b>ALSci:</b> ALS with cognitive impairment	<b>dpBS:</b> Dulbecco's Phosphate-buffered saline
<b>ALSFRS-R:</b> Revised Amyotrophic Lateral Sclerosis Functional Rating Scale	<b>DPR:</b> Dipeptide repeat
<b>AMPA:</b> Amino-3-hydroxy-5-methyl-4-isoxazolepropionic acid	<b>EAAT2:</b> Excitatory amino-acid transporter 2
<b>ARE:</b> Antioxidant response element	<b>EB:</b> Embryoid body
<b>ARM:</b> Activated response microglia	<b>ECAR:</b> Extracellular acidification rate
<b>ASO:</b> Antisense oligonucleotide	<b>EDTA:</b> Ethylenediaminetetraacetic acid
<b>A<math>\beta</math>:</b> Amyloid- $\beta$	<b>EMA:</b> European Medicine Agency
<b>BAC:</b> Bacterial artificial chromosome	<b>ER:</b> Endoplasmic reticulum
<b>BBB:</b> Blood-brain barrier	<b>ETC:</b> Electron transport chain
<b>Bcl-2:</b> B-cell lymphoma	<b>FACS:</b> Fluorescence activated cell sorting
<b>BDNF:</b> Brain-derived neurotrophic factor	<b>fALS:</b> familiar ALS
<b>BMP-4:</b> Bone morphogenetic protein 4	<b>FBS:</b> Foetal bovine serum
<b>bp:</b> Base pair	<b>FCCP:</b> Carbonyl cyanide-4-(trifluoromethoxy)-phenylhydrazone
<b>C1q:</b> Complement component 1q	<b>FDA:</b> Food and Drug Administration
<b>C9ORF72:</b> Chromosome 9 open reading frame 72	<b>FTD:</b> Frontotemporal dementia
<b>Ca<sup>+2</sup>:</b> Calcium	<b>FTL-3:</b> FMS- like tyrosine kinase 3
<b>CEBP<math>\alpha</math>:</b> CCAAT enhancer binding protein alpha	<b>FUS:</b> Fused in sarcoma
<b>CEBP<math>\beta</math>:</b> CCAAT enhancer binding protein beta	<b>Fw:</b> Forward
<b>CHCHD10:</b> Coiled-coil-helix-coiled-coil-helix domain-containing protein 10	<b>geoMFI:</b> Geometric mean fluorescence intensity
<b>CMAP:</b> Compound muscle action potential	<b>GFR:</b> Growth factor reduced
<b>CMV:</b> Cytomegalovirus	<b>GGGGCC:</b> G4C2
<b>CNS:</b> Central nervous system	<b>GM-CSF:</b> Granulocyte-macrophage colony-stimulating factor
<b>CRISPR:</b> Clustered Regularly Interspaced Short Palindromic Repeats	<b>GOF:</b> Gain of function
<b>CRM:</b> Cytokine response microglia	<b>GRN:</b> Progranulin
	<b>HAM:</b> Human AD microglia
	<b>HBSS:</b> Hank's Balanced Salt Solution
	<b>HD:</b> Huntington disease

## Abbreviations

<b>HDR:</b> Homologous directed repair	<b>NK:</b> Natural killer
<b>HLA:</b> Antigen presenting response	<b>NMDA:</b> N-methyl-D-aspartate
<b>HM:</b> Homeostatic microglia	<b>NO:</b> Nitric oxide
<b>hnRNPA1:</b> Heterogeneous nuclear ribonuclear protein A1	<b>NORT:</b> Novel object recognition test
<b>HPC:</b> Hematopoietic progenitor cells	<b>NRF2:</b> Nuclear factor erythroid 2-related factor 2
<b>HRE:</b> Hexanucleotide repeat expansion	<b>OCR:</b> Oxygen consumption rate
<b>Iba1:</b> Ionized calcium-binding adapter molecule 1	<b>OPC:</b> Oligodendrocyte progenitor cells
<b>IFN:</b> Interferon	<b>OT:</b> Off-target
<b>IGF-1:</b> Insulin-like growth factor-1	<b>P2RY12:</b> P2Y purinoreceptor 12
<b>IL:</b> Interleukin	<b>PAM:</b> Protospacer adjacent motif
<b>IL2<math>\gamma</math>:</b> Interleukin 2 receptor subunit gamma	<b>PB:</b> Phosphate buffer
<b>iPSC:</b> Induced pluripotent stem cell	<b>PBMC:</b> Peripheral blood mononuclear cells
<b>IRF5:</b> Interferon Regulatory Factor 5	<b>PBS:</b> Phosphate buffer saline
<b>IRF8:</b> Interferon regulatory factor 8	<b>PCR:</b> Polymerase chain reaction
<b>IRM:</b> Interferon response microglia	<b>PD:</b> Parkinson's disease
<b>IS:</b> Intraspinal	<b>PET:</b> Positron emission tomography
<b>KI:</b> Knock-in	<b>PFA:</b> Paraformaldehyde
<b>KO:</b> Knockout	<b>PNS:</b> Peripheral nervous system
<b>LDAM:</b> Lipid-droplet-accumulating microglia	<b>Poly-GA:</b> Poly-glycine-alanine
<b>LOF:</b> Loss of function	<b>Poly-GP:</b> Poly-glycine-proline
<b>LPS:</b> Lipopolysaccharide	<b>Poly-GR:</b> Poly-glycine-arginine
<b>MAFB:</b> MAF BZIP transcription factor B	<b>Poly-PA:</b> Poly-proline-alanine
<b>MAPT:</b> Microtubule-associated protein tau	<b>Poly-PR:</b> Poly-proline-arginine
<b>M-CSF:</b> Macrophage colony stimulating factor	<b>qPCR:</b> Quantitative PCR
<b>MGnD:</b> Microglial neurodegenerative phenotype	<b>Rag2:</b> Recombination activating gene 2
<b>MIMS:</b> Microglia inflamed in multiple sclerosis	<b>RAN:</b> Repeat Associated Non-AUG
<b>MN:</b> Motor neuron	<b>RBP:</b> RNA-binding protein
<b>MND:</b> Motor neuron disease	<b>RM:</b> Ribosomal microglia
<b>MP:</b> Microglial progenitor	<b>RNAseq:</b> RNA sequencing
<b>mtDNA:</b> mitochondrial DNA	<b>RNP:</b> Ribonucleoprotein
<b>NCL:</b> Nucleolin	<b>RNS:</b> Reactive nitrogen species
<b>NfH:</b> Neurofilament heavy chain	<b>ROCKi:</b> ROCK inhibitor
<b>NfL:</b> Neurofilament light chain	<b>ROS:</b> Reactive oxygen species
<b>NF-<math>\kappa</math>B:</b> Nuclear factor- $\kappa$ B	<b>Rot/AA:</b> Rotenone/antimycin
	<b>RRIM:</b> RIPK1-regulated inflammatory microglia
	<b>Rv:</b> Reverse

<b>sALS:</b> Sporadic ALS	<b>TDP-43:</b> Transactive response DNA binding protein of 43 kDa
<b>SC35:</b> Serine/arginine-rich splicing factor	<b>Th:</b> T-helper lymphocytes
<b>SCF:</b> Stem cell factor	<b>TMEM119:</b> Transmembrane protein 119
<b>SCOC:</b> Spinal cord organotypic culture	<b>TNFR1:</b> TNF- $\alpha$ receptor 1
<b>scRNAseq:</b> single-cell RNAseq	<b>TNF-<math>\alpha</math>:</b> Tumour necrosis factor-alpha
<b>SEM:</b> Standard error of the mean	<b>TPO:</b> Thrombopoietin
<b>SIP:</b> Stock Isotonic Percoll	<b>Treg:</b> Regulatory T-lymphocytes
<b>SOD1:</b> Superoxide dismutase 1	<b>UBQLN2:</b> Ubiquilin 2
<b>SPI1:</b> SFFV pro-viral integration 1	<b>UDP:</b> Uridine diphosphate
<b>SQSTM1:</b> Sequestosome 1	<b>UPR:</b> Unfolded protein response
<b>SST:</b> Sucrose splash test	<b>UPS:</b> Ubiquitin-proteasome system
<b>TARDBP:</b> TAR DNA-binding protein 43	<b>VEGF:</b> Vascular endothelial growth factor
<b>TBK1:</b> TANK-binding kinase 1	
<b>tCRM:</b> Transitioning CRM	





## III. Introduction

---



## 1. Amyotrophic lateral sclerosis - Frontotemporal dementia spectrum disorder

Historically, amyotrophic lateral sclerosis (ALS) and frontotemporal dementia (FTD) have been regarded as two distinct neurodegenerative diseases, with ALS affecting the motor nervous system and FTD, the cognitive functions. However, nowadays they are more commonly viewed as part of a continuous spectrum with overlapping symptoms due to shared pathological and genetic features (Gao et al., 2017). At one end of the spectrum, ALS patients exhibit pure motor symptoms while at the other end, FTD patients have behavioural and cognitive deficits. In between some patients fulfil the diagnostic criteria for both ALS and FTD (ALS/FTD). Additionally, some patients do not meet these strict criteria for both conditions, giving rise to some variants (Figure 1). Cognitive and behavioural alterations occur in 35-50% of ALS patients, including loss of normal language or executive function, apathy, irritability, depression, or sleep alterations, among others. About 15% of ALS patients have a concomitant diagnosis of FTD (Feldman et al., 2022).

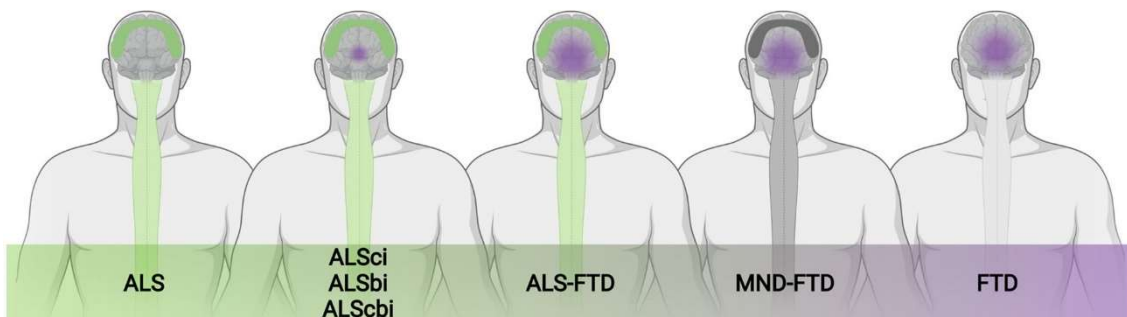


**Figure 1. ALS/FTD spectrum disorder.** ALSci=ALS with cognitive impairment; ALSbi=ALS with behavioural impairment; ALSbi=ALS with cognitive and behavioural impairment. MND=motor neuron disease. Extracted from Feldman et al., 2022.

ALS, also known as Lou Gehrig's Disease, is the third neurodegenerative disease with higher incidence, after Alzheimer's (AD) and Parkinson's (PD) diseases. ALS is characterized by the degeneration of upper motor neurons (MNs), located in the cortex and brainstem, and lower MNs, situated in the brainstem and ventral horn of the spinal cord (Figure 2). ALS was first described by Jean-Marie Charcot in the late 19<sup>th</sup> century, since he linked the spasticity and muscle atrophy seen in patients' legs with the MN death and sclerosis observed in their spinal cord.

Nowadays, global ALS incidence is approximately 1.68/100,000 person-years and is projected to increase in the coming decades, largely due to aging population. Incidence can vary across regions and populations: Europe and North America have higher ALS incidence whereas Asian people show lower incidence (Feldman et al., 2022; Longinetti & Fang, 2019). ALS prevalence is about 6-9 cases/100,000 people (Mead et al., 2023), being more common in males than females (ratio 1.34) (Feldman et al., 2022). ALS mostly debuts in adults between 50 and 65 years old, with a progressive weakness and atrophy of voluntary skeletal muscles in the extremities, dysphagia, and dysarthria, as a consequence of MN dysfunction. The disease progresses over time leading to paralysis and respiratory failure and ultimately causing death within 2 and 5 years after the disease onset in 80% of patients. There are some forms of ALS that are diagnosed in patients before the 25 years of age, referred to as juvenile ALS. This form of ALS usually progresses more slowly with some patients reported to become bedridden by 12 to 50 years. ALS has a heterogeneous phenotype depending on the affectation of upper and lower MNs and the location of the primary pathology, being the most common presentations the bulbar-onset and spinal-onset ALS (Feldman et al., 2022; Hardiman et al., 2017; Longinetti & Fang, 2019). Most ALS cases are sporadic, but there is a positive family history in ~10% of patients, typically with an autosomal dominant pattern of inheritance and reduced penetrance (Feldman et al., 2022; Mead et al., 2023).

FTD it is the third most common cause of dementia and the second most common early-onset dementia after AD, involving patients ranging from 45 to 65 years old (Bang et al., 2015). FTD is characterized by the degeneration of the frontal cerebral lobule which can be extended until the temporal one, and courses with progressive changes in behaviour and executive function (behavioural variant), and/or language alterations (language variant) (Boeve et al., 2022). In ~30% of FTD cases, there is a family history of dementia, indicating a significant genetic contribution. FTD patients' survival varies from 3-14 years, depending on the phenotype. The estimated prevalence is 15-22/100,000 people worldwide, and its incidence 2.7-4.1/100,000 people-years, with apparently no differences between sexes (Onyike & Diehl-Schmid, 2013).

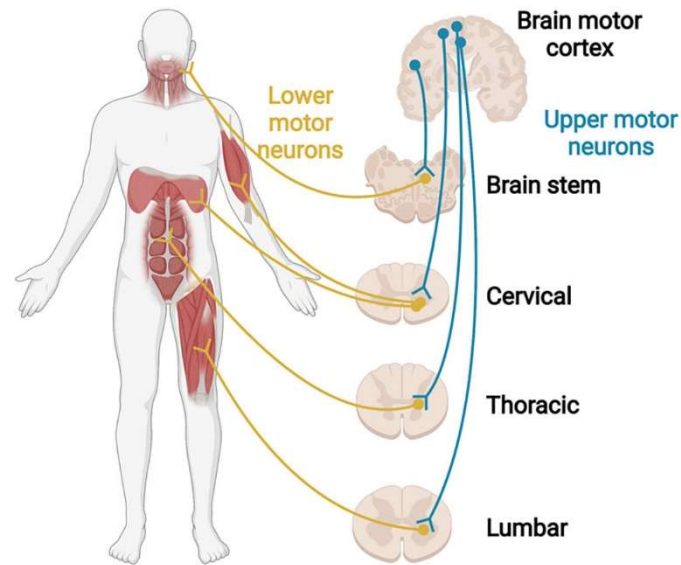


**Figure 2. Upper and lower MNs degenerate progressively in ALS.** Upper MNs are located in the motor cortex and brainstem and control lower MNs, which innervate skeletal muscles. Extracted from Mead et al., 2023.

### 1.1. ALS/FTD genetics

The discovery of genetic alterations implicated in both ALS and FTD strengthened the current notion that ALS and FTD share common pathogenic features (Figure 3, Table 1). It was particularly evident in 2011, when two independent studies identified a GGGGCC (G4C2) hexanucleotide repeat expansion (HRE) in the first intronic region of chromosome 9 open reading frame 72 (*C9ORF72*) gene (DeJesus-Hernandez et al., 2011; Renton et al., 2011). This genetic mutation is currently the most prevalent in both diseases, accounting for 50% of familiar ALS (fALS) cases and 25% of familiar FTD cases. Besides, other genes related to ALS are also involved in FTD, and vice versa, such as, TAR DNA-binding protein 43 (*TARDBP*), fused in sarcoma (*FUS*), TANK-binding kinase 1 (*TBK1*), Valosin-containing protein (*VCP*), Coiled-coil–helix-coiled–coil-helix domain-containing protein 10 (*CHCHD10*), Ubiquilin 2 (*UBQLN2*) or Sequestosome 1 (*SQSTM1*), among others (Figure 3) (Gao et al., 2017; Zampatti et al., 2022). This expanding list of ALS/FTD-related genes opens interesting questions to fully elucidate why different genes cause the same diseases or how mutations in the same gene produce different clinical phenotype.

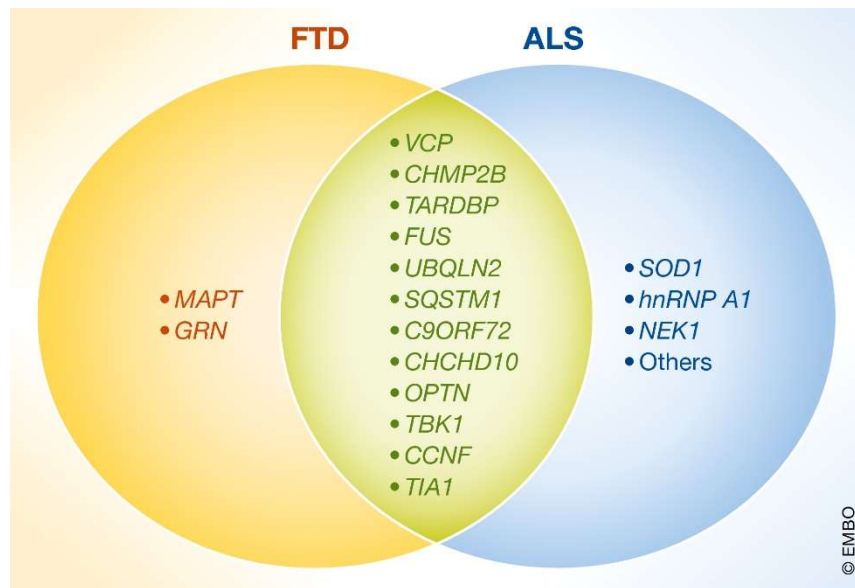


**Figure 3. Genetic overlap in ALS/FTD spectrum disorder.** Extracted from *Gao et al., 2017*.

The understanding of ALS genetic landscape has expanded significantly since 1993, when the first ALS-causing gene, the superoxide dismutase 1 (*SOD1*) gene, was discovered (Rosen et al., 1993). Since then, important efforts have been made to elucidate the complex genetic architecture of this disease. Currently, more than 40 genes have been linked to ALS as cause or disease modifiers, with varying levels of genetic support in replication and functional data and overlapping with other diseases (Chia et al., 2018; Feldman et al., 2022; Goutman et al., 2022). In 10-15% of ALS cases, the disease is inherited within a family and the genetic alterations underlying the disease are known. The type of inheritance is mainly dominant with reduced penetrance, although recessive mutations have been also described. This ALS form is the so-called fALS (Table 1). As mentioned before, the G4C2 HRE is the most common genetic alteration found in fALS patients (40%), but other common ALS genes involved are *SOD1* (12%), *TARDBP* (4%) and *FUS* (4%) (Table 1) (Goutman et al., 2022). The list of potential ALS genes (e.g. *GLT8D1*, *TIA1*, *C21orf2*, *DNAJC7*, *LGALS1*, *KANK1*, *CAV1*, *SPTLC1*, *ACSL5*) is still growing, but establishing the causality of many of these mutations is still challenging for geneticists and requires further validation (Mead et al., 2023). Nevertheless, in the vast majority of ALS patients (85%-90%), there is not an apparent family history, and it is known as sporadic ALS (sALS). In about 15% of sALS patients, they carry private mutations in the known ALS-associated genes, but not observed in their relatives (Table 1).

Importantly, in 85% of sALS patients, there is not a known cause explaining the disease (Feldman et al., 2022).

Regarding FTD genetics, 30% of FTD patients are considered familial, being 60% of those explained by mutations in microtubule-associated protein tau (*MAPT*), progranulin (*GRN*) and *C9ORF72*. Less common mutations, each accounting for less than 5% of cases, occur in genes such as *TARDBP*, *FUS*, *TBK1* or Charged multivesicular body protein 2B (*CHMP2B*). The remaining 70% of FTD patients accounts for sporadic cases (Olszewska et al., 2016; M. R. Turner et al., 2017).

Gene	Encoded protein	Locus	fALS	sALS	FTD
<b>ALS genes</b>					
<i>SOD1</i>	Cu-Zn superoxide dismutase	21q22.11	12%	1-2%	
<i>ALS2</i>	Alsin	2q33.1	<1%	<1%	
<i>SETX</i>	Senataxin	9q34.13	<1%	<1%	
<i>SPG11</i>	Spatacsin	15q21.1	<1%	<1%	
<i>VAPB</i>	Vesicle-associated membrane protein	20q13.32	<1%	<1%	
<i>ANG</i>	Angiogenin	16p11.2	<1%	<1%	
<i>FIG4</i>	Polyphosphoinositide phosphate	6q21	3%		
<i>SIGMAR1</i>	Sigma non-opioid intracellular receptor 1	9p13.3	<1%	<1%	
<i>OPTN</i>	Optineurin	10p13	<1%	<1%	
<i>PFN1</i>	Profilin-1	17p13.2	<1%	<1%	
<i>ERBB4</i>	Receptor tyrosine-protein kinase erbB-4	2q34	<1%		
<i>HNRNPA1</i>	Heterogeneous nuclear riboprotein A1	12q13.13	<1%	<1%	
<i>MATR3</i>	Matrin-3	5q31.2	<1%	<1%	
<i>ANXA11</i>	Annexin A11	10q22.2	1%	1.7%	
<i>NEK1</i>	Serine-threonine protein kinase Nek1	4q33	1-2%	<1%	
<i>KIF5A</i>	Kinesin heavy chain isoform 5A	12q13.3	0.5-3%	<1%	
<i>GLT8D1</i>	Glycosyltransferase 8 domain-containing protein 1	3p21.1	<1%	<1%	
<i>C21orf2 (CFAP410)</i>	Cilia and flagella-associated protein 410	21q22.3	<1%	<1%	
<i>DNAJC7</i>	DnaJ heat shock protein family (Hsp40) member C7	17q21.2	<1%	<1%	
<i>LGALS1</i>	Galectin-related protein	2p14	<1%	<1%	
<b>ALS/FTD genes</b>					
<i>C9ORF72</i>	Chromosome 9 open reading frame 72	9p21.2	40%	7%	25%
<i>CHCHD10</i>	Coiled-coil-helix-coiled-coil-helix domain-containing protein 10	22q11.23	<1%	<1%	2%
<i>SQSTM1</i>	Sequestosome-1	5q35.3	1%	<1%	1%
<i>TBK1</i>	TANK-binding kinase 1	12q14.2	3%	<1%	1%
<i>CCNF</i>	Cyclin F	16p13.3	1-3.3%	<1%	1%
<b>Predominantly ALS genes also found in FTD</b>					
<i>TARDBP</i>	TAR DNA binding protein 43 (TDP-43)	1p36.22	4%	1%	Rare
<i>FUS</i>	Fused in sarcoma	16p11.2	4%	1%	Rare
<i>UBQLN2</i>	Ubiquilin 2	Xp11.21	<1%	<1%	Rare

(Table continues in the next page)



Gene	Encoded protein	Locus	fALS	sALS	FTD
<b>Predominantly ALS genes also found in FTD</b>					
<i>OPTN</i>	Optineurin	10p13	<1%	<1%	Rare
<i>TUBA4A</i>	Tubulin $\alpha$ 4A chain	2q35	<1%	<1%	Rare
<i>ATXN2</i>	Ataxin 2	12q24.12	<1%	<1%	Rare
<i>TIA1</i>	TIA1 Cytotoxic Granule Associated RNA Binding Protein	2p13.3	2.2%	<1%	Rare
<b>Predominantly FTD genes also found in ALS</b>					
<i>VCP</i>	Valosin-containing protein	9p13.3	1%	1%	1.6%
<i>CHMP2B</i>	Charged multivesicular body protein 2B	3p11.2	<1%	<1%	1%
<b>FTD genes</b>					
<i>GRN</i>	Progranulin	17q21.31	-	-	5%
<i>MAPT</i>	Microtubule-associated protein tau	17q21.2	-	-	25%

**Table 1. Genes implicated in ALS and FTD.** Information extracted from Roggenbuck et al., 2017; Chia et al., 2018; Gregory et al., 2020; Saez-Atienzar et al., 2021; Goutman et al., 2022; Mead et al., 2023.

## 2. Amyotrophic lateral sclerosis

### 2.1 ALS pathophysiology

Several pathogenic mechanisms driving MN degeneration in ALS have been elucidated thanks to the identification of ALS genetic causes and the development of animal models (Figure 4) (Hardiman et al., 2017; Mead et al., 2023). However, as occurs in other neurodegenerative diseases, MN loss in ALS is likely the result of many interrelated pathways that disrupt a larger system progressively. The primary drivers underlying the disease and the relative extent to which each factor contributes to the pathology remain uncertain and, given the ALS heterogeneity observed in humans, probably not all the pathogenic mechanisms are involved in all ALS cases. In the following sections, the main ALS pathogenic mechanisms will be discussed.

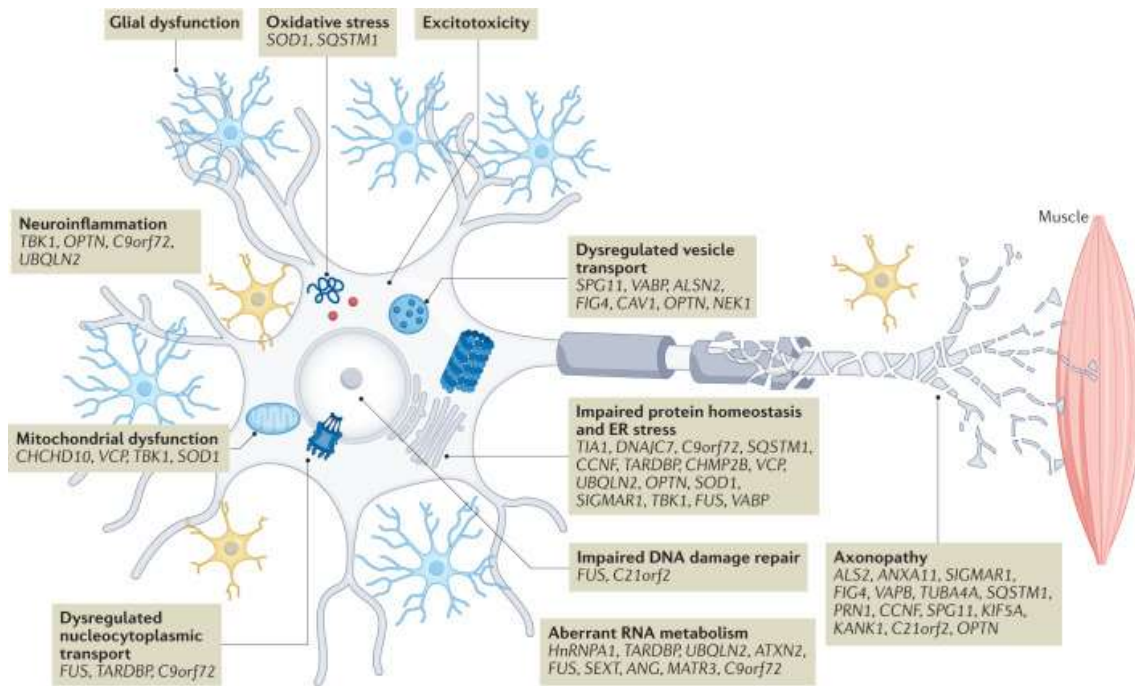


**Figure 4. Main pathogenic mechanisms involved in ALS.** ER: Endoplasmic reticulum. Extracted from Mead et al.,2023.

### ***i. Aberrant RNA processing***

Proper RNA metabolism is fundamental for a correct cellular function and involves its transcription, splicing, nuclear export, and translation. The involvement of aberrant RNA processing as a key pathway affected in ALS pathophysiology arose from the discovery of neuronal cytoplasmic inclusions of transactive response DNA binding protein of 43 kDa (TDP-43) in 95% of ALS patients, except for SOD1-linked ALS (Neumann et al., 2006). TDP-43 (encoded by *TARDBP*) is a DNA- and RNA-binding protein, which usually localizes in the nucleus where is essential for a proper RNA regulation. However, in pathological conditions, TDP-43 accumulates into the cytoplasm as aggregates, thus its exclusion from its nuclear location induces dramatic changes in gene expression. Targeted transcripts are essential for healthy neuronal functioning, including RNA splicing, synapse function, neurotransmitter metabolism or neurite development, whose altered expression may directly affect the well-functioning of MNs (Sephton et al., 2011). TDP-43 associates with cytoplasmic miRNA complexes, being involved in miRNA formation and maturation. TDP-43-targeted miRNA were abnormally produced in ALS patients, in line with the altered miRNA observed when TDP-43 is silenced in *in vitro* conditions (Freischmidt et al., 2013; Kawahara & Mieda-Sato, 2012). Moreover, some ALS-causing mutations

are harboured in RNA-binding protein genes, including heterogeneous nuclear ribonuclear protein A1 (*hnRNPA1*) or *FUS*. In a similar manner to TDP-43, *FUS* is involved in mRNA splicing. It has been seen that both mutant proteins altered splicing events in neuronal function and support genes, such as neurexins,  $\alpha$ -amino-3-hydroxy-5-methyl-4-isoxazolepropionic acid (AMPA) receptor GluR2 subunit or brain-derived neurotrophic factor (BDNF) (Arnold et al., 2013; Polymenidou et al., 2011; Qiu et al., 2014). Finally, repeated expansions in *C9ORF72* trigger the formation of abnormal RNA species and recruitment of RNA-binding proteins into RNA foci (Barmada, 2015; Kapeli et al., 2017).

**ii. Impaired proteostasis and protein aggregation**

Protein homeostasis, also known as proteostasis, consists of maintaining all proteins in the cell proteome in a conformation, concentration and location required for their correct function. It requires a proper protein synthesis, folding, trafficking and degradation. As in other neurodegenerative diseases, certain mutant proteins tend to misfold and assemble in neurotoxic aggregates (Lambert-Smith et al., 2022). In ALS, ubiquitinated TDP-43 inclusions (Mackenzie et al., 2007; Neumann et al., 2006), *FUS* aggregates (Hewitt et al., 2010), SOD1 inclusions (Forsberg et al., 2019; Shibata et al., 1994) or dipeptide repeat (DPR) proteins in *C9orf72* cases (Schipper et al., 2016) are observed in spinal MNs and glial cells in ALS postmortem samples, providing clear evidence of proteostasis dysfunction in the disease.

The accumulation of misfolded proteins induces endoplasmic reticulum (ER) stress, which triggers the unfolded protein response (UPR) to restore homeostasis (Jeon et al., 2023). However, in neurodegenerative diseases, including ALS, chronic ER stress and prolonged UPR induce apoptosis in MNs and glial cells (Ito et al., 2009). In fact, reducing ER stress by pharmacological treatment in ALS mouse models slowed progression and attenuated clinical manifestations (Saxena et al., 2009). On the other hand, the formation of aberrant proteins requires a proper degradation by autophagy and ubiquitin-proteasome system (UPS). Ubiquitin is specially known for its role in targeting proteins for quick degradation through the proteasome. The fact that intracellular inclusions in ALS-affected cells are ubiquitin-positive (Leigh et al., 1991; Neumann et al., 2006) suggests a defective UPS pathway in ALS pathogenesis as these inclusions are not degraded (Bendotti et al., 2012).

Importantly, some of ALS-linked mutations affect proteins that interact with the UPS, such as VCP, are known to be substrates for this system (SOD1, TDP-43 or OPTN).

Finally, both TDP-43 and FUS contain prion-like domains in its protein structures, which are fundamental for its self-aggregation properties. The prion-like domains are involved in stress granule formation, which are transient RNA-protein complexes formed in response to cellular stress. These granules sequester specific mRNAs to temporarily prevent their translation (Lambert-Smith et al., 2022). In physiological conditions, there is a balance between the formation and disruption of this stress granules. However, in ALS this balance is disrupted leading to a more persistent and pathogenic accumulation of stress granules (Barmada, 2015).

### ***iii. Excitotoxicity***

Glutamate-mediated excitotoxicity refers to neuronal death triggered by a massive calcium ( $\text{Ca}^{+2}$ ) entry as a result of excessive or prolonged glutamate stimulation (Mead et al., 2023). It has been established as a major pathogenic mechanism in ALS given the presence of increased glutamate levels in cerebrospinal fluid (CSF) from ALS patients (Perry et al., 1990; Spreux-Varoquaux et al., 2002). Besides, Riluzole, the only approved drug for all ALS forms in Europe, inhibits glutamate release, a mechanism that seems to be shared among all ALS forms (Bensimon et al., 1994).

Glutamate is the main excitatory neurotransmitter in the central nervous system (CNS) and acts through ionotropic and metabotropic receptors in the postsynaptic neurons. In pathological conditions, excitotoxicity is induced due to glutamate accumulation in the synaptic cleft and hypersensibilization of its receptors. Astrocytes are the main controllers of extracellular glutamate levels by removing it through the excitatory amino-acid transporter 2 (EAAT2). In this line, the loss of EAAT2 has been described in ALS patients (Bristol & Rothstein, 1996) and mouse models (Trotti et al., 1999), which would facilitate the accumulation of extracellular glutamate. Neuronal damage is induced by an increase of intracellular  $\text{Ca}^{+2}$ , triggering mitochondrial damage, activation of  $\text{Ca}^{+2}$ -dependent enzymes (e.g. nucleases, proteases, or lipases) and reactive oxygen species (ROS) generation (Mancuso & Navarro, 2015). MNs are particularly vulnerable to excitotoxicity

insults because they have lower expression of Ca<sup>2+</sup>-buffering proteins (e.g. parvalbumin and calbindin) (Ince et al., 1993) and high expression of N-methyl-D-aspartate (NMDA) and AMPA receptors lacking GluR2 subunit, which are more Ca<sup>2+</sup> permeable (Williams et al., 1997). In contrast, MNs that show resistance to neurodegeneration in ALS (e.g. oculomotor or trochlear MNs) display higher expression of these proteins (Alexianu et al., 1994), supporting the relevance of excitotoxicity to MN vulnerability in ALS.

#### **iv. Oxidative stress**

Oxidative stress is produced by excessive formation of ROS and reactive nitrogen species (RNS) in the mitochondria and/or by deficient activity of the antioxidant systems (Mead et al., 2023). Evidence of the involvement of oxidative stress arose from studies in ALS patients that show increased presence of ROS- and RNS-oxidized proteins, lipid peroxidation, and DNA damage in CSF and spinal cord (Aoyama et al., 2000; Beal et al., 1997; Chang et al., 2008; Ferrante et al., 1997). Oxidation of mRNA has also been observed in ALS mouse models, occurring at early stages of the disease and resulting in decreased protein translation in MNs (Chang et al., 2008). Impairment in oxidative stress defence systems is also reported in ALS, including dysregulation of glutathione homeostasis (Kiyoun, 2021) and alterations in the nuclear factor erythroid 2-related factor 2 (NRF2) antioxidant response element (ARE) system (Jiménez-Villegas et al., 2021). Besides, oxidative stress can contribute to other ALS pathogenic mechanisms. For instance, it can promote TDP-43 hyperphosphorylation and aggregation into insoluble inclusions (Goh et al., 2018). Despite the importance of oxidative stress in the pathogenesis of ALS, a recent press release by Ferrer International SA announced that the free radical scavenger FAB122, an investigational oral formulation of Edaravone, failed to achieve its primary efficacy and key secondary endpoints in the Phase III ADORE (ALS Declaration with Oral Edaravone) trial (NCT0178810) for ALS.

#### v. **Mitochondrial dysfunction**

Mitochondria are the cell organelle in charge of essential functions, including energy metabolism,  $\text{Ca}^{+2}$  homeostasis or programmed cell death. A proper mitochondrial functioning is especially relevant in MN survival and function, because they have high energetic demands, they are long-lived postmitotic cells prone to accumulate DNA damage arising from mitochondrial dysfunction and they require a fine regulation local  $\text{Ca}^{+2}$  dynamics. In this sense, it is extensively reported that mitochondrial impairment is linked to ALS, being one of the earliest events in the disease even before onset (Smith et al., 2019; J. Zhao et al., 2022).

Decreased activity of the mitochondrial electron transport chain (ETC) along with reduced ATP production and reduced mitochondrial DNA (mtDNA) content have been described in spinal cord and skeletal muscle from ALS patients (Ghiasi et al., 2012; Vielhaber et al., 2000; Wiedemann et al., 1998, 2002). Mitochondria also exhibit morphological abnormalities, such as swelling and vacuolization, as observed in ALS patients and SOD1 and TDP-43 mouse models (Magrané et al., 2014; Sasaki & Iwata, 2007). The exact mechanisms leading to mitochondrial dysfunction in ALS remain uncertain. However, it has been described that protein aggregates such as those generated by mutant SOD1, TDP-43 or C9orf72 can penetrate the mitochondrial membrane and disrupt the normal functioning of the mitochondrial ETC, increasing also oxidative stress (Ferri et al., 2006; Lopez-Gonzalez et al., 2016; W. Wang et al., 2013). Moreover, and as stated earlier, mitochondria play a key role in intracellular  $\text{Ca}^{+2}$  homeostasis. This is important since studies in SOD1 mouse models have elucidated that MNs display a deficient  $\text{Ca}^{+2}$  influx into the mitochondria before the symptomatology of the disease leading to mitochondrial  $\text{Ca}^{+2}$  overload (M. Damiano et al., 2006; Fuchs et al., 2013). Mitochondrial  $\text{Ca}^{+2}$  overload is one of the pro-apoptotic ways to induce the swelling of mitochondria, with perturbation or rupture of the outer membrane, and in turn the release of mitochondrial apoptotic factors into the cytosol, such as cytochrome c, apoptosis inducing factor (AIF), procaspase-9, among others, and lead to neuronal cell death. Several B-cell lymphoma 2 (Bcl-2) protein family members prevent apoptosis upon mitochondrial  $\text{Ca}^{+2}$  overload since it stabilizes mitochondrial membrane. SOD1 protein can interact with Bcl-2. However, mutant SOD1 leads to

pro-apoptotic gain of function of Bcl-2, and thus, further increases MN apoptosis (Pedrini et al., 2010).

**vi. Cytoskeletal and trafficking defects**

MNs have notably long axons, extending across substantial distances, sometimes up to a meter in humans. This extensive axonal length necessitates efficient transport systems to ensure proper neuron function. Both anterograde (from the cell body towards the axon terminals) and retrograde (from the axon terminals back to the cell body) axonal transport are critical for delivering necessary components like mitochondria, signalling endosomes, proteins, and other cellular cargo. Impairment of axonal transport is known to be involved in ALS pathogenesis, as evidenced in ALS mouse models and in the human disease, with an accumulation of neurofilaments and organelles in proximal axons and MN somas (Hirano et al., 1984; Sasaki & Iwata, 2007; Schmidt et al., 1987). Additionally, some ALS-associated mutations are present in cytoskeleton and trafficking genes, such as *TUBA4A*, *PFN1*, *ALS2* or *ANXA11*, or other ALS-linked genes (*FUS*, *TDP-43*, or *C9ORF72*) affect indirectly this mechanism (Burk & Pasterkamp, 2019). For instance, TDP-43 has been reported to be involved in endosomal recycling pathway, decreasing the number and motility of recycling endosomes in dendrites in TDP-43-knockdown neurons (Schwenk et al., 2016). Overall, these defects may result in MNs being unable to deliver fundamental components to their synapses or transmit information back to soma, potentially initiating degeneration processes.

**vii. Neuroinflammation**

It is well-established in the field that although ALS is a MN disease, non-neuronal cells also play a crucial role in the pathology, actively contributing to MN degeneration. This was evidenced in mice specifically expressing mutant SOD1 only in MNs, which did not show either MN degeneration or the typical ALS signs (Lino et al., 2002; Pramatarova et al., 2001). As in other neurodegenerative diseases, CNS inflammation is a prominent pathological feature in ALS. It is characterized by reactive microglia and astrocytes at sites of MN degeneration and, to lesser extent, to infiltration of peripheral immune cells (monocytes/macrophages, T-, B-, and natural killer (NK)-lymphocytes) into the CNS (E. Liu et al., 2021). Innate and



adaptative immune responses are evident during the whole disease course, even in presymptomatic stages (J. Liu & Wang, 2017).

First evidence that inflammation might contribute to ALS pathology emerged from human postmortem studies which revealed marked microglial and astrocytic reactivity in degenerative areas of the CNS (T. Kawamata et al., 1992; Philips & Robberecht, 2011; Schiffer et al., 1996). Notably, patients from fast-progressing ALS exhibited a higher microglial reactivity in postmortem CNS compared to those with slower progression (Brettschneider et al., 2012). Recently, RNA sequencing (RNAseq) analysis in postmortem motor cortex samples showed an overrepresentation of microglial cells in sALS patients compared to healthy controls (Dols-Icardo et al., 2020). ALS patients also exhibited more activated dendritic cells, the professional antigen presenting cells that initiate the adaptative immune response, and T- and B-lymphocytes in the ventral horn of the spinal cord and degenerating corticospinal tracts compared to controls. In this line, positron emission tomography (PET) neuroimaging studies in presymptomatic and symptomatic ALS patients also reported widespread microglial activation in motor and non-motor CNS regions, even in early stages of the disease (Corcia et al., 2012; Tondo et al., 2020; M. R. Turner et al., 2004).

Similar to immune cells, cytokine and chemokine levels in CSF and plasma samples from ALS patients also mirror CNS inflammation. Several studies have reported elevated levels of pro-inflammatory chemokines and cytokines in biofluids from ALS patients, sometimes with contradictory results (E. Liu et al., 2021; Lu et al., 2016; Moreno-Martinez et al., 2019; Tortelli et al., 2020). Hu et al., 2017 performed a metanalysis assessing peripheral cytokines levels in ALS blood samples, confirming the increased concentration of tumour necrosis factor-alpha (TNF- $\alpha$ ), TNF- $\alpha$  receptor 1 (TNFR1), interleukin (IL)-6, IL-1 $\beta$  and vascular endothelial growth factor (VEGF) in ALS patients. Interestingly, cytokine patterns in plasma and CSF correlates with patient survival (Olesen et al., 2020), further supporting the important contribution of inflammation to ALS pathogenesis.



### **CNS-resident glial cells**

Microglia and astrocytes are the main CNS glial cells involved in inflammatory processes in pathological conditions. Astrocytes constitute a large proportion of glial cells that develop important physiological functions (structural, metabolic, and trophic function) to ensure the correct functioning of neurons. Among them, astrocytes are involved in the brain-blood barrier (BBB), the release of neurotrophic factors and synaptic activity. Indeed, astrocytes play a role in the “tripartite synapse” by modulating the neuronal connectivity and regulating the composition of the extracellular space. Indeed, astrocytes exacerbate excitotoxicity in ALS by failing to efficiently clear glutamate from the synaptic cleft.

Astrocytes respond to CNS degeneration through a process known as astrogliosis, which is characterized by an astrocytic proliferation, hypertrophy, expression changes and cytokine secretion (Pehar et al., 2017). Astrogliosis is recapitulated in several ALS mouse models and ALS patients (De Giorgio et al., 2019; Schiffer et al., 1996). Specific expression of mutant SOD1 in astrocytes resulted in astrogliosis but this was not sufficient to cause MN degeneration in mice (Gong et al., 2000). However, selective correction of mutant SOD1 in astrocytes or transplantation of wild-type astrocytes in SOD1 mice delayed disease onset and extended mouse survival, highlighting the involvement of astrocytes in ALS pathogenesis (Lepore et al., 2008; L. Wang et al., 2011; Yamanaka et al., 2008). A recent meta-analysis comparing the transcriptome of human ALS induced pluripotent stem cell (iPSC)-derived astrocytes and astrocytes from different ALS mouse models described that ALS astrocytes adopt a reactive pro-inflammatory state (Ziff et al., 2022). Astrocyte-mediated toxicity was confirmed *in vitro* since healthy MNs underwent cell death when cultured with ALS astrocytes (SOD1, C9orf72, sALS) (Haidet-Phillips et al., 2011; C. Zhao et al., 2020). The precise mechanism by which astrocytes mediate MN degeneration remains unclear, but it may be linked to alterations in their secretome. Studies suggest that this involves a reduction in neurotrophic factors and an increase in toxic elements, such as pro-inflammatory cytokines (Ng& Ng, 2022). Importantly, there is a direct crosstalk between astrocytes and microglia. The transformation of astrocytes into a reactive state depends on reactive microglia through the secretion of IL-1 $\alpha$ , TNF- $\alpha$  and complement component 1q (C1q). It has been demonstrated that colony stimulating

factor 1 (CSF1) receptor (CSF1R) knockout (KO) mice, which lack microglia, fail to induce the reactive inflammatory phenotype in astrocytes when exposed to lipopolysaccharide (LPS) injection (Liddel et al., 2017). Since reactive pro-inflammatory astrocytes are observed in human neurodegenerative diseases, including ALS, this finding is considered significant for understanding ALS pathogenesis. Given the central focus on microglial cells in this thesis, their role in ALS will be explored in greater detail in section 3 (Microglia in ALS).

### **Peripheral immune system**

Monocytes and macrophages are phagocytes from the innate immune system. Monocytes circulate through the bloodstream, and they become resident macrophages and dendritic cells once recruited into body tissues. Their main physiological functions include antigen presentation, chemokines secretion to recruit other immune cells and phagocytosis of pathogens and cellular debris (Ginhoux & Jung, 2014). Whereas the proportion of monocytes among leucocytes in blood are not altered in ALS patients, it is reported that ALS monocytes are skewed towards a pro-inflammatory phenotype compared to controls (W. Zhao et al., 2017; Zondler et al., 2016). In fact, these differences are exacerbated in rapidly progressing patients in comparison with slowly progressing patients (W. Zhao et al., 2017).

Macrophage activation and infiltration into both CNS and peripheral nervous system (PNS) occurs in early stages of the disease and increases with disease progression, as seen in SOD1 mouse models (Chiot et al., 2020; Chiu et al., 2009; Martínez-Muriana et al., 2016; Nardo et al., 2016) and postmortem ALS patients (Chiot et al., 2020). Some studies illustrating the role of non-neuronal cells in ALS pathogenesis showed attenuation of disease progression and increased lifespan of SOD1 mice when the expression of mutant SOD1 was decreased in microglia and macrophages (Beers et al., 2006; Boillée et al., 2006). Interestingly, targeting macrophages at the periphery has a therapeutic impact on ALS course. For instance, a study from our group reported that pharmacological inhibition of CSF1R slowed ALS progression by reducing macrophage PNS infiltration (Martínez-Muriana et al., 2016). In this line, a recent study demonstrated that replacement of peripheral SOD1 by WT macrophages modified some ALS disease parameters by changing microglial reactivity (Chiot et al., 2020). Specifically, ALS disease onset was delayed

when macrophages were replaced at pre-symptomatic stage while SOD1<sup>G93A</sup> mouse survival was extended when replacement took place at the disease onset (Chiot et al., 2020).

NK cells are the innate effector lymphocytes, whose main function is to eliminate virus-infected cells and tumour cells. Its interest as players in ALS pathogenesis started few years ago when ALS patients were shown to exhibit an increased population of NK cells (Gustafson et al., 2017; Jin et al., 2020; Murdock et al., 2017). However, another study showed that ALS patients have a lower frequency of NK cells relative to other peripheral blood mononuclear cells (PBMC) (Garofalo et al., 2020). NK cells infiltration into the motor cortex and spinal cord was observed in ALS postmortem samples and in the mutant SOD1<sup>G93A</sup> mouse model (Garofalo et al., 2020). Interestingly, NK cells depletion in mutant SOD1<sup>G93A</sup> and TDP-43<sup>A315T</sup> mice increased mouse survival and delayed disease onset. Decrease in NK cells also affects other immune populations, leading to reduced microgliosis and a shift toward a more protective microglial phenotype, as well as an increase in the recruitment of regulatory T-lymphocytes (Tregs) into the CNS (Garofalo et al., 2020).

Amongst the cells that constitute the adaptative immune system, B-lymphocytes and T-lymphocytes are the main components. Whereas some studies describe that B-cells, the antibody-producing cells, are not particularly involved in ALS, peripheral T-lymphocytes are key players in ALS pathogenesis (E. Liu et al., 2021). Based on markers expression, T-cells can be classified as CD4<sup>+</sup> cells and CD8<sup>+</sup> cells. CD4<sup>+</sup> T-cells, also known as T helper (Th) lymphocytes, are the responsible of orchestrating an appropriate and specific immune response against a pathogen by providing the necessary activation signals to CD8<sup>+</sup> T-cells and B-cells. Upon activation, they can be polarized to several subsets (Th1, Th2, Th17, Treg) defined by their transcription factor expression patterns and their cytokine production (J. Liu & Wang, 2017; W. Zhao et al., 2013). In ALS patients, there are increased counts of pro-inflammatory Th1 and Th17 cells in the bloodstream (Jin et al., 2020; Saresella et al., 2013) whereas the number of Treg lymphocytes, which suppress immune reactions, are reduced (Henkel et al., 2013; Jin et al., 2020; Saresella et al., 2013). These findings correlate with those observed in SOD1<sup>G93A</sup> mice since blood

Th1 and Th17 cells increase at late disease stages while Treg population decreases over disease progression (Beers et al., 2011; Zhao, Beers, et al., 2012). It is unclear whether the counts of Th2 lymphocytes, which are neuroprotective, are altered in ALS since some studies report a reduction in ALS blood samples (Henkel et al., 2013; Jin et al., 2020) while others an increase (Saresella et al., 2013).

On the other hand, CD8<sup>+</sup> T-cells or cytotoxic T cells can eliminate both infected and tumour cells. Nevertheless, its involvement in ALS pathogenesis remains unclear. There is not a consensus about the percentages of CD8<sup>+</sup> T cells in ALS patients' blood. Whereas some studies report an increase in blood CD8<sup>+</sup> T cells in ALS patients (Jin et al., 2020; Rentzos et al., 2012), others show a reduction (Mantovani et al., 2009) or no significant change (Murdock et al., 2017). In SOD1<sup>G93A</sup> mice, cytotoxic CD8<sup>+</sup> cells infiltrate into the CNS (Beers et al., 2008; Chiu et al., 2008; Figueroa-Romero et al., 2020). Interestingly, SOD1<sup>G93A</sup> mice lacking CD8<sup>+</sup> T-lymphocytes exhibit greater MN survival and decreased neuroinflammation, suggesting the detrimental role of this T-cell subset in ALS pathogenesis (Nardo et al., 2018).

## 2.2. ALS experimental models

### *i. In vitro models*

Cell culture models allow the study of specific cellular mechanisms in a simpler scenario and to test the potential of pharmacological targets before moving to animal models. In the ALS field, a common cell line is NSC-34, a murine hybrid cell line generated by the fusion of mouse embryonic MN-enriched spinal cord cells and neuroblastoma cells. When differentiated, NSC-34 cells display several morphological and physiological MN features (Cashman et al., 1992). NSC-34 cells expressing mutant SOD1 exhibit cytoplasmic aggregation triggering some toxicity (B. J. Turner et al., 2005). Nevertheless, an important limitation of this model is the inability to model glutamate-induced excitotoxicity (Hounoum et al., 2016). Primary MNs from dissociated spinal cords from rat and mouse embryos are a more suitable model to assess neurotoxicity or neuroprotection (Nagai et al., 2007; Petrozziello et al., 2017). Also, primary co-cultures with MNs and glial cells (Díaz-Amarilla et al.,

2011) or organotypic cultures, such as spinal cord organotypic culture (SCOC) (Guzmán-Lenis et al., 2009), can be developed in order to study the interaction between cell types.

An increasing growing approach is the use of iPSCs. Their generation is based on reprogramming somatic cells from patients or healthy donors using the Yamanaka cocktail (Oct4, Sox2, Klf4 and Myc) (Takahashi & Yamanaka, 2006) and they can be differentiated into cell types relevant to human diseases in order to study the relationship between a complex genetic background and the associated phenotype. In the ALS field, several groups have differentiated iPSC into MNs (Workman et al., 2023) or glial cells (Birger et al., 2019; Funes et al., 2024; Lorenzini et al., 2023; Noh et al., 2023) harbouring ALS-related mutations or sporadic causes, giving some insights about the cell-autonomous pathogenic mechanisms.

## **ii. *In vivo mouse models***

The discovery of the genetic alterations underlying ALS (*SOD1*, *C9ORF72*, *TARDBP* and *FUS*) has facilitated the generation of transgenic mouse models that recapitulate some of the ALS clinical symptoms and pathogenic mechanisms (De Giorgio et al., 2019; Lutz, 2018). The first ALS mouse model featured a high copy number of human mutant *SOD1*, which overexpresses ubiquitously mutant SOD1 protein with glycine-to-alanine transition at the 93<sup>th</sup> codon (Gurney et al., 1994). These mice develop a rapid progressive disease, being the ALS onset around 12 weeks of age and leading to the endpoint at 4-5 months. *SOD1*<sup>G93A</sup> mouse model recapitulates some symptoms observed in ALS patients, for instance, muscle atrophy, denervation and paralysis in the hindlimbs, and the most characteristic histopathological hallmarks: MN loss and gliosis (Mancuso & Navarro, 2015). Other *SOD1* mouse models have been developed harbouring other mutations (*SOD1*<sup>G37R</sup>, *SOD1*<sup>G85R</sup>), which would mimic a more slow-progressing disease (Todd & Petrucelli, 2022). *SOD1* mice are still the gold standard in ALS research even though (i) *SOD1*-related cases represent a minimal percentage of all ALS patients (2%); (ii) there is no TDP-43 deposition in contrast to most ALS forms; (iii), these mice have several *SOD1*<sup>G93A</sup> copies and thus *SOD1* protein is not expressed at the physiological levels; and (iv) the allele instability can alter the gene copy numbers, leading to variations in the phenotype (Acevedo-Arozena et al., 2011; Fisher et al., 2023). To overcome

these limitations, Joyce et al., 2014 generated a mouse model carrying a homozygous D83G mutation in the endogenous mouse *SOD1* gene. These mice develop progressive degeneration of lower and upper MNs, likely due to the same unknown toxic gain of function as occurs in human fALS cases, but intriguingly lower MN cell death appears to stop in early adulthood and the mice do not become paralyzed. Humanized knock-in (KI) mouse models have been developed by replacing the mouse *SOD1* gene by the human ortholog (Devoy et al., 2021). However, these humanized *SOD1* mice carrying *SOD1*-causing mutations have not been reported in the literature.

Given the central TDP-43 pathology observed in most ALS cases, several TDP-43 mouse models have been generated overexpressing wild-type or mutant human TDP-43, leading to a dose-dependent and variable motor and behavioural phenotype and neuronal loss (Xu et al., 2010; Arnold et al., 2013). However, these mice showed some limitations: (i) they fail to fully develop the expected ALS-phenotype; (ii) cytoplasmic TDP-43 inclusions are not detected; and (iii) the endogenous mouse TDP-43 remains intact and nuclear (De Giorgio et al., 2019; Fisher et al., 2023; Lutz, 2018; Todd & Petrucelli, 2022). To induce TDP-43 aggregation in the cytoplasm, Igaz et al., 2011 generated a mouse model carrying TDP-43 missing the nuclear localization signal (TDP43 $\Delta$ NLS). They observed cytoplasmic TDP-43 accumulation but poor aggregation (Igaz et al., 2011; Walker et al., 2015). Recent TDP-43 models have focused on expressing TDP-43 in a more physiological level by introducing point mutations in the mouse *TARDBP* gene (Q331K, M337V, G298S, N390D). These mice show mild MN degeneration and a subtle ALS-phenotype, often at advanced ages (White et al., 2018; Ebstein et al., 2019; Huang et al., 2020; Kim, White, et al., 2020). Similar to TDP-43 models, *FUS* rodent models can be broadly classified into those overexpressing wild-type *FUS*, *FUS*-null models, and mutant models. Unlike TDP-43 models, mouse models carrying *FUS* mutations exhibit ALS-like locomotor deficits and progressive MN degeneration (López-Erauskin et al., 2018; X. Zhang et al., 2020). Finally, reported *C9orf72* mouse models harbouring the pathogenic G4C2 HRE have varying numbers of repeats and distinct phenotypes. They will be discussed more extensively given the importance within this PhD thesis.

### 2.3. ALS treatment

Nowadays, there is not an effective cure for ALS. Even though more than 60 compounds have been evaluated in clinical trials, only 4 treatments have been approved for clinical use (Genge et al., 2023; Mead et al., 2023). Riluzole was the first ALS treatment approved by Food and Drug Administration (FDA), the United States (US) regulatory agency, in 1995. This drug is an ant glutamatergic agent that reduces excitotoxicity and, although it triggers a modest improvement, it increases patient survival by 3 months (Bensimon et al., 1994; Lacomblez et al., 1996). Twenty years later, Edaravone, an antioxidant agent, was approved for ALS treatment in Japan (2015), US (2017), Canada (2018) and some Asian countries (China, 2019; Indonesia, 2020; Thailand, 2021), but not by the European Medicine Agency (EMA) (Mead et al., 2023). Its beneficial effect remains controversial, since there was not a significant improvement in ALS progression in treated patients compared to placebo (Abe et al., 2014). However, post-hoc analysis revealed a significant effect in disease progression in a subset of patients with rapid ALS progression treated early in the disease (Abe et al., 2017). However, on 10 January of 2024, a press release by Ferrer Internacional SA announced that its anticipated free radical scavenger FAB122, an investigational oral formulation of Edaravone, failed to achieve its primary efficacy and key secondary endpoints in the Phase III ADORE (ALS Declaration with Oral Edaravone) trial (NCT0178810) for ALS.

Recently, AMX0035, a combination of sodium phenylbutyrate and taurursodiol which targets mitochondrial dysfunction and ER stress, was approved in 2022 by the FDA. Although, efficacy studies showed that AMX0035 decreases the rate of decline and increases survival by 10 months (Paganoni et al., 2020, 2021), results from phase III (PHOENIX trial; NCT05021536) reported a lack of efficacy as ALS treatment (Amylyx Pharmaceuticals, 2024). Finally, in 2023, Tofersen (BIIB067) received an accelerated FDA approval for the treatment of SOD1-ALS specifically. Tofersen is an antisense oligonucleotide (ASO) that target mutant SOD1 mRNA, hence reducing toxic SOD1 protein. Indeed, Tofersen was shown to reduce toxic SOD1 protein levels in treated patients' CSF, and neurofilament light chain (NfL), a neuronal damage marker, in plasma (Miller et al., 2020, 2022). In a first phase III trial (VALOR clinical trial; NCT02623699), there was a tendency, but not statistically significant, in slowing the rate of disease progression (Miller et al.,

2022). An on-going phase III trial (ATLAS clinical trial; NCT03070119), which is expected to be finished in 2027, recruited presymptomatic SOD1-ALS patients in order to evaluate if Tofersen can delay the symptoms onset or slow disease progression once it appears.

The high failure rate in ALS clinicals trials is evident after almost 30 years of research since the first ALS treatment approval and demands a reflection to improve translation from animal models to clinical use (Genge et al., 2023; Mead et al., 2023). In the past clinical trials, ALS patients were considered as a homogenous group, and as clearly stated beforehand, the heterogeneity in ALS is high. Therefore, patients in clinical trials must be stratified by the driving pathogenic mechanisms, such as the genetic cause, and by the disease progression rate. Besides, given the late diagnosis of ALS patients and its rapid progression, it prevents the recruitment of early-stage patients which are more suitable for probably having a better improvement and response to the treatment. Moreover, there is a lack of reliable biomarkers of treatment efficacy or disease progression, which currently is only based on Revised Amyotrophic Lateral Sclerosis Functional Rating Scale (ALSFRS-R) score. There is not a surrogate biomarker for it, although some promising biomarkers are neurofilament heavy chain (NfH) and NfL in CSF and blood (Irwin et al., 2024). Importantly, this lack of translation to the clinics may be probably also due to the limitations in ALS mouse models. ALS field has mainly focused in the SOD1<sup>G93A</sup> mouse model, but as previously described SOD1-ALS represents a small proportion of human cases, and it does not develop TDP-43 pathology as most ALS patients. There is still a need of developing more reliable murine models of other genetic ALS subtypes for proper therapeutic testing.



### 3. Microglia in ALS

---

#### 3.1. Microglia generalities

Microglia, the CNS-resident immune cells, were first described by Pío del Río-Hortega in 1919 (Sierra et al., 2019). This myeloid population is originated via lineage-specific transcription factors Pu.1 and Irf8 during primitive haematopoiesis in the yolk sac, invading the CNS in the early embryonic stages (Ginhoux et al., 2010; Kierdorf et al., 2013). Maintenance of the microglial pool along life is facilitated by its self-renewal capacity, meaning that microglia are maintained by local proliferation without peripheral input. It is highly dependent on CSF1R-signalling, driven by two ligands: IL-34, which is produced by neurons; and CSF1, which is secreted by astrocytes and oligodendrocytes (Borst et al., 2021; Paolicelli et al., 2022). Microglial cells share markers with other CNS-associated myeloid cells (perivascular, meningeal, and choroid plexus macrophages), such as ionized Ca<sup>2+</sup>-binding adapter molecule 1 (Iba1), C-X3-C motif chemokine receptor 1 (CX3CR1), CD11b or low expression of CD45. Nevertheless, there are some microglial-specific markers, such as P2Y purinoreceptor 12 (P2RY12) or Transmembrane protein 119 (TMEM119), even though its expression may vary depending on its state (Paolicelli et al., 2022).

Microglia are dynamic cells which are continuously scanning the local CNS environment through their motile ramified processes, being crucial for CNS homeostasis. Although microglia were particularly known for its pro-inflammatory actions following CNS insults, they also play a key role in several biological functions in homeostatic conditions: synapse modelling, myelination, neurogenesis, neuronal function, tissue repair, BBB permeability or vasculogenesis (Paolicelli et al., 2022; Salter & Stevens, 2017). Microglia are involved in synaptic pruning in development by engulfment of non-functional synapses to ensure a correct modelling and functioning of the neuronal circuits (Paolicelli et al., 2011). Besides, in CNS development, adult homeostasis and aging, apoptotic cells and myelin debris are generated and must be phagocytosed by microglia for an optimal neuronal activity (Galloway et al., 2019; Li & Barres, 2018). It has been also described that microglial cells are key in the maturation and differentiation of oligodendrocyte progenitor cells (OPC) to mature oligodendrocytes for a correct myelination process (Borst et

al., 2021). Finally, microglia are important in the CNS protection against external injurious agents, such as infectious agents, or self-aberrant proteins, including amyloid- $\beta$  (A $\beta$ ),  $\alpha$ -synuclein, SOD1 or prions. Through a plethora of membrane receptors -the so-called sensome-, these noxious agents are detected by microglia. An inflammatory response is then triggered by the production of cytokines and chemokines to recruit more cells and to clear the injurious agent with the final purpose of promoting tissue repair and rescuing CNS homeostasis (Hickman et al., 2018). This physiological inflammatory phenomenon must be efficient and transient. However, when it becomes chronic and/or out of control, as occurs in neurological disorders, such as AD, PD or ALS, it is detrimental and contributes to neurodegeneration.

Microglia are characterized by their heterogeneity and plasticity in terms of microglial states, being temporary and highly dependent on the context. Traditionally, microglia were classified using the M1/M2 dichotomy: M1, the classical activation, considered as pro-inflammatory and neurotoxic; and M2, the alternative activation, regarded as anti-inflammatory and neuroprotective. However, microglial cells *in vivo* do not strictly align with either of these categories, frequently displaying co-expression of M1 and M2 markers (Paolicelli et al., 2022; Ransohoff, 2016). With the advances in single-cell technologies and multi-omics, a growing list of microglial states have been proposed depending on the context (development, health, injury, and disease), disease models and species, based on its transcriptomics which reflect the biological pathways implicated. Some reported microglial states related with neurodegenerative diseases and ageing are disease-associated microglia (DAM) (Keren-Shaul et al., 2017), microglial neurodegenerative phenotype (MGnD) (Krasemann et al., 2017), activated response microglia (ARM) (Frigerio et al., 2019), interferon-responsive microglia (IRM) (Frigerio et al., 2019), lipid-droplet-accumulating microglia (LDAM) (Marschallinger et al., 2020), human AD microglia (HAM) (Srinivasan et al., 2020), microglia inflamed in multiple sclerosis (MIMS) (Absinta et al., 2021) or RIPK1-regulated inflammatory microglia (RRIM) (Mifflin et al., 2021), among others. Nevertheless, the functional implications of these microglial states and the relationships between them remain elusive and further studies are required to

completely understand the complexity of microglia in physiological and pathological conditions.

### 3.2. Microglia in ALS pathogenesis

Microglial cells play an undeniable role in ALS, but delineating the precise contribution of microglia to disease is being challenging. Literature evidences both neurotoxic and neuroprotective microglial roles in ALS, which may be related with a spatiotemporal regulation of microglial activation over the disease (Brites & Vaz, 2014; Clarke & Patani, 2020; Geloso et al., 2017; Haukedal & Freude, 2019; Hickman et al., 2018; Motataianu et al., 2020; You et al., 2023).

Some *in vitro* studies with primary mouse mutant SOD1<sup>G93A</sup> microglia pointed out the detrimental role of microglia in ALS pathology. Weydt et al., 2004 described that SOD1<sup>G93A</sup> microglia exhibit an enhanced secretion of TNF $\alpha$  when stimulated with LPS, compared to wild-type microglia. In this line, other studies showed that SOD1<sup>G93A</sup> microglia are potentially toxic compared to the wild-type, through an increased production of ROS and nitric oxide (NO), and a decrease in the production of neurotrophic factors, such as insulin-like growth factor-1 (IGF-1). This neurotoxic potential was confirmed in co-cultures with MNs and SOD1<sup>G93A</sup> microglia, in which a decrease in MN survival was observed in comparison with control microglia (Beers et al., 2006; Liao et al., 2012; Q. Xiao et al., 2007).

Evidence from ALS mouse models *in vivo* also proved the involvement of microglia in the disease. On one hand, microglia are established to be a determinant cell type involved in the disease course rather than ALS onset. It was described that removing mutant SOD1 expression specifically in microglia/macrophages, throughout Cre-Lox recombination by crossing CD11b-Cre recombinase and Lox-SOD1<sup>G37R</sup> mice, was not able to change ALS onset, but it delayed ALS progression and increased survival (Boillée et al., 2006). Similarly, transplantation of wild-type microglia/macrophages in SOD1<sup>G93A</sup>-PU.1 KO mice, which lack myeloid and lymphoid cells, was able to increase MN survival, to delay ALS progression and to improve survival (Beers et al., 2006). Interestingly, transplanting SOD1<sup>G93A</sup> microglia/macrophages in PU.1 KO mice was not sufficient to induce MN disease (Beers et al., 2006). Modulating microglia specifically *in vivo* has been shown to

influence ALS progression. In this line, nuclear factor- $\kappa$ B (NF- $\kappa$ B) inhibition specifically in microglia rescued MN degeneration *in vitro* and increased SOD1<sup>G93A</sup> mice survival (Frakes et al., 2014). Besides, targeting microglia proliferation by a selective CSF1R inhibitor increased MN survival and ameliorated the disease in SOD1<sup>G93A</sup> mice (Martínez-Muriana et al., 2016).

On the other hand, it has been described that there is a shift in the microglial phenotype from more neuroprotective in the early disease to more neurotoxic in the late stages. Despite the use of the old-fashioned M1/M2 dichotomy, Liao et al., 2012 showed that, in the ALS onset, microglia have a more neuroprotective phenotype with an increased expression of *Ym1*, *Cd163* and *Bdnf*, whereas microglia in end-stage ALS late stage exhibit an increased *Nox2* expression. However, transcriptomic analysis of isolated microglia from SOD1<sup>G93A</sup> mice at different disease time points (pre-symptomatic, early symptomatic and end-stage) showed a neurodegenerative-specific transcriptome, in which microglia co-express neurotoxic (*Mmp2*, *Optn* or *Cybb*) and neuroprotective genes (*Igf1* or *Grn*), whose expression is exacerbated with ALS progression (Chiu et al., 2013).

Even though most transcriptomic studies describing microglial states in neurodegenerative diseases have focused on AD mouse models and human patients, some single-cell RNAseq (scRNAseq) studies have centred in elucidating the presence of different microglial states in ALS pathogenesis. The microglial state triggering more interest in the field is DAM, since it was the earliest in being identified. Its expression profile is characterized by downregulation of homeostatic genes (*P2ry12*, *Cx3cr1*, *Tmem119*), an upregulation of AD-associated risk genes (*ApoE*, *Ctsd*, *Lpl*, *Tyrobp*, *Trem2*) and genes related with phagocytic, lysosomal and lipid metabolism-related pathways (You et al., 2023). DAM are observed close to neurodegenerative areas, playing a protective role involving the clearance of misfolded and aggregated proteins that accumulate in neurodegenerative diseases (e.g. A $\beta$  or SOD1 aggregates). It is thought that DAM are not necessarily associated with the specific primary cause of disease, suggesting that DAM are rather a general microglial response to neurodegeneration. In SOD1<sup>G93A</sup> mouse model, DAM accumulate in the spinal cord over disease progression (Keren-Shaul et al., 2017) and their presence in human postmortem samples has been confirmed by

quantitative polymerase chain reaction (qPCR) of key DAM genes (Jauregui et al., 2023). RNAseq studies in postmortem cortex of sALS samples revealed an increased representation of a microglial subpopulation that overlapped with the DAM signature (Dols-Icardo et al., 2020). On the other hand, Krasemann et al., 2017 described a MGnD phenotype triggered in a *Trem2/Apoe*-dependent manner, observed in ALS and AD mouse models. MGnD microglia are induced by phagocytosis of apoptotic neurons, which are a hallmark of neurodegeneration. Additionally, Mifflin et al., 2021 described RRIM specifically in SOD1<sup>G93A</sup> and OPTN KO ALS mouse models. RRIM are characterized by RIPK1-dependent production of classical pro-inflammatory cytokines, including an upregulation of *Tnfa* and *Il1b*. RRIM are increased in both ALS mouse models, although to a greater extent in OPTN KO mice, and their peak occurs at earlier timepoints in ALS pathogenesis compared to DAM. Whereas OPTN KO mice do not have protein aggregates, SOD1<sup>G93A</sup> mice do exhibit misfolded SOD1 protein. It may suggest that RRIM represent a different path in early ALS stages independent from protein aggregation, which would be more associated to DAM (Mifflin et al., 2021). The functional role and implication of these context-dependent and temporary microglial states in ALS pathogenesis needs to be fully understood. However, it opens new therapeutic avenues targeting specifically microglial states to restore homeostatic microglia as a treatment for neurodegenerative diseases.

Although most advances have been done using mutant SOD1 mouse, other studies have focused on other ALS mouse models. Spiller et al., 2018 used the rNLS8 mouse which expresses human TDP-43 in neurons in a doxycycline-dependent manner and demonstrated that microglia play a neuroprotective role in this ALS mouse model, by clearing the TDP-43 aggregates in neurons. This beneficial effect was confirmed by blocking microgliosis with a CSF1R inhibitor, being the animals unable to regain motor function (Spiller et al., 2018). Moreover, C9orf72 deficiency triggers a microglial transcriptome change from a homeostatic signature to an inflammatory type I interferon (IFN) signature (Lall et al., 2021).

Genetic studies in patients and matched controls have identified loci associated with an increased risk for neurodegenerative diseases which are highly or preferentially expressed in microglia (Salter & Stevens, 2017). Notably,

polymorphisms in genes such as *TREM2*, *C9orf72*, *GRN*, *PFN1*, *TBK1*, *OPTN*, and *UBQLN2* have been strongly associated with ALS (Haukedal & Freude, 2019; Limone et al., 2024). These genes encode proteins implicated in crucial microglial pathways, such as autophagy or regulating their activation. Consequently, understanding the impact of newly identified ALS-associated genetic variants on microglial activity may uncover the role of microglial cells in this complex disease.

Modelling of iPSC-derived microglia from ALS patients *in vitro* have provided a valuable tool to study more in depth the pathological alterations in microglia driven by different ALS-related genes. Focusing in human *C9orf72* iPSC-derived microglia, it has been described that mutant *C9orf72* microglia have a deficit in autophagy and phagocytosis, an exacerbated response to LPS and, when cocultured with MNs, *C9orf72* microglia increase MN vulnerability to excitotoxicity (Banerjee et al., 2023). In this line, another study found metalloprotease-9 (MMP-9) as a microglial mediator of MN toxicity (Vahsen et al., 2023). However, Lorenzini et al., 2023 provided opposite results in their study, in which they described mild changes in gene expression and an increased phagocytosis in *C9orf72* microglia compared to control microglia, and they did not observe an exacerbated reactivity to LPS. On the other side, mutant *PFN1* iPSC-derived microglia exhibit an altered lipid metabolism and deficits in autophagy, which correlated in an inefficient phagocytic degradation. Mutant *PFN1* microglia did not show an exacerbated response to LPS (Funes et al., 2024). Furthermore, mutant *FUS* iPSC-derived microglia did show altered chemoreceptor-activated  $Ca^{+2}$  signalling, but phagocytosis and cytokine release remained unchanged (Kerk et al., 2022). Lastly, sALS microglia exhibited an impairment in phagocytosis, which correlates with the disease progression. Interestingly, those fast-progressing ALS patients had a greater deficit in phagocytosis (Noh et al., 2023; Quek et al., 2022). Additionally, sALS microglia had an altered cytokine profile, an increased DNA damage and inflammasome activity (Quek et al., 2022) and an exaggerated response to stimuli (Noh et al., 2023). Overall, although each study focused on a specific ALS gene or sALS patients, they do observe a cell-autonomous dysfunction in microglial cells, generally affecting the phagocytosing activity and the cytokine production.

### 3.3. Modelling human microglia *in vitro* and *in vivo*

The need of moving to more human-based research, especially in the microglia field, relies in several reasons. First, rodents do not illustrate human genetic complexity, which is particularly important in polygenic diseases, such as ALS (Hasselmann & Blurton-Jones, 2020). Besides, a significant proportion of human genes lack a convincing ortholog in the murine genome (Mancuso et al., 2019). For instance, some studies have shown that more than a half of AD-associated risk genes enriched in microglial cells do not have a clear mouse ortholog in terms of protein homology (Hasselmann & Blurton-Jones, 2020). It is also noteworthy to mention that gene expression can also differ between species. It has been described that even though mouse and human microglial transcriptome overlap considerably, there are notable species-specific differences in human genes regarding complement system, inflammatory cytokines, or neurodegenerative disease-associated genes (AD, PD) (Galatro et al., 2017; Geirsdottir et al., 2019; Gosselin et al., 2017; Lloyd et al., 2022). This divergence is exacerbated by ageing, which is particularly relevant for neurodegenerative diseases occurring in the late life stages (Galatro et al., 2017). Lastly, recent single-cell transcriptomic studies have revealed that human microglia display a much more heterogeneous and complex response to disease rather than mouse counterparts (Geirsdottir et al., 2019; Mancuso et al., 2024; Masuda et al., 2019). Overall, mouse microglia exhibit significant limitations for the study of microglia in human healthy and pathological conditions.

Accessibility to human fresh CNS tissue is limited and, if so, the amount of material obtained is low for research purposes. Human primary microglia sources have been restricted to postmortem samples or surgery biopsies from patients (Hasselmann & Blurton-Jones, 2020). It supposes some limitations, such as the artefacts derived from the postmortem delay, the rapid microglial changes when placed outside the brain or the influence of the underlying pathology (epilepsy, brain tumour, etc) in the microglia phenotype (Bohlen et al., 2017; Butovsky et al., 2014; Gosselin et al., 2017). Moreover, human microglial cell lines derive from primary microglia from embryonic or adult CNS that have been immortalized by viral transduction with oncogenes (Timmerman et al., 2018). However, this transformation may interfere in the microglial phenotype. Indeed, several studies have shown that human microglial cell lines do not proper recapitulate primary

human microglia genetically (Melief et al., 2016). There is therefore notorious limitation when working with human microglia.

***i. Human iPSC-derived microglia***

Since the discovery of the microglial ontogeny in 2010, several groups have designed different protocols to generate microglia-like cells from human iPSCs or embryonic stem cells (ESCs) (Sabogal-Guáqueta et al., 2020) (Table 2). In general, these protocols try to mimic *in vitro* the microglial ontogeny, first generating hematopoietic progenitor cells (HPC) to further mature into microglia-like cells (Hasselmann & Blurton-Jones, 2020; Timmerman et al., 2018). However, there is not still a consensus in the most appropriate method to produce human iPSC-derived microglia. First, the strategies used to produce microglial progenitors (MPs) differ. The most widely used method include the formation of embryoid bodies (EBs) and its differentiation into the mesoderm lineage to further induce haematopoiesis and produce HPC (Brownjohn et al., 2018; Haenseler et al., 2017; Muffat et al., 2016), even though others prefer to generate directly HPC using a monolayer approach (Abud et al., 2017; Douvaras et al., 2017; Pandya et al., 2017; Takata et al., 2017). Another point of divergence is the medium formulations for differentiation and maturation into microglia. While some protocols use different cocktails of cytokines or growth factors, others differentiate and mature microglia by co-culturing with neurons or astrocytes (Table 2), which complicates the standardization and comparison of human iPSC-derived microglia studies. This controversy arises from the fact that what defines microglia identity in the CNS is still unclear. It has been described that interactions with other CNS resident cells (neurons, astrocytes and oligodendrocytes) are key in its maturation, thus culturing iPSC-derived microglia in the absence of other CNS cells may trigger some deficiencies in the microglia generated (Borst et al., 2021). Although the use of the microglial survival factor, IL-34 or CSF1, is generalized among cultures, the other supplementations are still on debate. A recent work from Washer et al., 2022 performed a systematic comparison of all the published microglial protocols in order to identify which growth factors are necessary and which ones are redundant to produce microglial monocultures. They concluded that the cytokines that are beneficial to have a proper microglial specification are IL-34, granulocyte-macrophage colony-stimulating factor (GM-



CSF), macrophage colony stimulating factor (M-CSF) and transforming growth factor beta (TFG $\beta$ ).

PROTOCOL	Duration (days)	HPC production	Microglial Medium
Muffat et al., 2016	75	EB	CSF1 / IL-34
Pandya et al., 2017	30	Direct diff.	GM-CSF / M-CSF / IL-3 + Astrocyte coculture
Abud et al., 2017	38	Direct diff.	Insulin / IL-34 / M-CSF / TFG $\beta$ / CD200 / CX3CL1 + FACS
Haenseler et al., 2017	45	EB	IL-34 / GM-CSF
Douvaras et al., 2017	60	Direct diff.	IL-34 / GM-CSF / M-CSF / FLT-3
Takata et al., 2017	46	Direct diff.	CSF1
Brownjohn et al., 2018	30	EB	IL-34 / GM-CSF / FBS
McQuade et al., 2018	60	Direct diff.	IL-34 / M-CSF / TGF $\beta$ / CX3CL1 / CD200
Konttinen et al., 2019	42	Direct diff.	IL-34 / M-CSF
Claes et al., 2019	38	Direct diff.	IL-34 / M-CSF + FACS
Svoboda et al., 2019	35	Direct diff.	B27 / N2 / Albumax / NaCl / Pyruvate / Glutamax / TGF $\beta$ / IL-34 / CSF1
Guttikonda et al., 2021	30	Direct diff.	IL-34 / M-CSF / FBS
Reich et al., 2021	60	EB	IL-34 / M-CSF / TFG $\beta$
Lanfer et al., 2022	28	Direct diff.	IL-34 / GM-CSF / FBS
Dräger et al., 2022	15	Direct diff.	IL-34 / GM-CSF / M-CSF / TFG $\beta$

**Table 2. Microglial differentiation protocols from human stem cells.** HPC: Hematopoietic progenitor cells; Diff: Differentiation; EB: Embryoid body; CSF1: Colony stimulating factor 1; IL-34: Interleukin 34; GM-CSF: Granulocyte-macrophage colony-stimulating factor; M-CSF: Macrophage colony stimulating factor; TGF $\beta$ : Transforming growth factor beta; CX3CL1: C-X3-C Motif Chemokine Ligand 1; FACS: Fluorescence-activated cell sorting; FLT-3: FMS- like tyrosine kinase 3; NaCl: Sodium chloride; FBS: foetal bovine serum. Modified from María Sabogal-Guáqueta et al., 2020; Washer et al., 2022.

Another innovative method to produce iPSC-derived microglia in a more straight-forward way and in shorter time is the overexpression of key transcription factors, known as forward reprogramming strategy (Csatári et al., 2024). For instance, Chen et al., 2021 were able to generate microglia directly from iPSC in 10 days by overexpression of SFFV pro-viral integration 1 (SPI1) and its cofactor CCAAT/enhancer-binding protein  $\alpha$  (CEBP $\alpha$ ) by viral transfection. Another study from Dräger et al., 2022 obtained iPSC-derived microglia in 8 days from an engineered iPSC line that overexpresses six transcription factors highly expressed in microglia (PU.1, MAF BZIP transcription factor B (MAFB), CEBP $\alpha$ , CCAAT

enhancer binding protein  $\beta$  (CEBP $\beta$ ), interferon regulatory factor 5 (IRF5) and interferon regulatory factor 8 (IRF8)), in a doxycycline-dependent manner.

In parallel, some studies have focused on the generation of microglial-like cells from definitive hematopoietic stem cells, such as CD34<sup>+</sup> cord blood cells (Capotondo et al., 2017; Mathews et al., 2019), or directly from PBMCs obtained from patients (Quek et al., 2022). Although they obtained phenotypically compatible microglia-like cells, the origin source differs from yolk sac-derived primitive progenitors, which may influence the expression of key genes. It may suggest that these cord- or PBMC-derived cells could mimic more closely brain-infiltrating blood monocytes rather than resident microglia (Hasselmann & Blurton-Jones, 2020).

However, microglia are highly sensitive to their environment, thus *in vitro* microglia exhibit significant transcriptomic and proteomic changes compared to *ex vivo* microglia (Gosselin et al., 2017; Lloyd et al., 2022; Mancuso et al., 2019). RNAseq studies from *in vitro* and *ex vivo* human microglia revealed an upregulation of genes related to inflammation and stress responses and a downregulation of pathways related with immune cell function and signalling, among others, when cultured *in vitro* (Gosselin et al., 2017). Importantly, some AD-associated risk genes also changed its expression in *in vitro* conditions (Gosselin et al., 2017). Moreover, *in vitro* human microglia resemble more accurately foetal rather than human adult microglia at the transcriptomic level (Timmerman et al., 2018). Besides, microglia in cell-culture conditions show a basal level of activation, given the proteomic similarities observed between *in vitro* microglia and the DAM microglia phenotype, and lack key receptors in the microglia sensome, such as P2RY12 or CX3CR1, suggesting a limitation in the ability to sense and respond to the environment (Lloyd et al., 2024). This evidences that *in vitro* human microglia do not properly represent the complex microglial biology observed in *in vivo* conditions and brings to light the need of new models to explore microglia in health and disease.

**ii. Xenotransplantation of human microglia in the mouse CNS**

In recent years, chimeric mouse with human microglia have been developed to model more accurately human microglia in the living CNS (Abud et al., 2017; Capotondo et al., 2017; Hasselmann et al., 2019; Mancuso et al., 2019; Svoboda et al., 2019; Xu, Li, et al., 2020; Fattorelli et al., 2021). *Grosso modo*, this innovative approach involves the differentiation of human iPSC to MPs, which are transplanted into neonatal mouse brain. Previously to the administration, endogenous mouse microglia are depleted pharmacologically by a CSF1R inhibitor to ease human microglia survival and colonization across the CNS (Fattorelli et al., 2021) (Figure 5A).

Xenotransplantation of MPs into the neonatal mouse brain results in *in vivo* differentiation of human microglia, which acquire a comparable transcriptome and proteome to human primary microglia. Indeed, xenotransplanted microglia adopt a homeostatic phenotype, restoring the expression of homeostatic microglial markers TMEM119, P2RY12 or CX3CR1 and decreasing DAM-associated markers, which is not observed in *in vitro* conditions (Lloyd et al., 2022; Mancuso et al., 2019). Human xenotransplanted microglia are able to spread widely across the CNS and persist in the long term. It has been shown that xenotransplanted microglia can persist up to 6-month post-transplantation in the mouse brain (Figure 5B) (Xu et al., 2020; Hasselmann et al., 2019; Mancuso et al., 2024). Reported publications describe a human microglia chimerism ranging from 8-9% up to 80%, depending on the study (Fattorelli et al., 2021). However, Fattorelli et al., 2021 described a refined and optimized protocol for *in vitro* and xenotransplantation steps, having 60-80% of human xenotransplanted microglia consistently among several iPSC tested.

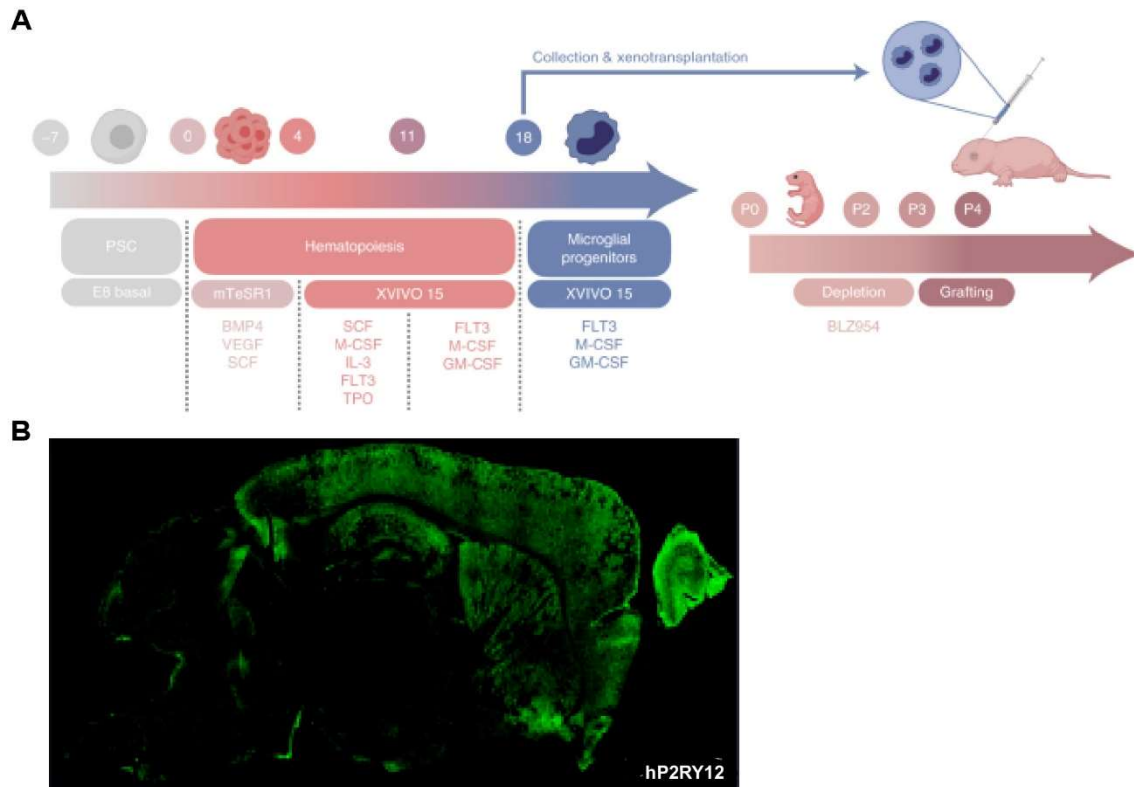


**Figure 5. Human microglia xenotransplantation into the mouse CNS. A)** Schematic diagram illustrating xenotransplantation protocol, which requires a coordinated *in vitro* differentiation into MPs and *in vivo* work. In this protocol, MPs are injected at P4 neonates after pharmacological microglial depletion; **B)** Representative image showing a high proportion of human engrafted microglia (human P2RY12<sup>+</sup>) 6-month post-transplantation. Extracted from Fattorelli et al., 2021.

Human xenotransplanted microglia are functional in the mouse brain, since 2-photon imaging *in vivo* showed how xenotransplanted microglia actively survey the CNS microenvironment by constant expansion and retraction of their ramifications (Hasselmann et al., 2019), and do interact with mouse neuronal cells, as seen with the observation of engulfed synaptic material inside the human microglia (Xu, Li, et al., 2020). Importantly, human xenotransplanted microglia can respond to acute stimuli, such as focal brain injury (Hasselmann et al., 2019), systemic LPS administration (Hasselmann et al., 2019; Svoboda et al., 2019) or A $\beta$  oligomers injection (Mancuso et al., 2019), as well as chronic insults, for instance cuprizone-induced demyelination (Xu, Li, et al., 2020) or insoluble A $\beta$  plaques accumulation (Hasselmann et al., 2019; Mancuso et al., 2024).

This strategy involves the use of immunodeficient mice to avoid rejection of human cells. First published works used MITRG mice, which are recombination activating gene 2 (Rag2)- and interleukin 2 receptor subunit gamma (IL2 $\gamma$ )-

deficient and express the human forms of M-CSF, IL-3, GM-CSF and thrombopoietin (TPO), to perform the development of these humanized mouse models (Abud et al., 2017; Hasselmann et al., 2019). Simplification of this transgenic mouse for this purpose was achieved afterwards, when it was proved that, apart from knocking-out the genes triggering the immunodeficiency status, only the expression of human CSF1 was required to increase differentiation, engraftment, and survival of the human microglia (Hasselmann et al., 2019). This correlates with previous reports demonstrating that mouse CSF1 is not able to activate completely the human CSF1R signalling, indispensable for microglial survival (Rathinam et al., 2011). Therefore, the use of hCSF1<sup>KI</sup> Rag2<sup>-/-</sup> IL2r $\gamma$ <sup>-/-</sup> transgenic mouse is the most widely used transgenic mouse for xenotransplantation purposes in the field (Xu, Li, et al., 2020; Fattorelli et al., 2021).

Although this innovative experimental approach has overcome some of the previously described difficulties in the human microglia modelling, there are some limitations that must be considered. On one hand, xenotransplantation-compatible immunodeficient mice lack the adaptive immune system. Peripheral immune cells, such as T-cells, are described to influence microglial function in neurological diseases (E. Liu et al., 2021; W. Zhao et al., 2013). Thus, these humanized mouse models with human microglia do not recapitulate these interactions and roles in the pathology. In this line, Parajuli et al., 2021 performed xenotransplantation in immunocompetent adult mice using a trans-nasal administration, a less invasive approach than the intracranial normally used, after 1-week CSF1R inhibitor treatment for mouse microglia depletion. They reported that human microglia were able to colonize and persist 2 months after transplantation. On the other hand, even though mouse microglia are depleted by CSF1R inhibitors, they can repopulate and compete with human microglia for the niche, and it is yet unknown whether endogenous mouse microglia may interfere somehow in the human microglia (Hasselmann & Blurton-Jones, 2020). Finally, these chimeric mouse models lack the ability to assess how human xenotransplanted microglia interact with the surrounding human neuronal environment, which is important to understand the pathogenesis in neurological disorders.

Up to the date, in the neurodegenerative diseases field, published studies using this cutting-edge approach to assess human microglia *in vivo* have basically focused on AD. It has been described that human xenotransplanted microglia in an AD mouse model actively interact with A $\beta$  plaques (Abud et al., 2017). Besides, human xenotransplanted microglia is able to respond to an acute injection of oligomeric A $\beta$ , an AD-related challenge, as seen with a significant increase of the cytokine response microglia (CRM) (Mancuso et al., 2019). Comparison of the trajectory analysis of the human microglia response triggered with the mouse counterpart revealed a divergence sequence towards CRM cluster in the human microglia whereas to DAM in the mouse case (Mancuso et al., 2019). Recently, Mancuso et al (2024) described extensively the response of human microglia to A $\beta$  pathology by performing single cell transcriptomic analysis from xenotransplanted microglia in 6-month AD mouse models. They observed a complex and heterogeneous response to A $\beta$  pathology with several microglial clusters: homeostatic (HM), ribosomal response (RM), DAM, IRM, antigen presenting response (HLA), CRM-1, CRM-2, and transitioning CRM (tCRM). Comparison with mouse microglia datasets revealed that DAM and IRM clusters do have similar counterparts in mouse; nevertheless, CRM and HLA clusters are human specific transcriptomic states. Interestingly, they also showed that human microglia display two main co-occurring transcriptional trajectories from HM to CRM, which are linked to soluble A $\beta$ , or HM to DAM to HLA, which are more dependent on A $\beta$  plaques (Mancuso et al., 2024). Overall, this opens a new avenue to explore human microglia response in other neurodegenerative diseases, such as ALS.

#### 4. C9orf72 ALS/FTD

---

As stated before, C9orf72 G4C2 HRE is the most prevalent genetic alteration in ALS and FTD. An arbitrary number of 30 repeats is considered as the threshold to be pathogenic. However, most healthy individuals have less than 10 repeats, whereas ALS/FTD patients have between twenty and thousands of G4C2 repeats (Balendra & Isaacs, 2018). Interestingly, a somatic mosaicism in the HRE length is observed between CNS regions and other tissues within the same individual, due to genetic instability caused by the expansion (Nordin et al., 2014; van Blitterswijk et

al., 2013). Additionally, there is not a clear correlation between the number of repeats and the disease progression (Dols-Icardo et al., 2014; van Blitterswijk et al., 2013).

#### 4.1. C9orf72 gene, protein, and function

C9orf72 architecture is complex, since its gene includes 11 exons, produces 3 alternatively spliced transcripts and 2 protein isoforms (Figure 6). Transcript variant 1 encodes for the short C9orf72 protein (222 amino acids) as it encompasses only non-coding 1a and coding 2<sup>nd</sup>-5<sup>th</sup> exons. On the other hand, mRNA variants 2 and 3 produce the long protein isoform (481 amino acids) since it includes all 11 exons. They differ in the inclusion of non-coding exon 1a (variant 2) or exon 1b (variant 3). The G4C2 HRE of interest is found in an intronic region between non-coding exon 1a and 1b (Figure 6). Given the alternatively spliced mRNA produced, their location within the mRNA and its functional consequences will differ among them. In the transcripts 1 and 3, the repeats are included in the mRNA. When pathogenic, this region is expanded and mRNA acquires secondary structures, such as hairpins or G-quadruplexes, whose relevance will be discussed afterwards. In contrast, in variant 2, the repeats are placed in the promoter region, thus the HRE is not incorporated, but it may affect the transcript expression (Balendra & Isaacs, 2018; Smeyers et al., 2021).

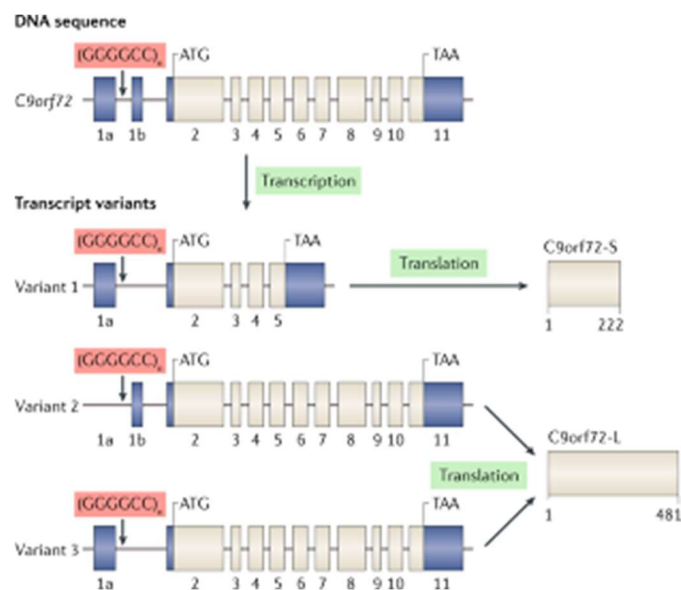


**Figure 6. C9ORF72 gene, transcripts variants and protein isoforms.** *C9orf72* gene includes 11 exons, produces 3 transcript variants and codifies for 2 protein isoforms (short and long). Extracted from Balendra & Isaacs, 2018.

C9orf72 protein is mainly found in the CNS and immune system, and to a lesser extent in other organs, such as lung, heart, liver, kidney, and skeletal muscle. At the cellular level, it is particularly enriched in peripheral myeloid cells (CD14<sup>+</sup> monocytes, eosinophils, and neutrophils) and microglia (Masrori et al., 2023; Rizzu et al., 2016). C9orf72 protein is highly conserved among species, sharing 98% of homology the mouse and human orthologs (Balendra & Isaacs, 2018).

C9orf72 function is still a matter of research, but it seems to be involved in autophagy, endo-lysosomal trafficking and immune response (Beckers et al., 2021; Smeyers et al., 2021). It has been described that a decreased C9orf72 expression leads to a reduction in autophagy and lysosome trafficking and an accumulation of the substrates, such as p62 or TDP-43 (Banerjee et al., 2023; Beckers et al., 2023; Lall et al., 2021; O'rourke et al., 2016; Sellier et al., 2016; Sullivan et al., 2016; Webster et al., 2016). Besides, C9orf72 has been suggested to play an important role in the immune system, since C9orf72 KO mice exhibit an immune system dysregulation (Balendra & Isaacs, 2018; Jiang et al., 2016; O'rourke et al., 2016; Sullivan et al., 2016).

#### **4.2. C9orf72 pathogenesis**

Since the discovery of G4C2 HRE as a genetic cause of ALS/FTD, the scientific community have tried to elucidate the pathogenic mechanisms underlying the disease. Three potential mechanisms have been described: C9orf72 protein loss of function (LOF) or haploinsufficiency; a gain of function (GOF) of the repetitive RNA with the sequestration of RNA-binding proteins (RBPs) into RNA foci; and the formation of DPRs (Figure 7). However, the exact contribution and relevance of each one in ALS/FTD is still unclear.



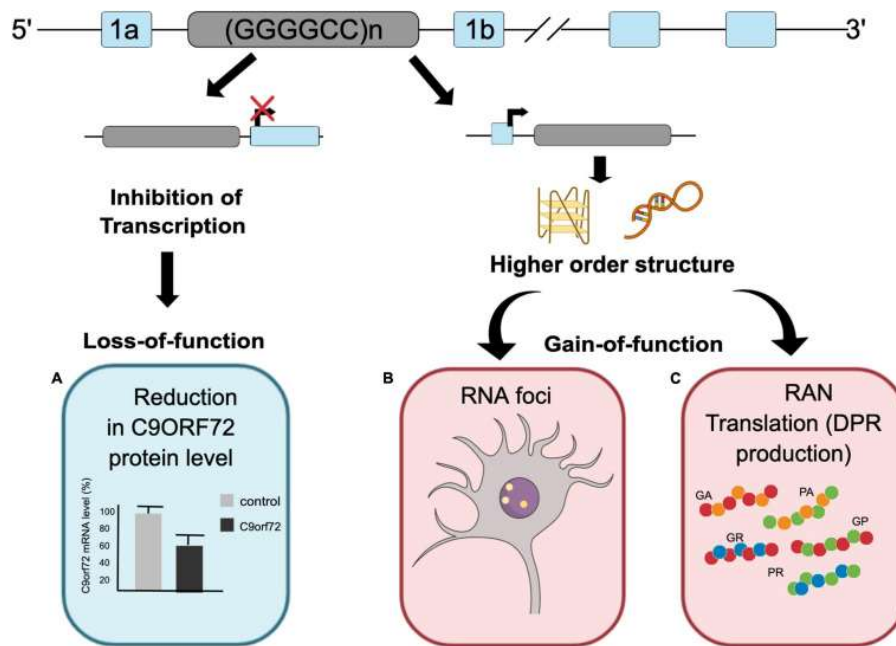


**Figure 7. LOF and GOF C9orf72 pathogenic mechanisms.** RAN: Repeat Associated Non-AUG; DPR: Dipeptide repeat. Extracted from Schmitz et al., 2021.

### i. C9orf72 loss of function

C9orf72 protein haploinsufficiency is due to the presence of the pathogenic G4C2 HRE mutation in the 1<sup>st</sup> intron, which causes an abortive transcription from exon 1a and a decreased promoter activity by epigenetic mechanisms (Balendra & Isaacs, 2018; Smeyers et al., 2021). It has been described that the expanded repeats are able to trigger DNA hypermethylation (Xi et al., 2015) and to bind trimethylated histones (Belzil et al., 2013), which would trigger a decreased transcription. In this sense, reduced *C9ORF72* mRNA and protein is observed in frontal cortex and spinal cord of human C9orf72 ALS/FTD patients (Belzil et al., 2013; DeJesus-Hernandez et al., 2011; Gijssels et al., 2012; Waite et al., 2014; S. Xiao et al., 2015).

To fully understand the pathogenic contribution of LOF mechanisms in ALS/FTD, several animal models have been developed over the last decade. Whereas *Caenorhabditis elegans* and zebrafish C9orf72 LOF models do exhibit locomotion alterations (Ciura et al., 2013; Therrien et al., 2013), no neurological and motor phenotypes are observed in C9orf72-null mouse models. First, Koppers et al (2015) generated a conditional C9orf72-KO mouse lacking C9orf72 expression specifically in neurons. This C9orf72 LOF mouse model did not show MN degeneration, either motor dysfunction or altered survival (Koppers et al., 2015). Additionally, general C9orf72-null mice exhibited a robust immune phenotype,

including splenomegaly, lymphadenopathy, accumulation of enlarged macrophage-like cells, expansion of myeloid and lymphoid cell populations and age-related neuroinflammation (Atanasio et al., 2016; O’rourke et al., 2016). Even, it was described that the severe autoimmunity induced led to a premature mortality compared to wild-type mice (Burberry et al., 2016). At the behavioural level, some studies reported altered social recognition and mild motor deficits (Atanasio et al., 2016; Jiang et al., 2016), or late learning and memory deficits associated with exacerbated synaptic pruning (Lall et al., 2021). It was recently published that ubiquitous C9orf72 knock-down mice, which correlates better with the decreased expression observed in patients rather than a complete loss, had some FTD-like pathological signs, such as depression-like behaviour or social interaction abnormalities, and subtle motor alterations in aged mice (Lopez-Herdoiza et al., 2023). Overall, it suggests that C9orf72 haploinsufficiency by itself is insufficient to trigger MN disease.

## ***ii. C9orf72 gain of function***

Gain of toxicity of the repetitive RNA is another important driver of C9orf72 pathogenesis. On one hand, the G4C2 HRE is bidirectionally transcribed into repetitive RNA, forming sense and antisense RNA foci. This repetitive RNA forms stable secondary structures, such as hairpins and G-quadruplexes, which recruit RBPs. RNA foci are usually found in the neuronal nucleus, being less frequent in glial cells, and are detected widely in the CNS of C9orf72 HRE carriers (frontal and motor cortex, hippocampus, cerebellum, and spinal cord) (Gendron et al., 2014; McEachin et al., 2020). Many of the proteins sequestered in RNA foci are essential for normal RNA processing (e.g. hnRNPA1, hnRNPA3, hnRNPH, nucleolin (NCL), adhesion and degranulation-promoting adapter protein (ADAP), serine/arginine-rich splicing factor (SC35), Pur $\alpha$ ), thus their functional depletion could trigger neuronal toxicity (Barmada, 2015; Gendron et al., 2014).

On the other hand, repetitive RNA can be translated into DPRs through non-canonical repeat associated non-AUG-dependent (RAN) translation. They can be found in the neuronal cytoplasm as soluble oligomers or insoluble aggregates. Five different DPRs are produced: poly-GA (glycine-alanine), poly-GP (glycine-proline), poly-GR (glycine-arginine), poly-PA (proline-alanine) and poly-PR (proline-

arginine). DPR inclusions are observed in different CNS regions, such as hippocampus, frontal cortex, motor cortex, cerebellum, and basal ganglia, and in less frequency in the spinal cord (Freibaum & Taylor, 2017; Schipper et al., 2016; Schmitz et al., 2021).

Although poly-GA is the most abundant DPR, it seems that arginine-enriched DPRs (poly-GR and poly-PR) are the most neurotoxic ones due to their physicochemical properties. Some studies have shown that arginine-enriched DPRs are able to induce neurodegeneration in *Drosophila* models (Mizielinska et al., 2014) and TDP-43 proteinopathy in mice overexpressing poly-GR (Cook et al., 2020). Interestingly, Verdone et al., 2022 developed a knock-in mouse model with widespread expression poly-GR, which had sex-specific chronic ALS/FTD-like phenotypes, including mild MN loss and subtle motor and behavioural alterations. Poly-GR and poly-PR-mediated toxicity seems to be related with inhibition of translation and RNA decay (Moens et al., 2019; Sun et al., 2020) and interfering in the formation of membrane-less organelles, such as nucleolus (Lee et al., 2016). Nevertheless, the exact contribution of DPR pathology in ALS/FTD course remains unclear. It is described that DPR pathology appears early in the disease, before TDP-43 pathology is triggered (Baborie et al., 2015; Vatsavayai et al., 2016). Regarding the correlation between DPRs burden and neurodegeneration, some studies report that poly-GR correlates better with neurodegeneration than other DPRs in disease-related compared to unrelated CNS regions (MacKenzie et al., 2013; Saberi et al., 2018; Sakae et al., 2018). In contrast to it, Davidson et al., 2016 did not observe any correlation in their study, suggesting that probably it is due to methodological issues that underestimates the burden of soluble DPRs in comparison with large insoluble inclusions and the absence of degenerating neurons in postmortem samples.

Over the last years, experimental mouse models that express the C9orf72 HRE mutation have been generated and they exhibit the previously described GOF-related pathological mechanisms (Chew et al., 2015; Jiang et al., 2016; Y. Liu et al., 2016; O'Rourke et al., 2015; Peters et al., 2015) (Table 3). However, they differ considerably in several aspects: (i) transgenesis methodology (bacterial artificial chromosome (BAC) or non-integrative viral vectors); (ii) extent of human *C9ORF72* gene in the transgenic expression cassette; (iii) number of G4C2 repeats; (iv)

spatiotemporal pattern of RNA foci and DPR aggregates; (v) neuropathological features; and (vi) ALS/FTD-related signs. Unfortunately, these models do not exhibit clinical phenotype of the disease, and the only one of them that did show ALS/FTD signs has not been replicated in some laboratories (Y. Liu et al., 2016; Mordes et al., 2020; Nguyen et al., 2020). The absence of a clear ALS/FTD phenotype in these models is likely because the G4C2 HRE introduced in the animals does not localize in the *C9orf72* mouse gene and thus it does not alter the expression and function of the endogenous gene (Shao et al., 2019).

Recently, multiple evidences support that a decrease of *C9orf72* expression is an early contributor to the disease development, which would synergize with GOF mechanisms to produce ALS/FTD phenotype. Reduced *C9orf72* activity triggers neurodegeneration in human iPSC-derived MNs by modulating their vulnerability to degenerative stimuli, such as DPR pathology or glutamate-mediated excitotoxicity (Shi et al., 2018). In a similar way, it was observed in *C9orf72*-null rats which were more susceptible to excitotoxic insults, triggering an ALS-compatible phenotype (Dong et al., 2021). Other *in vivo* studies revealed that *C9orf72* loss increased gain of toxicity, exacerbating motor deficits and behavioural alterations in G4C2 HRE expressing animal models (Shao et al., 2019; Zhu et al., 2020). In conclusion, the current knowledge about *C9orf72* pathogenesis relies on the necessary contribution of both LOF and GOF mechanisms to produce an ALS/FTD phenotype. As it has been described extensively, current murine *C9orf72* models are not useful enough to study new therapies for ALS/FTD. Given that this mutation is the main cause of genetic forms of ALS and FTD, there is an urgent need to generate new murine *C9orf72* models carrying G4C2 HRE that do recapitulate both LOF and GOF pathogenic mechanisms and do exhibit clinical signs of the disease.

Paper	Chew et al (2015)	Peters et al (2015)	O'Rourke et al (2015)	Jiang et al (2016)	Liu et al (2016)	
<b>Transgenesis</b>	AAV2/9	BAC	BAC	BAC	BAC	
<b>C9orf72 gene</b>	Full sequence	Exon 1-6	Full sequence	Exon 1-5	Full sequence	
<b>G4C2 HRE size</b>	66	500/300	100-1000	450	500	
<b>Flanking regions</b>	5': 119 bp 3': 100 bp	5': 141 Kb	5': 110 Kb 3': 20 Kb	5': 140 Kb	5': 52 Kb 3': 19 Kb	
<b>C9orf72 pathology</b>	<b>RNA foci</b>	Yes (6 months)	Yes (3,10,24 months)	Yes (3,6,8 months)	Yes (2, 6 months)	Yes (2 months)
	<b>DPRs</b>	Yes (Poly-GA, -GP, -GR) (6 months)	Yes (Poly-GP) (4, 10, 24 months)	Yes (Poly-GP) (20 months)	Yes (Poly-GA,-GP, -GR) (3, 6, 22 months)	Yes (Poly-GA, -GP) (Acute-progressing mice)
	<b>TDP-43 pathology</b>	Nuclear pTDP-43 inclusions (6 months)	Not detectable	Not detectable	pTDP-43, but not mislocalized or in aggregates (22 months)	Nuclear and cytoplasmic aggregates (Acute-progressing mice)
	<b>Neuronal loss</b>	Yes (Mild) Whole cortex, motor cortex and cerebellar Purkinje cells (6 months)	Not detectable	Not detectable	Yes (Mild): Hippocampus No: SC	Yes: SC, cortex, hippocampus (Acute progression mice)
<b>Motor phenotype</b>	↓ Motor coordination (6 months)	Normal	Normal	Normal	Gait abnormalities, ↓ grip strength (16 weeks) (Acute-progressing mice)	
<b>Behaviour</b>	↑ Anxiety ↑ Hyperactivity ↓ Socialization (6 months)	Normal	Normal	↑ Anxiety ↓ Spatial learning ↓ Working memory (12 months)	↑ Anxiety (12 months)	
<b>Survival</b>	Not analysed	Normal	Not analysed	Not analysed	Decreased	
<b>Others</b>					Acute-progressing mice: 5-7 months Slow-progressing mice: 12-17 months	

**Table 3. Summary of C9orf72 GOF mouse models reported in the literature.** AAV: Adeno-associated viral vector; BAC: Bacterial artificial chromosome; pTDP-43: phosphorylated TDP-43; SC: Spinal cord. Adapted from Batra & Lee, 2017; Balendra & Isaacs, 2018.

## IV. Hypothesis and objectives

---



## Hypothesis

The general objective of the current thesis is to generate and characterize new experimental models for ALS and FTD that will facilitate the understanding of the pathogenic mechanisms of these two neurodegenerative diseases. Our main hypotheses are the following:

1. Our gene editing strategy will allow us the generation of a human ESC line carrying the ALS-causing SOD1<sup>G93A</sup> mutation.
2. The ALS-linked mutant SOD1<sup>G93A</sup> will directly alter key microglial functions in human ESC-derived microglia.
3. Human microglia xenotransplantation into the mouse spinal cord will result in a chimeric, humanized, mouse model with human microglia colonization throughout all the mouse spinal cord.
4. The C9orf72 G4C2 HRE knock-in mouse model will develop a phenotype that mimic ALS and/or FTD.

## Objectives

This PhD thesis has been structured into three chapters according to the following specific aims.

### **Chapter 1. ALS-linked SOD1<sup>G93A</sup> mutation disrupts microglial functions in a cell-autonomous manner in human embryonic stem cell-derived microglia *in vitro*.**

- To generate an isogenic cell line carrying the SOD1<sup>G93A</sup> mutation in human ESC using Clustered Regularly Interspaced Short Palindromic Repeats (CRISPR)/Cas9 technology.
- To establish an *in vitro* differentiation protocol for differentiating human ESC into microglia.
- To assess the impact of the SOD1<sup>G93A</sup> mutation on distinct microglial functions (cytokine production, phagocytosis and cell metabolism) in *in vitro* human ESC-derived microglia.



## **Chapter 2. Xenotransplantation of human microglia into the mouse spinal cord.**

- To establish a protocol of human microglia xenotransplantation into the neonatal Rag2<sup>-/-</sup> IL2r $\gamma$ <sup>-/-</sup> hCSF1<sup>KI</sup> mouse spinal cord.
- To evaluate the extent of the human microglia engraftment throughout the mouse spinal cord over time, with a particular interest in the lumbar spinal cord.

## **Chapter 3. Phenotypic characterization of a novel C9orf72 G4C2 HRE knock-in mouse model**

- To assess whether the C9orf72 G4C2 HRE knock-in mouse model develops ALS-like motor deficits.
- To evaluate whether the C9orf72 G4C2 HRE knock-in mouse model recapitulates FTD-like behavioural deficits.

## V. Material and methods

---



## Chapter 1. ALS-linked SOD1<sup>G93A</sup> mutation disrupts microglial functions in a cell-autonomous manner in ESC-derived microglia *in vitro*

---

### Stem cell maintenance

Human ESC (WA09 also referred to as H9, Lot RB66492, WiCell) were cultured in feeder-free conditions in Matrigel Growth Factor Reduced (GFR) Basement Membrane Matrix (#356230, Corning)-coated 6-well plates in mTeSR1 medium (#85850, StemCell Technologies) with 100 U/mL Penicillin-Streptomycin (#15140-122, Gibco). Medium was changed daily. ESC cells passing was performed weekly using Versene (#15040-066, Gibco). ESC were maintained in a 5% CO<sub>2</sub> incubator (Heraeus HERAcell 150) at 37°C.

To cryopreserve ESC, cells were washed with Dulbecco's Phosphate-buffered saline (dPBS) (#14190-144, Gibco), detached with Versene and resuspended in CryoStor CS10 freezing medium (#07959, StemCell Technologies). Cryovials were kept in Mr Frosty freezing recipient (#5100-0036, ThermoFisher) at -80°C overnight and then transferred to a nitrogen tank the following day.

### CRISPR/Cas9 genome editing

CRISPR/Cas9 strategy design was performed by Sigma-Aldrich CRISPR Design customer service in collaboration with Transgenic Animal Unit (UAT, CBATEG-UAB). CRISPR reagents were delivered into ESC by electroporation using a Super Electroporator NEPA21 Type II (Nepagene) according to manufacturer's protocol. Briefly, ESC were pre-treated with 10 μM Y-27632 ROCK inhibitor (ROCKi) (#Y0503, Sigma-Aldrich) to ease survival before dissociating in a single cell suspension with TrypLE Select Enzyme (#12563-011, Gibco) for 3-5 min at 37°C, which was inactivated by diluting 10 times with dPBS. Cells were then washed twice with Opti-MEM medium (#11058-021, Gibco) to remove any residual medium from stem cell culture. 10<sup>6</sup> cells were transfected with 1.6 μM sgRNA (5'-GAATCTTCAATAGACACAT-3'; custom-made, Sigma-Aldrich), 0.8 μM Cas9 ribonucleoprotein (RNP) (#C120010, Sigma-Aldrich) and 5 μg single-stranded oligodonor (ssODN) (5'-ATGCTTTTTTCATTATTAGGCATGTTGGAGACTTGGGCAATGTGACTGCTGACAAAGATGCTGTGGCTGATGTGTCTATTGAAGATTCTGTGATCTCACTCTCAGGAGACCATTGCAT

CAT-3'; custom-made, Sigma-Aldrich) in a total volume of 100  $\mu$ L. Electroporation conditions are summarized in Table 4. After electroporation, ESC were seeded at a low density of 100,000 cells/well from 6-well plate in mTeSR1 medium containing 10  $\mu$ M ROCKi for 24h. The following day, a full medium change was performed to remove ROCKi. Three or four days later, individual colonies were picked up manually and plated in a Matrigel-coated 96-well plate. When clones showed optimal size, they were duplicated to obtain DNA for genotyping and to cryopreserve as a backup.

	Voltage	Length	Interval	Number	Decay Rate	Polarity
<b>Poring pulse</b>	135 V	2.5 ms	50 ms	2	10 %	+
<b>Transfer pulse</b>	20 V	50 ms	50 ms	5	40 %	+/-

**Table 4.** Electroporation conditions for ESC (WA09) CRISPR/Cas9 gene editing.

### Potential off-target sites analysis

Potential off-target arisen from CRISPR/Cas9 technology were predicted *in silico* by COSMID bioinformatics-based tool (Cradick et al., 2014). Relevant parameters introduced in the search were: *Homo sapiens* GRCh38 (hg38) (target genome); 5'-GAATCTTCAATAGACACAT-3' (sgRNA); NGG (Protospacer adjacent motif (PAM) suffix); and  $\leq 3$  mismatches, 1-base deletion and/or 1-base insertion allowed. According to the score, top 10 off-target sites (OT1-OT10) were selected for further analysis.

### Genotyping

DNA was extracted using Genomic DNA Kit (#0603, DANAGEN) following manufacturer's protocol. ESC were detached by TrypLE Select (#12563-011, Gibco) dissociation and then, digested with lysis buffer for 15 min at 55°C. Proteins were eliminated using protein precipitation buffer and DNA was precipitated with 2-propanol (#131090, Panreac) and further washed with 70% ethanol. Finally, DNA pellets were dried at room temperature for approximately 30 min and then solubilized with DNA hydration solution for 1h at 65°C. DNA concentration was quantified using a NanoDrop 2000 spectrophotometer (ThermoFisher).

To screen positive clones for SOD1<sup>G93A</sup> knock-in, the region flanking the SNP of interest in *SOD1* gene was amplified by PCR using Taq DNA polymerase (#10342-020, Invitrogen). Primers and cycle conditions are specified in Table 5. The PCR

product was digested by BclI (#R0508L, New England Biolabs) or EaeI (#R0704S, New England Biolabs) restriction enzymes (10U) for 1h at 37°C and then BclI and EaeI were inactivated at 65°C for 20 min and 10 min, respectively. Expected bands in non-edited and edited clones were predicted using the *Restriction analyser* tool from *Molecular Biology tools* (*Molbiotools*) (<https://molbiotools.com/restrictionanalyzer.php>) (Table 6). Finally, resulting digestions, together with a 100bp DNA ladder (#G210A, Promega) were analysed by standard electrophoresis in a 4% agarose gel and imaged in a ChemiDoc MP Imaging System (BioRad).

Gene	Fw/Rv	Sequence (5'→3')	PCR Product	PCR Conditions
SOD1	Fw	CATCAGCCCTAATCCATCTGA	236 bp	95°C for 3 min, 35x (95°C for 15s, 60°C for 30s, 72°C for 45s) and 72°C for 2 min
	Rv	CGCGACTAACAATCAAAGTGA		
OT 1	Fw	CCAGGCACTGTGTAAGCCTTTACC	276 bp	
	Rv	AGCTTGCCTGACCTTCGCCT		
OT 3	Fw	CCACGTCCATCAGTTTGGAGC	285 bp	
	Rv	CCGCAAGCTAAATGACTTCCAGTG		
OT 5	Fw	CAAGCTCAGTGGATTTTCTGGACG	314 bp	
	Rv	CAGAATTGGTAGAGAGAAGGGGAG		
OT 8	Fw	GGACCATTTATATCCACATACGAAACAACAG AG	292 bp	
	Rv	CCATTAGATGGCTAGATCGTGGAG		
OT 9	Fw	ACCCTGAAATACTGTTTCATATAGGAACGCC	275 bp	
	Rv	TCATGTAACTGGACTCAGGAGCC		
OT 10	Fw	ATGCAAGGTCATTTCAACTGCAAAACAGAGG	310 bp	
	Rv	GTGACTAAGGTACCTCAGTGAATTAGAACTC		
OT 2	Fw	GGGTTTTGTGTAGACTTGTACCACTCAG	326 bp	
	Rv	CTGGACCAGAGCTAGTCAACAGA		
OT 4	Fw	CCCAGAGACTCAAGGACCTTTTC	325 bp	
	Rv	GAGGTGGGATGAGGGAAGTC		
OT 6	Fw	AAACCATTCTTAATTCTACTCTCGAAAGAAA ACCAGC	307 bp	
	Rv	CATTGGAGCAGAACAGAGAGGTAG		
OT 7	Fw	GTTGAGTCCTTTAAAAGTGGTTATGAAATCTC TGG	294 bp	
	Rv	CATAGTTAGATTAAGTGGGTCTTATGTCCAA GAG		

**Table 5.** Primer sequences and PCR conditions. OT: Off-target; Fw: Forward; Rv: Reserve; bp: base pair.

To confirm the absence of any undesired genetic modification in SOD1 locus and potential off-target sites, specific PCR products were analysed by Sanger sequencing in Servei de Genòmica (UAB). Primers and PCR conditions for each locus are specified in Table 5. Forward and reverse sequences for each gene were analysed using Geneious Prime software.

	<b>BclI</b>	<b>EaeI</b>
<b>Sequence recognition</b>	5'...CCATC(N) <sub>4</sub> ↓...3' 3'...GGTAG(N) <sub>5</sub> ↑...5'	5'...Y <sup>4</sup> GGCCR...3' 3'...RCCGG <sub>r</sub> R...5'
<b>No gene edition</b>	166 bp	95 bp
	48 bp	83 bp
	22 bp	58 bp
<b>Gene edition</b>	214 bp	141 bp
	22 bp	95 bp

**Table 6.** Expected bands in non-edited and edited clones after BclI or EaeI digestion.

### Directed differentiation of human ESC into microglia

Human control and SOD1<sup>G93A</sup> ESC were differentiated into microglia based on previously published protocols from (Douvaras et al., 2017; Fattorelli et al., 2021; Haenseler et al., 2017) with few modifications. At ~75% confluency, ESCs were dissociated into single cell suspension using TrypLE Select (#12563-011, Gibco) and plated into AggreWell™ 800 24-well plate (#34811, StemCell Technologies) at a density of 4·10<sup>6</sup> cells/well in mTeSR1 medium (#85850, StemCell Technologies) with 10 μM Y-27632 ROCKi (#Y0503, Sigma-Aldrich), 50 ng/mL BMP-4 (#120-05, PeproTech), 50 ng/mL VEGF (#100-20, PeproTech) and 20 ng/mL SCF (#300-07, PeproTech). After seeding, the plate was centrifuged at 100g for 3 min to ensure a proper cell distribution among the microwells. During the following 3 days, 75% medium change was performed daily with the same medium (mTeSR1 medium with BMP-4, VEGF and SCF) without ROCKi. On day 4, embryoid bodies were harvested and transferred to a reversible 37 μm cell strainer (#27250, StemCell Technologies). Approximately 20 EBs per well were plated in 6-well plates in X-VIVO 15 medium (#BE02-060F, Lonza) supplemented with 1 mM Glutamax (#35050-038, ThermoFisher), 100 U/mL Penicillin-Streptomycin (#15140-122, Gibco), 50 μM 2-mercaptoethanol (#31350-010, ThermoFisher), 50 ng/mL SCF (#300-07, PeproTech), 50 ng/mL M-CSF (#300-25, PeproTech), 50 ng/mL IL-3 (#200-03, PeproTech), 50 ng/mL FLT3 (#300-19, PeproTech) and 5 ng/mL TPO (#300-18, PeproTech). EBs were cultured with the previous medium for 7 days, followed by a

complete medium change on day 8. On day 11, differentiation medium was replaced with X-VIVO 15 medium (#BE02-060F, Lonza) with 1 mM Glutamax (#35050-038, ThermoFisher), 100 U/mL Penicillin-Streptomycin (#15140-122, Gibco), 50  $\mu$ M 2-mercaptoethanol (#31350-010, ThermoFisher), 50 ng/mL FLT3 (#300-19, PeproTech), 50 ng/mL M-CSF (#300-25, PeproTech) and 25 ng/mL GM-CSF (#300-03, PeproTech). On day 18 onwards, human MPs accumulated in the supernatant were collected weekly to differentiate into microglia. MPs were plated in different plate formats and density depending on the assay (specified in following sections) in microglia differentiation medium, formed by advanced Dulbecco's Modified Eagle Medium/Ham's F-12 (DMEM/F12) medium (#12634-010, Gibco) supplemented with 1 mM Glutamax (#35050-038, ThermoFisher), 50 U/mL Penicillin-Streptomycin (#15140-122, Gibco), 50  $\mu$ M 2-mercaptoethanol (#31350-010, ThermoFisher), 100 ng/mL IL-34 (#200-34, Peprotech) and 10 ng/mL GM-CSF (#300-03, PeproTech). 50% of the medium was changed 3 times per week for 2 weeks, being used for functional assays at day 12-14. During all the process, pictures were taken using an Olympus CSK1 inverted microscope.

### **Fluorescence activated cell sorting (FACS)**

At day 14<sup>th</sup> of differentiation, microglia were detached by incubation of trypsin (T4674, Sigma-Aldrich), diluted at 0.25% in Hank's Balanced Salt Solution (HBSS) without Ca<sup>2+</sup> and Mg<sup>2+</sup> buffer (#14170-088, Gibco), at 37°C for 7 minutes. To stop the trypsin reaction, DMEM medium containing 10% heat-inactivated FBS (#A5256701, Gibco) was added and by pipetting gently, cells were harvested in 1.5 mL microcentrifuge tubes. Cells were centrifuged at 900g for 10 min at 4°C. Primary antibodies (1:300; CD45-PerCP (#GTX79950, GeneTex), CD11b-PE/Cy7 (#101216, BioLegend), P2RY12 (#GTX16888, GeneTex) were diluted in DEMEM-10% FBS and incubated for 1h at 4°C in soft agitation. For P2RY12 staining, the secondary antibody Alexa Fluor 647 (1:500; #ab150075, Invitrogen) was incubated for 45 min at room temperature in agitation. Cells were finally washed with DMEM-10% FBS, centrifuged at 900g for 6 min at 4°C and fixed with 2% paraformaldehyde (PFA). Unstained samples, single stainings and isotype-matched control samples were used to determine nonspecific binding and autofluorescence. Samples were processed on



a FACS Canto Flow Cytometer (BD Bioscience) or CytoFLEX (Beckman Coulter) and all data were processed using FlowJo® software V.10.

### **Immunofluorescence**

Microglial cells, cultured on 12 mm-glass coverslips at a density of 50,000/well in 24-well plate, were fixed with 4% PFA for 15 min at room temperature at 14<sup>th</sup> day of differentiation and kept with dPBS at 4°C until needed. Cells were washed twice with phosphate buffer saline (PBS), PBS with 0.1M Glycine (#G8898, Sigma-Aldrich), PBS 0.1% Tween (P1379, Sigma-Aldrich) and PBS 0.1% Triton X-100 (#X-100, Sigma-Aldrich). Each wash was performed for 5 min. Cells were incubated with the blocking solution (PBS containing 0.1% Triton X-100 and 5% donkey serum (#S30-100ML, Sigma-Aldrich) for 30 min at room temperature in continuous agitation. Primary antibodies anti-Iba1 (1:400; #019-19714, Wako Chemicals) and anti-P2RY12 (1:200; #GTX16888, GeneTex) were diluted with PBS 0.1% Triton X-100 and incubated overnight at 4°C in agitation. The following day, cells were washed with PBS 0.1% Triton X-100 and incubated with the corresponding secondary antibodies (anti-rabbit Alexa Fluor 488 (1:200; #A-21206, Invitrogen); anti-rabbit Alexa Fluor 594 (1:200; #A-21207, Invitrogen) which were diluted in PBS 0.1% Triton X-100 supplemented with 1.5% donkey serum for 1h at room temperature. Finally, coverslips were dehydrated with series of graded ethanol and mounted in DPX mounting medium (#44581, Sigma-Aldrich). Representative images were captured using an Olympus BX51 microscope attached to Olympus DP73 Camera.

### **Luminex (bead-based multiplex assay)**

Conditioned medium from SOD1<sup>G93A</sup> and control microglia, which were plated in 96-well plates at a density of 25,000 cells/well (n=3-4), was collected in basal conditions and after 6h, 14h and 24h of 10 ng/mL LPS (#L2880, Sigma-Aldrich) stimulation. IL-1 $\beta$ , IL-10 and IL-17A concentration was measured using ProcartaPlex™ Human Essential Panel 2, 4 plex (#EPX040-10008-901, ThermoFisher) Multiplex Immunoassay, following its specific commercial protocol on a MAGPIX Luminex Analyzer (ThermoFisher).

### Isolation of myelin debris and conjugation to pHrodo

Microglial phagocytosis was assessed by pHrodo-conjugated myelin internalization, prepared as described in Gómez-López et al., 2021. Myelin debris were extracted from wild-type C57BL6/J 4-month female mice, which were euthanised with an overdose of pentobarbital sodium (Dolethal) (#07400060, Vetoquinol, >200mg/kg) and perfused transcardially with saline (0.9% NaCl). Each brain hemisphere was first cut in small pieces and then digested enzymatically with dPBS containing 0.1% collagenase (#C-2674, Sigma-Aldrich) and 0.1% DNase I (#11284932001, Roche) for 30 min at 37°C (Amo-Aparicio et al., 2018). Brains were diluted with dPBS (#14190-144, Gibco), 7 mM ethylenediaminetetraacetic acid (EDTA) (#E5134, Sigma-Aldrich) and 2% heat-inactivated FBS (#A5256701, Gibco) and passed through a 70µm filter mesh (#141379C, ClearLine). Myelin debris were obtained after 70%/30% Percoll gradient, prepared by diluting Stock Isotonic Percoll (SIP) (#P1644, Sigma-Aldrich) in dPBS. Percoll gradient containing the cell suspension was centrifuged at 18°C at 500g for 30 min and myelin debris were collected with a Pasteur pipette and quantified by BCA™ protein Assay kit (#23250, ThermoFisher) according to manufacturers' protocol. Myelin debris were conjugated with pHrodo Green STP Ester (#P35369, ThermoFisher). Briefly, 0.277 mg myelin debris were diluted with dPBS (pH=8) up to a volume of 225 µL, which was incubated with 25 µL pHrodo (8.9 mM) for 45 min at room temperature protected from light in agitation. Then, it was resuspended with dPBS (pH=7) having a final concentration of 0.3 mg/mL.

### Phagocytosis assay

Control and SOD1<sup>G93A</sup> MPs were plated in 96-well plate at a density of 25,000 cells/well for 14 days (n=4). Six replicates were plated per differentiation (three for basal conditions and three for LPS stimulation). In treated microglia, LPS (10 ng/mL) (#L2880, Sigma-Aldrich) was added to the medium for 24h before adding myelin. 1 µg of pHrodo-myelin was added for 30 min, 3h and 24h in fresh medium to eliminate LPS. Finally, cells were collected for flow cytometry analysis as described before. Microglia population was defined by CD45<sup>+</sup> CD11b<sup>+</sup> cells and, within it, the proportion of positive cells for pHrodo signal and the geometric mean

fluorescence intensity (geoMFI), as a measure of the quantity of myelin phagocytosed by phagocytic microglia, were calculated.

### **Cell metabolism assay**

Mitochondrial respiration was evaluated using the Seahorse XF Cell Mito Stress Test Kit (Agilent) in a Seahorse XFe96 analyser (Agilent). Independent microglial differentiations (n=3-4) were carried out in parallel. 20,000 MPs were seeded per well in a Seahorse XF96 cell culture microplate (#103794-100, Agilent) for 14 days of differentiation. Ten replicates were plated per differentiation (five for basal conditions and five for LPS stimulation). 24 hours prior to the experiment, five replicates were stimulated with LPS (10 ng/mL). On the day of experiment itself, microglial cells were incubated in Seahorse XF DMEM medium (#103575-100, Agilent) supplemented with 10 mM Glucose (#103577-100, Agilent), 1 mM Pyruvate (#103578-100, Agilent) and 2 mM L-Glutamine (#103579-100, Agilent) for 1 hour in a non-CO<sub>2</sub> incubator at 37°C. Oxygen consumption rate (OCR) and extracellular acidification rate (ECAR) were monitored three times in basal conditions and in response to the sequential injection of 2 µM Oligomycin, 1 µM carbonyl cyanide-4-(trifluoromethoxy)-phenylhydrazone (FCCP) and 0.5 µM rotenone/antimycin A (Rot/AA), according to the assay manual. Data was analysed using Wave software. For normalization, Hoescht staining (2 µM) was performed to label nuclei. Nine images per well covering 40% of the central area were taken with a Zeiss Axio Observer Z1 equipped with Apotome inverted fluorescent microscope, then mosaic of the well images was made using ZenBlue software and nuclei were quantified with Fiji software.

### **Measurement of ROS levels**

Control and SOD1<sup>G93A</sup> MPs were seeded at 25,000 cells/well on 12 mm glass coverslips for 14 days. Each biological replicate (n=4) included two technical replicates. Cells were washed with dPBS and incubated for 20 min in HBSS medium (#14170-088, Gibco) supplemented with 200 nM MitoTracker™ Deep Red FM (#M46753, ThermoFisher) and 3 µM MitoSOX™ Red (#M36008, ThermoFisher). Then, cells were washed with dPBS, fixed with 4% PFA in 0.1M phosphate buffer (PB) for 15 min at room temperature. Finally, cells were mounted with DAPI-Fluoromount G mounting medium (#0100-20, Southern Biotech). Five random

images per technical replicate were acquired with a digital camera Nikon DS-Ri2 attached to a Nikon Eclipse Ni-E microscope. Fluorescence intensity and area of MitoSOX and Mitotracker stainings were analysed using Image J software. Normalization of results was performed by DAPI nuclei counting.

### **Statistical analysis**

Statistical analysis and graphical representations were performed using GraphPad Prism version 9.0.0 (GraphPad Software). The normality of data distribution was assessed using Shapiro-Wilk test. Specific statistical tests for each analysis are specified in the results section. All data are shown as mean  $\pm$  standard error of the mean (SEM). Statistically significant was considered at  $p < 0.05$ .

## Chapter 2. Xenotransplantation of human microglia into the mouse spinal cord

---

### **Ethical statement**

All experimental procedures were performed under the approval from the Animal Experimentation Ethics and Biosafety Committees of the Universitat Autònoma de Barcelona (CEEAH 6500 and HR-725-23) and followed the European Communities Council Directive 2010/63/EU and the Spanish regulations for the use of laboratory animals (RD 53/2013) and biosafety (RD 664-97, RD 178/04).

### **Animals**

Rag2<sup>-/-</sup> IL2r $\gamma$ <sup>-/-</sup> hCSF1<sup>KI</sup> mice (strain #017708) were purchased from The Jackson Laboratory and bred and maintained in the animal facilities from Universitat Autònoma de Barcelona. Mice were housed in microisolator cages under a controlled environment (22  $\pm$  2°C, 12h light/dark cycle) with food and water *ad libitum*.

Eight-week-old females were used for mating in trios to generate pups for cell transplantation. Coordination between mice mating and the *in vitro* differentiation of human MPs from ESC (WA09) was required to ensure that postnatal day 4 (P4) mice coincide with the 18<sup>th</sup> day of the *in vitro* microglia differentiation protocol for successful cell transplantation. To assess the likelihood of pregnancy, vaginal plugs were checked the morning after mating.

### **Mouse microglia depletion**

Endogenous mouse microglia were depleted pharmacologically by administering the CSF1R inhibitor, Sotuletinib (BLZ945) (#S7725, Selleck Chem), prepared with 20% (2-hydroxypropyl)- $\beta$ -cyclodextrin (#H0979, TCI Chemicals). Rag2<sup>-/-</sup> IL2r $\gamma$ <sup>-/-</sup> hCSF1<sup>KI</sup> pups were administered intraperitoneally at 48 hours (P2 day) and 24 hours (P3 day) before cell transplantation, at a dose of 200 mg/kg, using an insulin syringe (29G, 0,33x12mm needle; #N14107, ICO Plus3).

### **Human MPs generation**

*In vitro* human ESC (WA09, Lot RB66492, WiCell) differentiation to MPs were performed as described in Chapter 1. At the day 18<sup>th</sup>, MPs accumulated in the

supernatant were collected and resuspended in dPBS (#14190-144, Gibco) at a concentration of 50,000 cells/ $\mu$ L.

### **Human microglia transplantation**

The xenotransplantation protocol was adapted from Ayers et al., 2015; Fattorelli et al., 2021. In brief, human MPs were resuspended in dPBS at a concentration of 50,000 MPs/ $\mu$ L. P4 pups were anesthetized by hypothermia induced by ice immersion, and then an injection of the cell suspension (1 $\mu$ L/spinal cord) was performed into the spinal cord, at the level of the hips, using a 10  $\mu$ L-Hamilton syringe (#7635-01; Hamilton Co.) coupled to a 26G needle (#7804-03; Hamilton Co.). More details about the intraspinal (IS) injection will be described in the results section. As a proof of concept of the injection, fast green (#F7258, Sigma-Aldrich) diluted in dPBS was used. Afterwards, mice were placed on a heating pad at 37 °C to recover before being returned to their cage.

### **Histological analysis**

Animals were euthanized with an overdose of pentobarbital sodium (Dolethal) (#07400060, Vetoquinol, >200mg/kg) at different timepoints after the cell transplantation (5 days, 1 month, 2 months, 5 months and 10 months) and perfused transcardially with cold 4% PFA in PBS for approximately 15 min. Spinal cords were harvested, post-fixed in cold 4% PFA in PBS for 1h and embedded in 30% sucrose (#A2211, PanReac AppliChem) solution in PB, with 0.05% sodium azide, for cryopreservation.

Tissues were embedded in O.C.T. Compound (#4583, Tissue-Tek) and quickly frozen on a plate in contact with nitrogen liquid. Spinal cords were cut longitudinally (P9) or transversally at a thickness of 20  $\mu$ m using a cryostat (Leica). Slides were stored at -20°C until needed.

For immunofluorescence staining, spinal cord sections were first washed with PBS and then permeabilized with PBS 0.3% Triton X-100 (#X-100, Sigma-Aldrich) (10 min/wash). Slides were incubated with the blocking solution, containing 10% normal donkey serum (#S30-100ML, Sigma-Aldrich) for 1h at room temperature. Then, primary antibodies were incubated overnight at 4°C diluted with the blocking solution. The primary antibodies used were anti-Iba1 (1:400;

#019-19714, Wako Chemicals), anti-human P2RY12 (1:1000; #HPA014518, Merck) and anti-human CD45 (1:200; 368502, Biolegend). The following day, sections were washed with PBS 0.3% Triton X-100 and the corresponding secondary antibodies were incubated for 2h at room temperature. The secondary antibodies used were, respectively, anti-rabbit Alexa Fluor 488 (1:200; #A-21206, Invitrogen); anti-rabbit Alexa Fluor 594 (1:200; #A21207, Invitrogen); anti-mouse Alexa Fluor 647 (1:200; #A31571, Invitrogen) or anti-mouse Alexa Fluor 594 (1:200; #A21203, Invitrogen). Finally, sections were washed with PBS 0.3% Triton X-100, PBS and PB, and mounted in DAPI-Fluoromount G medium (#0100-20, Southern Biotech).

Representative pictures of human microglia engraftment were taken in BX51 Olympus microscope equipped to a DP50 digital camera at 10X magnification. For the quantification of the human microglia chimerism across the spinal cord at 2, 5 and 10 months of age, images were taken with a digital camera Nikon DS-Ri2 attached to a Nikon Eclipse Ni-E microscope. For each spinal cord section, six pictures were taken at 40X magnification, capturing the dorsal horn, ventral horn and white matter surrounding the ventral horn, from both hemi-spinal cords. Quantification of the percentage of human microglia in the distinct areas of the spinal cord were performed using Image J software, by analysing the proportion of Iba1<sup>+</sup> cells expressing also human CD45 in a region of interest of 84,240  $\mu\text{m}^2$ . The average of 3 spinal cord sections was calculated per animal.

### **Statistical analysis**

GraphPad Prism version 9.0.0 (GraphPad Software) was used to perform data representation and statistical analysis. Data was expressed as mean  $\pm$  SEM. To analyse the chimerism of human microglia in the spinal cord over the months, data normality was checked using Shapiro-Wilk test and then, Kruskal-Wallis test with Dunn's multiple comparisons was performed. Differences were considered significant at  $p < 0.05$ .

## Chapter 3. Phenotypic characterization of a novel C9orf72 G4C2 HRE knock-in mouse model

---

### **Ethical statement**

All experimental procedures were approved by the Universitat Autònoma de Barcelona Animal Experimentation Ethical Committee (CEEAH 6500) and followed the European Communities Council Directive 2010/63/EU and the Spanish regulations for the use of laboratory animals (RD 53/2013).

### **Animals**

Mice were housed in a controlled environment ( $22 \pm 2^{\circ}\text{C}$ , 12h light/dark cycle) in conventional open cages with food and water *ad libitum*, in the Universitat Autònoma de Barcelona animal facilities.

Mice carrying 30 repeats of G4C2 HRE in the first intron of the C9orf72 gene (C9orf72 HRE knock-in or C9) were generated in the Transgenic Animal Unit (UAT, CBATEG-UAB). The G4C2 HRE is preceded by a STOP region flanked by two loxP sites. Briefly, a gene targeting approach was employed using u129/Sv ESCs to introduce the desired mutation. Recombinant clones were then injected into blastocytes of C57BL/6J01aHsd, which were subsequently transferred to recipient females. Chimeric mice were crossed with wild-type C57BL/6J mice to determine germ line transmission and C9orf72 HRE knock-in animals were selected in the descendancy and confirmed by genotyping.

Both heterozygous and homozygous C9orf72 HRE knock-in animals were generated. These animals were crossed with CAGGCre-ER<sup>TM</sup> mice (#004682, Jackson Labs), a strain which has a tamoxifen-inducible cre recombinase driven by ubiquitous chicken beta actin promoter/enhancer coupled with the cytomegalovirus (CMV) enhancer. When bred, Cre-mediated recombination results in the deletion of the floxed stop region. CAGGCre-ER<sup>TM</sup> mice were bred as heterozygous, since homozygous mice are not viable or fertile.

### **Body weight and survival analysis**

Body weight of all animals was monitored monthly using a standard scale. For the survival study, animals were followed up for two years. The human endpoint



for animal euthanasia included a weight loss of more than 20%, apathy to human manipulation or veterinarian criteria (e.g. idiopathic ulcerative dermatitis or tumour development).

### Genotyping

DNA was extracted from mouse tails using Genomic DNA Mouse Tail Kit (#0603, DANAGEN) following manufacturer's protocol. Briefly, tissue was digested with lysis buffer overnight at 55°C. The following day, proteins were eliminated using protein precipitation buffer and DNA precipitation was performed with 2-propanol (#131090, Panreac). After washing with 70% ethanol, DNA pellets were dried at room temperature for approximately 30 min and then solubilized with DNA hydration solution for 1h at 65°C. DNA concentration was quantified using a NanoDrop 2000 spectrophotometer (ThermoFisher). For further assays, DNA was diluted at 50 ng/μL with RNase-free water (#AM9915G, Invitrogen).

*CreER* and *Neo* genotyping was performed by PCR reaction using DreamTaq DNA polymerase (#EP0703, ThermoFisher) using the primers and cycle conditions listed in Table 7. Heterozygous and homozygous *C9orf72* animals were determined by qPCR using iTaq Universal SYBR Green Supermix (#1725124, Bio-Rad) in a CFX384 Touch CFX384 Touch Real-Time PCR Detection System (Bio-Rad). Relative expression of *Neo* versus the housekeeping gene *Gapdh* was performed (Table 7) using the  $2^{-\Delta\Delta Ct}$  method. Wild-type and heterozygous animals were used as controls and homozygous animals were considered when fold change (vs heterozygous)  $\geq 2$ .

Gene	Fw/Rv	Sequence (5'→3')	PCR Product	PCR Conditions
<b>Conventional PCR</b>				
<b><i>CreER</i></b>	Fw	GCTAACCATGTTTCATGCCTTC	180 pb	94°C for 2 min, 11x (94°C for 20s, 65°C for 15s (-0.5°C per cycle decrease), 68°C for 15s), 28x (94°C for 15s, 60°C for 15s and 72°C for 10s) and 72°C for 2 min
	Rv	AGGCAAATTTTGGTGTACGG		
<b>Internal control (CreER)</b>	Fw	CAAATGTTGCTTGTCTGGTG	200 pb	
	Rv	GTCAGTCGAGTGCACAGTTT		
<b><i>Neo</i></b>	Fw	CTTGGGTGGAGAGGCTATTC	280 pb	
	Rv	AGGTGAGATGACAGGAGATC		
<b><i>Trpv1</i></b>	Fw	TTCAGGGAGAACTGGAAGAA	490 pb	
	Rv	TAGTCCCAGCCATCCAAAAG		

(Table continues in the next page)

Gene	Fw/Rv	Sequence (5'→3')	PCR product	PCR conditions
<b>qPCR</b>				
<i>Neo</i>	Fw	CTTGGGTGGAGAGGCTATTC		95°C for 3 min, 40x (95°C for 10s, 60°C for 30s)
	Rv	AGGTGAGATGACAGGAGATC		
<i>Gapdh</i>	Fw	TCAACAGCAACTCCCCTCTTCCA		
	Rv	ACCCTGTTGCTGTAGCCGTATTCA		

**Table 7.** Primer sequences and PCR conditions. Fw: Forward; Rv: Reverse; bp: base pair.

### Tamoxifen induction

CreER tamoxifen-mediated induction was performed as described in Sanchis et al., 2020 to 8 weeks old animals for 11 consecutive days. CreER<sup>+/-</sup> animals, but also CreER<sup>-/-</sup> littermates, were administered to control tamoxifen effects in the model. Tamoxifen (#T5648, Sigma-Aldrich) was dissolved in ethanol (#32205, Sigma-Aldrich) at 10 mg/100 µL in continuous agitation at 37°C. Then, it was diluted to 10 mg/mL in corn oil (#C8267, Sigma-Aldrich). A daily dose of 1 mg (100 µl) was administered intraperitoneally to each mouse.

### Functional assessment

Distinct functional tests to evaluate motor and behavioural features were performed at 2, 8, 12 and 18 months of age. Exceptionally, novel object recognition test (NORT) was done at 14 months of age instead of 12 months of age. Basal measurements were done at young adult 2-months-old animals. 8-months-old mice were considered between mature adult and middle-aged; 12/14-months-old mice, middle-aged; and 18-months-old animals belonged to the elderly group (Flurkey et al., 2007).

### Rotarod test

Rotarod test was performed to assess locomotor coordination, strength and balance (Mancuso et al., 2011). Mice were placed on a rotating rod (Ugo Basile®) at a constant speed of 14 rpm and the duration each animal remained on the rod was measured. For each animal, three trials were given and the longest latency before failing was recorded. An arbitrary cut-off time of 180 s was chosen. At 2 months of age, animals were trained to achieve baseline levels (180 s at 14 rpm). The training consisted of achieving 180s on the rod first at 8 rpm, then at 11 rpm and finally 14rpm, distributed during several days.

### **Electrophysiological tests**

Motor nerve conduction tests were used to assess the neuromuscular integrity (Mancuso et al., 2011; Navarro & Udina, 2009). Electrophysiological tests were performed under anaesthesia (sodium pentobarbital sodium; 50mg/kg i.p.; #P3761, Sigma-Aldrich) and animals were immobilized in a prone position on a thermostated to maintain body temperature. The sciatic nerve was stimulated percutaneously by a single electrical pulse of 20 $\mu$ s (Grass S88) delivered by a monopolar needle placed in the sciatic notch. The impulse conducted through  $\alpha$ -motor axons initiates synaptic transmission at the neuromuscular junction, which leads to the production of an action potential in the membrane of the skeletal muscles. The evoked compound muscle action potential (CMAP) of plantar interosseus, tibialis anterior and gastrocnemius muscles were recorded using microelectrodes carefully inserted in the desired muscle. The recorded action potential was amplified and digitized with Power Lab recording system (PowerLab16SP, ADInstrument) to measure the CMAP amplitude.

### **Open field test**

Open field test was used to evaluate general locomotor activity (Seibenhener & Wooten, 2015). Prior to the test, mice were allowed to acclimate to the behavioural room for a minimum of 30 min. Mice were individually placed into a white methacrylate box (50 x 50 x 33 cm) and allowed to explore for a period of 6 min. Their exploratory behaviour was recorded for automated assessment by ANY-maze Video Tracking software version 7.20 (Stoelting Co.). The time spent in the central area, corresponding to the inner 900 cm<sup>2</sup>, was measured to evaluate anxiety-like behaviour. The arena was cleaned with 70% ethanol between trials to exclude possible interferences.

### **Sucrose splash test**

Sucrose splash test (SST) was used to measure depression-like and anhedonic behaviour as performed in Lago et al., 2020. Previously to the test, animals were habituated for, at least, 30 min in the test room. A 10% sucrose (#A2211, PanReac) solution, diluted in tap water, was applied to the dorsal coat of the mice. Thereafter, mice were placed individually in a glass container (10,5 x 10,5 x 13,5 cm) and the grooming behaviour was recorded for 5 minutes. Latency from

the sucrose splash to the first grooming and the total grooming time were measured as indicator of motivational behaviour, anhedonia, and self-care. Recipients were cleaned with 70% ethanol before placing new animals to avoid possible olfactive clues.

### **Novel object recognition test**

NORT was performed to evaluate memory (Lueptow, 2017). The test, performed in an arena sized 45 x 45 x 30 cm, was distributed in 3 consecutive days: habituation, familiarization and testing sessions. Each day, before the session, mice were acclimated to the behavioural room for a minimum of 30 min. The arena was cleaned with 70% ethanol between trials to avoid any possible olfactive interferences. The first day (habituation session), mice were placed in the open arena in the absence of any object for 10 min. The second day (familiarization session), two identical objects (A1 and A2) were placed in opposite corners of the arena and mice were allowed to explore them for 10 min. 24 hours after, memory was assessed in the testing session by putting back the animal for 10 min to the arena, where one of the familial objects was substituted by a novel object (B). Novel and familial objects were randomly changed to avoid any place preference. Both training and testing sessions were recorded using the ANY-maze Video Tracking software version 7.20 (Stoelting Co.) and further analysed manually. The time of active exploration (sniffing or touching) to each object was measured in the training and testing sessions. Animals that did not reach a minimum total exploration time for both objects of 15s were excluded in the analysis. The fraction of time exploring each object over the total exploration time was analysed.

### **Statistical analysis**

GraphPad Prism version 9.0.0 (GraphPad Software) was used for statistical analysis. Normal distribution of the data was checked by Shapiro-Wilk test. The statistical test used in each analysis was specified in the figure caption in the results section. Data are shown as mean  $\pm$  SEM. Differences were considered statistically significant if  $p < 0.05$ .



## VI. Results

---



# Chapter 1

---

**ALS-linked SOD1<sup>G93A</sup> mutation disrupts microglial functions in a cell-autonomous manner in human ESC-derived microglia *in vitro***





## Overview

---

Microglia are well-established to contribute to ALS pathogenesis. Mutations in the *SOD1* gene are among the genetic factors that cause ALS, which have facilitated the generation of ALS mouse models. However, the most widely used ALS mouse model overexpresses human mutant SOD1<sup>G93A</sup>, hindering the possibility to fully elucidate the physiopathological contribution of mutant SOD1 to ALS-relevant cell types. Besides, species differences have been shown to be relevant in microglia, especially regarding the altered expression of neurodegenerative disease-associated risk genes in the mouse microglial transcriptome and the incomplete representation of the heterogeneity and complexity of human microglial states in the mouse microglia. Moving to more human-based biomedical research, the ability to differentiate human stem cells to microglia *in vitro*, combined with the advances in gene editing approaches, allows a more accurate assessment of the causative relationship between a genetic background and the associated phenotype.

In this context, we aimed at assessing the effects of mutant SOD1 to microglial function *in vitro*. By generating an isogenic human ESC line carrier for the SOD1<sup>G93A</sup> point mutation by CRISPR/Cas9 technology, we characterized SOD1<sup>G93A</sup> ESC-derived microglia phenotypically and functionally *in vitro* compared to the control. In this sense, we evaluated how mutant SOD1<sup>G93A</sup> affects the microglial cytokine profile, phagocytic function and cell metabolism in basal and in response to a pro-inflammatory stimulus.

**CRISPR/Cas9 gene editing of SOD1<sup>G93A</sup> knock-in in a human ESC line**

Considering that SOD1<sup>G93A</sup> mouse model is the most widely used in ALS field (Gurney et al., 1994; Lutz, 2018), we focused on SOD1<sup>G93A</sup> mutation to assess its cell-autonomous effects specifically on human ESC-derived microglia. Via CRISPR/Cas9 technology, we engineered human ESC line (WA09) with the aim of generating two isogenic cell lines that differ only by the pathogenic point mutation of interest. We targeted the 4<sup>th</sup> exon of *SOD1* gene, where the Gly-to-Ala mutation in 93<sup>rd</sup> position is located, by a sgRNA followed by the PAM sequence. To promote editing by homologous directed repair (HDR), we introduced a ssODN, which included three main features: GGT>GCT codon conversion of interest (Gly93Ala); GCC>GCT synonymous substitution (Ala95Ala) that mutates PAM to avoid Cas9 re-cutting upon editing; and 59-pb and 53-pb left and right homology to ensure proper recombination in the desired locus. Importantly, these two genetic modifications abolished the recognition site for BclI and EaeI restriction enzymes, respectively, useful for genotype analysis (Figure 8A). Positive clones for SOD1<sup>G93A</sup> knock-in were screened by BclI and EaeI digestion of SOD1 region, since edited clones showed longer bands (BclI: 214 pb; EaeI: 141 pb) compared to non-edited ones (BclI: 166 pb; EaeI: 95 pb) (Figure 8B). Finally, Sanger sequencing confirmed the presence of both homozygous SOD1<sup>G93A</sup> and PAM mutations, without other non-desired modifications in the SOD1 locus (Figure 8C).

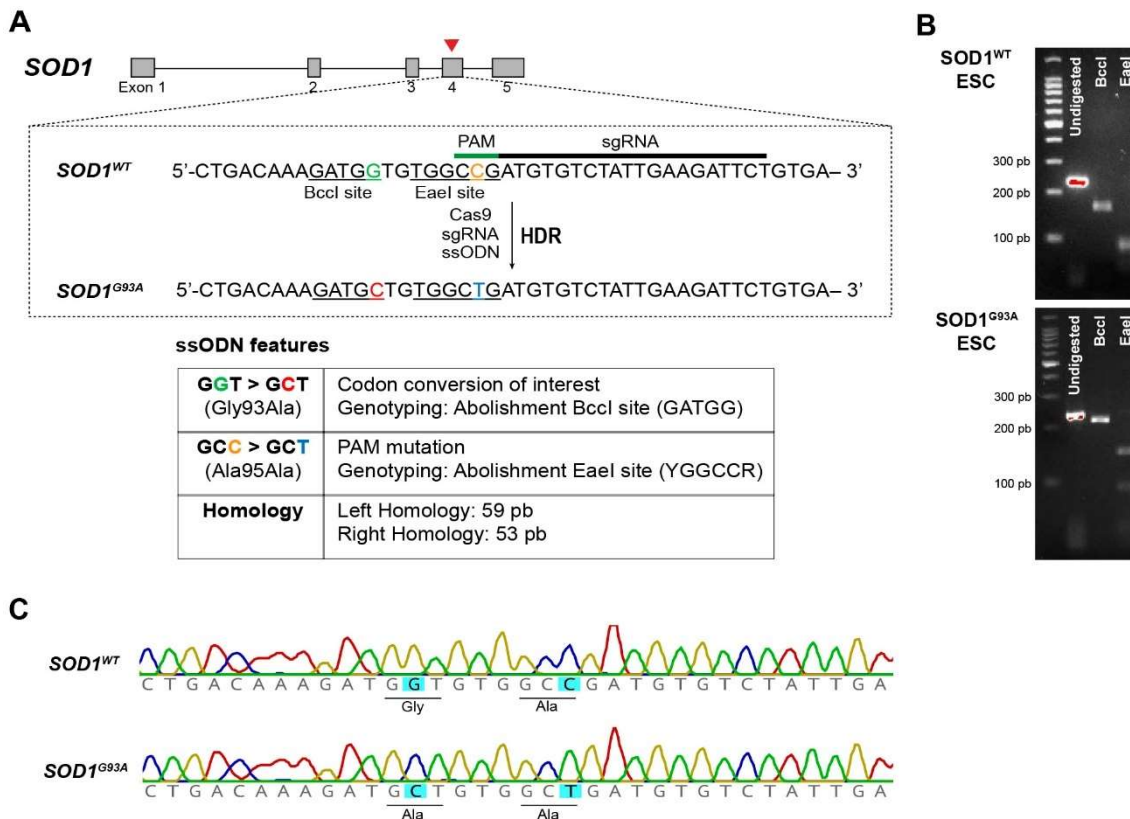


**Figure 8. CRISPR/Cas9 engineering of *SOD1*<sup>G93A</sup> knock-in in human ESC (WA09).** **A**) Schematic representation of the human *SOD1* locus and CRISPR/Cas9 strategy, including single guide RNA (sgRNA) target site and single stranded oligodonor (ssODN) features. Full sequence of ssODN is not shown. PAM, protospacer-adjacent motif; HDR, homology-directed repair. **B**) Representative electrophoresis gels of *SOD1* locus in non-edited (*SOD1*<sup>WT</sup> ESC) and edited (*SOD1*<sup>G93A</sup> ESC) in undigested conditions, after Bccl and EaeI digestion. **C**) Sanger sequencing results from *SOD1*<sup>WT</sup> and *SOD1*<sup>G93A</sup> region of interest, showing inclusion of both genetic alterations: GGT>GCT (Gly93Ala) and GCC>GCT (Ala95Ala).

Off-target effects of CRISPR/Cas9 technology, caused by unintended editing of genomic sites similar to the targeted region, remains a major concern. Therefore, top 10 potential off-target sites were predicted *in silico* by COSMID bioinformatics-based tool (Figure 9A) (Cradick et al., 2014). None of the 10 potential off-target sites analysed (OT1-OT10) by Sanger sequencing showed differences in the sequence between control and edited *SOD1*<sup>G93A</sup> cell line (Figure 9B). In summary, isogenic human control and homozygous *SOD1*<sup>G93A</sup> ESC lines were successfully engineered to further assess the impact of mutant *SOD1* on relevant cell types in ALS pathology, in our case, microglia.

**A**

	Sequence	Mismatches	Score	Chromosome position	Cut site	Strand
<b>SOD1</b>	GAATCTTCAATAGACACATCGG	0	0	Chr21:31667305-31667326	31667311	-
<b>OT 1</b>	CAAAATTC AATAGACACATGGG	3	0,53	Chr15:25520090-25520111	25520105	+
<b>OT 2</b>	GTA A CTGCAATAGACACATGGG	3	0,61	Chr1:107789864-107789885	107789870	-
<b>OT 3</b>	GAATCTTCA G TAGACACATTGG	1	0,7	Chr6:53196867-53196888	53196882	+
<b>OT 4</b>	GTATATTC CATAGACACATGGG	3	0,86	Chr4:109681139-109681160	109681154	+
<b>OT 5</b>	TCATCTTCAA AAGACACATTGG	3	1,08	Chr13:46227046-46227067	46227061	+
<b>OT 6</b>	GTATCTT GAAAAGACACATGGG	3	1,3	Chr11:87945053-87945074	87945068	+
<b>OT 7</b>	GATTCTCAAT G GACACATTGG	3	1,54	Chr12:24874767-24874788	24874773	-
<b>OT 8</b>	GAATTTCCAAT G GACACATTGG	3	1,58	Chr7:134494940-134494961	134494946	-
<b>OT 9</b>	GATTCTTAAATA A ACACATTGG	3	1,82	Chr1:33543890-33543911	33543896	-
<b>OT 10</b>	GAATCTGCA G TGGACACATAGG	3	2,07	Chr9:79338631-79338652	79338637	-

**B**

<b>OT1</b>	<b>Control</b>	ATTGCCAAAATTCAATAGACACATGGGAAATTGTCTACCAG
	<b>SOD1<sup>G93A</sup></b>	ATTGCCAAAATTCAATAGACACATGGGAAATTGTCTACCAG
<b>OT2</b>	<b>Control</b>	GAGCTGTAAGTCAATAGACACATGGGATTTTGAAGAGTTA
	<b>SOD1<sup>G93A</sup></b>	GAGCTGTAAGTCAATAGACACATGGGATTTTGAAGAGTTA
<b>OT3</b>	<b>Control</b>	AAAGTGAATCTTTCAGTAGACACATTGGCCACACCATCTTTG
	<b>SOD1<sup>G93A</sup></b>	AAAGTGAATCTTTCAGTAGACACATTGGCCACACCATCTTTG
<b>OT4</b>	<b>Control</b>	AATGTGTATATTCATAGACACATGGGAGGTATCCAAGGAA
	<b>SOD1<sup>G93A</sup></b>	AATGTGTATATTCATAGACACATGGGAGGTATCCAAGGAA
<b>OT5</b>	<b>Control</b>	TGTTATCATCTTCAAAGACACATTGGTCTGACATCTGGCA
	<b>SOD1<sup>G93A</sup></b>	TGTTATCATCTTCAAAGACACATTGGTCTGACATCTGGCA
<b>OT6</b>	<b>Control</b>	ACAAGGTATCTTGAAAAGACACATGGGTAAATTTTAAATTTT
	<b>SOD1<sup>G93A</sup></b>	ACAAGGTATCTTGAAAAGACACATGGGTAAATTTTAAATTTT
<b>OT7</b>	<b>Control</b>	TTGAGGATTCTACAATGGACACATTGGTGTGGGCCCCAGC
	<b>SOD1<sup>G93A</sup></b>	TTGAGGATTCTACAATGGACACATTGGTGTGGGCCCCAGC
<b>OT8</b>	<b>Control</b>	ATCCTGAATTTCCAATGGACACATTGGAAAAATAACTTGATT
	<b>SOD1<sup>G93A</sup></b>	ATCCTGAATTTCCAATGGACACATTGGAAAAATAACTTGATT
<b>OT9</b>	<b>Control</b>	AAAATGATTCTTAAATAAACACATTGGTCACCTTTGGAGTTT
	<b>SOD1<sup>G93A</sup></b>	AAAATGATTCTTAAATAAACACATTGGTCACCTTTGGAGTTT
<b>OT10</b>	<b>Control</b>	AAGGGAATCTGCAG(C/T)GGACACATAGGGGAGGGCAACAT
	<b>SOD1<sup>G93A</sup></b>	AAGGGAATCTGCAG(C/T)GGACACATAGGGGAGGGCAACAT

**Figure 9. Off-target analysis of SOD1-sgRNA. A)** Computationally predicted top 10 off-target sites by COSMID tool ranked according to decreasing likelihood of occurrence (score value). For each off-target site, mismatches in relation to sgRNA target site (*SOD1* gene), genomic location, the predicted Cas9 cut site and DNA strand (+/-) are also shown. **B)** Sanger sequencing of the top 10 off-target sites in control and SOD1<sup>G93A</sup> ESC lines. Shaded region marks the sgRNA recognition sequence in the off-target locus.

### **Generation of microglia-like cells from human ESC *in vitro***

Our differentiation protocol was based on previously established protocols (Douvaras et al., 2017; Fattorelli et al., 2021; Haenseler et al., 2017) to sequentially direct SOD1<sup>G93A</sup> and isogenic control ESC (WA09) to microglia-like cells (Figure 10A). This strategy aims at recapitulating the *in vivo* microglial developmental ontogeny (Ginhoux et al., 2010). As a first stage, stem cells constitute EBs, which are 3D spherical aggregates which comprise components from the three embryonic layers (endoderm, mesoderm and endoderm) (Van Wilgenburg et al., 2013) (Figure 10B.2). EBs were initially derived for 4 days to the mesodermal lineage through the addition of bone morphogenetic protein 4 (BMP-4) and, VEGF and stem cell factor (SCF) factors to induce HPC (Pick et al., 2007). For the generation of hematopoietic cells, EBs were cultured for 1 week with medium containing SCF, M-CSF, IL-3, Flt-3 and TPO cytokines (Figure 10B.3-4). Then, in the final myeloid stage, through the addition of Flt-3, M-CSF and GM-CSF, EBs produced MPs which could be collected weekly from the supernatant (Figure 10B.5) (Yanagimachi et al., 2013). Finally, MPs were terminally differentiated into microglia-like cells for 12-14 days by using GM-CSF and IL-34, essential for microglia survival and development (Y. Wang et al., 2012) (Figure 10B.6).

To confirm that human ESC-derived microglia-like cells were in fact microglial cells, we analysed the expression profile of specific surface microglial markers. First, we confirmed that 92.3% of cells were CD45<sup>low</sup> CD11b, demonstrating the microglial phenotype of the differentiated cells (Figure 10C). To further corroborate that our cells were microglia, we evaluated the expression of P2RY12, whose expression is restricted to homeostatic microglia in the CNS but not found in other myeloid cells (Butovsky et al., 2014). Again, most CD45<sup>+</sup>CD11b<sup>+</sup> cells (99.6%) were also positive for P2RY12 (Figure 10C,D). Overall, these data prove that our protocol yielded large amounts of microglia from human ESC.



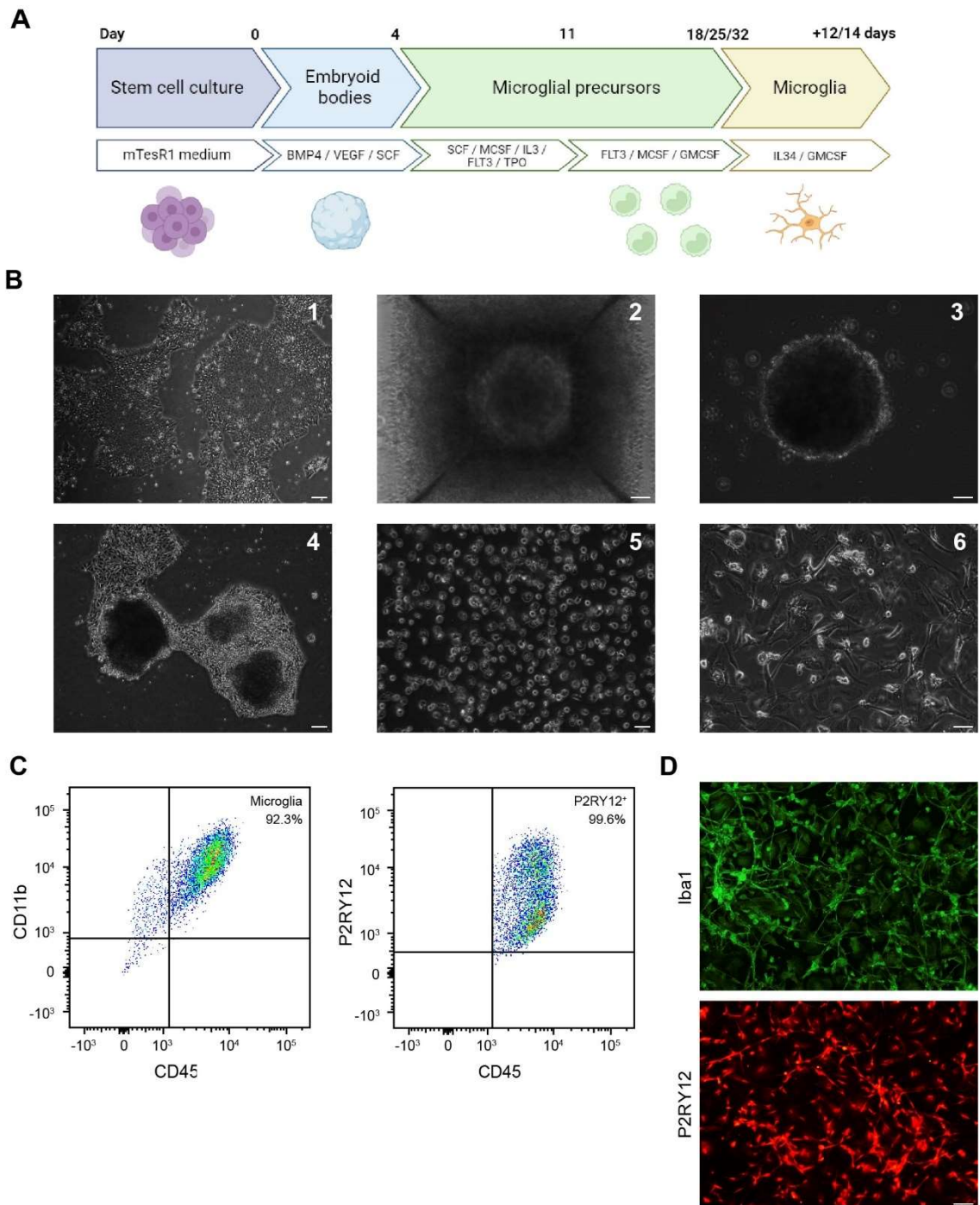


**Figure 10. Generation and characterization of microglial-like cells derived from human ESC.**

**A)** Schematic timeline of the microglial differentiation protocol created with BioRender.com. **B)** Representative pictures of the microglial differentiation at different time points of the protocol. (1) Stem cell (WA09) culture before starting the differentiation; (2) Growing EB present in a microwell from an AggreWell™ 800 plate (Day 3); (3) EB plated in regular 6-well plates with differentiation medium supplemented with SCF, M-CSF, IL-3, Flt-3 and TPO (Day 4); (4) EBs tend to attach and to be surrounded by stromal cells (Day 8); (5) MPs in the supernatant before collection for microglia differentiation (Day 15); (6) Microglia-like cells at the end of the protocol (Day 14 of microglia differentiation). Scale bar: 100  $\mu$ m (1,4,5); 50  $\mu$ m (2,3,6). **C)** Flow cytometry graphs defining the microglial population based on CD45 and CD11b expression; and P2RY12 expression within CD45+

CD11b<sup>+</sup> population. **D)** Representative immunofluorescence images of human ESC-derived microglia against Iba1 and P2RY12. Scale bar: 50  $\mu$ m.

### ***In vitro* SOD1<sup>G93A</sup> microglia exhibit an altered cytokine profile in basal conditions and an exacerbated response to pro-inflammatory stimuli**

We first evaluated the cytokine profile of SOD1<sup>G93A</sup> and control microglia in basal conditions by measuring cytokine concentration in the conditioned medium. We found that the anti-inflammatory cytokine IL-10 secretion was significantly higher in SOD1<sup>G93A</sup> microglia ( $56.72 \pm 8.95$  pg/mL) compared to control microglia ( $14.14 \pm 4.03$  pg/mL,  $p=0.0286$ ) (Figure 11A). Regarding the pro-inflammatory cytokine IL-1 $\beta$ , we found undetectable levels in the supernatants of control microglia ( $<2.26$  pg/mL), whereas those from mutant SOD1<sup>G93A</sup> microglia had a higher, although non-statistically significant, secretion ( $2.89 \pm 0.48$  pg/mL,  $p=0.4286$ ) (Figure 11A). Finally, the pro-inflammatory cytokine IL-17A did not show any significant change in the supernatants of mutant SOD1 ( $3.57 \pm 0.47$  pg/mL) compared to the control SOD1<sup>G93A</sup> microglia ( $3.29 \pm 0.19$  pg/mL,  $p>0.9999$ ) (Figure 11A). These results suggest that the SOD1<sup>G93A</sup> mutation alters cytokine secretion in unstimulated microglia.

To assess how SOD1<sup>G93A</sup> microglia respond to a pro-inflammatory stimulus, we incubated microglial cells with LPS (10 ng/mL) for 6, 14 and 24h and we then evaluated the levels of cytokines in the supernatant over time. We observed that the secretion of all cytokines analysed was pronounced in SOD1<sup>G93A</sup> compared to control microglia (Figure 11B). At 6h after LPS stimulation, we found a significantly stronger secretion of IL-1 $\beta$  ( $50.9 \pm 3.86$  pg/mL) and IL-10 ( $4,948.33 \pm 2,864.89$  pg/mL) in LPS-treated SOD1<sup>G93A</sup> microglia in comparison with control microglial production (IL-1 $\beta$ :  $26.53 \pm 6.45$  pg/mL,  $p=0.0215$ ; IL-10:  $354.19 \pm 103.35$  pg/mL,  $p=0.0126$ ) (Figure 11B). IL-17A secretion was increased in a significant manner after 14h of LPS-stimulation in SOD1<sup>G93A</sup> microglia ( $10.92 \pm 1.03$  pg/mL) compared to the control ( $7.21 \pm 1.28$  pg/mL,  $p=0.0497$ ) (Figure 11B). These results evidence that SOD1<sup>G93A</sup> microglia exhibit an exacerbated response to pro-inflammatory stimuli.



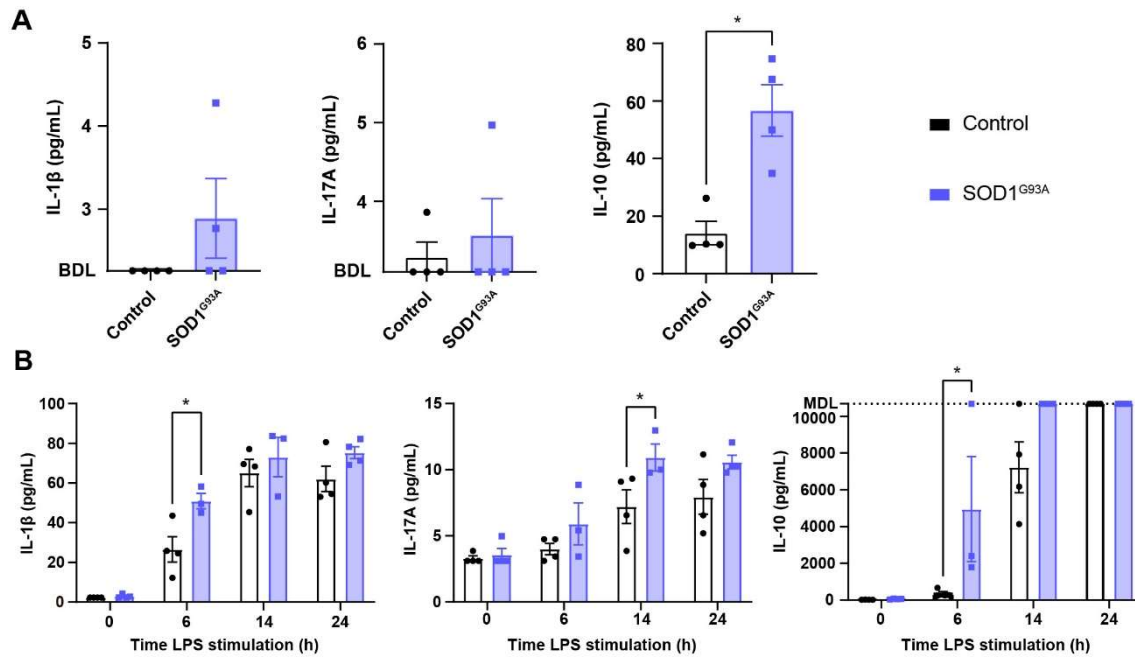


**Figure 11. Cytokine profile in control and SOD1<sup>G93A</sup> microglial conditioned medium at baseline conditions and upon LPS stimulation. A)** Levels of IL-1 $\beta$ , IL-17A and IL-10 in the conditioned media secreted by SOD1<sup>G93A</sup> and control microglia in baseline conditions. **B)** Levels of IL-1 $\beta$ , IL-17A and IL-10 in the conditioned media secreted by SOD1<sup>G93A</sup> and control microglia after 6, 14 and 24h of LPS stimulation (10 ng/mL). N=3-4 differentiation/condition. \*p<0.05. Mann-Whitney test in **A**; Two-way ANOVA with Bonferroni's post hoc correction in **B**. Data shown as mean  $\pm$  SEM. BDL: Below detection limit; MDL: Method detection limit.

### Mutant SOD1<sup>G93A</sup> affects microglial phagocytosis *in vitro*

Next, we aimed at assessing whether SOD1<sup>G93A</sup> mutation had an impact on microglial phagocytic function in an unstimulated state. We exposed control and SOD1<sup>G93A</sup> microglia with 1  $\mu$ g pHrodo-myelin for 30 min and 3h and then we quantified pHrodo signal by flow cytometry. It is a pH-sensitive dye that becomes fluorescent only in acidic environments, such as phagosomes at the end of the phagocytosis process (Gómez-López et al., 2021). Regarding the proportion of phagocytic microglia, meaning those microglia with positive signal for pHrodo, we observed a significant reduction of phagocytic cells after 3h of myelin exposure in SOD1<sup>G93A</sup> microglia ( $52.73 \pm 1.85\%$ ) versus control microglia ( $61.25 \pm 2.51\%$ ,  $p=0.0340$ ) (Figure 12A, B). In parallel, we quantified the pHrodo-geoMFI within the population of phagocytic microglia as a quantitative parameter for the myelin internalization or degradation within the phagolysosome. Phagocytic SOD1<sup>G93A</sup> microglia tended to have a decrease in pHrodo signal at 30 min ( $151,575 \pm 7,978$  AU) compared to control ( $177,158 \pm 7,978$  AU,  $p=0.0591$ ). This slight decrease

reached the significance after 3h of myelin exposure (Control:  $268,092 \pm 10,833$  AU; SOD1<sup>G93A</sup>:  $235,557 \pm 7,593$  AU,  $p=0.0286$ ) (Figure 12A, C). Overall, these results suggest that SOD1<sup>G93A</sup> mutation affects microglial phagocytosis *in vitro*.

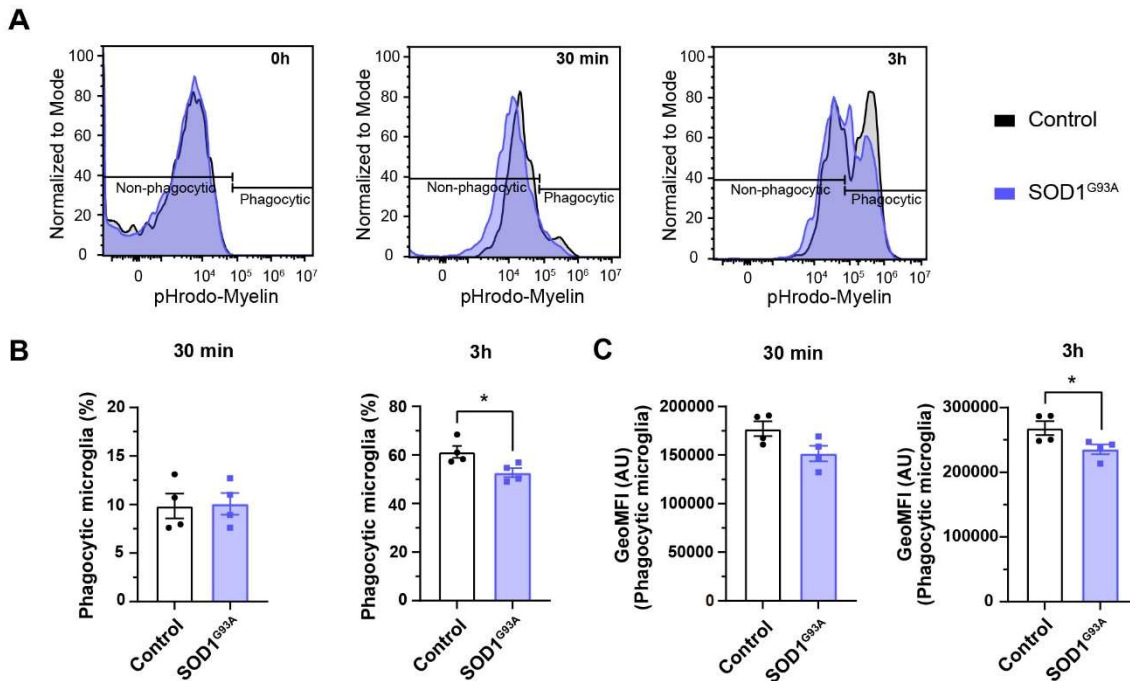


**Figure 12. Functional phagocytosis assay in SOD1<sup>G93A</sup> and control microglia at baseline conditions *in vitro*.** **A)** Representative flow cytometry histograms at 0h, 30 min and 3h after exposure to pHrodo-conjugated myelin. **B)** Quantification of the proportion of phagocytic control and SOD1<sup>G93A</sup> microglia 30 min and 3h after myelin exposure. **C)** Quantification of pHrodo-Myelin phagocytosed within the phagocytic population expressed as geoMFI (AU) after 30 min and 3h of myelin exposure. N=4 differentiations/condition. \* $p<0.05$ . Unpaired t-test in **B** (30 min, 3h) and **C** (30 min); Mann-Whitney test in **C** (3h). Data shown as mean  $\pm$  SEM. GeoMFI: Geometric mean fluorescence intensity; AU: Arbitrary units.

### ***In vitro* SOD1<sup>G93A</sup> microglia display metabolic disturbances in basal conditions**

Alterations in energy metabolism have been described in ALS (H. Kawamata & Manfredi, 2017; Vandoorne et al., 2018). To study whether energy metabolism is affected in *in vitro* microglia carrying the SOD1<sup>G93A</sup> mutation, we evaluated mitochondrial respiration by measuring the OCR after treatment with distinct ETC modulators in control and SOD1<sup>G93A</sup> microglia in basal conditions. Simultaneously, ECAR was measured as an indirect parameter of the glycolytic metabolism. We did not find any significant differences in basal OCR levels between control and SOD1<sup>G93A</sup> microglia. Although basal ECAR values tended to be higher in SOD1<sup>G93A</sup> microglia, this increase did not reach statistical significance (time 7.76 min:

$p=0.0520$ ) (Figure 13A). Upon exposition to oligomycin, an inhibitor of the mitochondrial ATP-synthase (complex V), both control and SOD1<sup>G93A</sup> microglia exhibited a similar decrease in OCR ( $p>0.05$ ). However, oligomycin also caused a more pronounced reduction in ECAR in SOD1<sup>G93A</sup> microglia compared to control (Figure 13A).

We then treated microglia with FCCP, an uncoupling agent that collapses the proton gradient and mimics a physiological energy demand by pushing the ETC to operate at maximum capacity. Interestingly, SOD1<sup>G93A</sup> microglia showed a significant increase in both OCR and ECAR upon FCCP treatment in comparison with control microglia ( $p<0.0001$ ) (Figure 13A), resulting in an increased maximal respiration capacity. This suggests that SOD1<sup>G93A</sup> microglia possess a higher capacity to operate to the maximum respiration in response to a physiological energy demand.

Finally, mitochondrial respiration was shut down by a combination of rotenone, a complex I inhibitor, and antimycin A, a complex III inhibitor. OCR was reduced to similar values in both control and SOD1<sup>G93A</sup> microglia, indicating that the SOD1<sup>G93A</sup> mutation did not alter non-mitochondrial respiration in microglia ( $p>0.05$ ). ECAR was also reduced upon rotenone incubation, but SOD1<sup>G93A</sup> microglia display non-significantly higher values compared to the control (time=55.61 min:  $p=0.0880$ ; time 66.06 min, 75.51 min:  $p>0.05$ ) (Figure 13A).

To elucidate some possible mechanisms underlying the previous metabolism disturbances detected in SOD1<sup>G93A</sup> microglia, we measured ROS levels and active mitochondria content in control and SOD1<sup>G93A</sup> microglia. As expected, due to the antioxidant function of SOD1 enzyme, mutant SOD1<sup>G93A</sup> microglia exhibit a significant increase in ROS levels in terms of area (Control:  $576.0 \pm 41.34 \mu\text{m}^2$ ; SOD1<sup>G93A</sup>:  $792.6 \pm 47.18 \mu\text{m}^2$ ,  $p=0.0136$ ) and intensity (Control:  $8,664 \pm 1,323 \text{ AU}$ ; SOD1<sup>G93A</sup>:  $13,208 \pm 1,375 \text{ AU}$ ,  $p=0.0547$ ) (Figure 13B, D). Nevertheless, we did not find differences in mitochondria content between control (Area:  $508.3 \pm 43.44 \mu\text{m}^2$ ; Intensity:  $7,373 \pm 347 \text{ AU}$ ) and SOD1<sup>G93A</sup> microglia (Area:  $696.3 \pm 100.5 \mu\text{m}^2$ ,  $p=0.1369$ ; Intensity:  $9,106 \pm 1,689 \text{ AU}$ ,  $p=0.3537$ ) (Figure 13C, E), discarding that the increased maximal respiration capacity observed in SOD1<sup>G93A</sup> was due to higher mitochondria content.

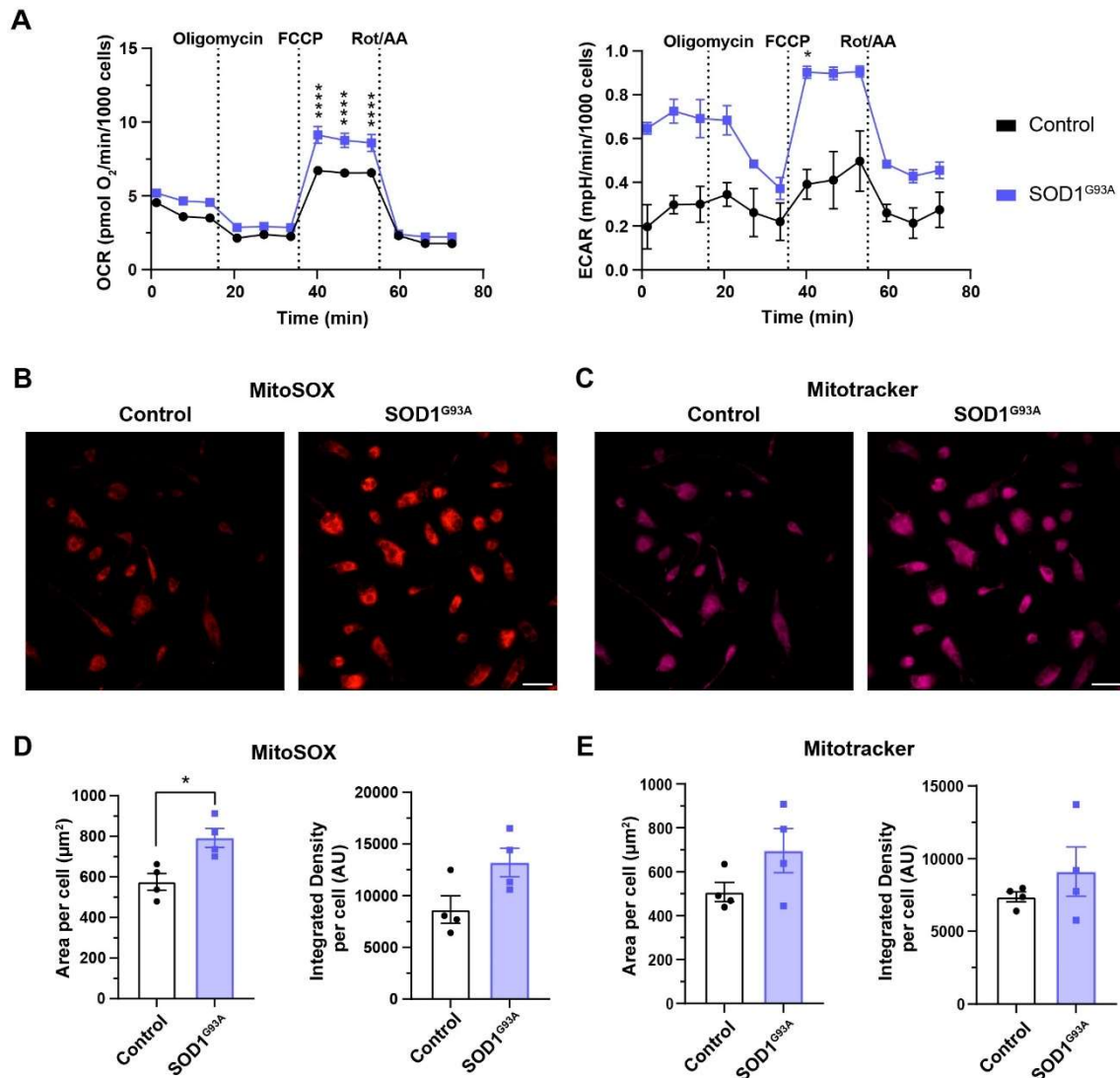


**Figure 13. SOD1<sup>G93A</sup> microglia cell metabolism in basal conditions.** **A**) OCR and **B**) ECAR values in control and SOD1<sup>G93A</sup> microglia at baseline conditions and after the sequential injection of different mitochondrial electron transport chain complex inhibitors (oligomycin and Rot/AA) and the mitochondrial uncoupling agent FCCP. OCR and ECAR were measured three times initially and after each injection. Values are normalized by 1000 cells. N=3-4 differentiations/condition. **C**) Representative images of MitoSOX (ROS levels) and **D**) Mitotracker (active mitochondria) stainings in control and SOD1<sup>G93A</sup> microglia. Scale bar: 50 μm. **E**) MitoSOX and **F**) Mitotracker area (μm<sup>2</sup>) and fluorescence intensity (AU) quantification normalized by cell number. N=4 differentiations/condition. \*\*\*\* p<0.0001, \*p<0.05. Two-way RM ANOVA in **A** (OCR) and Mixed-effects analysis in **A** (ECAR) with Bonferroni's post hoc correction; unpaired t-test in **D**, **E**. Data shown as mean ± SEM. OCR: Oxygen consumption rate; ECAR: Extracellular acidification rate; Rot/AA: Rotenone/antimycin A; FCCP: carbonyl cyanide-4-(trifluoromethoxy)-phenylhydrazone; AU: Arbitrary units.

### ***In vitro* SOD1<sup>G93A</sup> microglia adapt differently their metabolism in response to LPS**

Metabolic reprogramming towards glycolysis is required to transform microglia from a resting to an activated state (Strogulski et al., 2023; Q. Wang et al., 2022). To evaluate how SOD1<sup>G93A</sup> microglia adapt metabolically to pro-inflammatory stimulus, we evaluated mitochondria respiration (OCR values) and glycolysis (ECAR values) after 24h of LPS treatment. Compared to LPS-stimulated control microglia, LPS-stimulated SOD1<sup>G93A</sup> microglia showed lower, although not significant, mitochondrial oxidative phosphorylation activity, reflected with decreased OCR values specially at baseline timepoints (time 1.31 min:  $p=0.0745$ ) (Figure 14A). This correlates with the higher ECAR values (glycolytic metabolism) observed in LPS-stimulated SOD1<sup>G93A</sup> microglia, being significant at baseline conditions ( $p<0.05$ ) (Figure 14A). In response to different mitochondrial stressors (oligomycin, FCCP and Rot/AA), LPS-SOD1<sup>G93A</sup> microglia showed a slight decrease, but non-significant, in OCR compared to LPS-control microglia ( $p>0.05$ ). Regarding the glycolytic metabolism, LPS-control microglia were able to slightly increase ECAR values in response to the mitochondrial stressors. Contrarywise, the ECAR values were not modified by the mitochondrial stressors in LPS-SOD1<sup>G93A</sup> microglia, which is likely due to their higher ECAR values observed at baseline timepoints (Figure 14A).

No differences in ROS levels were found in microglia carrying or not the SOD1<sup>G93A</sup> mutation after LPS stimulation, neither in MitoSox area (LPS-Control:  $735.9 \pm 113.7 \mu\text{m}^2$ ; LPS-SOD1<sup>G93A</sup>:  $834.1 \pm 53.61 \mu\text{m}^2$ ,  $p=0.6857$ ) nor in MitoSox fluorescence intensity (LPS-Control:  $12,741 \pm 835 \text{ AU}$ ; LPS-SOD1<sup>G93A</sup>:  $13,057 \pm 1,734 \text{ AU}$ ,  $p=0.8747$ ) (Figure 14B,D). Indeed, MitoSox values were elevated in LPS-stimulated control microglia compared to unstimulated controls, but this increase was not observed in SOD1<sup>G93A</sup> microglia (see Figures 13D and 14D). These findings suggest that while control microglia increase ROS levels upon LPS stimulation, this response is absent in SOD1<sup>G93A</sup> microglia, likely due to their already elevated basal ROS levels. Similar to unstimulated conditions, mitochondrial content did not vary upon LPS stimulation in control and SOD1<sup>G93A</sup> microglia as shown by Mitotracker area (LPS-Control:  $616.3 \pm 58.3 \mu\text{m}^2$ ; SOD1<sup>G93A</sup>:  $678 \pm 104.2 \mu\text{m}^2$ ,  $p=0.6235$ ) and

Mitotracker fluorescence intensity (LPS-Control:  $7,876 \pm 1,335$  AU; SOD1<sup>G93A</sup>:  $8,193 \pm 2,116$  AU,  $p=0.9033$ ).

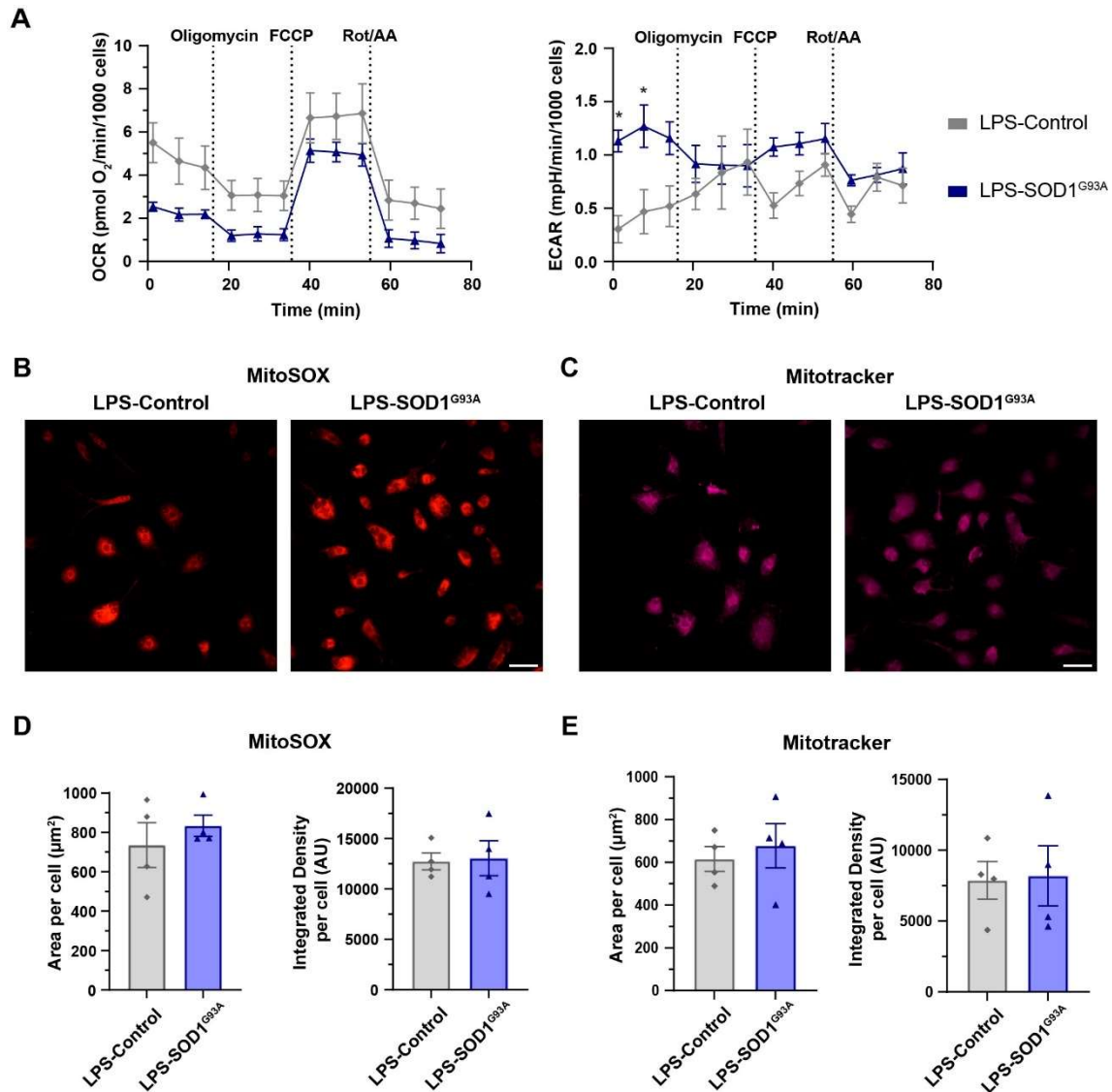


**Figure 14. SOD1<sup>G93A</sup> microglia cell metabolism upon LPS stimulation. A)** OCR and **B)** ECAR values in LPS-stimulated control and SOD1<sup>G93A</sup> microglia at baseline conditions and after the sequential injection of different mitochondrial electron transport chain complex inhibitors (oligomycin and Rot/AA) and the mitochondrial uncoupling agent FCCP. OCR and ECAR were measured three times initially and after each injection. Values are normalized by 1000 cells. N=3 differentiations/condition. **C)** Representative images of MitoSOX (ROS levels) and **D)** Mitotracker (active mitochondria) staining in LPS-stimulated control and SOD1<sup>G93A</sup> microglia. Scale bar: 50  $\mu$ m. **E)** MitoSOX and **F)** Mitotracker area ( $\mu$ m<sup>2</sup>) and fluorescence intensity (AU) quantification normalized by cell number. N=4 differentiations/condition. LPS stimulation was performed at 10ng/mL for 24h prior to the assays. \* $p<0.05$ . Two-way RM ANOVA in **A** with Bonferroni's post hoc correction; Mann Whitney test in **D** (area); unpaired t-test in **D** (Integrated density), **E**. Data shown as mean  $\pm$  SEM. OCR: Oxygen consumption rate; ECAR: Extracellular acidification rate; Rot/AA: Rotenone/antimycin A; FCCP: carbonyl cyanide-4-(trifluoromethoxy)-phenylhydrazone; AU: Arbitrary units.



## Chapter 2

---

**Xenotransplantation of human microglia  
into the mouse spinal cord**





## Overview

---

A proper human microglia modelling is being a challenge for decades. Although mouse microglia is comparable to the human in general terms, species-specific differences in neurodegenerative-associated risk microglial genes and the absence of a clear ortholog in the mouse genome hinders a good understanding of their contribution to pathology. Importantly, the generation of human iPSC-derived microglia *in vitro* has overcome partially these limitations. However, microglia are highly sensitive to the environment as important transcriptomic changes have been described in microglia grown in cell-culture conditions compared to *ex vivo* microglia. For this reason, there is an urgent need to explore new microglia experimental models. In the recent years, chimeric mouse with human microglia in the living mouse brain have been developed. Interestingly, human microglia grown in the mouse CNS mimics more closely the primary human microglia. Thus, these cutting-edge humanized mouse models may be an innovative tool to elucidate the role on microglia in healthy and disease.

In this chapter, we aimed at developing a chimeric mouse model with human microglia in the mouse spinal cord, a model of particular relevance to the ALS field. By adapting previous works of human microglia xenotransplantation into the mouse brain, we set up a protocol to administrate human microglia into the spinal cord and we characterized its engraftment and distribution in the mouse spinal cord, monitoring them for up to 10 months post-transplantation.

### **Xenotransplantation of human microglia into the mouse spinal cord**

All published protocols aimed at integrating human microglia into the mouse CNS are performed in the brain (Abud et al., 2017; Hasselmann et al., 2019; Mancuso et al., 2019; Svoboda et al., 2019; Xu, Li, et al., 2020; Fattorelli et al., 2021). However, we are interested in setting up this strategy in the mouse spinal cord, since lower MNs located in the spinal cord degenerate in ALS and, most studies in the ALS field, particularly using the SOD1<sup>G93A</sup> mouse model, are focused on spinal MNs (Mancuso & Navarro, 2015). Thus, we consider interesting to develop a chimeric mouse model with human microglia engrafted in the mouse spinal cord to assess the role of microglia in ALS pathology. For this purpose, we adapted the already published protocol from Fattorelli et al., 2021, but using an IS administration in neonatal mice as described in Ayers et al., 2015 (Figure 15A).

First, as a proof-of-concept of the administration, we injected Fast Green dye through IS administration to P4 neonates to quickly visualize its localization and distribution in the spinal cord. Given the small size of P4 mice and the immunosuppressive status of Rag2<sup>-/-</sup> IL2 $\gamma$ <sup>-/-</sup> hCSF1<sup>KI</sup> mice, which is needed to avoid rejection of the injected human cells, we decided not to open any scission to minimize the risk of infection. Therefore, we set two references to define the injection point: the intersection between the hip level and the tail (Figure 15A). Moreover, the injection was performed in a depth of 1-2 mm. As a reference point to ensure proper needle placement within the spinal cord, we observed that the ventral portion of the vertebra in P4 mice is already ossified and firm, while the dorsal portion remains softer and easily penetrated. With these considerations, we successfully visualized the spinal cord turning green within 5 minutes following the IS injection of Fast Green, confirming the effectiveness of the IS protocol (Figure 15B). To further validate the success of the IS administration, we injected 50,000 MPs as described previously. Since Iba1 labels both mouse and human microglia, we tracked the human cells using a specific antibody against human CD45 (hCD45). Five days post-transplantation, we confirmed the engraftment of human cells (Iba1<sup>+</sup> hCD45<sup>+</sup>) into the spinal cord, particularly in the most lateral areas, in close association to the meninges (Figure 15C).

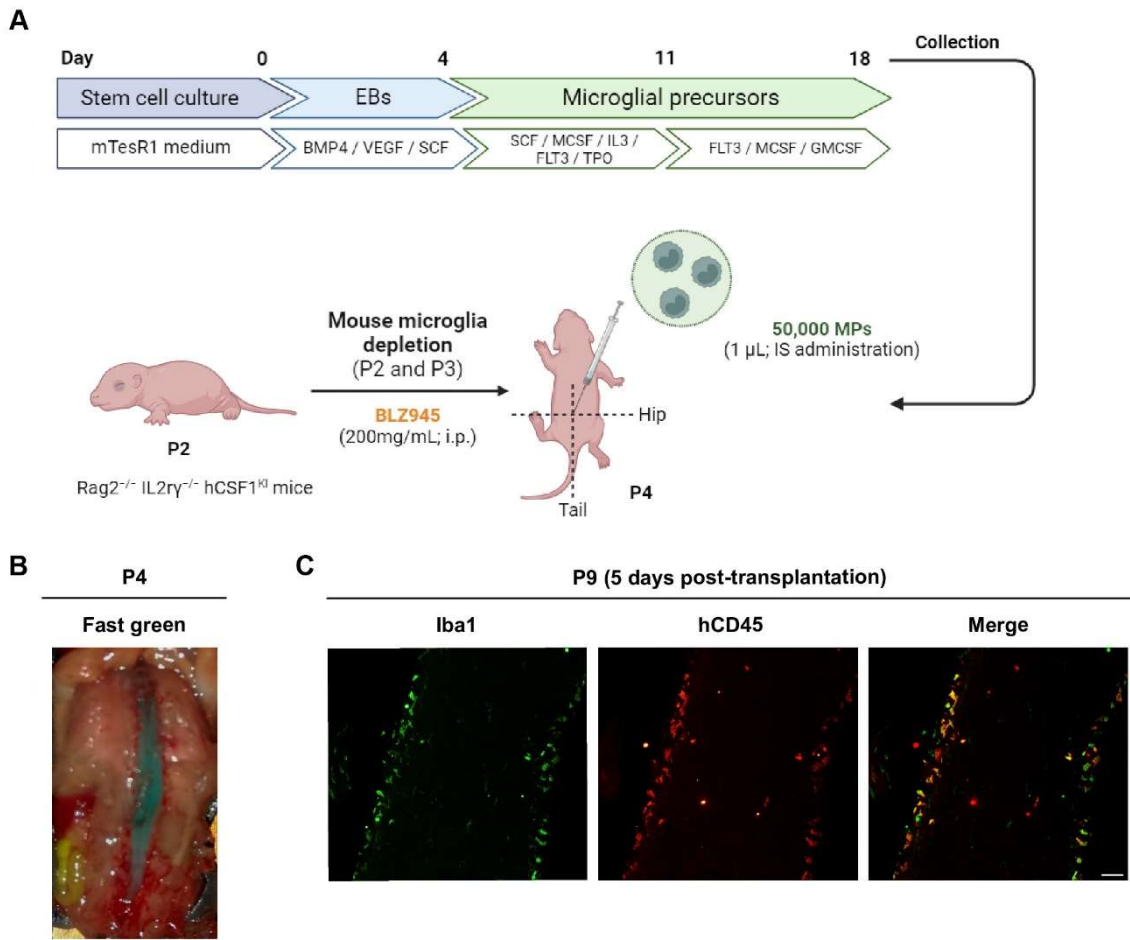


**Figure 15. Xenotransplantation protocol of human microglia into the mouse spinal cord. A)** Schematic representation of the xenotransplantation protocol into the mouse spinal cord used in our study, which requires a coordinated work of *in vitro* iPSC-derived microglial precursors generation and *in vivo* work Rag2<sup>-/-</sup> IL2ry<sup>-/-</sup> hCSF1<sup>KI</sup> mice. Created with Biorender.com. EBs: Embryoid bodies; IS: Intraspinal; MPs: Microglial precursors; i.p.: intraperitoneally; P2/3/4: Postnatal day 2/3/4. **B)** Picture showing green staining in all spinal cord after Fast Green IS administration at P4 neonate. **C)** Representative images of Iba1 (mouse and human microglia), human CD45 (hCD45) and merge in the spinal cord at P9. Scale bar=50  $\mu$ m. hCD45: human CD45.

### Engrafted human microglia co-express the prototypical microglial markers P2RY12 and CD45

First, we studied whether the human MPs injected intraspinaly could differentiate into microglia *in vivo* and persist in the mouse spinal cord 1 month after transplantation. Histological spinal cord section of xenotransplanted mice showed the presence of engrafted human microglia as verified by the expression of human P2RY12 (Figure 16A), a cell marker restricted to homeostatic microglia in the CNS (Butovsky et al., 2014), indicating that human MPs differentiate into microglia and survived for 1 month. Similarly, we also observed the expression of human CD45

(Figure 16B), a common marker of myeloid cells (Paolicelli et al., 2022). Indeed, most human P2RY12<sup>+</sup> cells co-labelled with the human CD45 marker, indicating engrafted human microglia expressed both prototypical microglial markers in the mouse spinal cord (Figure 16C). In contrast to day 5 post-transplantation, the presence of human microglia was not restricted to the outermost area of the spinal cord at 1-month post-transplantation, since they were observed within the spinal cord parenchyma, particularly, in white matter regions.

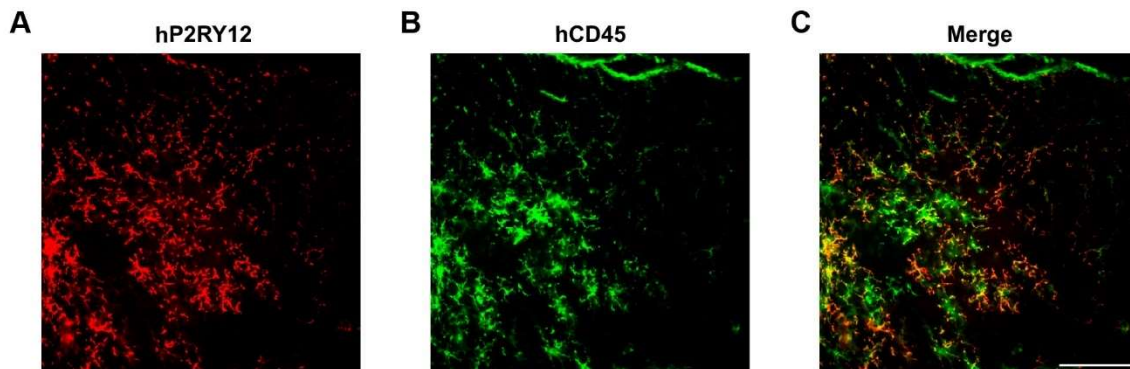


**Figure 16. CD45 and P2RY12 expression in engrafted human microglia in the mouse spinal cord.** Representative pictures of xenotransplanted human microglia in the lumbar spinal cord 1-month post-transplantation showing labelling against **A)** human P2RY12 (hP2RY12); **B)** human CD45 (hCD45) and **C)** merge. Scale bar=100  $\mu$ m.

### **Human microglia populate and persist throughout the lumbar spinal cord over a period of at least of 10 months**

The most widely used ALS mouse model, SOD1<sup>G93A</sup> model, exhibits hindlimb atrophy and paralysis as one the main symptoms. These muscles are mainly innervated by MNs whose soma are located in the lumbar spinal cord (Mancuso & Navarro, 2015). Given the interest of this spinal cord region in ALS, we characterize the survival and distribution of human microglia in the lumbar spinal cord of xenotransplanted mice for 10 months. As expected, the presence of human microglia (hP2RY12<sup>+</sup>) in the lumbar spinal cord increased with the age (Figure 17A). Engrafted human microglia started to populate the spinal cord from the periphery to the central part. At 2 months of age, we observed that human microglia were mainly detected in the white matter of the spinal cord, to a lesser extent, in the grey matter, including the ventral horn. In 5-month-age transplanted mice, human microglia were already present in almost all white matter and started to populate, to a greater extent than at 2 months post-transplantation, the dorsal and ventral

horns. Finally, at 10 month of age, human microglia were detected in virtually all the spinal cord including white and grey matter (Figure 17A).

We then quantified the degree of human microglia chimerism in specific areas of the lumbar spinal cord white and grey matter at various timepoints post-transplantation. Microglia were identified as those Iba1<sup>+</sup> cells, which include both human and mouse microglia. Human microglia were distinguished from mouse microglia by using the hCD45 marker. At 2 months of age, we observed that the percentage human microglia chimerism (% of human microglia relative to total microglia) was 49% in the dorsal horn (Figure 17B,E), 68% in the ventral horn (Figure 17C,E) and 72% in the white matter (Figure 17D,E). Over time, the proportion of human chimerism increased in both grey and white matter. In the dorsal horn, we observed that human microglia engraftment was approximately 71% at 5 months post-transplantation and about 84% at 10 months (Figure 17B,E). In the ventral horn, chimerism was around 79% and 91% at 5 and 10 months, respectively (Figure 17C,E). Despite the greater degree of chimerism observed in the grey matter areas at 10 months post-transplantation relative to 5 months, no statistical differences were observed. Importantly, the highest degree of chimerism was observed in the white matter, reaching values of 98% at both 5 and 10 months post-transplantation (Figure 17D,E).



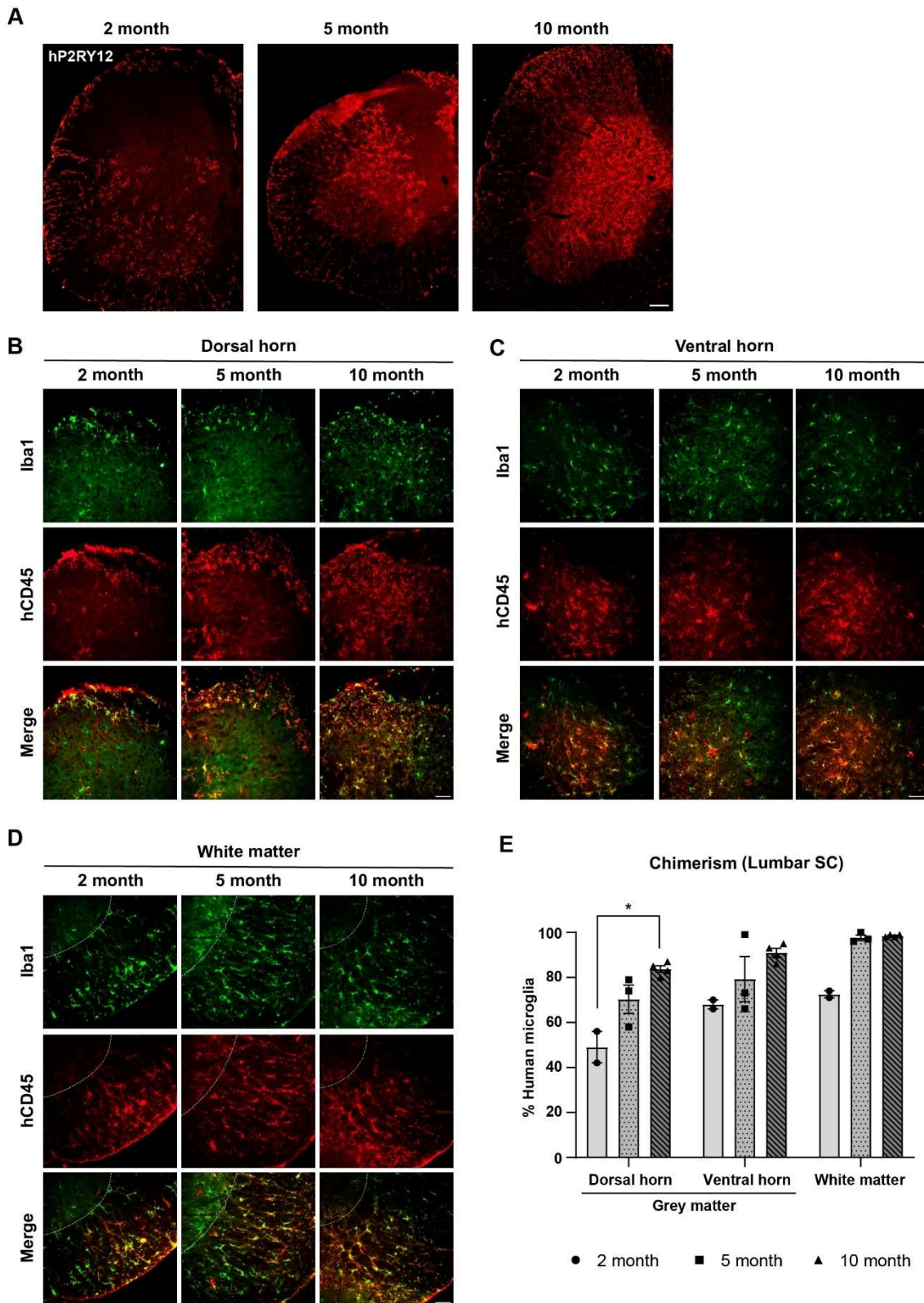


**Figure 17. Human microglia chimerism in the lumbar spinal cord over time.** **A)** Representative pictures of xenotransplanted human microglia (hP2RY12<sup>+</sup>) in the lumbar spinal cord at 2, 5 and 10 months post transplantation. Scale bar=100 $\mu$ m. **B)** Representative images of Iba1 (mouse and human microglia), human CD45 (hCD45) and merge in the dorsal horn of the lumbar spinal cord at 2, 5 and 10 months post-transplantation. Scale bar=50 $\mu$ m. **C)** Representative images of Iba1 (mouse and

human microglia), hCD45 and merge in the ventral horn of the lumbar spinal cord at 2, 5 and 10 months of transplantation. Scale bar=50 $\mu$ m. **D)** Representative images of Iba1 (mouse and human microglia), hCD45 and merge in the white matter of the lumbar spinal cord at 2, 5 and 10 months post-transplantation. Scale bar=50 $\mu$ m. **E)** Quantification of human chimerism, as the proportion of human CD45<sup>+</sup> relative to Iba1<sup>+</sup> cells, in the dorsal horn, ventral horn and white matter from the lumbar spinal cord at 2, 5 and 10 months post-transplantation. n=2 (2 month); n=3 (5 month); n=4 (10 month). \*p<0.05. Kruskal-Wallis test with Dunn's multiple comparisons per region. Data shown as mean  $\pm$  SEM. SC: Spinal cord.

### Human microglia spread throughout all the mouse spinal cord over time

Finally, we investigate whether human microglia were able to populate other regions beyond the lumbar spinal cord in the xenotransplanted mice. We observed a wide population of human microglia (hP2RY12<sup>+</sup>) in cervical and thoracic spinal cord at 5 months post-transplantation (Figure 18A). Similarly, hP2RY12<sup>+</sup> human microglia populate white and grey matter of thoracic and sacral mouse spinal cord at 10 months of age (Figure 18B).

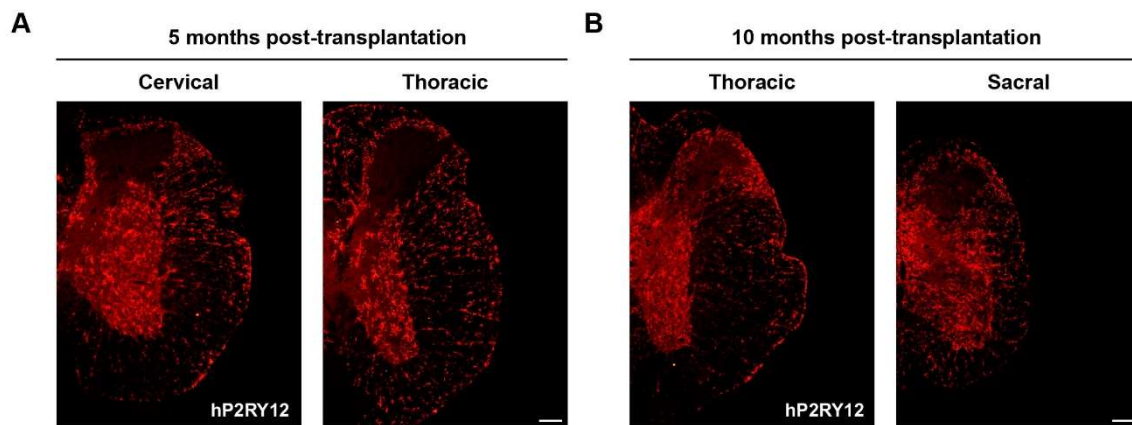


**Figure 18. Human microglia engraftment in all spinal cord. A)** Representative pictures of xenotransplanted human microglia (hP2RY12<sup>+</sup>) in the cervical and thoracic spinal cord at 5 months post-transplantation. Scale bar=100  $\mu$ m. **B)** Representative pictures of xenotransplanted human microglia (hP2RY12<sup>+</sup>) in the thoracic and sacral spinal cord at 10 months post-transplantation. Scale bar=100  $\mu$ m.





## Chapter 3

---

**Phenotypic characterization of a novel C9orf72  
G4C2 HRE knock-in mouse model**



## Overview

---

Pathogenic G4C2 HRE in *C9ORF72* gene is the most prevalent genetic cause in ALS and FTD. However, current *C9orf72* mouse models fail to fully recapitulate motor ALS-like and behavioural FTD-like signs and symptoms. Nowadays, it is quite established that both *C9orf72* LOF and GOF pathogenic mechanisms are required to produce an ALS/FTD phenotype. Whereas *C9orf72* haploinsufficiency by itself is not enough to trigger MN disease, GOF animal models that expressed the human pathogenic G4C2 HRE exogenously by BAC or viral vectors do not exhibit a clear phenotype of ALS/FTD. Importantly, in current *C9orf72* GOF mouse models, the endogenous mouse *C9orf72* gene remains intact due to the non-integrative methodology used to generate the model, and therefore the expression and function of the mouse *C9orf72* is not affected.

Some years ago, in our research group, we generated a transgenic mouse carrier for 30 G4C2 repeats in the mouse *C9orf72* gene, specifically in the intronic region between exon 1a and 1b, where the HRE are usually located. Therefore, in this context, we have characterized our novel *C9orf72* mouse model phenotypically at the motor level, in order to elucidate whether ALS- and/FTD-like phenotype is reproduced.

### Generation of our C9orf72 G4C2 HRE knock-in mouse model

Current C9orf72 mouse models express the human *C9ORF72* gene containing the pathogenic G4C2 repeats through BACs or adeno-associated viral vectors (AAVs), meaning that the endogenous mouse *C9orf72* gene remains intact (Chew et al., 2015; Jiang et al., 2016; Y. Liu et al., 2016; O'Rourke et al., 2015; Peters et al., 2015). In this context, we developed a mouse model including G4C2 HRE in the mouse *C9orf72* gene, specifically in the intronic region between exon 1a and 1b, where the HRE are usually located. The vector used to engineer this mouse (shown in Figure 19A) includes several features: i) 5'- (3K pb) and 3'- (5K pb) homology arms to ensure proper gene targeting; ii) a STOP region; iii) the neomycin-resistance gene (neo) under the control of phosphoglycerate kinase 1 (PGK) promoter, with the purpose of selecting the recombinant clones; iv) LoxP sites flanking the STOP and Neo sites; v) FRT sites flanking the neo region; vi) 30x G4C2 repeats; and vii) C9orf72 exon 1b. Given the inclusion of LoxP sites, we could remove the STOP region and neo cassette by crossing our C9orf72 G4C2 HRE knock-in mouse model (abbreviated hereinafter as C9 animals) with mice expressing a tamoxifen-inducible Cre recombinase (CreER) ubiquitously. Cre-mediated recombination was induced by tamoxifen administration at 8 weeks-old mice for 11 consecutive days (Figure 19B).

In this study, we characterized our C9 mice phenotypically for two years (Figure 19B). We focused on the motor function and behaviour as these are the main symptoms of C9orf72-related ALS/FTD. We included six experimental groups as shown in Figure 19C. No CreER-expressing mice (CreER<sup>-/-</sup>) include (i) wild-type (WT) animals; (ii) CreER<sup>-/-</sup> C9<sup>STOP/+</sup>, which are heterozygous animals; and (iii) CreER<sup>-/-</sup> C9<sup>STOP/STOP</sup>, which are homozygous (Figure 19C). In these groups, the 30x G4C2 repeats are preceded by the STOP and neo cassette. Since these mice do not express the tamoxifen-inducible Cre recombinase, the STOP region and neo cassette are not cleaved. Given that the pathogenic G4C2 HRE is located in an intronic region, we hypothesize that this STOP region may not have any direct effect on the C9orf72 expression. On the other hand, CreER-expressing animals (CreER<sup>+/-</sup>) comprise (iv) CreER<sup>+/-</sup> animals as controls; (v) CreER<sup>+/-</sup> C9<sup>fl/+</sup>, which are heterozygous mice; (vi) CreER<sup>+/-</sup> C9<sup>fl/fl</sup>, which are homozygous animals (Figure 19C). CreER<sup>+/-</sup>, CreER<sup>+/-</sup> C9<sup>fl/+</sup> and CreER<sup>+/-</sup> C9<sup>fl/fl</sup> animals have the STOP-neo region floxed and thus, it would

express the *C9orf72* gene in a physiopathological manner without any potential interference of the STOP-neo presence.

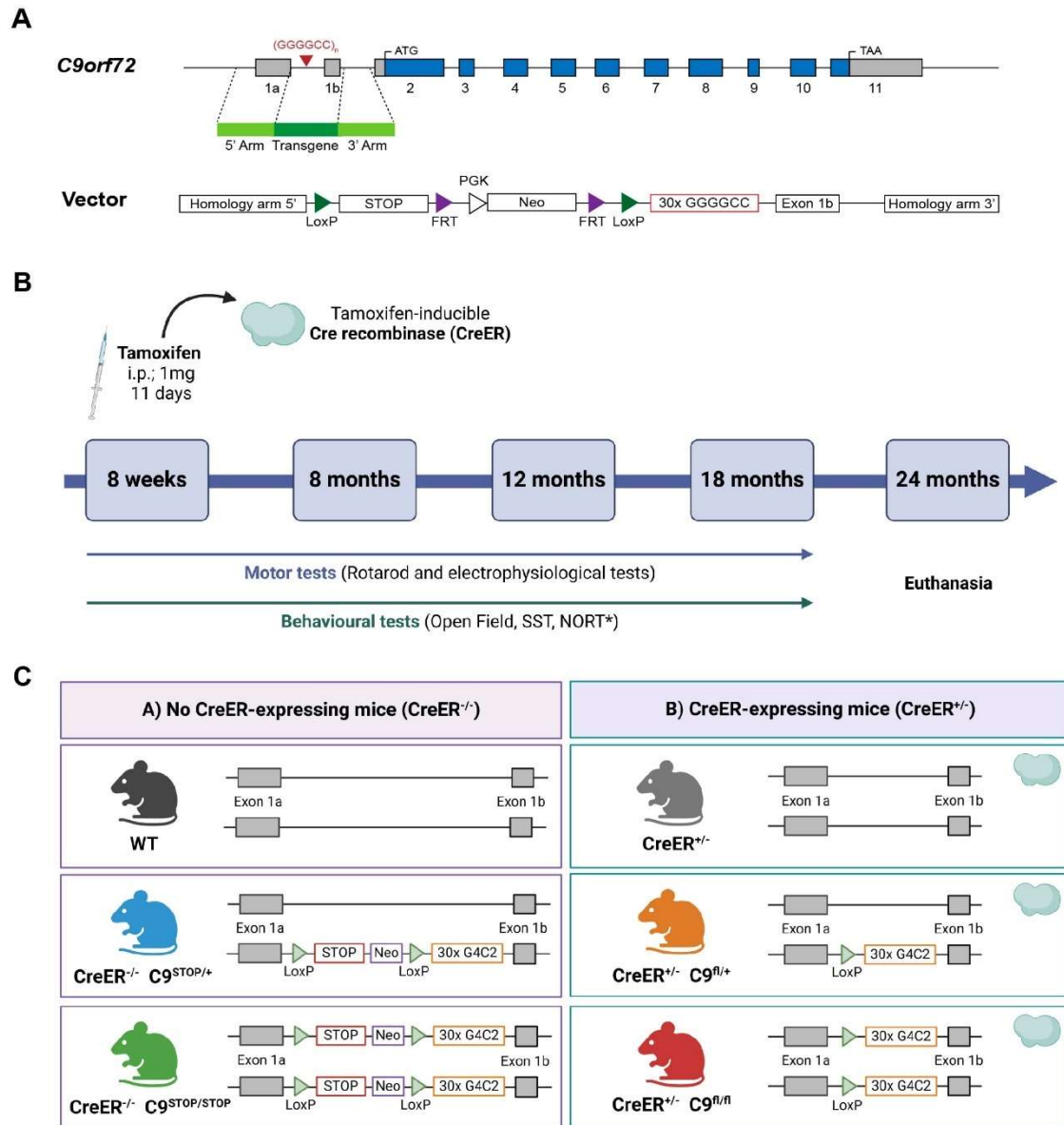


**Figure 19. Study design for the characterization of our *C9orf72* G4C2 HRE knock-in (C9) mouse model.** **A)** Schematic representation of the targeted region of the *C9orf72* gene and the vector used to generate our transgenic C9 mice. PGK: Phosphoglycerate kinase. **B)** Study design for the phenotypic characterization at the motor and behavioural level of C9 mice for two years of follow-up. Created with BioRender.com. i.p.: intraperitoneal administration; SST: Sucrose splash test; NORT: Novel object recognition test. \*NORT was performed at 14 months of age instead of at 12 months as the other tests. **C)** Summary of the experimental groups analysed in this study. Created with BioRender.com.

**C9 animals do not exhibit reduced lifespan and relevant body weight changes**

Since we characterized these C9 animals for the first time and ALS/FTD debuts in adult people, we followed up the animals for two years. First, we evaluated the survival rate of heterozygous and homozygous C9 animals compared to controls. We did not find any significant difference in survival between WT and CreER<sup>-/-</sup> C9<sup>STOP/+</sup> or CreER<sup>-/-</sup> C9<sup>STOP/STOP</sup> mice ( $p=0.5490$ ; Figure 20A) or between CreER<sup>+/-</sup> and CreER<sup>+/-</sup> C9<sup>fl/+</sup> or CreER<sup>+/-</sup> C9<sup>fl/fl</sup> animals ( $p=0.1544$ ; Figure 20B).

ALS mouse models exhibit body weight loss with disease progression due to muscle atrophy (Todd & Petrucelli, 2022). Consequently, we assessed body weight of mice as indicator of animal welfare. We found that mice from all the experimental groups increased their body weight with aging (Figure 20C-F), both in males (Figure 20C,D) and in females (Figure 20E,F). Notably, C9 mice exhibited reduced body weight, statistically significant observed in heterozygous C9 mice, both in CreER<sup>-/-</sup> C9<sup>STOP/+</sup> animals (males and females; Figure 20C,E) and CreER<sup>+/-</sup> C9<sup>fl/+</sup> females, but not in homozygous C9 mice (Figure 20F).

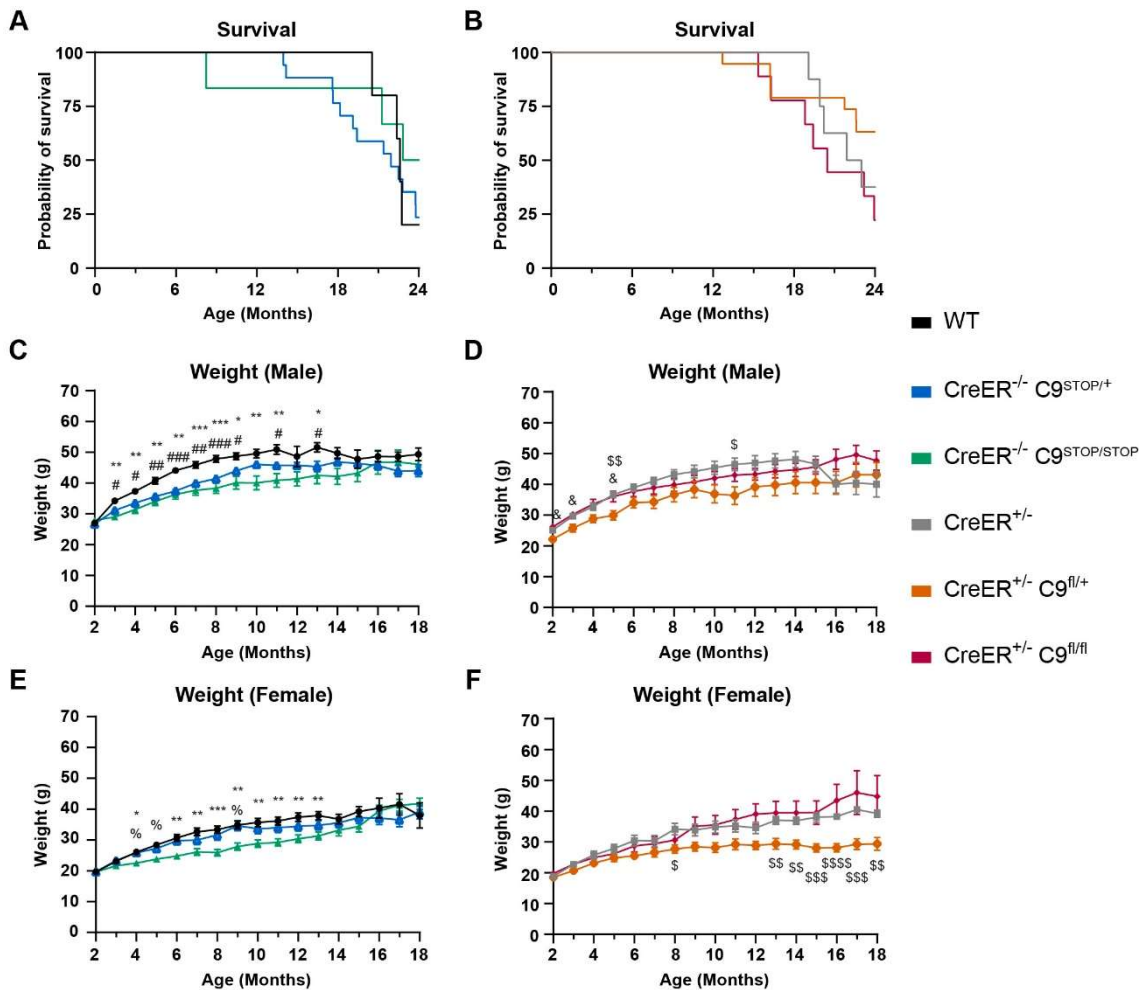


**Figure 20. Follow-up of control, heterozygous and homozygous C9 animals for 2 years. A)** Survival rate of WT (N=5), CreER<sup>-/-</sup> C9<sup>STOP/+</sup> (N=17) and CreER<sup>-/-</sup> C9<sup>STOP/STOP</sup> (N=6) animals for 24 months. **B)** Survival rate of CreER<sup>+/-</sup> (N=8), CreER<sup>+/-</sup> C9<sup>fl/+</sup> (N=19) and CreER<sup>+/-</sup> C9<sup>fl/fl</sup> (N=9) animals for 24 months. **C)** Body weight in WT (N=3-12), CreER<sup>-/-</sup> C9<sup>STOP/+</sup> (N=7-9) and CreER<sup>-/-</sup> C9<sup>STOP/STOP</sup> (N=7-13) males for 18 months. **D)** Body weight in CreER<sup>+/-</sup> (N=3-13), CreER<sup>+/-</sup> C9<sup>fl/+</sup> (N=7-8) and CreER<sup>+/-</sup> C9<sup>fl/fl</sup> (N=8-16) males for 18 months. **E)** Body weight in WT (N=5-16), CreER<sup>-/-</sup> C9<sup>STOP/+</sup> (N=8) and CreER<sup>-/-</sup> C9<sup>STOP/STOP</sup> (N=5-14) females for 18 months. **F)** Body weight in CreER<sup>+/-</sup> (N=5-14), CreER<sup>+/-</sup> C9<sup>fl/+</sup> (N=8-13) and CreER<sup>+/-</sup> C9<sup>fl/fl</sup> (N=3-12) males for 18 months. \*p<0.05, \*\*p<0.01, \*\*\*p<0.001, \*\*\*\*p<0.0001. \*WT vs CreER<sup>-/-</sup> C9<sup>STOP/STOP</sup>, # WT vs CreER<sup>-/-</sup> C9<sup>STOP/+</sup>, % CreER<sup>-/-</sup> C9<sup>STOP/+</sup> vs CreER<sup>-/-</sup> C9<sup>STOP/STOP</sup>, \$ CreER<sup>+/-</sup> vs CreER<sup>+/-</sup> C9<sup>fl/+</sup>, & CreER<sup>+/-</sup> C9<sup>fl/fl</sup> vs CreER<sup>+/-</sup> C9<sup>fl/+</sup>. Mantel-Cox test in **A, B**; Mixed-effects analysis with Bonferroni's post hoc correction in **C, D, E, F**. Data shown as mean ± SEM.



### **C9 mice do not develop an ALS-like phenotype**

Our primary interest was first to assess whether our C9 animals developed motor alterations, compatible with an ALS phenotype. We monitored rotarod performance as the main functional outcome to evaluate motor coordination. We found that control (WT and CreER<sup>+/-</sup>) and homozygous C9 (CreER<sup>-/-</sup> C9<sup>STOP/STOP</sup> and CreER<sup>+/-</sup> C9<sup>fl/fl</sup>) animals remained on the rotating rod for the full test duration of 180s without falling (Figure 21A,B), indicating no motor impairment. A slight decreased in rotarod performance was observed in some groups at 18 months of age, probably due to the high body weight in aged animals. Heterozygous animals (CreER<sup>-/-</sup> C9<sup>STOP/+</sup> and CreER<sup>+/-</sup> C9<sup>fl/+</sup> animals) were excluded from the rotarod analysis, because they were uncooperative. Despite they had the ability to perform well (as shown with the EMG results, Figure 21C-H), they did not execute the rotarod task effectively.

To identify any potential damage in spinal MNs that may not have been detectable in the rotarod assessments, we performed electrophysiological tests to evaluate neuromuscular integrity by measuring the evoked CMAP in the plantar, tibialis anterior, and gastrocnemius muscles. In males, the electrophysiological results (Figure 21C-H) showed no substantial differences in CMAP amplitudes across the time points analysed (2, 8, 12, and 18 months of age) when comparing WT, CreER<sup>-/-</sup> C9<sup>STOP/+</sup>, and CreER<sup>-/-</sup> C9<sup>STOP/STOP</sup> experimental groups (Figure 21C-E), as well as CreER<sup>+/-</sup>, CreER<sup>+/-</sup> C9<sup>fl/+</sup> and CreER<sup>+/-</sup> C9<sup>fl/fl</sup> animals (Figure 21F-H). Similar electrophysiological results were observed in females (Figures 21I-N), with no differences in CMAP amplitudes noted in the plantar (Figure 21I,L), tibialis anterior (Figure 21J,M), and gastrocnemius muscles (Figure 21K,N) across any of the experimental groups analysed as they aged (up to 18 months).

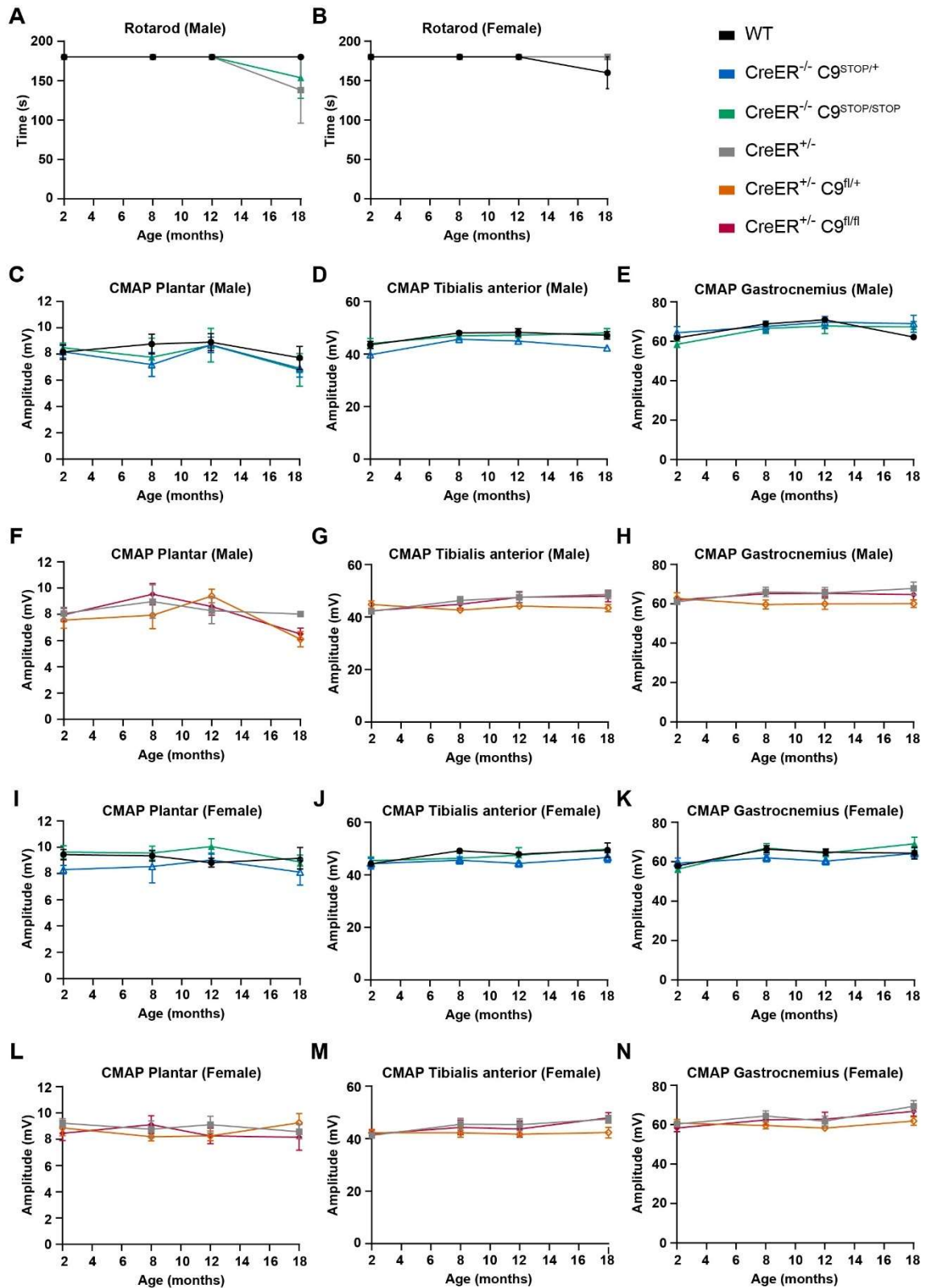


**Figure 21. Motor function evaluation in C9 and control animals for 18 months.** **A)** Rotarod test performance in WT (N=4-12), CreER<sup>+/-</sup> (N=3-8), CreER<sup>-/-</sup> C9<sup>STOP/STOP</sup> (N=6-8) and CreER<sup>+/-</sup> C9<sup>fl/fl</sup> (N=6-16) males. **B)** Rotarod test performance in WT (N=7-16), CreER<sup>+/-</sup> (N=4-8), CreER<sup>-/-</sup> C9<sup>STOP/STOP</sup> (N=6-9) and CreER<sup>+/-</sup> C9<sup>fl/fl</sup> (N=3-6) females. **C)** CMAP amplitudes of the plantar, **D)** tibialis anterior and **E)** gastrocnemius muscles in WT (N=3-12), CreER<sup>-/-</sup> C9<sup>STOP/+</sup> (N=7-9) and CreER<sup>-/-</sup> C9<sup>STOP/STOP</sup> (N=5-8) males. **F)** CMAP amplitudes of the plantar, **G)** tibialis anterior and **H)** gastrocnemius muscles in

CreER<sup>+/-</sup> (N=3-8), CreER<sup>+/-</sup> C9<sup>fl/+</sup> (N=7-8) and CreER<sup>+/-</sup> C9<sup>fl/fl</sup> (N=9-16) males. **I**) CMAP amplitudes of the plantar, **J**) tibialis anterior and **K**) gastrocnemius muscles in WT (N=5-16), CreER<sup>-/-</sup> C9<sup>STOP/+</sup> (N=6-9) and CreER<sup>-/-</sup> C9<sup>STOP/STOP</sup> (N=5-10) females. **L**) CMAP amplitudes of the plantar, **M**) tibialis anterior and **N**) gastrocnemius muscles in CreER<sup>+/-</sup> (N=5-8), CreER<sup>+/-</sup> C9<sup>fl/+</sup> (N=8-11) and CreER<sup>+/-</sup> C9<sup>fl/fl</sup> (N=3-6) females. Mixed-effects analysis with Bonferroni's post hoc correction between groups. Data shown as mean ± SEM.

### Control and homozygous C9 animals display similar ambulatory ability

Next, we aimed to determine whether our C9 mouse model could exhibit some behavioural deficits related with FTD-like symptoms. In the behavioural characterization, we only included control (WT and CreER<sup>+/-</sup>) and homozygous C9 (CreER<sup>-/-</sup> C9<sup>STOP/STOP</sup> and CreER<sup>+/-</sup> C9<sup>fl/fl</sup>) animals, since we reasoned that, in case of any alteration, it would be more evident in homozygotes than in heterozygotes, as the G4C2 repeats affects both copies of the *C9orf72* gene. We first evaluated the general ambulatory ability of the mice in an open field at various timepoints (2, 8, 12 and 18 months of age). While the total distance traversed decreases with ageing, no significant differences were observed between groups (Figure 22A). This trend was consistent when analysing males and females separately (Figure 22B,C), confirming the absence of sex differences. These findings suggest that homozygous C9 (CreER<sup>-/-</sup> C9<sup>STOP/STOP</sup> and CreER<sup>+/-</sup> C9<sup>fl/fl</sup>) animals exhibit similar ambulatory ability than controls.

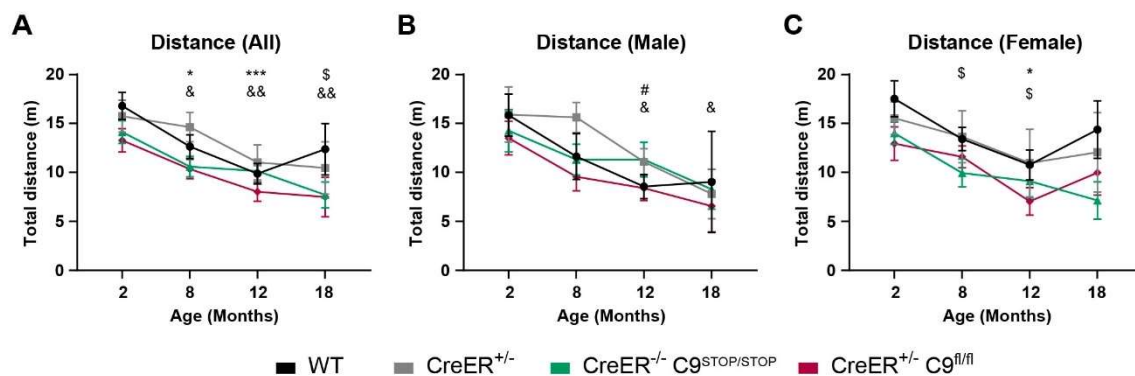


**Figure 22. Open field test in control and homozygous C9 animals for 18 months of age.** **A**) Total ambulatory distance of all WT, CreER<sup>+/-</sup>, CreER<sup>-/-</sup> C9<sup>STOP/STOP</sup> and CreER<sup>+/-</sup> C9<sup>fl/fl</sup> animals in an open field arena. **B**) Total ambulatory distance in males. **C**) Total ambulatory distance in females. N: WT= 3-12M, 5-16F; CreER<sup>+/-</sup>= 3-10M, 5-10F; CreER<sup>-/-</sup> C9<sup>STOP/STOP</sup>= 5-12M, 5-14F; CreER<sup>+/-</sup> C9<sup>fl/fl</sup>= 8-16M, 3-10F. \*p<0.05, \*\*p<0.01, \*\*\*p<0.001. \*WT; # CreER<sup>+/-</sup>; \$ CreER<sup>-/-</sup> C9<sup>STOP/STOP</sup>; & CreER<sup>+/-</sup> C9<sup>fl/fl</sup> (vs 2-month). Mixed-effects analysis with Bonferroni's post hoc correction between groups and versus basal measurements (2-month). Data shown as mean ± SEM.

### C9 animals display anhedonia and depressive-like behaviour

FTD patients present distinct behavioural changes, including apathy, decreased motivation or lack of interest in former hobbies (Ahmed et al., 2017). To assess whether our C9 mouse model developed depressive-like behaviour, we conducted the sucrose splash test. At 2 months of age, we found no significant differences in grooming time between the groups (WT:  $132 \pm 8$ s; CreER<sup>-/-</sup> C9<sup>STOP/STOP</sup>:  $128 \pm 8$ s;  $p > 0.9999$ ; Cre<sup>+/-</sup>:  $128 \pm 10$ s; CreER<sup>+/-</sup> C9<sup>fl/fl</sup>:  $131 \pm 9$ s;  $p > 0.9999$ ) (Figure 23A). However, as the animals aged, C9 mice, both CreER<sup>-/-</sup> C9<sup>STOP/STOP</sup> and CreER<sup>+/-</sup> C9<sup>fl/fl</sup>, spent less time grooming after the sucrose splash compared to WT and CreER<sup>+/-</sup> animals, respectively, suggesting anhedonic behaviour (Figure 23A). This reduction was already apparent at 8 months of age, with C9 animals showing a significant decrease in total grooming time (CreER<sup>-/-</sup> C9<sup>STOP/STOP</sup>:  $78 \pm 8$ s; CreER<sup>+/-</sup> C9<sup>fl/fl</sup>:  $87 \pm 8$ s) compared to their respective controls (WT:  $132 \pm 7$ s,  $p < 0.001$ ; Cre<sup>+/-</sup>:  $138 \pm 10$ s,  $p = 0.0021$ ) and their baseline measurements at 2 months of age (Figure 23A). This trend persisted as the animals continued to age (12 and 18 months).

When separated by sex, differences in the onset of depressive-like behaviour were observed. In males, the reduction in grooming time was particularly evident at 8 months of age, in both C9 groups (CreER<sup>-/-</sup> C9<sup>STOP/STOP</sup> and CreER<sup>+/-</sup> C9<sup>fl/fl</sup>) (Figure 23B). Although female C9 mice also developed an anhedonic phenotype, it emerged at later stages (18 months) compared to males (Figure 23C).

Latency to start grooming is a parameter to evaluate motivational behaviour. At 8 months of age, C9 animals exhibited a significant longer latency to start grooming after the sucrose splash in comparison with control animals (WT:  $15 \pm 2$ s, CreER<sup>-/-</sup> C9<sup>STOP/STOP</sup>:  $43 \pm 8$ s,  $p = 0.0110$ ; Cre<sup>+/-</sup>:  $12 \pm 2$ s, CreER<sup>+/-</sup> C9<sup>fl/fl</sup>:  $22 \pm 3$ s,  $p = 0.0425$ ) at the age of 8 months. (Figure 23D). However, this was a transient observation, as no differences were detected at 12 and 18 months of age. A similar pattern emerged when males and females were analysed separately over 18 months. Overall, these results indicate that C9 animals exhibit anhedonia and depressive-like behaviour.

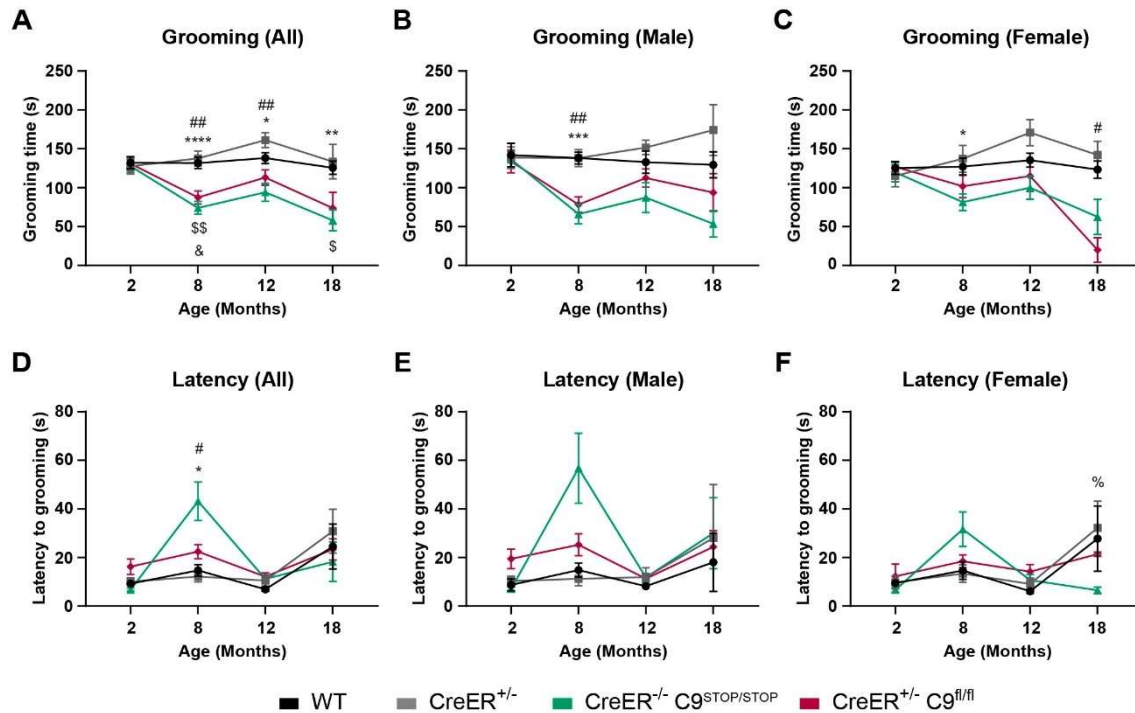


**Figure 23. Sucrose splash test in control and homozygous C9 animals for 18 months of age. A)** Total grooming time in all WT, CreER<sup>+/-</sup>, CreER<sup>-/-</sup> C9<sup>STOP/STOP</sup> and CreER<sup>+/-</sup> C9<sup>fl/fl</sup> animals. **B)** Total grooming time males. **C)** Total grooming time in females. **D)** Latency to start grooming behaviour in all WT, CreER<sup>+/-</sup>, CreER<sup>-/-</sup> C9<sup>STOP/STOP</sup> and CreER<sup>+/-</sup> C9<sup>fl/fl</sup> animals. **E)** Latency to start grooming behaviour in males. **F)** Latency to start grooming behaviour in females. N: WT= 2-13M, 4-18F; CreER<sup>+/-</sup>= 2-10M, 4-9F; CreER<sup>-/-</sup> C9<sup>STOP/STOP</sup>= 4-12M, 4-13F; CreER<sup>+/-</sup> C9<sup>fl/fl</sup>= 6-16M, 3-10F. \*p<0.05, \*\*p<0.01, \*\*\*p<0.001, \*\*\*\*p<0.0001. \*WT vs CreER<sup>-/-</sup> C9<sup>STOP/STOP</sup>; # CreER<sup>+/-</sup> vs CreER<sup>+/-</sup> C9<sup>fl/fl</sup>; % CreER<sup>-/-</sup> C9<sup>STOP/STOP</sup> vs CreER<sup>+/-</sup> C9<sup>fl/fl</sup>; \$ CreER<sup>-/-</sup> C9<sup>STOP/STOP</sup> (vs 2-month); & CreER<sup>+/-</sup> C9<sup>fl/fl</sup> (vs 2-month). Mixed-effects analysis with Bonferroni's post hoc correction between groups and versus basal measurements (2-month). Data shown as mean ± SEM.

### Aged C9 animals do not exhibit anxiety-like behaviour

Some of the reported C9orf72 mouse models and FTD patients have some anxiety-related symptoms (Ahmed et al., 2017). The anxiety-like behaviour was screened in our homozygous C9 animals and controls by measuring the time spent in the central area of the open field. The tendency to remain close to the walls, the so-called thigmotaxis, is an anxiety index in mice (Seibenhener & Wooten, 2015). WT and CreER<sup>-/-</sup> C9<sup>STOP/STOP</sup> animals and CreER<sup>+/-</sup> and CreER<sup>+/-</sup> C9orf72<sup>fl/fl</sup> animals spent comparable time in the inner area in all the timepoints tested (Figure 24A). Similarly, we did not find differences between the experimental groups when studied males (Figure 24B) and females (Figure 24C) separately. Thus, these results indicate that our C9 mouse model do not acquire anxiety-like behaviour with ageing.

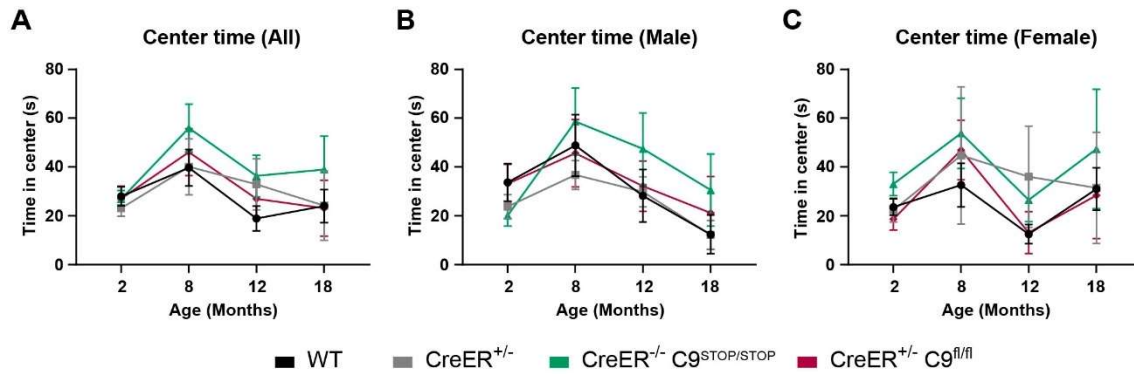


**Figure 24. Anxiety assessment in control and homozygous C9 animals for 18 months of age. A)** Time spent in the central area of all WT, CreER<sup>+/-</sup>, CreER<sup>-/-</sup> C9<sup>STOP/STOP</sup> and CreER<sup>+/-</sup> C9<sup>fl/fl</sup> animals in an open field arena. **B)** Time spent in the central area in males. **C)** Time spent in the central area in females. N: WT= 3-11M, 5-16F; CreER<sup>+/-</sup>= 3-10M, 5-9F; CreER<sup>-/-</sup> C9<sup>STOP/STOP</sup>= 5-10M, 5-11F; CreER<sup>+/-</sup> C9<sup>fl/fl</sup>= 8-11M, 3-8F. Mixed-effects analysis with Bonferroni's post hoc correction between groups and versus basal measurements (2-month). Data shown as mean ± SEM.

### Aged C9 animals exhibit memory decline

Memory dysfunction is a feature of some FTD variants and has been recapitulated in some FTD mouse models (Ahmed et al., 2017). Therefore, we investigated whether our C9 model have also alterations in this type of memory. To assess this, we performed NORT with a retention period of 24h, which evaluates recognition memory by measuring rodent's spontaneous preference for novelty.

First, we performed NORT in young adult 2-months-old animals as basal measurements. In the familiarization day (2<sup>nd</sup> day of test), we did not observe differences in the total exploration time among controls (WT and CreER<sup>+/-</sup>) and C9 animals (CreER<sup>-/-</sup> C9<sup>STOP/STOP</sup> and CreER<sup>+/-</sup> C9<sup>fl/fl</sup>) (Figure 25A). No sex differences were found regarding total exploration time at this age (Figure 25B). As expected, since both objects (A1 and A2) are identical in the familiarization session, the fraction of time exploring each object was equal (fraction≈0.5) in all the experimental groups (Figure 25C), meaning that there is not preference for any object. Same results were observed when analysed by sex (Figure 25D,E). In the testing day (3<sup>rd</sup> day of test), WT, CreER<sup>+/-</sup>, CreER<sup>-/-</sup> C9<sup>STOP/STOP</sup> and CreER<sup>+/-</sup> C9<sup>fl/fl</sup> animals exhibited similar total exploration time (Figure 25F) and not sex differences were observed, although CreER<sup>+/-</sup> C9<sup>fl/fl</sup> females tended to explore less than CreER<sup>+/-</sup> C9<sup>fl/fl</sup> males (p=0.0701) (Figure 25G). As expected, 2-months-old controls (WT and CreER<sup>+/-</sup>) and C9 animals (CreER<sup>-/-</sup> C9<sup>STOP/STOP</sup> and CreER<sup>+/-</sup> C9<sup>fl/fl</sup>) had a preference



for the novel object, as the time fraction exploring it was significantly higher than the familiar one in all the groups (Figure 25H) and per sex (Figure 25I,J). Overall, these results indicate that controls (WT and CreER<sup>+/-</sup>) and C9 animals (CreER<sup>-/-</sup> C9<sup>STOP/STOP</sup> and CreER<sup>+/-</sup> C9<sup>fl/fl</sup>) display proper episodic memory at 2 months of age.

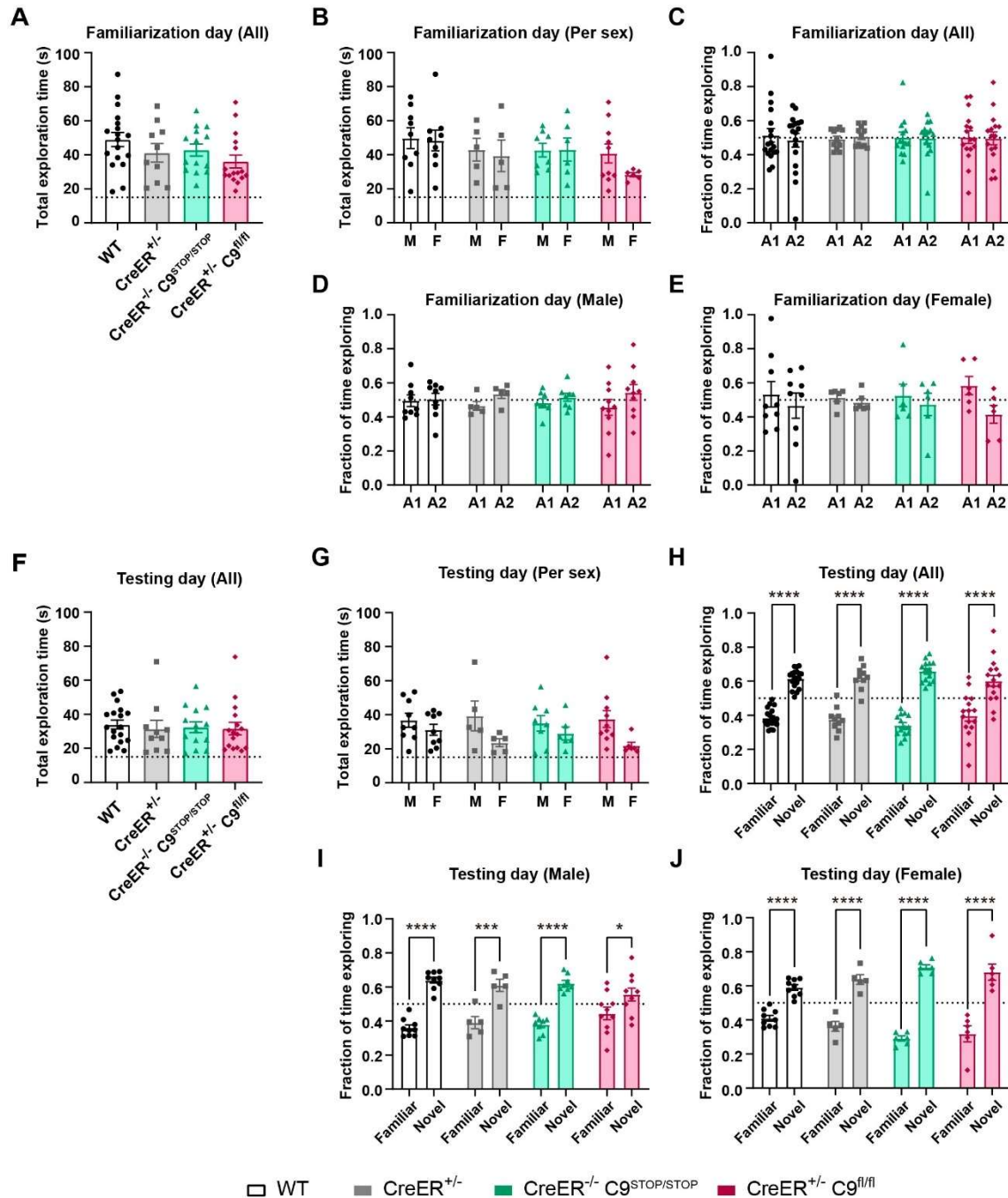


**Figure 25. NOR in control and homozygous C9 animals at 2 months of age.** **A)** Total exploration time of WT, CreER<sup>+/-</sup>, CreER<sup>-/-</sup> C9<sup>STOP/STOP</sup> and CreER<sup>+/-</sup> C9<sup>fl/fl</sup> animals in the familiarization session (Day 2), and **B)** distributed per sex. **C)** Fraction of time exploring A1 and A2 objects (A1=A2) of WT, CreER<sup>+/-</sup>, CreER<sup>-/-</sup> C9<sup>STOP/STOP</sup> and CreER<sup>+/-</sup> C9<sup>fl/fl</sup> animals in the familiarization session (Day 2); **D)** in males and **E)** females. **F)** Total exploration time of WT, CreER<sup>+/-</sup>, CreER<sup>-/-</sup> C9<sup>STOP/STOP</sup> and CreER<sup>+/-</sup> C9<sup>fl/fl</sup> animals in the testing session (Day 3), and **G)** distributed per sex. **H)** Fraction of time exploring

familial and novel objects of WT, CreER<sup>+/-</sup>, CreER<sup>-/-</sup> C9<sup>STOP/STOP</sup> and CreER<sup>+/-</sup> C9<sup>fl/fl</sup> animals in the testing session (Day 3); **I** in males and **J** females. N: WT= 18 (9M, 9F); CreER<sup>+/-</sup>= 10 (5M, 5F); CreER<sup>-/-</sup> C9<sup>STOP/STOP</sup>= 14 (8M, 6F); CreER<sup>+/-</sup> C9<sup>fl/fl</sup>= 16 (10M, 6F). \*p<0.05, \*\*\*p<0.001, \*\*\*\*p<0.0001. Kruskal-Wallis test with Dunn's multiple comparisons in **A** and **F**; Two-way ANOVA with Bonferroni's post hoc correction in **B, C, D, E, G, H, I, J**. Data shown as mean ± SEM. M: Male; F: Female.

We also evaluated episodic memory by NORT in 8-months-old animals, an age range considered to be between mature adult and middle-aged (Flurkey et al., 2007). No statistical differences were observed in the total exploration time between the control groups (WT, CreER<sup>+/-</sup>) and C9 (CreER<sup>-/-</sup> C9<sup>STOP/STOP</sup> and CreER<sup>+/-</sup> C9<sup>fl/fl</sup>) during the familiarization (Figure 26A) and testing sessions (Figure 26F). Additionally, not sex differences were found within each group during familiarization (Figure 26B) or testing session (Figure 26G). As seen in 2-months-old animals, WT, CreER<sup>+/-</sup>, CreER<sup>-/-</sup> C9<sup>STOP/STOP</sup> and CreER<sup>+/-</sup> C9<sup>fl/fl</sup> animals spent similar amounts of time exploring identical A1 and A2 objects during familiarization (Figure 26C). However, when analysed per sex, CreER<sup>+/-</sup> C9<sup>fl/fl</sup> males showed a preference for A1 object in (Figure 26D) while CreER<sup>+/-</sup> C9<sup>fl/fl</sup> females preferred object A2 (Figure 26E). In the testing session, control mice (WT, CreER<sup>+/-</sup>) and CreER<sup>-/-</sup> C9<sup>STOP/STOP</sup> animals showed significant preference for the novel object, but this was not observed in CreER<sup>+/-</sup> C9<sup>fl/fl</sup> mice (Figure 26H). Interestingly, all 8-months-old females demonstrated significant novel object discrimination, indicating intact episodic memory (Figure 26J). In contrast, males did not show this ability, with only CreER<sup>+/-</sup> males significantly preferring the novel object compared to WT, CreER<sup>-/-</sup> C9<sup>STOP/STOP</sup> and CreER<sup>+/-</sup> C9<sup>fl/fl</sup> males (Figure 26I).



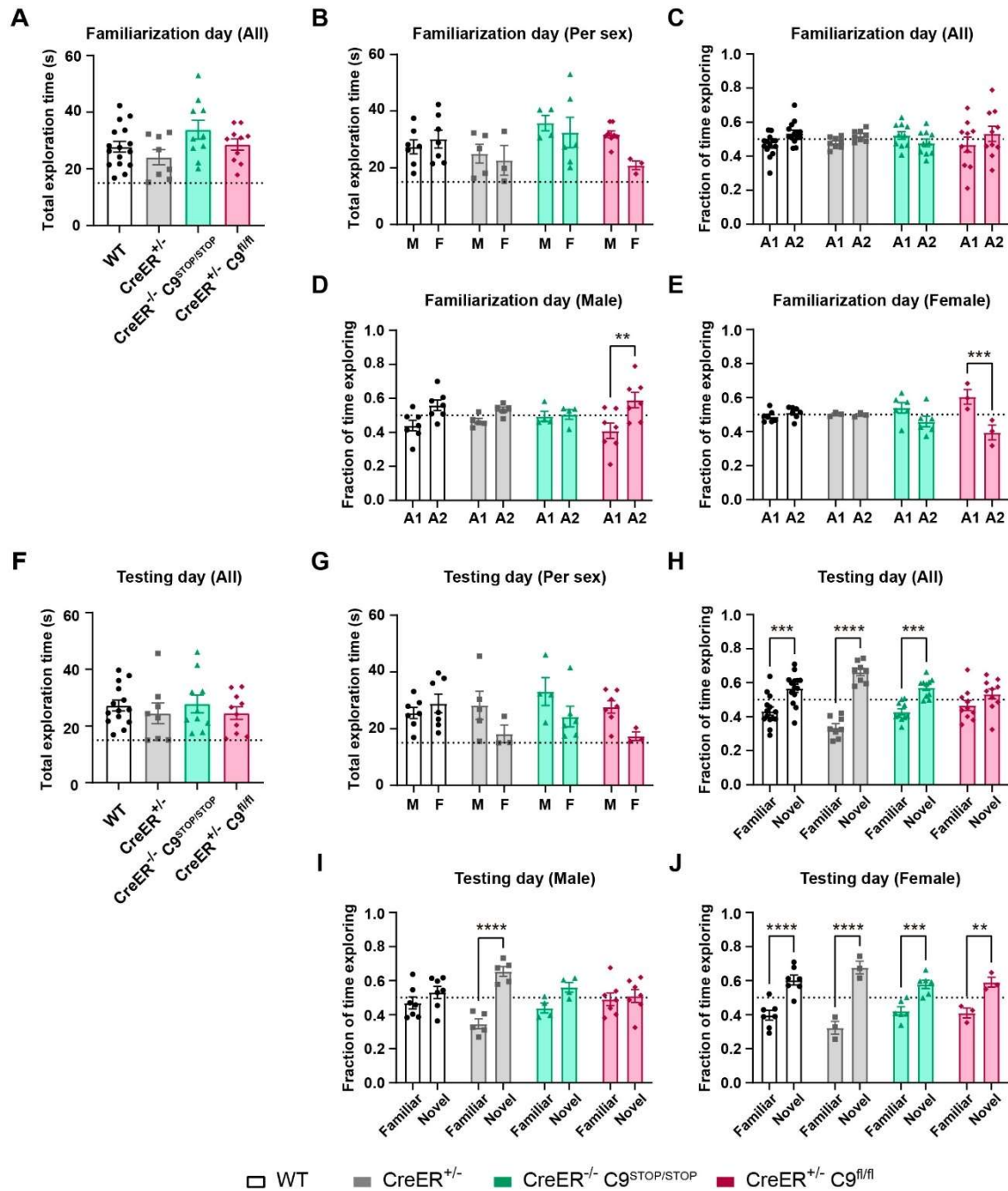


**Figure 26. NOR in control and homozygous C9 animals at 8 months of age.** **A)** Total exploration time of WT, CreER<sup>+/-</sup>, CreER<sup>-/-</sup> C9<sup>STOP/STOP</sup> and CreER<sup>+/-</sup> C9<sup>fl/fl</sup> animals in the familiarization session (Day 2), and **B)** distributed per sex. **C)** Fraction of time exploring A1 and A2 objects (A1=A2) of WT, CreER<sup>+/-</sup>, CreER<sup>-/-</sup> C9<sup>STOP/STOP</sup> and CreER<sup>+/-</sup> C9<sup>fl/fl</sup> animals in the familiarization session (Day 2); **D)** in males and **E)** females. **F)** Total exploration time of WT, CreER<sup>+/-</sup>, CreER<sup>-/-</sup> C9<sup>STOP/STOP</sup> and CreER<sup>+/-</sup> C9<sup>fl/fl</sup> animals in the testing session (Day 3), and **G)** distributed per sex. **H)** Fraction of time exploring familiar and novel objects of WT, CreER<sup>+/-</sup>, CreER<sup>-/-</sup> C9<sup>STOP/STOP</sup> and CreER<sup>+/-</sup> C9<sup>fl/fl</sup> animals in the testing session (Day 3); **I)** in males and **J)** females. N: WT= 14 (7M, 7F); CreER<sup>+/-</sup>= 8 (5M, 3F); CreER<sup>-/-</sup> C9<sup>STOP/STOP</sup>= 10 (4M, 6F); CreER<sup>+/-</sup> C9<sup>fl/fl</sup>= 10 (7M, 3F). \*\*p<0.01, \*\*\*p<0.001, \*\*\*\*p<0.0001. One-way ANOVA with Bonferroni's post hoc correction in **A** and **F**; Two-way ANOVA with Bonferroni's post hoc correction in **B, C, D, E, G, H, I, J**. Data shown as mean ± SEM. M: Male; F: Female.

Next, we focused on episodic memory of middle-aged 14-months-old C9 animals (Flurkey et al., 2007). We did not observe significant differences in the total exploration time between control (WT, CreER<sup>+/-</sup>) and C9 (CreER<sup>-/-</sup> C9<sup>STOP/STOP</sup> and CreER<sup>+/-</sup> C9<sup>fl/fl</sup>) animals during both familiarization (Figure 27A) and testing (Figure 27F) sessions. Nevertheless, CreER<sup>-/-</sup> C9<sup>STOP/STOP</sup> animals showed a trend toward less exploration compared to their WT control animals ( $p=0.0711$ ) in the familiarization session (Figure 27A). No sex differences were noted for this parameter (Figure 27B, G). In the familiarization session, when animals were exposed to two identical objects (A1 and A2), all groups spent an equal amount of time on each object (fraction  $\approx 0.5$ ) (Figure 27C), with no significant sex differences (Figure 27D,E). Interestingly, control animals (WT and CreER<sup>+/-</sup>) exhibited a significant preference for the novel object over the familiar one in the testing session, while C9 animals (CreER<sup>-/-</sup> C9<sup>STOP/STOP</sup> and CreER<sup>+/-</sup> C9<sup>fl/fl</sup>) were unable to discriminate between the novel and familiar objects (Figure 27H), indicating impairments in memory. When analysed by sex, control females showed a clear preference for the novel object, while C9 females did not (Figure 27J). Similar to 8 months of age, CreER<sup>-/-</sup> males displayed a preference for the novel object, while this was not observed in WT and C9 males (Figure 27I).

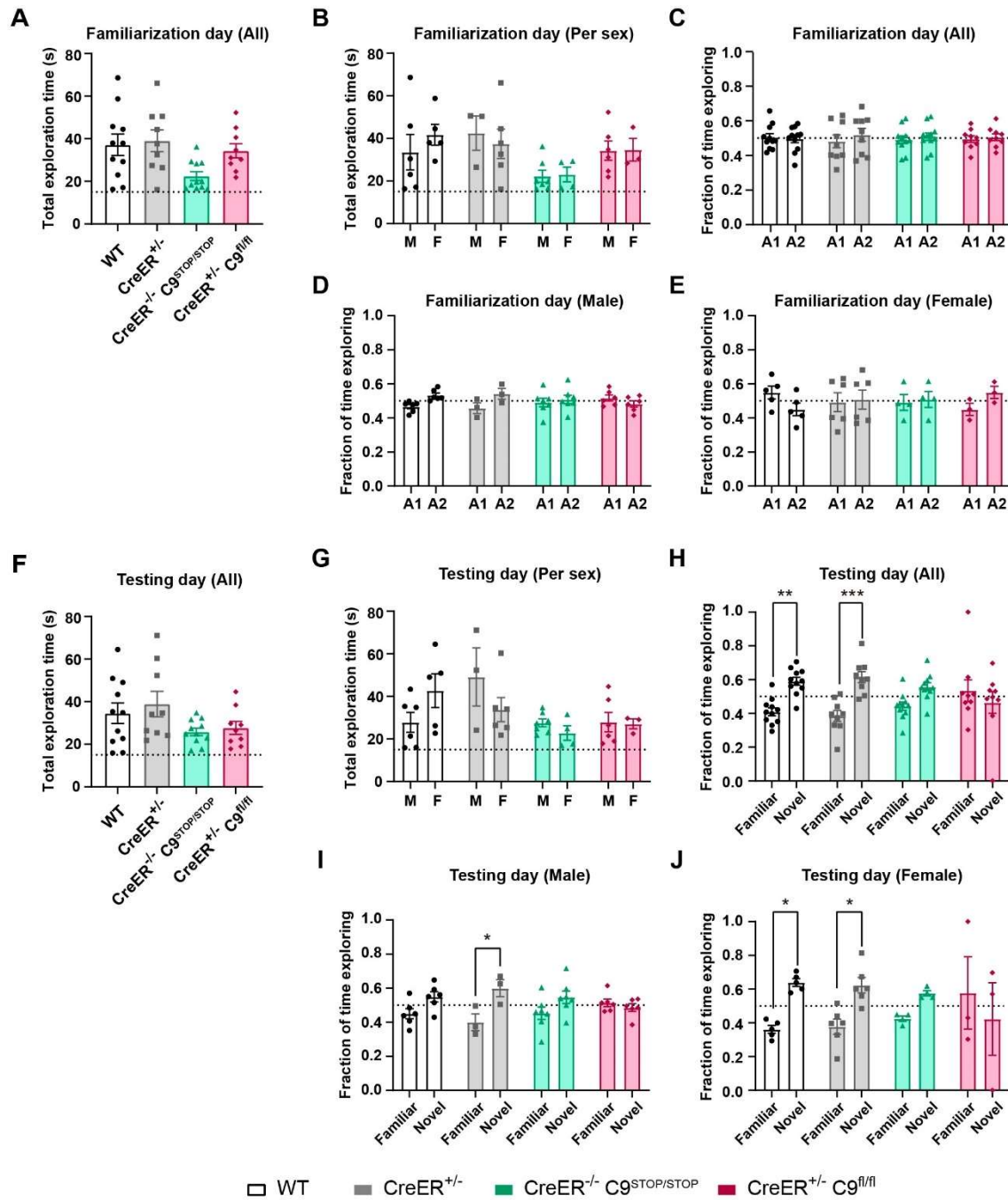


**Figure 27. NORT in control and homozygous C9 animals at 14 months of age.** **A)** Total exploration time of WT, CreER<sup>+/-</sup>, CreER<sup>-/-</sup> C9<sup>STOP/STOP</sup> and CreER<sup>+/-</sup> C9<sup>fl/fl</sup> animals in the familiarization session (Day 2), and **B)** distributed per sex. **C)** Fraction of time exploring A1 and A2 objects (A1=A2) of WT, CreER<sup>+/-</sup>, CreER<sup>-/-</sup> C9<sup>STOP/STOP</sup> and CreER<sup>+/-</sup> C9<sup>fl/fl</sup> animals in the familiarization session (Day 2); **D)** in males and **E)** females. **F)** Total exploration time of WT, CreER<sup>+/-</sup>, CreER<sup>-/-</sup> C9<sup>STOP/STOP</sup> and CreER<sup>+/-</sup> C9<sup>fl/fl</sup> animals in the testing session (Day 3), and **G)** distributed per sex. **H)** Fraction of time exploring familiar and novel objects of WT, CreER<sup>+/-</sup>, CreER<sup>-/-</sup> C9<sup>STOP/STOP</sup> and CreER<sup>+/-</sup> C9<sup>fl/fl</sup> animals in the testing session (Day 3); **I)** in males and **J)** females. N: WT= 11 (6M, 5F); CreER<sup>+/-</sup>= 9 (3M, 6F); CreER<sup>-/-</sup> C9<sup>STOP/STOP</sup>= 11 (7M, 4F); CreER<sup>+/-</sup> C9<sup>fl/fl</sup>= 9 (6M, 3F). \*p<0.05, \*\*p<0.01; \*\*\*p<0.001. Kruskal-Wallis test with Dunn's multiple comparisons in **A**; One-way ANOVA with Bonferroni's post hoc correction in **F**; Two-way ANOVA with Bonferroni's post hoc correction in **B, C, D, E, G, H, I, J**. Data shown as mean ± SEM. M: Male; F: Female.

Finally, as preliminary results, we performed NORT on old 18-months-old animals (Flurkey et al., 2007). Control (WT and CreER<sup>+/-</sup>) and C9 (CreER<sup>-/-</sup> C9<sup>STOP/STOP</sup> and CreER<sup>+/-</sup> C9<sup>fl/fl</sup>) animals spent similar amount of time exploring objects during the familiarization (Figure 28A) and testing sessions (Figure 28C). On the second day, all the groups spent comparable time fraction exploring A1 and A2 objects, although WT mice showed a trend towards spending more time with the A2 object ( $p=0.0907$ ) (Figure 28B). In the testing, CreER<sup>-/-</sup> C9<sup>STOP/STOP</sup> and CreER<sup>+/-</sup> C9<sup>fl/fl</sup> animals did not exhibit a preference for the novel object, unlike WT mice (Figure 28D). CreER<sup>+/-</sup> animals also showed a trend towards a preference for the novel object, but this was not significant. Overall, consistent with the results from 14-month-old animals, these findings suggest that 18-month-old C9 animals may also exhibit memory impairments.

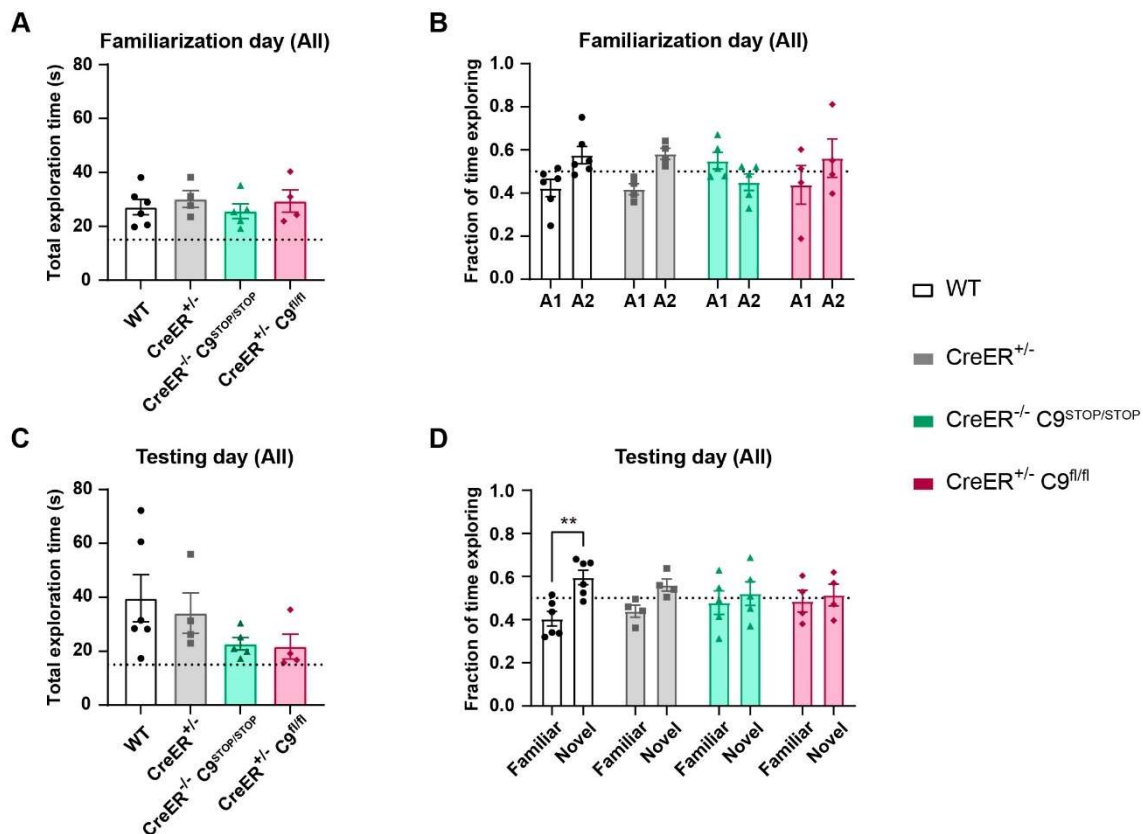


**Figure 28. NORT in control and homozygous C9 animals at 18 months of age. A)** Total exploration time of WT, CreER<sup>+/-</sup>, CreER<sup>-/-</sup> C9<sup>STOP/STOP</sup> and CreER<sup>+/-</sup> C9<sup>fl/fl</sup> animals in the familiarization session (Day 2). **B)** Fraction of time exploring A1 and A2 objects (A1=A2) of WT, CreER<sup>+/-</sup>, CreER<sup>-/-</sup> C9<sup>STOP/STOP</sup> and CreER<sup>+/-</sup> C9<sup>fl/fl</sup> animals in the familiarization session (Day 2). **C)** Total exploration time of WT, CreER<sup>+/-</sup>, CreER<sup>-/-</sup> C9<sup>STOP/STOP</sup> and CreER<sup>+/-</sup> C9<sup>fl/fl</sup> animals in the testing session (Day 3). **D)** Fraction of time exploring familiar and novel objects of WT, CreER<sup>+/-</sup>, CreER<sup>-/-</sup> C9<sup>STOP/STOP</sup> and CreER<sup>+/-</sup> C9<sup>fl/fl</sup> animals in the testing session (Day 3). N: WT= 6 (3M, 3F); CreER<sup>+/-</sup>= 4 (2M, 2F); CreER<sup>-/-</sup>

C9<sup>STOP/STOP</sup>= 5 (2M, 3F); CreER<sup>+/-</sup> C9<sup>fl/fl</sup>= 4 (2M, 2F). \*\*p<0.01. One-way ANOVA with Bonferroni's post hoc correction in **A**; Kruskal-Wallis test with Dunn's multiple comparisons in **C**; Two-way ANOVA with Bonferroni's post hoc correction in **B** and **D**. Data shown as mean ± SEM.

## VII. Discussion

---



ALS field faces an urgent need to find new experimental models to fully elucidate neuronal and non-neuronal mechanisms that lead to MN degeneration and to evaluate new therapeutical approaches. This need is partially responsible for the absence of effective therapies for ALS as findings from animal models have not reliably translated to clinical success. Until recently, most clinical trials included sALS and fALS patients, carriers for distinct mutations, despite relying on data obtained from a single animal model, predominantly the most widely used SOD1<sup>G93A</sup> mouse model (Mead et al., 2023). In this doctoral thesis, we pretend to address this gap in the ALS field. On one hand, we tackled the limitations of mouse microglia, moving to a more human-based microglial approach by studying ALS iPSC-derived microglia *in vitro*, and then by generating an *in vivo* model by xenotransplanting human microglia in the mouse spinal cord. On the other hand, we faced the lack of a C9orf72 ALS/FTD mouse model that fully recapitulates clinical signs and histopathological features.

## Human SOD1<sup>G93A</sup> ALS microglia

---

Among non-neuronal cells involved in ALS physiopathology, we focused our interest on microglial cells. Several studies support both neurotoxic and neuroprotective roles during the disease course in several ALS mouse models (Beers et al., 2006; Boillée et al., 2006; Chiu et al., 2013; Clarke & Patani, 2020; Spiller et al., 2018; You et al., 2023). Besides, mutations in ALS-related genes, such as *C9ORF72* (Banerjee et al., 2023; Lorenzini et al., 2023; Vahsen et al., 2023), *PFN1* (Funes et al., 2024), *FUS* (Kerk et al., 2022), as well as sALS microglia (Noh et al., 2023; Quek et al., 2022), seem to show altered physiological functions in human ALS iPSC-derived microglia. Although the gold standard animal model in ALS field is the SOD1<sup>G93A</sup> mouse, an extensive study of the contribution of mutant SOD1 on human microglial functioning has not been reported.

To address this limitation, we engineered human ESC to introduce the G93A mutation in the *SOD1* gene using CRISPR/Cas9 technology. Although most SOD1 mutations found in ALS patients, including G93A, are usually heterozygous, with only a few exceptions being homozygous variants (e.g. L84F, N86S, D90A, L117V, L126S, L144S, G27delGGACCA) (Gagliardi et al., 2022; Saccon et al., 2013), we opted



to use a homozygous SOD1<sup>G93A</sup> cell line. This approach was chosen because it is likely to cause greater cellular dysfunction than heterozygous SOD1<sup>G93A</sup> cell line. Additionally, CRISPR/Cas9 gene editing allowed us to have the control isogenic cell line, which shares the same genetic background except for this point mutation of interest. This allowed us to assess the impact of mutant SOD1 in the human genetic background, accounting for both known and unknown genetic modifiers.

Most studies investigating the impact of mutant SOD1<sup>G93A</sup> on microglial phenotype have been performed in rodent models that overexpress the mutant human SOD1<sup>G93A</sup> gene (Beers et al., 2006; Boillée et al., 2006; Chiu et al., 2013; Liao et al., 2012; Y. Liu et al., 2009; Vaz et al., 2019; Weydt et al., 2004; Q. Xiao et al., 2007). However, this may not provide the most appropriate experimental setting, as SOD1<sup>G93A</sup> in these models is often expressed at levels up to 25 times higher than endogenous murine SOD1, making it non-physiological (Fisher et al., 2023; Jonsson et al., 2006). As a result, the phenotype observed in SOD1<sup>G93A</sup> mouse model may not fully represent the disease as seen in ALS patients, who carry only a single copy of the mutant *SOD1* gene. It is debated that the phenotypic features observed in the SOD1<sup>G93A</sup> mouse model may result from a high overexpression of SOD1 protein, rather than being solely attributed to the SOD1<sup>G93A</sup> mutation itself (Shibata, 2001). In fact, even overexpression of wild-type human SOD1 in mice results in axonopathy and mitochondrial vacuolation (Jaarsma et al., 2001) and can cause ALS-like disease when expressed at similar levels as mutant SOD1<sup>G93A</sup> in SOD1<sup>G93A</sup> mice (Graffmo et al., 2013). Thus, our human ESC line expresses mutant SOD1 at more disease-relevant levels as seen in ALS patients, overcoming this genetic artifact.

Besides these concerns regarding SOD1, species differences between mouse and human have been described to be relevant in the microglia field. For instance, a substantial portion of human genes do not have a clear ortholog in the mouse genome, as observed in some AD-related risk microglial genes (Hasselmann & Blurton-Jones, 2020; Mancuso et al., 2019). Furthermore, differential gene expression have been detected in mouse and human microglia regarding interesting pathways in ALS pathology, such as inflammatory-related genes, or some neurodegenerative disease-associated genes (Galatro et al., 2017; Geirsdottir et al., 2019; Gosselin et al., 2017; Lloyd et al., 2024). Importantly, these differences

become more pronounced with aging (Galatro et al., 2017). Overall, considering these limitations, we shifted our focus to a more human-based model using human stem cell-derived microglia.

The pathological phenotype caused by mutant SOD1 in human relevant ALS cell-types have been described in SOD1<sup>G93A</sup> iPSC-derived MNs, which showed proteinopathy, axonopathy, synaptic alterations and functional deficits (B. W. Kim et al., 2020), and SOD1<sup>A4V</sup> and SOD1<sup>D90A</sup> iPSC-derived astrocytes, which display a reactive transformation phenotype with nuclear oxidative stress and DNA damage (Soubannier et al., 2024). However, to the best of our knowledge, only one study has investigated human SOD1 iPSC-derived microglia, specifically with the A4V mutation (Allison & Ebert, 2024), though this study focused primarily on astrocyte-microglia interactions rather than the direct effects of mutant SOD1 on microglial function. For this reason, we chose to investigate the relevance of SOD1<sup>G93A</sup> to key physiological functions in human microglial cells.

Given the relatively recent discovery of microglial ontogeny (Ginhoux et al., 2010), microglial differentiation protocols from human iPSC started to emerge from 2016. However, this is a field in constant evolution, and there is still no consensus on the most reliable method to obtain human microglia (Washer et al., 2022). Focusing on the last stages in the protocol, we used IL-34 and GM-CSF as the main cytokines to produce microglial cells (Haenseler et al., 2017). However, recent studies have shown that TGF $\beta$  is relevant for proper microglial maturation and microglial identity in the adult CNS (Butovsky et al., 2014; Zöllner et al., 2018). Hence, we do believe that incorporating TGF- $\beta$  and M-CSF, as outlined in the systematic study by Washer et al. (2022), will enhance our microglial differentiation protocol.

### **Inflammatory phenotype in *in vitro* SOD1<sup>G93A</sup> microglia**

Regarding the cytokine profile of human SOD1<sup>G93A</sup> microglia, we found moderate changes in the cytokine profile in unstimulated state. SOD1<sup>G93A</sup> microglia showed a significant increase of the anti-inflammatory cytokine IL-10, as well as a tendency to exhibit increased levels of the pro-inflammatory IL-1 $\beta$ , which was undetectable in all control microglial cultures but not in these carrying the SOD1

mutation. In contrast, the pro-inflammatory cytokine IL-17A did not show changes in mutant SOD1 microglia.

Previous studies done in SOD1<sup>G93A</sup> mouse microglia under basal conditions showed that these cells display a pro-inflammatory phenotype, with increased production of superoxide, nitrates and nitrites (Beers et al., 2006; Y. Liu et al., 2009; Q. Xiao et al., 2007) and a decrease in production of neurotrophic factors, such as IGF-1 (Q. Xiao et al., 2007). However, how mutant SOD1 affect the cytokine production in unstimulated microglia has been poorly studied with conflicting results. Some studies reported similar TNF $\alpha$  and IL-6 secretion levels between wild-type and mutant SOD1<sup>G93A</sup> mouse microglia (Weydt et al., 2004), while others showed increased expression of pro-inflammatory (TNF $\alpha$ , IL-1 $\beta$ , iNOS) and anti-inflammatory markers (Arg1, SOCS1) in microglia overexpressing human SOD1<sup>G93A</sup>.

Upon activation, microglia release bioactive substances, such as the pro-inflammatory cytokine IL-1 $\beta$  (Burm et al., 2015), whose overproduction has been implicated in pathophysiological conditions characterized by acute and chronic inflammation, including ALS (Olesen et al., 2020; Ren & Torres, 2009). Nevertheless, SOD1<sup>G93A</sup> microglia secreted this cytokine even in unstimulated conditions, suggesting a basal reactive state not observed in control microglia. Indeed, mouse SOD1<sup>G93A</sup> microglia have been shown to express NLRP3 inflammasome components, necessary for a proper maturation IL-1 $\beta$ , including active caspase 1, which can be activated by misfolded SOD1 (Bellezza et al., 2018; Meissner et al., 2010).

On the other hand, IL-17A is a pro-inflammatory cytokine involved in inflammatory and autoimmune diseases, such as multiple sclerosis (Tzartos et al., 2008), inflammatory bowel disease (Fujino et al., 2003) or rheumatoid arthritis (Metawi et al., 2011), among others. In ALS, IL-17A has been detected in the serum of 65% of ALS patients (Fiala et al., 2010). The low levels of IL-17A (found in both control and SOD1<sup>G93A</sup> microglia conditioned medium (detectable in one of the control and SOD1<sup>G93A</sup> microglial cultures) may be due to the fact that IL-17A is primarily produced by circulating and infiltrating immune cells, such as Th17 cells, CD8<sup>+</sup> T cells, and mast cells, rather than by microglia (Fiala et al., 2010). In fact, one study described undetectable IL-17A mRNA levels production in unstimulated wild-type microglia (Kawanokuchi et al., 2008).

Surprisingly, untreated SOD1<sup>G93A</sup> microglia showed an increased production of the anti-inflammatory cytokine IL-10, compared to the control. This does not necessarily imply a polarization towards a more anti-inflammatory microglial phenotype. The IL-10 increase is likely a compensatory mechanism to counterbalance the basal activation in SOD1<sup>G93A</sup> microglia, similar to what is observed after LPS stimulation (Y. Wang et al., 2021). Besides, sALS PBMCs treated with misfolded SOD1 showed increased IL-10 levels alongside pro-inflammatory cytokines (G. Liu et al., 2012). Similarly, *ex vivo* murine SOD1<sup>G93A</sup> microglia (Chiu et al., 2013) and SOD1<sup>G93A</sup> N9 murine microglia cell line (Vaz et al., 2019) co-express neurotoxic and neuroprotective markers, as seen in our unstimulated human SOD1<sup>G93A</sup> microglia.

To our knowledge, no studies have been published on cytokine and chemokine secretion in human mutant SOD1 iPSC-derived microglia, although it has been assessed in other ALS-related mutations. For instance, mutant C9orf72 (Banerjee et al., 2023; Lorenzini et al., 2023), FUS (Kerk et al., 2022), PFN1 (Funes et al., 2024) and sALS microglia (Noh et al., 2023) produced comparable cytokine (IL-1 $\alpha$ , IL-1 $\beta$ , IL-6, IL-8, TNF $\alpha$ , among others) and chemokine (CCL5) levels as controls in unstimulated conditions. In contrast, Vahsen et al., 2023 described an altered cytokine profile in C9orf72-ALS iPSC-derived microglia, reporting upregulation of dipeptidyl peptidase 4 (DPP4) and CXCL1 in the supernatant of basal C9orf72 microglia-MN cocultures compared to healthy microglia-MNs. Quek et al., 2022 observed upregulation of *IL8* and *TFG $\beta$*  mRNA in sALS microglia along with increased IL-8, IL-18 and TNF $\alpha$  protein levels. Nevertheless, IL-10 secretion in basal ALS microglia remains more controversial. While we observed a clear increased IL-10 production in SOD1<sup>G93A</sup> microglia, others described an IL-10 decrease in sALS microglia (Allison et al., 2022), no change in PFN1 microglia (Funes et al., 2024) or a subtle, non-significant, increase in sALS (Quek et al., 2022).

On the other hand, SOD1<sup>G93A</sup> ESC-derived microglia displayed heightened immune response following LPS stimulation, as we observed higher secretion of IL-1 $\beta$ , IL-17A and IL-10, specially during the first 6 hours, compared to LPS-primed control microglia. This is consistent with findings in murine microglia overexpressing SOD1<sup>G93A</sup>, which also showed increased TNF $\alpha$  production despite a

reduction in IL-6 levels upon LPS stimulation (Weydt et al., 2004). Similar exacerbated immune response to pro-inflammatory stimuli has been observed in mutant C9orf72 iPSC-microglia, since LPS exposure resulted in an increased release of pro-inflammatory mediators, such as IL-1 $\beta$  and IL-6 (Banerjee et al., 2023) or MMP-9 (Vahsen et al., 2023), and in sALS microglia, where the response was more pronounced in rapid-progressing than in slow-progressing sALS (Noh et al., 2023). Nevertheless, the microglial inflammation triggered in response to stimulation seems to be dependent on the ALS-causing gene, treatment duration, and type of stimulus. For instance, mutant PFN1 microglia does not exhibit changes in the cytokine profile after 6h- and 24h after LPS stimulation (Funes et al., 2024). Similarly, mutant FUS microglia did not display an exacerbated immune response in response to uridine diphosphate (UDP) or apoptotic MN (Kerk et al., 2022), possibly because these stimuli were not potent enough to trigger a significant response compared to LPS. Interestingly, Lorenzini et al., 2023 observed no difference in the response to LPS between mutant C9orf72 and control microglia, in contrast to findings by Banerjee et al., 2023 and Vahsen et al., 2023. These differences may be explained due to different LPS treatment protocols used. While longer LPS treatments were done in Banerjee et al., 2023 (8h followed by 12h washout) and Vahsen et al., 2023 (48h), the shorter duration of LPS treatment (6h) used by Lorenzini et al., 2023 could not be long enough to elicit detectable differences, at least in microglia carrying the C9orf72 mutation.

An exaggerated microglial response can be noxious and contribute to neuronal damage, as excessive production of pro-inflammatory cytokines and other mediators can lead to neuronal death by either directly by affecting neurons or indirectly through the release of neurotoxic substances by glial cells (Chao et al., 1995; X. Liu & Quan, 2018; Thornton et al., 2006).

### Phagocytosis in *in vitro* SOD1<sup>G93A</sup> microglia

Phagocytosis is an essential process for tissue homeostasis, since it is involved in the removal of apoptotic and necrotic cells (e.g. apoptotic MNs), toxic protein aggregates (e.g. misfolded SOD1) or pathogens. In the CNS, microglia are the most important professional phagocytes (Uribe-Querol & Rosales, 2020). To evaluate whether mutant SOD1 affects microglial phagocytosis, we used pHrodo-conjugated myelin debris which offers a more physiological model than using beads. The pHrodo-labelled myelin allows its detection once internalized in the phagolysosome due to its acidic environment, thereby marking the later stages of phagocytosis (Gómez-López et al., 2021; Uribe-Querol & Rosales, 2020).

In our phagocytosis assay, we observed a reduction in the proportion of pHrodo-positive SOD1<sup>G93A</sup> microglial cells compared to control microglia after 3h of myelin exposure. Besides, when we focused our analysis on phagocytic cells, we also found that phagocytic SOD1<sup>G93A</sup> microglia displayed decreased pHrodo fluorescence intensity compared to phagocytic control microglia. This reduction in the pHrodo signal does not necessarily imply a deficit in phagocytosis capacity caused by the SOD1<sup>G93A</sup> mutation. One possibility is that SOD1<sup>G93A</sup> microglia have an impairment in the early stages of phagocytosis, affecting the internalization of the material to be digested. Alternatively, the reduction in pHrodo could result from increased degradation of the material in the phagolysosomes during the final stage of phagocytosis or by impaired lysosomal acidification.

Literature offers controversial results regarding phagocytosis in mutant SOD1 microglia. *In vitro* studies in a SOD1<sup>G93A</sup>-overexpressing N9 murine microglia cell line showed unaltered capacity to phagocytose beads (Sargsyan et al., 2011) while murine SOD1<sup>G93A</sup> microglia displayed reduced phagocytosis of apoptotic neuronal cells (Sargsyan et al., 2011) and impaired autophagy, which is relevant for proper degradation of the ingested material (Massenzio et al., 2018). To fully elucidate which phagocytosis step is affected, additional experiments are required. For instance, it would be useful to repeat our experiment and quantify pHrodo signal after 48h of washout (e.g. as performed in (Funes et al., 2024)) to determine whether the degradation stage is different between control and SOD1<sup>G93A</sup> microglia.

It has been shown that microglial phagocytosis of perineuronal nets is enhanced in SOD1<sup>G93A</sup> mice compared to wild-type mice, but this is likely due to the activation of microglia as a consequence of the disease (Cheung et al., 2024). This is in line with SOD1<sup>A4V</sup> iPSC-derived microglia, where a trend to show increased phagocytosis of beads was noted when stimulated by LPS (Allison & Ebert, 2024). However, in this study the authors did not compare the phagocytic capacity relative to control microglia. Generally, in resting conditions, phagocytic activity is relatively low, and it is enhanced in reactive microglia to face stimuli (Uribe-Querol & Rosales, 2020). It would be interesting to assess how our SOD1<sup>G93A</sup> ESC-microglia adapt phagocytosis after chronic LPS stimulation. Due to time constraints, this was not done but it will be studied in the future.

When comparing our results with other ALS-related mutations, microglial phagocytic dysfunction seems to be a common feature in most ALS microglia. For instance, mutant C9orf72 and PFN1 iPSC-derived microglia show impaired autophagy, which causes an inefficient degradation (Banerjee et al., 2023; Funes et al., 2024). Additionally, sALS microglia display a deficit in phagocytosis, with greater impairment in rapid-progressing than slow-progressing sALS microglia (Quek et al., 2022), suggesting a link between microglia phagocytosis deficit and disease progression. It is noteworthy to mention that this link is not all always observed, since mutant FUS iPSC-derived microglia have unaltered apoptotic MN phagocytosis (Kerk et al., 2022) and mutant C9orf72-derived microglia show increased A $\beta$  phagocytosis and unaltered synaptoneuroosomes phagocytosis (Lorenzini et al., 2023). Thus, it is likely that the material to be ingested may also influence the ability of ALS microglia to effectively trigger phagocytosis and digestion.

### **Immunometabolism in *in vitro* SOD1<sup>G93A</sup> microglia**

Mitochondrial dysfunction is a well-established early pathogenic mechanism in ALS (Cozzolino et al., 2013; S. Damiano et al., 2020). As a result, energy disturbances have been described in both ALS patients (Dupuis et al., 2011) and SOD1<sup>G93A</sup> mouse models (Dupuis et al., 2004). Mutant SOD1 diminishes the activity of mitochondrial ETC complexes, leading to defective mitochondrial bioenergetics and ATP production in rodent SOD1<sup>G93A</sup> models (Irvin et al., 2015). Thus, we assessed how SOD1<sup>G93A</sup> affected microglia metabolism at baseline conditions. We

observed that SOD1<sup>G93A</sup> microglia showed greater glycolytic metabolism compared to the isogenic control but also showed increased maximal respiration.

Most metabolic studies on SOD1-related ALS have been performed in homogenates obtained from mouse SOD1<sup>G93A</sup> spinal cord and brain (M. Damiano et al., 2006; Igoudjil et al., 2011; Kirkinezos et al., 2005; Mattiazzi et al., 2002; Miquel et al., 2012; Wendt et al., 2002) or muscle fibres (Leclerc et al., 2001). This strategy can combine affected and unaffected regions in ALS pathology, thus reducing the potential detectable changes in mitochondrial activities in the vulnerable areas. To date, cell-specific metabolic effects in ALS have been mainly described in human iPSC-derived MNs, which exhibited hypo-oxidative and hyper-glycolytic metabolism regardless of the ALS cause (SOD1<sup>L144F</sup>, TDP43<sup>G298S</sup>, C9ORF72-HRE and sALS) (Hor et al., 2021; Singh et al., 2021). Similarly, SOD1<sup>G93A</sup> NSC-34 MN-like cells rely on glycolytic metabolism due to reduced ETC activity (Menziés et al., 2002). In this line, metabolic changes in glial cells have been only reported in primary rat SOD1<sup>G93A</sup> astrocytes, which showed impaired mitochondrial respiration with uncoupling of ATP production (Cassina et al., 2008; Miquel et al., 2012). Only one study has described increased maximal respiration by mutant SOD1, and this was done in yeast expressing distinct SOD1 mutations (Bastow et al., 2016). This work demonstrated that expression of mutant SOD1 isoforms in yeast resulted in reduced cell viability, whose toxicity did not correlate with mitochondrial dysfunction or oxidative stress rather on the inability to control central metabolic processes. However, immunometabolism assessment in ALS microglia have not been previously assessed. Considering our contrary results, it may suggest a particular microglial metabolic effect in SOD1-related ALS.

A plausible explanation may be the metabolic preferences in each CNS cell type. In resting conditions, astrocytes rely their metabolism on glycolysis and lactate production, with limited dependence on mitochondrial oxidation (Y. M. Zhang et al., 2023). In contrast, oxidative phosphorylation, which is more efficient than glycolysis in terms of ATP production, is the main energy source to fuel the high metabolic demands in neurons, thus being highly sensitive to any mitochondrial disturbance (Breuer et al., 2013). Regarding microglia metabolism, they are more plastic cells that can utilize both glycolytic and oxidative metabolism (Lynch, 2020).



Although it has been postulated that metabolic reprogramming towards glycolysis occurs in activated pro-inflammatory microglia and oxidative phosphorylation is the main metabolism in the anti-inflammatory state (Amo-Aparicio et al., 2024). A recent study has shown that sustained oxidative phosphorylation is a feature of pro-inflammatory microglia that contributes to the CNS inflammation perpetuation (Peruzzotti-Jametti et al., 2024). Our hypothesis is that mutant SOD1<sup>G93A</sup> microglia have a basal activated state, which imply active aerobic oxidative phosphorylation and to a greater extent, glycolytic metabolism, to support essential phagocytic, migratory and mitotic mechanisms, among others. Mutant SOD1 may exacerbate this metabolic demand as a compensatory mechanism, increasing maximal respiration to produce more energy, potentially as a response to impaired mitochondrial function. This could lead to detrimental consequences, such as excessive ROS generation and oxidation of critical biomolecules, especially if antioxidant defences, like SOD1, are overwhelmed. However, further exploration needs to be done to understand the biological impact of the metabolic alterations observed in SOD1<sup>G93A</sup> microglia.

Some methodological and interpretation issues must be taken into account. On one hand, mitochondrial CO<sub>2</sub> could act as a confounding variable to interpreting ECAR as glycolytic flux, since the entire breakdown of one molecule of glucose through oxidative phosphorylation generates six CO<sub>2</sub> molecules (Divakaruni et al., 2014). In our data, we observed ECAR changes after injection of ETC inhibitors, particularly in the SOD1<sup>G93A</sup> microglia, where ECAR decreased after oligomycin and Rot/AA and an increase following FCCP. If the glycolytic turnover were the main contributor, ECAR values would remain constant or increase after ETC modulators injection. Overall, it may indicate that Krebs cycle activity and coupled mitochondrial respiration likely contributes to the ECAR signal. Thus, to interpretate better the glycolytic results, it would be useful to perform an additional specific glycolysis assay. On the other hand, most published studies describing metabolism in SOD1-related ALS, they used isolated live mitochondria (Cassina et al., 2008; M. Damiano et al., 2006; Igoudjil et al., 2011; Kirkinezos et al., 2005; Mattiazzi et al., 2002; Panov et al., 2011; Wendt et al., 2002; W. Zhao, Varghese, et al., 2012), which is especially useful in *ex vivo* studies from tissues as the quality and yields of mitochondria are appropriate. However, some limitations must be

considered as the isolation process could trigger some artifacts in terms of morphological ultrastructure and mitochondrial subselection. Additionally, isolated mitochondria studies miss cell-intrinsic effects on mitochondrial function (Divakaruni & Jastroch, 2022). In contrast, by conducting studies in intact cells, we preserved the physiological interactions between organelles and signalling pathways, providing a more accurate representation of cellular metabolisms (Divakaruni & Jastroch, 2022).

Microglia reprogram their metabolism from oxidative phosphorylation towards aerobic glycolysis upon activation by a pro-inflammatory stimulus to fulfil the high energy demands, in a similar way as the Warburg effect observed in cancer cells (Amo-Aparicio et al., 2024; Cassina et al., 2021). Hence, we stimulated control and SOD1<sup>G93A</sup> microglia with LPS for 24 hours, known to induce the pro-inflammatory phenotype, to assess how immunometabolism is adapted. Since some species-particularities have been reported in metabolic reprogramming in mouse and human microglia (Sabogal-Guáqueta et al., 2023), we first confirmed that our metabolic profile observed in LPS-control microglia was reproduced in the literature. No detectable OCR changes were detected between basal and LPS-stimulated control microglia, in line with the unchanged oxidative phosphorylation seen in LPS-stimulated human macrophages (Vijayan et al., 2019). Moreover, similar basal ECAR values were observed between untreated and LPS-treated control microglia, in a similar manner to human iPSC-derived microglia (Sabogal-Guáqueta et al., 2023). At baseline measurements, LPS-SOD1<sup>G93A</sup> microglia exhibited decreased oxidative phosphorylation values with a concomitant increased glycolytic metabolism compared to LPS-control microglia. Importantly, in response to oligomycin, a mitochondrial ATP synthase inhibitor, LPS-control microglia showed an increment in ECAR, suggesting an increased glycolytic capacity in line with (Sangineto et al., 2023). Nevertheless, this ECAR increase was not observed in LPS-SOD1<sup>G93A</sup> microglia, suggesting an inability to further enhance glycolysis, likely due to an already high basal glycolytic rate, potentially as a response to SOD1-related pathology.

To assess whether our metabolic findings in basal SOD1<sup>G93A</sup> microglia were intrinsic to mitochondria or were due to changes in mitochondrial biogenesis, we

first tracked live mitochondria with Mitotracker dye. We did not find differences in mitochondrial content between SOD1<sup>G93A</sup> and control microglia either in basal or LPS-stimulation conditions. Thus, this indicates that the increased maximal respiration observed at baseline states is not due to an increment in mitochondrial formation. In contrast with our findings, a qualitative decrease in Mitotracker labelling was visible in primary SOD1<sup>G93A</sup> astrocytes (Cassina et al., 2008).

Mitochondrial ROS, specifically superoxide anion, was quantified with the MitoSOX probe. As expected, SOD1<sup>G93A</sup> microglia showed significant higher superoxide levels, which indicates increased ROS generation or impaired clearance. Increased ROS production has been described extensively as a pathogenic mechanism in MN death (Hardiman et al., 2017; Mead et al., 2023; Park & Yang, 2021), but also in glial cells, including mutant SOD1 astrocytes (Cassina et al., 2008; Soubannier et al., 2024) and microglia (Beers et al., 2006; Y. Liu et al., 2009; Q. Xiao et al., 2007). The linkage between ROS and mitochondrial dysfunction is clear. Mitochondria are the main source of ROS and consequent oxidative stress as a result of mitochondrial dysfunction can affect its functioning. ROS generation also takes place in microglia after adopting the pro-inflammatory phenotype induced by LPS (Hsu & Wen, 2002). LPS-control microglia showed elevated superoxide levels to a similar extent to LPS-stimulated SOD1<sup>G93A</sup>. Interestingly, compared to basal conditions, control microglia increased ROS production upon LPS stimulation, as part of the inflammatory response. Contrarily, SOD1<sup>G93A</sup> microglia did not exhibit any change in ROS levels between basal and stimulated conditions, probably due to the already elevated basal ROS levels. Controlled ROS production is known to be necessary to activate a proper pro-inflammatory signalling pathway, regulate the resolution of inflammatory response and induce the expression of antioxidant proteins. However, excessive ROS production can contribute to exacerbate inflammation and oxidative damage production of pro-inflammatory cytokines (Checa & Aran, 2020), as it may occur in SOD1<sup>G93A</sup> microglia. In this line, we showed that human microglia carrying this mutation produced greater levels of cytokines, further linking impaired metabolism, ROS production and inflammation.

## **Pendant experiments for a complete *in vitro* SOD1<sup>G93A</sup> microglia characterization**

To fully characterize *in vitro* SOD1<sup>G93A</sup> microglia in an ALS context, we consider that assessing microglial-mediated MN toxicity is fundamental. As a part of this work, we collected microglial conditioned medium from control and SOD1<sup>G93A</sup> microglia, from both untreated and LPS-stimulated conditions, to test the neurotoxic potential of the factors secreted by mutant microglia. During this PhD, we have performed some trials consisting of treating differentiated NSC-34 MN-like cells or primary mouse cortical neurons with microglial conditioned medium at different dilutions. However, these experiments were unsuccessful, likely due to the lack of a complete differentiation of the NSC-34 hybridoma cell line into MN or the high sensitivity of cortical neurons.

Currently, we are performing the same approach with human iPSC-derived MN in the context of a collaboration (Alberto Ortega Cano Research group, IDIBELL) with more promising results. We also included LPS treatment as variable, as it remains unclear whether microglia require to be activated to a certain degree to exert toxicity. Although some previous studies reported microglial toxicity in MN co-cultured with untreated ALS microglia (Liao et al., 2012; Q. Xiao et al., 2007), others suggest that stimulation is needed to produce cytotoxicity (Banerjee et al., 2023; Vahsen et al., 2023; Weydt et al., 2004). Finally, it would be also interesting to study SOD1<sup>G93A</sup> microglial morphology more extensively and to see whether misfolded SOD1 aggregates are accumulated in our human ESC-derived microglia.

During this PhD, a short-term international internship was done in Mancuso Lab (VIB-UAntwerp Center for Molecular Neurology (Antwerp, Belgium)). Microglial conditioned medium from two sALS patients and one control iPSC line was collected with the purpose of screening their neurotoxic potential and prioritizing the most neurotoxic one in future *in vivo* experiments of xenotransplantation in the mouse spinal cord. However, due to the lack of success in the neurotoxicity assays with our SOD1<sup>G93A</sup> microglia supernatant, this experiment is pendant and cannot be included in the present manuscript.

## Xenotransplantation of microglia into the mouse spinal cord

---

Transplantation of human MPs into the mouse CNS results in functional human microglia, which closely resembles *in vivo* adult human microglia (Hasselmann et al., 2019), providing a more accurate model for human microglia. This idea arose from the fact that microglia behaviour differs *in vitro* and *ex vivo* due to the lack of the CNS environment and its fundamental clues for proper microglial identity (Gosselin et al., 2017; Lloyd et al., 2024; Mancuso et al., 2019). This cutting-edge system could be useful to assess the effect of human genetic variants relevant in neurological diseases in *in vivo* microglia. Studies using these chimeric mice consistently show human microglia engrafted into the brain (Abud et al., 2017; Capotondo et al., 2017; Fattorelli et al., 2021; Hasselmann et al., 2019; Mancuso et al., 2019, 2024; Svoboda et al., 2019; R. Xu et al., 2020), which is especially useful in diseases affecting mainly this anatomical region, such as AD, PD, Huntington disease (HD) or ischemic ictus, among others. While ALS also involves upper MN located in the motor cortex, most studies in animal models have focused on lower MN located in the spinal cord. In fact, SOD1<sup>G93A</sup> mouse model exhibits evident hindlimb muscles atrophy and paralysis, which is caused by lumbar MN degeneration (Mancuso & Navarro, 2015). Given our interest in ALS pathology, we set up the protocol to successfully engraft human microglia in newborn spinal cord for the first time, based on the methodology described by Fattorelli et al., 2021 for cell engraftment into the brain. The transplantation window is limited to the neonatal stage because microglia have not yet fully populated the entire CNS (Z. Xu et al., 2020). Therefore, our experimental setting is more challenging methodologically due to the smaller size of the spinal cord.

Previous studies achieved extensive human microglia engraftment across the brain using multiple injections at different brain coordinates, with cell concentrations ranging from 200,000 MPs/brain (R. Xu et al., 2020), 500,000 MPs/pup (Fattorelli et al., 2021; Hasselmann et al., 2019) or up to 1,000,000 MPs/mouse (Svoboda et al., 2019). In contrast, our approach used a single injection of 50,000 MPs in the caudal region of the spinal cord, which was sufficient to achieve widespread human microglia engraftment throughout the spinal cord. Importantly, at 5-months and 10-months after transplantation, human microglia expressing the

homeostatic marker P2RY12 were observed in the cervical, thoracic, lumbar and sacral regions of the spinal cord. Human microglia started to colonize the mouse spinal cord from the outer region of the spinal cord, adjacent to meninges, as seen at 5 days post-transplantation, and then progressively expanded to inner areas, as observed at 2-, 5- and 10-months post-transplantation.

Focusing on the lumbar spinal cord, human microglial chimerism increased over time following transplantation, ranging from 49-72% (2 months old), 71%-98% (5 months old) and 84-91% (10 months old), depending on the spinal cord area (white and grey matter). When comparing our results with previous studies performing human microglia brain xenotransplantation, our human microglia chimerism reached values comparable to the 80% (2 months old) described in Hasselmann et al., 2019, and 33% (3 weeks old) or 80% (3-6 months old) in Fattorelli et al., 2021. Notably, our engraftment rates surpassed other studies, which reported 9% chimerism at 8 weeks (8 weeks old) (Mancuso et al., 2019), 27% (4 months old) (Svoboda et al., 2019) or 8% (6 months old) (R. Xu et al., 2020). These findings confirm the success of our human microglial xenotransplantation model in the spinal cord and validate the robustness of our chimeric mouse model.

Within the lumbar spinal cord, regional differences in human microglia chimerism were detected regardless the timepoint analysed. The greater presence of human microglia was seen in the white matter, while lower levels were observed in the grey matter, particularly in the dorsal horn. This may be attributed to the migration of human microglia along white matter tracts, mirroring the pattern seen during microglial development (Abud et al., 2017; Menassa & Gomez-Nicola, 2018).

Our main interest of setting up human microglia xenotransplantation in the mouse spinal cord is to elucidate the involvement of microglia in the ALS pathogenesis. Given that SOD1<sup>G93A</sup> mouse has a lifespan of about 5 months (Mancuso & Navarro, 2015), it is important to achieve substantial human microglia engraftment at this timeframe to facilitate *in vivo* studies using human microglia in this ALS mouse model. Indeed, by 5 months, transplanted mice exhibited 71% chimerism in the dorsal horn, 79% in the ventral horn and 98% in the white matter, and no statistical differences in chimerism were observed between 5- and 10-month-old mice. At earlier timepoints, 2-months-old transplanted mice displayed a

human chimerism in the lumbar spinal cord of 49% in the dorsal horn, 68% in the ventral horn and 72% in the white matter. This age would correspond to the pre-symptomatic phase in SOD1<sup>G93A</sup> mouse (Mancuso & Navarro, 2015). Although the human microglia population in the dorsal horn is relatively lower, our main interest is the ventral horn where MN somas are located. Indeed, in this specific area we observed the greatest chimerism in the grey matter, reaching values about of 70%. This is particularly relevant as microglia have been described to be key players in ALS progression (Beers et al., 2006; Boillée et al., 2006) and, thus, achieving sufficient human microglial engraftment in this region is critical for studying ALS in this model.

During this thesis, we have generated a new transgenic mouse by crossing the immunodeficient Rag2<sup>-/-</sup> IL2r $\gamma$ <sup>-/-</sup> hCSF1<sup>KI</sup> mice with human SOD1<sup>G93A</sup>-overexpressing ALS mice, which would allow us future investigation of xenografted ALS human microglia in an ALS context *in vivo*. Although this innovative approach has been used previously in AD mouse models (Hasselmann et al., 2019; Mancuso et al., 2024; Romero-Molina et al., 2024), no studies have been performed in the ALS field to date, as far as we know.

This cutting-edge strategy opens numerous avenues for investigating the role of microglia in ALS pathogenesis. First, xenotransplantation of human SOD1<sup>G93A</sup> and control microglia in wild-type Rag2<sup>-/-</sup> IL2r $\gamma$ <sup>-/-</sup> hCSF1<sup>KI</sup> mice would allow to assess how mutant SOD1 affects directly microglial transcriptomic states. Additionally, it would be interesting to study how xenografted SOD1<sup>G93A</sup> microglia interacts with lumbar MNs in wild-type Rag2<sup>-/-</sup> IL2r $\gamma$ <sup>-/-</sup> hCSF1<sup>KI</sup> immunodeficient mice and whether mutant SOD1 microglia is enough to trigger any detectable MN damage. This approach could also be applied to SOD1<sup>G93A</sup> Rag2<sup>-/-</sup> IL2r $\gamma$ <sup>-/-</sup> hCSF1<sup>KI</sup> mice, allowing the evaluation of how an ALS context affects human control and SOD1<sup>G93A</sup> xenografted microglia.

A key question is whether we could replicate findings from Beers et al., 2006, which described extend survival in SOD1<sup>G93A</sup> mice by replacing of mutant microglia by control murine microglia transplantation. While we focused on mutant SOD1<sup>G93A</sup> as it is the most studied mutation, this can be extended to other ALS-related genes, such as *C9ORF72*, *TARDBP*, *FUS*, etc. Importantly, this holds particular relevance for

sALS, as lack a corresponding animal model to explore the contribution of microglia to ALS pathogenesis. Thus, this approach may offer a new experimental approach to study sALS microglia *in vivo*.

As with all the experimental models, limitations must be taken into consideration. One significant drawback is the lack of an adaptative immune system in the human microglia-recipient mice, which hinders the possibility to explore, for instance, the interaction between T-cells and microglia since T-cells infiltrate the CNS parenchyma in ALS (Chiu et al., 2008). Whereas neuroprotective CD4<sup>+</sup> Th2 cells have been described in earlier stages, pro-inflammatory CD8<sup>+</sup> CD4<sup>+</sup> Th1 and Th17 cells have been reported to be detrimental in the later ALS phases (W. Zhao et al., 2013). Microglial cells are widely known to influence the polarization of immune cells, and, in turn, T-cells have been shown to modulate ALS microglia *in vitro* (Zhao et al., 2012) and influence transcriptome signature in brain ischemia (Benakis et al., 2022), which could be also significant in ALS. Fortunately, a recent work developed the first fully functional human immune system in immunosuppressed mice (Chupp et al., 2024). Moving to a more humanized system would improve our understanding about human diseases and we would gain more translation from basic research to clinics. Moreover, although endogenous microglia pharmacological depletion is performed to ease human microglia integration and expansion, residual mouse microglia can repopulate rapidly after one week after treatment cessation (Elmore et al., 2015; Z. Xu et al., 2020). Finally, given the recent discovery of this microglia modelling approach, many questions about the model itself need to be explored. For instance, how persistent repopulated mouse microglia may influence engrafted human microglia requires further examination. Moreover, whether the regional microglia heterogeneity of engrafted microglia in physiological and pathological conditions is recapitulated needs to be addressed (Tan et al., 2020).



## Generation of a novel C9orf72 HRE knock-in mouse model

---

Developing a C9orf72 animal model, which recapitulates GOF and LOF pathogenic mechanisms as well as ALS/FTD symptoms and signs, remains challenging in the field. C9orf72-null mouse exhibits immune system dysregulation rather than CNS-related features (Atanasio et al., 2016; O'Rourke et al., 2016). In contrast, GOF animal models recapitulate typical C9orf72 pathology, including RNA foci and DPR accumulation, but fail to develop a complete ALS/FTD phenotype (Chew et al., 2015; Jiang et al., 2016; Y. Liu et al., 2016; O'Rourke et al., 2015; Peters et al., 2015). Current research suggests that C9orf72 haploinsufficiency may exacerbate pathogenesis when combined with the GOF factors, potentially contributing to a more complete ALS/FTD-phenotype (Shao et al., 2019; Zhu et al., 2020).

Here, we characterized phenotypically a newly generated C9orf72 knock-in with G4C2 HRE, in which the pathogenic repeats disrupt the endogenous *C9orf72* gene. This model differs from published GOF animal models, which incorporate the human C9orf72 G4C2 HRE through BACs or AAVs (Chew et al., 2015; Jiang et al., 2016; Y. Liu et al., 2016; O'Rourke et al., 2015; Peters et al., 2015). These GOF mouse models preserve the murine *C9orf72* gene intact and, thus, C9orf72 LOF mechanism is not modelled. This caveat was solved by expressing G4C2 HRE exogenously by viral vectors in a C9orf72 KO mouse (Zhu et al., 2020). However, in none of the previous mouse models, the pathogenic repeats were located in the corresponding murine C9orf72 ortholog. Our model is similar to the approach used by Dong et al., 2020 in which they targeted the rat *C9orf72* locus to incorporate 80 G4C2 repeats with human flanking fragments within exon 1a and exon 1b, replacing the rat exon 1. Our expression cassette includes 30 G4C2 repeats, which it is considered to be the pathogenic threshold (Balendra & Isaacs, 2018). However, the somatic and intergenerational repeat instability arose from the repetitive sequence may have modified the number of repeats, due to errors in DNA repair or replication that generate changes in the genome over time (Kojak et al., 2024). Although it would be interesting to measure the exact G4C2 repeat length in our model, it is methodologically challenging to precisely define the repeat length above 30 due to

the 100% GC content of the DNA sequence and long expansions found in patients (Van Der Ende et al., 2021).

Preliminary results on survival of our C9 mice did not show alterations in either heterozygous or homozygous animals. The only C9orf72 mouse model that reported decrease in survival was BAC-(G4C2)<sub>500</sub> (Y. Liu et al., 2016), while Peters et al., 2015 reported normal survival in BAC-(G4C2)<sub>500/300</sub> and other studies did not analyse mortality (Chew et al., 2015; Jiang et al., 2016; O'Rourke et al., 2015). Additionally, research indicates that survival is dramatically shortened when BAC-G4C2 HRE are expressed in C9orf72-null mice (Zhu et al., 2020), highlighting the importance of combining GOF and LOF mechanisms.

Both control and C9 animals in our study displayed body weight increase with age, although heterozygous animals surprisingly showed a notable smaller body weight gain. Although the exact cause is unclear, we hypothesize that the mixed genetic background (129/Sv and C57BL/6JOLA<sup>Hsd</sup>) of our animals could have influenced this parameter.

Despite 18 months of follow-up, our C9 mouse model did not exhibit an ALS-like phenotype. No motor deficits were detected in the rotarod test or through CMAP electrophysiological measurements of plantar, tibialis anterior and gastrocnemius muscles. Besides, the presence of the G4C2 HRE in heterozygosis or homozygosis, or the inclusion or exclusion of the STOP-neo region did not impact these outcomes. Although several C9orf72 models expressing the human *C9ORF72* gene with distinct G4C2 HRE length have been developed through BAC or viral vectors, a robust ALS-like phenotype has not been recapitulated. BAC transgenic C9orf72 mouse models do not exhibit any motor alteration (Jiang et al., 2016; O'Rourke et al., 2015; Peters et al., 2015) or only subtle motor deficits in the rotarod (Chew et al., 2015), gait abnormalities and decreased grip strength (Y. Liu et al., 2016; Nguyen et al., 2020; Pattamatta et al., 2020). C9orf72 LOF models, including C9orf72-null (Atanasio et al., 2016; Jiang et al., 2016) and knock-down (Lopez-Herdoiza et al., 2023) mice, do not develop a motor phenotype, with only subtle motor deficits in aged animals. Dong et al., 2020 attribute the motor deficits observed in 8-months-old C9orf72 HRE knock-in rats with the triggered C9orf72 haploinsufficiency, although GOF involvement cannot be excluded since this pathogenic mechanism was not

evaluated. Other studies using DPR<sup>KI</sup> C9orf72<sup>+/+</sup> (Verdone et al., 2022) and C9orf72<sup>+/-</sup> mice (Milioto et al., 2024) displayed MN damage and loss, accompanied by some rotarod deficits, but not recapitulating a full ALS phenotype. Thus, our C9 mouse model adds to the existing evidence that reproducing a complete ALS phenotype in *C9orf72* models remains elusive. It seems both GOF and LOF mechanisms are necessary for a robust ALS phenotype, yet further exploration is required to understand why these mice are resistant to developing full motor neuron disease.

In contrast to the lack of MN disease, our homozygous C9 mouse model (CreER<sup>-/-</sup>, C9<sup>STOP/STOP</sup> and CreER<sup>+/-</sup>, C9<sup>fl/fl</sup>) more closely recapitulates a FTD-compatible phenotype with depressive-like behaviour and memory dysfunction in advanced ages. Anhedonia in our C9 mice is evident from 8 months-old onwards. Although this behavioural feature has not been assessed in the reported BAC-G4C2 C9orf72 mice (Jiang et al., 2016; O'Rourke et al., 2015; Peters et al., 2015) and AAV-G4C2 C9orf72 models (Chew et al., 2015; Herranz-Martin et al., 2017), depressive-like behaviour was described for the first time in C9orf72 models by Lopez-Herdoiza et al., 2023 in aged C9orf72-knock down mice. Besides, FTD mouse models with other mutations, such as human mutated tau<sup>KI</sup> (Koss et al., 2016) or GRN-KO (Yin et al., 2010) also exhibit depressive-like behaviours, further supporting the FTD relevance of our C9 mouse model.

In terms of memory dysfunction, aged homozygous C9 mice display memory deficits in NORT from 8 months-old onwards, mirroring results from 12-months-old AAV-(G4C2)<sub>102</sub> mice (Herranz-Martin et al., 2017). Memory impairments in aged BAC-(G4C2)<sub>450</sub> mice, particularly spatial learning and working memory, have also been observed in (Jiang et al., 2016; Zhu et al., 2020), with severity increasing when *C9orf72* haploinsufficiency co-occurs (Zhu et al., 2020). However, some other studies reported no memory alterations in BAC-(G4C2)<sub>100-1000</sub> (O'Rourke et al., 2015) while did not evaluate memory skills (Chew et al., 2015; Y. Liu et al., 2016).

Here, we also showed that homozygous C9 animals exhibited similar ambulatory distance to their respective control mice, and as expected, these distances decreased with age in all the experimental groups. This aligns with observations from previous C9orf72 mouse models, as described in BAC-(G4C2)<sub>100-</sub>

<sup>1000</sup> (O'Rourke et al., 2015), BAC-(G4C2)<sub>500</sub> (Y. Liu et al., 2016) and DPR-overexpressing mice (Verdone et al., 2022). This is especially relevant since ambulatory behavior is significant because many of our behavioral tests rely on this parameter, and the absence of differences in locomotor activity validates the results of the other tests by eliminating it as a confounding factor. Interestingly, while anxiety-like behaviour is generally developed in several C9orf72 mouse models, including BAC-(G4C2)<sub>500</sub> (Y. Liu et al., 2016), BAC-(G4C2)<sub>450</sub> (Jiang et al., 2016), AAV-(G4C2)<sub>66</sub> (Chew et al., 2015) and DPR-overexpressing mice (Verdone et al., 2022), our homozygous C9 mouse model did not display an anxiety-like behaviour, as seen in 18-month-old BAC-(G4C2)<sub>100-1000</sub> mice (O'Rourke et al., 2015).

C9orf72 mouse models display plenty of variability in the phenotype developed, which could be influenced by the repeat length, differences in transgene expression, site of integration, regulatory elements or sequence differences within transgenes used to generate the models, mouse genetic background effects or variability in typical C9orf72 pathology recapitulated (RNA foci, DPR accumulation, TDP-43 mislocalization or neuronal loss). Elucidating how these variables affect to the ALS/FTD phenotype development in mice could help the field to understand the C9orf72 physiopathology and to have a robust C9orf72 mouse model to test potential therapies.

In terms of sex differences, no major differences were observed in motor and behavioural features in our C9 animals. However, it is worth noting that due to the small number of animals per sex at certain time points, these findings are preliminary. Still, we observed a tendency for male C9 mice to exhibit more pronounced depressive symptoms and to develop memory deficits earlier (at 8 months of age) than females, which showed these deficits later (at 14 months of age). In C9orf72 FTD and ALS/FTD patients, no sex differences have been observed in terms of prevalence (Curtis et al., 2017; Glasmacher et al., 2020). In contrast, female predominance has been observed in ALS-related C9orf72 cases (Curtis et al., 2017), with evidence suggesting that C9orf72 ALS males may experience shorter lifespan (Trojsi et al., 2019) and earlier disease onset (Murphy et al., 2017) in specific cohorts. In existing C9orf72 mouse models, no sex differences were detected in terms of neurodegeneration or behavioural phenotype, although specific studies

using AAV-(G4C2)<sub>66</sub> (Chew et al., 2015) and BAC-(G4C2)<sub>500</sub> (Y. Liu et al., 2016) showed higher disease vulnerability in females, with greater body weight reduction in the former study and more development of acute disease in the latter.

In our study, no differences were found in the motor and behavioural evaluation between CreER<sup>-/-</sup>, C9<sup>STOP/STOP</sup> and CreER<sup>+/-</sup>, C9<sup>fl/fl</sup> mice, suggesting that the presence of the STOP-neo region does not play any effect. One plausible explanation for this is the location of the stop-neo region within an intronic area, meaning it may not affect the expression of the *C9orf72* protein itself. Additionally, the synthesis of DPRs occurs via non-canonical RAN translation, which is driven by loop structures in the G4C2 repeat sequence (Freibaum & Taylor, 2017) Therefore, the presence of the STOP region preceding the repeats is unlikely to disrupt this pathogenic mechanism.

Beyond the phenotypic characterization of our C9 model, our next steps will be to explore histological and molecularly this mouse model. First, we have designed specific primers to confirm the recombination after tamoxifen-mediated CreER induction at 8 weeks-old-mice, which should result with the STOP-neo removal. Besides, we need to measure the protein levels of C9orf72 to elucidate whether our C9 model reproduces the LOF C9orf72 mechanism. Dong et al., 2020 reported C9orf72 haploinsufficiency in their C9orf72-KI rat model, with a 40% reduction in C9orf72 protein expression in the CNS. We hypothesize that, given the presence of the STOP region in the intronic region, the protein expression should not be different between CreER<sup>-/-</sup>, C9<sup>STOP/STOP</sup> and CreER<sup>+/-</sup>, C9<sup>fl/fl</sup> mice. In parallel, we are completing the phenotypic characterization of additional animal groups to determine the optimal age for conducting histological analyses. Key pathogenic features related to C9orf72 will be evaluated, including the formation of DPRs, the presence of RNA foci, and TDP-43 phosphorylation and mislocalization. Furthermore, we aim to correlate behavioural alterations, particularly those related to memory and depression, with histological findings in the hippocampus and prefrontal cortex. In these regions, we will examine neuronal death and glial reactivity, which could provide insight into the underlying mechanisms driving the observed cognitive and affective symptoms in our model.

This combined approach of molecular, histological, and behavioural analysis will allow us to better understand the pathogenic mechanisms at play in this C9orf72 model, which may ultimately shed light on ALS/FTD and provide a valuable platform for testing therapeutic interventions.



## VIII. Conclusions

---





**Chapter 1. ALS-linked SOD1<sup>G93A</sup> mutation disrupts microglial functions in a cell-autonomous manner in human embryonic stem cell-derived microglia *in vitro*.**

- Our CRISPR/Cas9 strategy has successfully allowed the generation of an isogenic cell line carrying the SOD1<sup>G93A</sup> mutation, without detectable off-target effects.
- Human ESCs differentiate into microglia-like cells following a 5-week protocol *in vitro*. The resulting cells are phenotypically compatible with microglial cells, since they express myeloid markers (Iba1, CD11b, CD45<sup>low</sup>) and specific microglial markers (P2RY12<sup>+</sup>).
- *In vitro* human SOD1<sup>G93A</sup> ESC-derived microglia exhibit altered cytokine profile at baseline conditions compared to control microglia.
- *In vitro* human SOD1<sup>G93A</sup> ESC-derived microglia display an exacerbated response to the pro-inflammatory stimulus LPS compared to control microglia.
- SOD1<sup>G93A</sup> mutation affects microglial phagocytosis *in vitro*.
- Under basal conditions, *in vitro* SOD1<sup>G93A</sup> microglia display metabolic disturbances with an increased glycolytic metabolism and maximal respiration rate.
- *In vitro* SOD1<sup>G93A</sup> microglia adapt differently their metabolism in response to LPS. Whereas control microglia increase glycolysis in response to mitochondrial ETC inhibitors, LPS-stimulated SOD1<sup>G93A</sup> microglia did not, probably due to their already basal high glycolytic metabolism.
- Control and SOD1<sup>G93A</sup> microglia exhibit similar mitochondria content both at basal conditions and after LPS stimulation.
- ROS production is elevated in SOD1<sup>G93A</sup> microglia compared to control microglia. Upon LPS stimulation, control microglia increase ROS production, but this increment is absent in SOD1<sup>G93A</sup> microglia, likely to their already higher basal levels.

## **Chapter 2. Xenotransplantation of human microglia into the mouse spinal cord.**

- Human microglia xenotransplantation into the neonatal Rag2<sup>-/-</sup> IL2ry<sup>-/-</sup> hCSF1<sup>KI</sup> mouse spinal cord is feasible.
- Xenotransplanted human microglia (P2RY12<sup>+</sup> CD45<sup>+</sup>) populate the lumbar mouse spinal cord starting from the outer regions of the spinal cord and extending inwards, and persist for at least 10 months.
- The degree of human microglia chimerism increases over time following transplantation.
- The highest levels of human microglia colonization are found in the white matter, although significant colonization is also observed in the grey matter.
- Human microglia progressively populate the entire mouse spinal cord, from the cervical to sacral regions, over time.

## **Chapter 3. Phenotypic characterization of a novel C9orf72 G4C2 HRE knock-in mouse model**

- Heterozygous and homozygous C9 animals do not exhibit reduced survival rates.
- Heterozygous and homozygous C9 animals do not display altered body weight changes.
- Heterozygous and homozygous C9 animals do not develop an ALS phenotype during the 18 months of follow-up.
- Homozygous C9 animals recapitulate a FTD phenotype with the following features:
  - Control and homozygous C9 animals display similar ambulatory ability, which decreases with ageing.
  - Aged homozygous C9 mice develop anhedonia and depressive-like behaviour from 8 months of age onwards.
  - Anxiety-like behaviour is not recapitulated in aged homozygous C9 animals during the 18 months of follow-up.
  - Aged homozygous C9 animals exhibit memory decline, particularly evident by 14 months of age.
- The presence of the STOP-neo region has no affect in the C9 phenotype.
- There are not major sex differences between male and female C9 animals.

## IX. References

---



- Abe, K., Aoki, M., Tsuji, S., Itoyama, Y., Sobue, G., Togo, M., Hamada, C., Tanaka, M., Akimoto, M., Nakamura, K., Takahashi, F., Kondo, K., Yoshino, H., Abe, K., Tsuji, S., Itoyama, Y., Sobue, G., Togo, M., Hamada, C., ... Yoshino, H. (2017). Safety and efficacy of edaravone in well defined patients with amyotrophic lateral sclerosis: a randomised, double-blind, placebo-controlled trial. *The Lancet Neurology*, *16*(7), 505–512. [https://doi.org/10.1016/S1474-4422\(17\)30115-1](https://doi.org/10.1016/S1474-4422(17)30115-1)
- Abe, K., Itoyama, Y., Sobue, G., Tsuji, S., Aoki, M., Doyu, M., Hamada, C., Kondo, K., Yoneoka, T., Akimoto, M., & Yoshino, H. (2014). Confirmatory double-blind, parallel-group, placebo-controlled study of efficacy and safety of edaravone (MCI-186) in amyotrophic lateral sclerosis patients. *Amyotrophic Lateral Sclerosis and Frontotemporal Degeneration*, *15*(7–8), 610–617. <https://doi.org/10.3109/21678421.2014.959024>
- Absinta, M., Maric, D., Gharagozloo, M., Garton, T., Smith, M. D., Jin, J., Fitzgerald, K. C., Song, A., Liu, P., Lin, J. P., Wu, T., Johnson, K. R., McGavern, D. B., Schafer, D. P., Calabresi, P. A., & Reich, D. S. (2021). A lymphocyte–microglia–astrocyte axis in chronic active multiple sclerosis. *Nature*, *597*(7878), 709–714. <https://doi.org/10.1038/s41586-021-03892-7>
- Abud, E. M., Ramirez, R. N., Martinez, E. S., Healy, L. M., Nguyen, C. H. H., Newman, S. A., Yeromin, A. V., Scarfone, V. M., Marsh, S. E., Fimbres, C., Caraway, C. A., Fote, G. M., Madany, A. M., Agrawal, A., Kayed, R., Gylys, K. H., Cahalan, M. D., Cummings, B. J., Antel, J. P., ... Blurton-Jones, M. (2017). iPSC-Derived Human Microglia-like Cells to Study Neurological Diseases. *Neuron*, *94*(2), 278–293.e9. <https://doi.org/10.1016/j.neuron.2017.03.042>
- Acevedo-Arozena, A., Kalmar, B., Essa, S., Ricketts, T., Joyce, P., Kent, R., Rowe, C., Parker, A., Gray, A., Hafezparast, M., Thorpe, J. R., Greensmith, L., & Fisher, E. M. C. (2011). A comprehensive assessment of the SOD1 G93A low-copy transgenic mouse, which models human amyotrophic lateral sclerosis. *Disease Models and Mechanisms*, *4*(5), 686–700. <https://doi.org/10.1242/dmm.007237>
- Ahmed, R. M., Irish, M., van Eersel, J., Ittner, A., Ke, Y. D., Volkerling, A., van der Hoven, J., Tanaka, K., Karl, T., Kassiou, M., Kril, J. J., Piguet, O., Götz, J., Kiernan, M. C., Halliday, G. M., Hodges, J. R., & Ittner, L. M. (2017). Mouse models of frontotemporal dementia: A comparison of phenotypes with clinical symptomatology. *Neuroscience and Biobehavioral Reviews*, *74*(Pt A), 126–138. <https://doi.org/10.1016/j.neubiorev.2017.01.004>
- Alexianu, M. E., Ho, B. -K, Mohamed, A. H., La Bella, V., Smith, R. G., & Appel, S. H. (1994). The role of calcium-binding proteins in selective motoneuron vulnerability in amyotrophic lateral sclerosis. *Annals of Neurology*, *36*(6), 846–858. <https://doi.org/10.1002/ANA.410360608>
- Allison, R. L., Adelman, J. W., Abrudan, J., Urrutia, R. A., Zimmermann, M. T., Mathison, A. J., & Ebert, A. D. (2022). Microglia Influence Neurofilament Deposition in ALS iPSC-Derived Motor Neurons. *Genes*, *13*(2), 241. <https://doi.org/10.3390/GENES13020241/S1>
- Allison, R. L., & Ebert, A. D. (2024). ALS iPSC-derived microglia and motor neurons respond to astrocyte-targeted IL-10 and CCL2 modulation. *Human Molecular Genetics*, *33*(6), 530–542. <https://doi.org/10.1093/hmg/ddad209>
- Amo-Aparicio, J., Dinarello, C. A., & Lopez-Vales, R. (2024). Metabolic reprogramming of the inflammatory response in the nervous system: the crossover between inflammation and metabolism. *Neural Regeneration Research*, *19*(10), 2189–2201. <https://doi.org/10.4103/1673-5374.391330>
- Amo-Aparicio, J., Martínez-Muriana, A., Sánchez-Fernández, A., & López-Vales, R. (2018). Neuroinflammation quantification for spinal cord injury. *Current Protocols in Immunology*, *123*(1), e57. <https://doi.org/10.1002/CPIM.57>

Amylyx Pharmaceuticals. (2024, March 8). *Amylyx Pharmaceuticals Announces Topline Results From Global Phase 3 PHOENIX Trial of AMX0035 in ALS*. <https://www.amylyx.com/news/amylyx-pharmaceuticals-announces-topline-results-from-global-phase-3-phoenix-trial-of-amx0035-in-als>.

Aoyama, K., Matsubara, K., Fujikawa, Y., Nagahiro, Y., Shimizu, K., Umegae, N., Hayase, N., Shiono, H., & Kobayashi, S. (2000). Nitration of manganese superoxide dismutase in cerebrospinal fluids is a marker for peroxynitrite-mediated oxidative stress in neurodegenerative diseases. *Annals of Neurology*, *47*(4), 524–527.

Arnold, E. S., Ling, S. C., Huelga, S. C., Lagier-Tourenne, C., Polymenidou, M., Ditsworth, D., Kordasiewicz, H. B., McAlonis-Downes, M., Platoshyn, O., Parone, P. A., Da Cruz, S., Clutario, K. M., Swing, D., Tessarollo, L., Marsala, M., Shaw, C. E., Yeo, G. W., & Cleveland, D. W. (2013). ALS-linked TDP-43 mutations produce aberrant RNA splicing and adult-onset motor neuron disease without aggregation or loss of nuclear TDP-43. *Proceedings of the National Academy of Sciences*, *110*(8), E736–45. <https://doi.org/10.1073/pnas.1222809110>

Atanasio, A., Decman, V., White, D., Ramos, M., Ikiz, B., Lee, H. C., Siao, C. J., Brydges, S., Larosa, E., Bai, Y., Fury, W., Burfeind, P., Zamfirova, R., Warshaw, G., Orengo, J., Oyejide, A., Fralish, M., Auerbach, W., Poueymirou, W., ... Lai, K. M. V. (2016). C9orf72 ablation causes immune dysregulation characterized by leukocyte expansion, autoantibody production and glomerulonephropathy in mice. *Scientific Reports*, *6*(1), 1–14. <https://doi.org/10.1038/srep23204>

Ayers, J. I., Fromholt, S., Sinyavskaya, O., Siemienski, Z., Rosario, A. M., Li, A., Crosby, K. W., Cruz, P. E., Dinunno, N. M., Janus, C., Ceballos-Diaz, C., Borchelt, D. R., Golde, T. E., Chakrabarty, P., & Levites, Y. (2015). Widespread and efficient transduction of spinal cord and brain following neonatal AAV injection and potential disease modifying effect in ALS mice. *Molecular Therapy*, *23*(1), 53–62. <https://doi.org/10.1038/mt.2014.180>

Baborie, A., Griffiths, T. D., Jaros, E., Perry, R., McKeith, I. G., Burn, D. J., Masuda-Suzukake, M., Hasegawa, M., Rollinson, S., Pickering-Brown, S., Robinson, A. C., Davidson, Y. S., & Mann, D. M. A. (2015). Accumulation of dipeptide repeat proteins predates that of TDP-43 in frontotemporal lobar degeneration associated with hexanucleotide repeat expansions in C9ORF72 gene. *Neuropathology and Applied Neurobiology*, *41*(5), 601–612. <https://doi.org/10.1111/nan.12178>

Balendra, R., & Isaacs, A. M. (2018). C9orf72-mediated ALS and FTD: multiple pathways to disease. *Nature Reviews Neurology*, *14*(9), 544–558. <https://doi.org/10.1038/s41582-018-0047-2>

Banerjee, P., Mehta, A. R., Nirujogi, R. S., Cooper, J., James, O. G., Nanda, J., Longden, J., Burr, K., Mcdade, K., Salzinger, A., Paza, E., Newton, J., Story, D., Pal, S., Smith, C., Alessi, D. R., Selvaraj, B. T., Priller, J., & Chandran, S. (2023). Cell-autonomous immune dysfunction driven by disrupted autophagy in C9orf72-ALS iPSC-derived microglia contributes to neurodegeneration. *Science Advances*, *9*(16), eabq0651. <https://doi.org/10.1126/sciadv.abq0651>

Bang, J., Spina, S., & Miller, B. L. (2015). Frontotemporal dementia. *The Lancet*, *386*(10004), 1672–1682. [https://doi.org/10.1016/S0140-6736\(15\)00461-4](https://doi.org/10.1016/S0140-6736(15)00461-4)

Barmada, S. J. (2015). Linking RNA dysfunction and neurodegeneration in amyotrophic lateral sclerosis. *Neurotherapeutics*, *12*(2), 340–351. <https://doi.org/10.1007/s13311-015-0340-3>

Bastow, E. L., Peswani, A. R., Tarrant, D. S. J., Pentland, D. R., Chen, X., Morgan, A., Staniforth, G. L., Tullet, J. M., Rowe, M. L., Howard, M. J., Tuite, M. F., & Gourlay, C. W. (2016). New links

- between SOD1 and metabolic dysfunction from a yeast model of amyotrophic lateral sclerosis. *Journal of Cell Science*, *129*(21), 4118–4129. <https://doi.org/10.1242/jcs.190298>
- Batra, R., & Lee, C. W. (2017). Mouse models of C9orf72 hexanucleotide repeat expansion in amyotrophic lateral sclerosis/ frontotemporal dementia. *Frontiers in Cellular Neuroscience*, *11*, 196. <https://doi.org/10.3389/fncel.2017.00196>
- Beal, M. F., Ferrante, R. J., Browne, S. E., Matthews, R. T., Kowall, N. W., & Brown, R. H. (1997). Increased 3-nitrotyrosine in both sporadic and familial amyotrophic lateral sclerosis. *Annals of Neurology*, *42*(4), 644–654. <https://doi.org/10.1002/ana.410420416>
- Beckers, J., Tharkeshwar, A. K., Fumagalli, L., Contardo, M., Van Schoor, E., Fazal, R., Thal, D. R., Chandran, S., Mancuso, R., Van Den Bosch, L., & Van Damme, P. (2023). A toxic gain-of-function mechanism in C9orf72 ALS impairs the autophagy-lysosome pathway in neurons. *Acta Neuropathologica Communications*, *11*(1), 151. <https://doi.org/10.1186/s40478-023-01648-0>
- Beckers, J., Tharkeshwar, A. K., & Van Damme, P. (2021). C9orf72 ALS-FTD: recent evidence for dysregulation of the autophagy-lysosome pathway at multiple levels. *Autophagy*, *17*(11), 3306–3322. <https://doi.org/10.1080/15548627.2021.1872189>
- Beers, D. R., Henkel, J. S., Xiao, Q., Zhao, W., Wang, J., Yen, A. A., Siklos, L., McKercher, S. R., & Appel, S. H. (2006). Wild-type microglia extend survival in PU.1 knockout mice with familial amyotrophic lateral sclerosis. *Proceedings of the National Academy of Sciences*, *103*(43), 16021–16026. <https://doi.org/10.1073/pnas.0607423103>
- Beers, D. R., Henkel, J. S., Zhao, W., Wang, J., & Appel, S. H. (2008). CD4+ T cells support glial neuroprotection, slow disease progression, and modify glial morphology in an animal model of inherited ALS. *Proceedings of the National Academy of Sciences*, *105*(40), 15558–15563. <https://doi.org/10.1073/PNAS.0807419105>
- Beers, D. R., Henkel, J. S., Zhao, W., Wang, J., Huang, A., Wen, S., Liao, B., & Appel, S. H. (2011). Endogenous regulatory T lymphocytes ameliorate amyotrophic lateral sclerosis in mice and correlate with disease progression in patients with amyotrophic lateral sclerosis. *Brain*, *134*(5), 1293–1314. <https://doi.org/10.1093/BRAIN/AWR074>
- Bellezza, I., Grottelli, S., Costanzi, E., Scarpelli, P., Pigna, E., Morozzi, G., Mezzasoma, L., Peirce, M. J., Moresi, V., Adamo, S., & Minelli, A. (2018). Peroxynitrite activates the NLRP3 inflammasome cascade in SOD1(G93A) mouse model of amyotrophic lateral sclerosis. *Molecular Neurobiology*, *55*(3), 2350–2361. <https://doi.org/10.1007/s12035-017-0502-x>
- Belzil, V. V., Bauer, P. O., Prudencio, M., Gendron, T. F., Stetler, C. T., Yan, I. K., Pregent, L., Daugherty, L., Baker, M. C., Rademakers, R., Boylan, K., Patel, T. C., Dickson, D. W., & Petrucelli, L. (2013). Reduced C9orf72 gene expression in C9FTD/ALS is caused by histone trimethylation, an epigenetic event detectable in blood. *Acta Neuropathologica*, *126*(6), 895–905. <https://doi.org/10.1007/s00401-013-1199-1>
- Benakis, C., Simats, A., Tritschler, S., Heindl, S., Besson-Girard, S., Llovera, G., Pinkham, K., Kolz, A., Ricci, A., Theis, F. J., Bittner, S., Gökce, Ö., Peters, A., & Liesz, A. (2022). T cells modulate the microglial response to brain ischemia. *Elife*, *11*, e82031. <https://doi.org/10.7554/eLife>
- Bendotti, C., Marino, M., Cheroni, C., Fontana, E., Crippa, V., Poletti, A., & De Biasi, S. (2012). Dysfunction of constitutive and inducible ubiquitin-proteasome system in amyotrophic lateral sclerosis: Implication for protein aggregation and immune response. *Progress in Neurobiology*, *97*(2), 101–126. <https://doi.org/10.1016/j.pneurobio.2011.10.001>



- Bensimon, G., Lacomblez, L., Meininger, V., & ALS/Riluzole Study Group. (1994). A Controlled Trial of Riluzole in Amyotrophic Lateral Sclerosis. *New England Journal of Medicine*, *330*, 585–591. <https://doi.org/10.1056/NEJM199403033300901>
- Birger, A., Ben-Dor, I., Ottolenghi, M., Turetsky, T., Gil, Y., Sweetat, S., Perez, L., Belzer, V., Casden, N., Steiner, D., Izrael, M., Galun, E., Feldman, E., Behar, O., & Reubinoff, B. (2019). Human iPSC-derived astrocytes from ALS patients with mutated C9ORF72 show increased oxidative stress and neurotoxicity. *EBioMedicine*, *50*, 274–289. <https://doi.org/10.1016/j.ebiom.2019.11.026>
- Boeve, B. F., Boxer, A. L., Kumfor, F., Pijnenburg, Y., & Rohrer, J. D. (2022). Advances and controversies in frontotemporal dementia: diagnosis, biomarkers, and therapeutic considerations. *The Lancet Neurology*, *21*(3), 258–272. [https://doi.org/10.1016/S1474-4422\(21\)00341-0](https://doi.org/10.1016/S1474-4422(21)00341-0)
- Bohlen, C. J., Bennett, F. C., Tucker, A. F., Collins, H. Y., Mulinyawe, S. B., & Barres, B. A. (2017). Diverse requirements for microglial survival, specification and function revealed by defined-medium cultures. *Neuron*, *94*(4), 759–773.e8. <https://doi.org/10.1016/j.neuron.2017.04.043>
- Boillée, S., Yamanaka, K., Lobsiger, C. S., Copeland, N. G., Jenkins, N. A., Kassiotis, G., Kollias, G., & Cleveland, D. W. (2006). Onset and progression in inherited ALS determined by motor neurons and microglia. *Science*, *312*(5778), 1389–1392. <https://doi.org/10.1126/science.1123511>
- Borst, K., Dumas, A. A., & Prinz, M. (2021). Microglia: Immune and non-immune functions. *Immunity*, *54*(10), 2194–2208. <https://doi.org/10.1016/j.immuni.2021.09.014>
- Brettschneider, J., Toledo, J. B., van Deerlin, V. M., Elman, L., McCluskey, L., Lee, V. M. Y., & Trojanowski, J. Q. (2012). Microglial activation correlates with disease progression and upper motor neuron clinical symptoms in amyotrophic lateral sclerosis. *PLoS One*, *7*(6), e39216. <https://doi.org/10.1371/journal.pone.0039216>
- Breuer, M. E., Koopman, W. J., Koene, S., Nootboom, M., Rodenburg, R. J., Willems, P. H., & Smeitink, J. A. M. (2013). The role of mitochondrial OXPHOS dysfunction in the development of neurologic diseases. *Neurobiology of Disease*, *51*, 27–34. <https://doi.org/10.1016/j.NBD.2012.03.007>
- Bristol, L. A., & Rothstein, J. D. (1996). Glutamate transporter gene expression in amyotrophic lateral sclerosis motor cortex. *Annals of Neurology*, *39*(5), 676–679. <https://doi.org/10.1002/ANA.410390519>
- Brites, D., & Vaz, A. R. (2014). Microglia centered pathogenesis in ALS: Insights in cell interconnectivity. *Frontiers in Cellular Neuroscience*, *8*, 117. <https://doi.org/10.3389/fncel.2014.00117>
- Brownjohn, P. W., Smith, J., Solanki, R., Lohmann, E., Houlden, H., Hardy, J., Dietmann, S., & Livesey, F. J. (2018). Functional studies of missense TREM2 mutations in human stem cell-derived microglia. *Stem Cell Reports*, *10*(4), 1294–1307. <https://doi.org/10.1016/j.stemcr.2018.03.003>
- Burberry, A., Suzuki, N., Wang, J. Y., Moccia, R., Mordes, D. A., Stewart, M. H., Suzuki-Uematsu, S., Ghosh, S., Singh, A., Merkle, F. T., Koszka, K., Li, Q. Z., Zon, L., Rossi, D. J., Trowbridge, J. J., Notarangelo, L. D., & Eggan, K. (2016). Loss-of-function mutations in the C9ORF72 mouse ortholog cause fatal autoimmune disease. *Science Translational Medicine*, *8*(347), 347ra93. <https://doi.org/10.1126/scitranslmed.aaf6038>

- Burk, K., & Pasterkamp, R. J. (2019). Disrupted neuronal trafficking in amyotrophic lateral sclerosis. *Acta Neuropathologica*, *137*(6), 859–877. <https://doi.org/10.1007/S00401-019-01964-7>
- Burm, S. M., Zuiderwijk-Sick, E. A., t' Jong, A. E. J., Van Der Putten, C., Veth, J., Kondova, I., & Bajramovic, J. J. (2015). Inflammasome-induced IL-1 secretion in microglia is characterized by delayed kinetics and is only partially dependent on inflammatory caspases. *The Journal of Neuroscience*, *35*(2), 678–687. <https://doi.org/10.1523/JNEUROSCI.2510-14.2015>
- Butovsky, O., Jedrychowski, M. P., Moore, C. S., Cialic, R., Lanser, A. J., Gabriely, G., Koeglsperger, T., Dake, B., Wu, P. M., Doykan, C. E., Fanek, Z., Liu, L., Chen, Z., Rothstein, J. D., Ransohoff, R. M., Gygi, S. P., Antel, J. P., & Weiner, H. L. (2014). Identification of a unique TGF- $\beta$ -dependent molecular and functional signature in microglia. *Nature Neuroscience*, *17*(1), 131–143. <https://doi.org/10.1038/nn.3599>
- Capotondo, A., Milazzo, R., Garcia-Manteiga, J. M., Cavalca, E., Montepeloso, A., Garrison, B. S., Peviani, M., Rossi, D. J., & Biffi, A. (2017). Intracerebroventricular delivery of hematopoietic progenitors results in rapid and robust engraftment of microglia-like cells. *Science Advances*, *3*(12), e1701211. <https://doi.org/10.1126/sciadv.1701211>
- Cashman, N. R., Durham, H. D., Blusztajn, J. K., Oda, K., Tabira, T., Shaw, I. T., Dahrouge, S., & Antel, J. P. (1992). Neuroblastoma x spinal cord (NSC) hybrid cell lines resemble developing motor neurons. *Developmental Dynamics*, *194*(3), 209–221. <https://doi.org/10.1002/AJA.1001940306>
- Cassina, P., Cassina, A., Pehar, M., Castellanos, R., Gandelman, M., De León, A., Robinson, K. M., Mason, R. P., Beckman, J. S., Barbeito, L., & Radi, R. (2008). Mitochondrial dysfunction in SOD1G93A-bearing astrocytes promotes motor neuron degeneration: Prevention by mitochondrial-targeted antioxidants. *The Journal of Neuroscience*, *28*(16), 4115–4122. <https://doi.org/10.1523/JNEUROSCI.5308-07.2008>
- Cassina, P., Miquel, E., Martínez-Palma, L., & Cassina, A. (2021). Glial metabolic reprogramming in amyotrophic lateral sclerosis. *Neuroimmunomodulation*, *28*(4), 204–212. <https://doi.org/10.1159/000516926>
- Chang, Y., Kong, Q., Shan, X., Tian, G., Ilieva, H., Cleveland, D. W., Rothstein, J. D., Borchelt, D. R., Wong, P. C., & Glenn Lin, C. (2008). Messenger RNA oxidation occurs early in disease pathogenesis and promotes motor neuron degeneration in ALS. *PLoS One*, *3*(8), e2849. <https://doi.org/10.1371/journal.pone.0002849>
- Chao, C. C., Hu, S. X., Ehrlich, L., & Peterson, P. K. (1995). Interleukin-1 and tumor necrosis factor- $\alpha$  synergistically mediate neurotoxicity: Involvement of nitric oxide and of N-methyl-D-aspartate receptors. *Brain, Behavior, and Immunity*, *9*(4), 355–365. <https://doi.org/10.1006/BRBI.1995.1033>
- Checa, J., & Aran, J. M. (2020). Reactive oxygen species: Drivers of physiological and pathological processes. *Journal of Inflammation Research*, *13*, 1057–1073. <https://doi.org/10.2147/JIR.S275595>
- Chen, S. W., Hung, Y. S., Fuh, J. L., Chen, N. J., Chu, Y. S., Chen, S. C., Fann, M. J., & Wong, Y. H. (2021). Efficient conversion of human induced pluripotent stem cells into microglia by defined transcription factors. *Stem Cell Reports*, *16*(5), 1363–1380. <https://doi.org/10.1016/j.stemcr.2021.03.010>
- Cheung, S. W., Bhavnani, E., Simmons, D. G., Bellingham, M. C., & Noakes, P. G. (2024). Perineuronal nets are phagocytosed by MMP-9 expressing microglia and astrocytes in the SOD1G93A ALS mouse model. *Neuropathology and Applied Neurobiology*, *50*(3), e12982. <https://doi.org/10.1111/NAN.12982>

- Chew, J., Gendron, T. F., Prudencio, M., Sasaguri, H., Zhang, Y. J., Castanedes-Casey, M., Lee, C. W., Jansen-West, K., Kurti, A., Murray, M. E., Bieniek, K. F., Bauer, P. O., Whitelaw, E. C., Rousseau, L., Stankowski, J. N., Stetler, C., Daugherty, L. M., Perkerson, E. A., Desaro, P., ... Petrucelli, L. (2015). C9ORF72 repeat expansions in mice cause TDP-43 pathology, neuronal loss, and behavioural deficits. *Science*, *348*(6239), 1151–1154. <https://doi.org/10.1126/science.aaa9344>
- Chia, R., Chiò, A., & Traynor, B. J. (2018). Novel genes associated with amyotrophic lateral sclerosis: diagnostic and clinical implications. *The Lancet Neurology*, *17*(1), 94–102. [https://doi.org/10.1016/S1474-4422\(17\)30401-5](https://doi.org/10.1016/S1474-4422(17)30401-5)
- Chiot, A., Zaïdi, S., Iltis, C., Ribon, M., Berriat, F., Schiaffino, L., Jolly, A., de la Grange, P., Mallat, M., Bohl, D., Millecamps, S., Seilhean, D., Lobsiger, C. S., & Boillée, S. (2020). Modifying macrophages at the periphery has the capacity to change microglial reactivity and to extend ALS survival. *Nature Neuroscience*, *23*(11), 1339–1351. <https://doi.org/10.1038/s41593-020-00718-z>
- Chiu, I. M., Chen, A., Zheng, Y., Kosaras, B., Tsiftoglou, S. A., Vartanian, T. K., Brown, R. H., & Carroll, M. C. (2008). T lymphocytes potentiate endogenous neuroprotective inflammation in a mouse model of ALS. *Proceedings of the National Academy of Sciences*, *105*(46), 17913–17918. <https://doi.org/10.1073/pnas.0804610105>
- Chiu, I. M., Morimoto, E. T. A., Goodarzi, H., Liao, J. T., Keeffe, S. O., Phatnani, H. P., Muratet, M., Carroll, M. C., Levy, S., Tavazoie, S., Myers, R. M., & Maniatis, T. (2013). A neurodegeneration-specific expression signature and immune profile of acutely isolated microglia from an ALS mouse model. *Cell Reports*, *4*(2), 385–401. <https://doi.org/10.1016/j.celrep.2013.06.018.A>
- Chiu, I. M., Phatnani, H., Kuligowski, M., Tapia, J. C., Carrasco, M. A., Zhang, M., Maniatis, T., & Carroll, M. C. (2009). Activation of innate and humoral immunity in the peripheral nervous system of ALS transgenic mice. *Proceedings of the National Academy of Sciences*, *106*(49), 20960–20965. <https://doi.org/10.1073/pnas.0911405106/>
- Chupp, D. P., Rivera, C. E., Zhou, Y., Xu, Y., Ramsey, P. S., Xu, Z., Zan, H., & Casali, P. (2024). A humanized mouse that mounts mature class-switched, hypermutated and neutralizing antibody responses. *Nature Immunology*, *25*(8), 1489–1506. <https://doi.org/10.1038/s41590-024-01880-3>
- Ciura, S., Lattante, S., Le Ber, I., Latouche, M., Tostivint, H., Brice, A., & Kabashi, E. (2013). Loss of function of C9orf72 causes motor deficits in a zebrafish model of amyotrophic lateral sclerosis. *Annals of Neurology*, *74*(2), 180–187. <https://doi.org/10.1002/ANA.23946>
- Claes, C., Van Den Daele, J., Boon, R., Schouteden, S., Colombo, A., Monasor, L. S., Fiers, M., Ordoñas, L., Nami, F. A., Bohrmann, B., Tahirovic, S., De Strooper, B., & Verfaillie, C. M. (2019). Human stem cell-derived monocytes and microglia-like cells reveal impaired amyloid plaque clearance upon heterozygous or homozygous loss of TREM2. *Alzheimer's and Dementia*, *15*(3), 453–464. <https://doi.org/10.1016/j.jalz.2018.09.006>
- Clarke, B. E., & Patani, R. (2020). The microglial component of amyotrophic lateral sclerosis. *Brain*, *143*(12), 3526–3539. <https://doi.org/10.1093/brain/awaa309>
- Cook, C. N., Wu, Y., Odeh, H. M., Gendron, T. F., Jansen-West, K., del Rosso, G., Yue, M., Jiang, P., Gomes, E., Tong, J., Daugherty, L. M., Avendano, N. M., Castanedes-Casey, M., Shao, W., Oskarsson, B., Tomassy, G. S., McCampbell, A., Rigo, F., Dickson, D. W., ... Petrucelli, L. (2020). C9orf72 poly(GR) aggregation induces TDP-43 proteinopathy. *Science Translational Medicine*, *12*(559), eabb3774. <https://doi.org/10.1126/scitranslmed.abb3774>

- Corcia, P., Tauber, C., Vercoullie, J., Arlicot, N., Prunier, C., Praline, J., Nicolas, G., Venel, Y., Hommet, C., Baulieu, J. L., Cottier, J. P., Roussel, C., Kassiou, M., Guilloteau, D., & Ribeiro, M. J. (2012). Molecular imaging of microglial activation in amyotrophic lateral sclerosis. *PLoS One*, 7(12), 6–12. <https://doi.org/10.1371/journal.pone.0052941>
- Cozzolino, M., Ferri, A., Valle, C., & Carri, M. T. (2013). Mitochondria and ALS: Implications from novel genes and pathways. *Molecular and Cellular Neuroscience*, 55, 44–49. <https://doi.org/10.1016/j.mcn.2012.06.001>
- Cradick, T. J., Qiu, P., Lee, C. M., Fine, E. J., & Bao, G. (2014). COSMID: A web-based tool for identifying and validating CRISPR/Cas off-target sites. *Molecular Therapy - Nucleic Acids*, 3(12), e214. <https://doi.org/10.1038/mtna.2014.64>
- Csatári, J., Wiendl, H., & Pawlowski, M. (2024). Forward programming human pluripotent stem cells into microglia. *Trends in Cell Biology*, 24, 69. <https://doi.org/10.1016/j.TCB.2024.03.006>
- Curtis, A. F., Masellis, M., Robin Hsiung, G.-Y., Moineddin, R., Zhang, K., Au, B., Millett, G., Mackenzie, I., Rogaeva, E., & Tierney, M. C. (2017). Sex differences in the prevalence of genetic mutations in FTD and ALS. *Neurology*, 89(15), 1633–1642. <https://doi.org/10.1212/WNL.0000000000004494>
- Damiano, M., Starkov, A. A., Petri, S., Kipiani, K., Kiaei, M., Mattiazzi, M., Flint Beal, M., & Manfredi, G. (2006). Neural mitochondrial Ca<sup>2+</sup> capacity impairment precedes the onset of motor symptoms in G93A Cu/Zn-superoxide dismutase mutant mice. *Journal of Neurochemistry*, 96(5), 1349–1361. <https://doi.org/10.1111/J.1471-4159.2006.03619.X>
- Damiano, S., Sozio, C., La Rosa, G., Guida, B., Faraonio, R., Santillo, M., & Mondola, P. (2020). Metabolism regulation and redox state: Insight into the role of superoxide dismutase 1. *International Journal of Molecular Sciences*, 21(18), 1–22. <https://doi.org/10.3390/ijms21186606>
- Davidson, Y., Robinson, A. C., Liu, X., Wu, D., Troakes, C., Rollinson, S., Masuda-Suzukake, M., Suzuki, G., Nonaka, T., Shi, J., Tian, J., Hamdalla, H., Ealing, J., Richardson, A., Jones, M., Pickering-Brown, S., Snowden, J. S., Hasegawa, M., & Mann, D. M. A. (2016). Neurodegeneration in frontotemporal lobar degeneration and motor neurone disease associated with expansions in C9orf72 is linked to TDP-43 pathology and not associated with aggregated forms of dipeptide repeat proteins. *Neuropathology and Applied Neurobiology*, 42(3), 242–254. <https://doi.org/10.1111/nan.12292>
- De Giorgio, F., Maduro, C., Fisher, E. M. C., & Acevedo-Arozena, A. (2019). Transgenic and physiological mouse models give insights into different aspects of amyotrophic lateral sclerosis. *Disease Models and Mechanisms*, 12(1), dmm037424. <https://doi.org/10.1242/dmm.037424>
- DeJesus-Hernandez, M., Mackenzie, I. R., Boeve, B. F., Boxer, A. L., Baker, M., Rutherford, N. J., Nicholson, A. M., Finch, N. C. A., Flynn, H., Adamson, J., Kouri, N., Wojtas, A., Sengdy, P., Hsiung, G. Y. R., Karydas, A., Seeley, W. W., Josephs, K. A., Coppola, G., Geschwind, D. H., ... Rademakers, R. (2011). Expanded GGGGCC Hexanucleotide Repeat in Noncoding Region of C9ORF72 Causes Chromosome 9p-Linked FTD and ALS. *Neuron*, 72(2), 245–256. <https://doi.org/10.1016/j.neuron.2011.09.011>
- Devoy, A., Price, G., De Giorgio, F., Bunton-Stasyshyn, R., Thompson, D., Gasco, S., Allan, A., Codner, G. F., Nair, R. R., Tibbit, C., McLeod, R., Ali, Z., Noda, J., Marrero-Gagliardi, A., Brito-Armas, J. M., Öztürk, M. M., Simon, M., O'Neill, E., Bryce-Smith, S., ... Cunningham, T. J. (2021). Generation and analysis of innovative genomically humanized knockin SOD1, TARDBP (TDP-43), and FUS mouse models. *iScience*, 24(12), 103463. <https://doi.org/10.1016/j.isci.2021.103463>

- Díaz-Amarilla, P., Olivera-Bravo, S., Trias, E., Cragnolini, A., Martínez-Palma, L., Cassina, P., Beckman, J., & Barbeito, L. (2011). Phenotypically aberrant astrocytes that promote motoneuron damage in a model of inherited amyotrophic lateral sclerosis. *Proceedings of the National Academy of Sciences*, *108*(44), 18126–18131. <https://doi.org/10.1073/pnas.1110689108/>
- Divakaruni, A. S., & Jastroch, M. (2022). A practical guide for the analysis, standardization and interpretation of oxygen consumption measurements. *Nature Metabolism*, *4*(8), 978–994. <https://doi.org/10.1038/s42255-022-00619-4>
- Divakaruni, A. S., Paradyse, A., Ferrick, D. A., Murphy, A. N., & Jastroch, M. (2014). Analysis and interpretation of microplate-based oxygen consumption and pH data. *Methods in Enzymology*, *547*, 309–354. <https://doi.org/10.1016/B978-0-12-801415-8.00016-3>
- Dols-Icardo, O., García-Redondo, A., Rojas-García, R., Sánchez-Valle, R., Noguera, A., Gómez-Tortosa, E., Pastor, P., Hernández, I., Esteban-Pérez, J., Suárez-Calvet, M., Antón-Aguirre, S., Amer, G., Ortega-Cubero, S., Blesa, R., Fortea, J., Alcolea, D., Capdevila, A., Antonell, A., Lladó, A., ... Clarimón, J. (2014). Characterization of the repeat expansion size in C9orf72 in amyotrophic lateral sclerosis and frontotemporal dementia. *Human Molecular Genetics*, *23*(3), 749–754. <https://doi.org/10.1093/hmg/ddt460>
- Dols-Icardo, O., Montal, V., Sirisi, S., López-Pernas, G., Cervera-Carles, L., Querol-Vilaseca, M., Muñoz, L., Belbin, O., Alcolea, D., Molina-Porcel, L., Pegueroles, J., Turón-Sans, J., Blesa, R., Lleó, A., Fortea, J., Rojas-García, R., & Clarimón, J. (2020). Motor cortex transcriptome reveals microglial key events in amyotrophic lateral sclerosis. *Neurology, Neuroimmunology & Neuroinflammation*, *7*(5), e829. <https://doi.org/10.1212/NXI.0000000000000829>
- Dong, W., Ma, Y., Guan, F., Zhang, X., Chen, W., Zhang, L., & Zhang, L. (2021). Ablation of C9orf72 together with excitotoxicity induces ALS in rats. *The FEBS Journal*, *288*(5), 1712–1723. <https://doi.org/10.1111/FEBS.15501>
- Dong, W., Zhang, L., Sun, C., Gao, X., Guan, F., Li, J., Chen, W., Ma, Y., & Zhang, L. (2020). Knock in of a hexanucleotide repeat expansion in the C9orf72 gene induces ALS in rats. *Animal Models and Experimental Medicine*, *3*(3), 237–244. <https://doi.org/10.1002/ame2.12129>
- Douvaras, P., Sun, B., Wang, M., Kruglikov, I., Lалlos, G., Zimmer, M., Terrenoire, C., Zhang, B., Gandy, S., Schadt, E., Freytes, D. O., Noggle, S., & Fossati, V. (2017). Directed differentiation of human pluripotent stem cells to microglia. *Stem Cell Reports*, *8*(6), 1516–1524. <https://doi.org/10.1016/j.stemcr.2017.04.023>
- Dräger, N. M., Sattler, S. M., Huang, C. T. L., Teter, O. M., Leng, K., Hashemi, S. H., Hong, J., Aviles, G., Clelland, C. D., Zhan, L., Udeochu, J. C., Kodama, L., Singleton, A. B., Nalls, M. A., Ichida, J., Ward, M. E., Faghri, F., Gan, L., & Kampmann, M. (2022). A CRISPRi/a platform in human iPSC-derived microglia uncovers regulators of disease states. *Nature Neuroscience*, *25*(9), 1149–1162. <https://doi.org/10.1038/s41593-022-01131-4>
- Dupuis, L., Oudart, H., René, F., Gonzalez De Aguilar, J. L., & Loeffler, J. P. (2004). Evidence for defective energy homeostasis in amyotrophic lateral sclerosis: Benefit of a high-energy diet in a transgenic mouse model. *Proceedings of the National Academy of Sciences*, *101*(30), 11159–11164. <https://doi.org/10.1073/pnas.0402026101/>
- Dupuis, L., Pradat, P.-F., Ludolph, A. C., & Loeffler, J.-P. (2011). Energy metabolism in amyotrophic lateral sclerosis. *The Lancet Neurology*, *10*(1), 75–82. <https://doi.org/10.1016/S1474>
- Ebstein, S. Y., Yagudayeva, I., & Shneider, N. A. (2019). Mutant TDP-43 causes early-stage dose-dependent motor neuron degeneration in a TARDBP knockin mouse model of ALS. *Cell Reports*, *26*(2), 364–373.e4. <https://doi.org/10.1016/j.celrep.2018.12.045>

- Elmore, M. R. P., Lee, R. J., West, B. L., & Green, K. N. (2015). Characterizing newly repopulated microglia in the adult mouse: Impacts on animal behavior, cell morphology, and neuroinflammation. *PLoS One*, *10*(4), e0122912. <https://doi.org/10.1371/journal.pone.0122912>
- Fattorelli, N., Martinez-Muriana, A., Wolfs, L., Geric, I., De Strooper, B., & Mancuso, R. (2021). Stem-cell-derived human microglia transplanted into mouse brain to study human disease. *Nature Protocols*, *16*(2), 1013–1033. <https://doi.org/10.1038/s41596-020-00447-4>
- Feldman, E. L., Goutman, S. A., Petri, S., Mazzini, L., Savelieff, M. G., Shaw, P. J., & Sobue, G. (2022). Amyotrophic lateral sclerosis. *The Lancet*, *400*(10360), 1363–1380. [https://doi.org/10.1016/S0140-6736\(22\)01272-7](https://doi.org/10.1016/S0140-6736(22)01272-7)
- Ferrante, R. J., Shinobu, L. A., Browne, S. E., Bowling, A. C., Schulz, J. B., Brown, R. H., & Beal, M. F. (1997). Evidence of increased oxidative damage in both sporadic and familial amyotrophic lateral sclerosis. *Journal of Neurochemistry*, *69*(5), 2064–2074. <https://doi.org/10.1046/j.1471-4159.1997.69052064.x>
- Ferri, A., Cozzolino, M., Crosio, C., Nencini, M., Casciati, A., Gralla, E. B., Rotilio, G., Valentine, J. S., & Carri, M. T. (2006). Familial ALS-superoxide dismutases associate with mitochondria and shift their redox potentials. *Proceedings of the National Academy of Sciences*, *103*(37), 13860–13865. <https://doi.org/10.1073/PNAS.0605814103/>
- Fiala, M., Chattopadhyay, M., La Cava, A., Tse, E., Liu, G., Lourenco, E., Eskin, A., Liu, P. T., Magpantay, L., Tse, S., Mahanian, M., Weitzman, R., Tong, J., Nguyen, C., Cho, T., Koo, P., Sayre, J., Martinez-Maza, O., Rosenthal, M. J., & Wiedau-Pazos, M. (2010). IL-17A is increased in the serum and in spinal cord CD8 and mast cells of ALS patients. *Journal of Neuroinflammation*, *7*, 79. <https://doi.org/10.1186/1742-2094-7-76>
- Figuroa-Romero, C., Guo, K., Murdock, B. J., Paez-Colasante, X., Bassis, C. M., Mikhail, K. A., Raue, K. D., Evans, M. C., Taubman, G. F., McDermott, A. J., O'Brien, P. D., Savelieff, M. G., Hur, J., & Feldman, E. L. (2020). Temporal evolution of the microbiome, immune system and epigenome with disease progression in ALS mice. *Disease Models and Mechanisms*, *13*(2), dmm041947. <https://doi.org/10.1242/DMM.041947/>
- Fisher, E. M. C., Greensmith, L., Malaspina, A., Fratta, P., Hanna, M. G., Schiavo, G., Isaacs, A. M., Orrell, R. W., Cunningham, T. J., & Arozena, A. A. (2023). Opinion: more mouse models and more translation needed for ALS. *Molecular Neurodegeneration*, *18*(1), 30. <https://doi.org/10.1186/s13024-023-00619-2>
- Flurkey, K., Curren, J. M., & Harrison, D. E. (2007). Mouse models in aging research. *The Mouse in Biomedical Research*, *3*, 637–672. <https://doi.org/10.1016/B978-012369454-6/50074-1>
- Forsberg, K., Graffmo, K., Pakkenberg, B., Weber, M., Nielsen, M., Marklund, S., Brännström, T., & Andersen, P. M. (2019). Misfolded SOD1 inclusions in patients with mutations in C9orf72 and other ALS/FTD-associated genes. *Journal of Neurology, Neurosurgery, and Psychiatry*, *90*(8), 861–869. <https://doi.org/10.1136/JNNP-2018-319386>
- Frakes, A. E., Ferraiuolo, L., Haidet-Phillips, A. M., Schmelzer, L., Braun, L., Miranda, C. J., Ladner, K. J., Bevan, A. K., Foust, K. D., Godbout, J. P., Popovich, P. G., Guttridge, D. C., & Kaspar, B. K. (2014). Microglia induce motor neuron death via the classical NF-κB pathway in amyotrophic lateral sclerosis. *Neuron*, *81*(5), 1009–1023. <https://doi.org/10.1016/j.neuron.2014.01.013>
- Freibaum, B. D., & Taylor, J. P. (2017). The role of dipeptide repeats in C9ORF72-related ALS-FTD. *Frontiers in Molecular Neuroscience*, *10*, 35. <https://doi.org/10.3389/fnmol.2017.00035>

- Freischmidt, A., Müller, K., Ludolph, A. C., & Weishaupt, J. H. (2013). Systemic dysregulation of TDP-43 binding microRNAs in amyotrophic lateral sclerosis. *Acta Neuropathologica Communications*, 1, 42. <https://doi.org/10.1186/2051-5960-1-42>
- Frigerio, C. S., Wolfs, L., Fattorelli, N., Perry, V. H., Fiers, M., & De Strooper, B. (2019). The major risk factors for Alzheimer's disease: Age, sex, and genes modulate the microglia response to Ab plaques. *Cell Reports*, 27(4), 1293–1306. <https://doi.org/10.1016/j.celrep.2019.03.099>
- Fuchs, A., Kutterer, S., Mühling, T., Duda, J., Schütz, B., Liss, B., Keller, B. U., & Roeper, J. (2013). Selective mitochondrial Ca<sup>2+</sup> uptake deficit in disease endstage vulnerable motoneurons of the SOD1G93A mouse model of amyotrophic lateral sclerosis. *Journal of Physiology*, 591(10), 2723–2745. <https://doi.org/10.1113/jphysiol.2012.247981>
- Fujino, S., Andoh, A., Bamba, S., Ogawa, A., Hata, K., Araki, Y., Bamba, T., & Fujiyama, Y. (2003). Increased expression of interleukin 17 in inflammatory bowel disease. *Gut*, 52(1), 65–70. <https://doi.org/10.1136/GUT.52.1.65>
- Funes, S., Jung, J., Hayden Gadd, D., Mosqueda, M., Zhong, J., Unger, M., Stallworth, K., Cameron, D., Rotunno, M. S., Dawes, P., Fowler-Magaw, M., Keagle, P. J., McDonough, J. A., Boopathy, S., Sena-Esteves, M., Nickerson, J. A., Lutz, C., Skarnes, W. C., Lim, E. T., ... Bosco, D. A. (2024). Expression of ALS-PFN1 impairs vesicular degradation in iPSC-derived microglia. *Nature Communications*, 15, 2497. <https://doi.org/10.1038/s41467-024-46695-w>
- Gagliardi, D., Ahmadinejad, M., Del Bo, R., Meneri, M., Comi, G. Pietro, Corti, S., & Ronchi, D. (2022). Homozygous SOD1 variation L144S produces a severe form of amyotrophic lateral sclerosis in an iranian family. *Neurology Genetics*, 8(1), e645. <https://doi.org/10.1212/NXG.0000000000000645>
- Galatro, T. F., Holtman, I. R., Lerario, A. M., Vainchtein, I. D., Brouwer, N., Sola, P. R., Veras, M. M., Pereira, T. F., Leite, R. E. P., Möller, T., Wes, P. D., Sogayar, M. C., Laman, J. D., Den Dunnen, W., Pasqualucci, C. A., Oba-Shinjo, S. M., Boddeke, E. W. G. M., Marie, S. K. N., & Eggen, B. J. L. (2017). Transcriptomic analysis of purified human cortical microglia reveals age-associated changes. *Nature Neuroscience*, 20(8), 1162–1171. <https://doi.org/10.1038/nn.4597>
- Galloway, D. A., Phillips, A. E. M., Owen, D. R. J., & Moore, C. S. (2019). Phagocytosis in the brain: Homeostasis and disease. *Frontiers in Immunology*, 10, 790. <https://doi.org/10.3389/fimmu.2019.00790>
- Gao, F., Almeida, S., & Lopez-Gonzalez, R. (2017). Dysregulated molecular pathways in amyotrophic lateral sclerosis–frontotemporal dementia spectrum disorder. *The EMBO Journal*, 36(20), 2931–2950. <https://doi.org/10.15252/embj.201797568>
- Garofalo, S., Cocozza, G., Porzia, A., Inghilleri, M., Raspa, M., Scavizzi, F., Aronica, E., Bernardini, G., Peng, L., Ransohoff, R. M., Santoni, A., & Limatola, C. (2020). Natural killer cells modulate motor neuron-immune cell cross talk in models of Amyotrophic Lateral Sclerosis. *Nature Communications*, 11(1), 1773. <https://doi.org/10.1038/s41467-020-15644-8>
- Geirsdottir, L., David, E., Keren-Shaul, H., Weiner, A., Bohlen, S. C., Neuber, J., Balic, A., Giladi, A., Sheban, F., Dutertre, C. A., Pfeifle, C., Peri, F., Raffo-Romero, A., Vizioli, J., Matiassek, K., Scheiwe, C., Meckel, S., Mätz-Rensing, K., van der Meer, F., ... Prinz, M. (2019). Cross-species single-cell analysis reveals divergence of the primate microglia program. *Cell*, 179(7), 1609–1622.e16. <https://doi.org/10.1016/j.cell.2019.11.010>
- Geloso, M. C., Corvino, V., Marchese, E., Serrano, A., Michetti, F., D'Ambrosi, N., Tang, Y., Diz-Chaves, Y., Vickers, J. C., & D'Ambrosi, N. (2017). The dual role of microglia in ALS:

- Mechanisms and therapeutic approaches. *Frontiers in Aging Neuroscience*, 9, 242. <https://doi.org/10.3389/fnagi.2017.00242>
- Gendron, T. F., Belzil, V. V., Zhang, Y. J., & Petrucelli, L. (2014). Mechanisms of toxicity in C9FTLD/ALS. *Acta Neuropathologica*, 127(3), 359–376. <https://doi.org/10.1007/s00401-013-1237-z>
- Genge, A., Wainwright, S., & Vande Velde, C. (2023). Amyotrophic lateral sclerosis: exploring pathophysiology in the context of treatment. *Amyotrophic Lateral Sclerosis and Frontotemporal Degeneration*, 25(3–4), 225–236. <https://doi.org/10.1080/21678421.2023.2278503>
- Ghiasi, P., Hosseinkhani, S., Noori, A., Nafissi, S., & Khajeh, K. (2012). Mitochondrial complex I deficiency and ATP/ADP ratio in lymphocytes of amyotrophic lateral sclerosis patients. *Neurological Research*, 34(3), 297–303. <https://doi.org/10.1179/1743132812Y.0000000012>
- Gijselinck, I., Langenhove, T. Van, Van Der Zee, J., Sleegers, K., Philtjens, S., Kleinberger, G., Janssens, J., Bettens, K., Cauwenberghe, C. Van, Pereson, S., Engelborghs, S., Sieben, A., De Jonghe, P., Vandenberghe, R., Santens, P., De Bleecker, J., Maes, G., Bäumer, V., Dillen, L., ... Van Broeckhoven, C. (2012). A C9orf72 promoter repeat expansion in a Flanders-Belgian cohort with disorders of the frontotemporal lobar degeneration-amyotrophic lateral sclerosis spectrum: a gene identification study. *The Lancet Neurology*, 11(1), 54–65. <https://doi.org/10.1016/S1474>
- Ginhoux, F., Greter, M., Leboeuf, M., Nandi, S., See, P., Gokhan, S., Mehler, M. F., Conway, S. J., Guan Ng, L., Stanley, E. R., Samokhvalov, I. M., & Merad, M. (2010). Fate mapping analysis reveals that adult microglia derive from primitive macrophages. *Science*, 330(6005), 841–845. <https://doi.org/10.1126/science.1194637>
- Ginhoux, F., & Jung, S. (2014). Monocytes and macrophages: developmental pathways and tissue homeostasis. *Nature Reviews Immunology*, 14, 392–404. <https://doi.org/10.1038/nri3671>
- Glasmacher, S. A., Wong, C., Pearson, I. E., & Pal, S. (2020). Survival and prognostic factors in C9orf72 repeat expansion carriers: A systematic review and meta-analysis. *JAMA Neurology*, 77(3), 367–376. <https://doi.org/10.1001/JAMANEUROL.2019.3924>
- Goh, C. W., Lee, I. C., Sundaram, J. R., George, S. E., Yusoff, P., Brush, M. H., Sze, N. S. K., & Shenolikar, S. (2018). Chronic oxidative stress promotes GADD34-mediated phosphorylation of the TAR DNA-binding protein TDP-43, a modification linked to neurodegeneration. *Journal of Biological Chemistry*, 293(1), 163–176. <https://doi.org/10.1074/JBC.M117.814111/>
- Gómez-López, A. R., Manich, G., Recasens, M., Almolda, B., González, B., & Castellano, B. (2021). Evaluation of myelin phagocytosis by microglia/macrophages in nervous tissue using flow cytometry. *Current Protocols*, 1(3), e73. <https://doi.org/10.1002/cpz1.73>
- Gong, Y. H., Parsadanian, A. S., Andreeva, A., Snider, W. D., & Elliott, J. L. (2000). Restricted expression of G86R Cu/Zn superoxide dismutase in astrocytes results in astrocytosis but does not cause motoneuron degeneration. *Journal of Neuroscience*, 20(2), 660–665. <https://doi.org/10.1523/JNEUROSCI.20-02-00660.2000>
- Gosselin, D., Skola, D., Coufal, N. G., Holtman, I. R., Schlachetzki, J. C. M., Sajti, E., Jaeger, B. N., O'Connor, C., Fitzpatrick, C., Pasillas, M. P., Pena, M., Adair, A., Gonda, D. D., Levy, M. L., Ransohoff, R. M., Gage, F. H., & Glass, C. K. (2017). An environment-dependent transcriptional network specifies human microglia identity. *Science*, 356(6344), 1248–1259. <https://doi.org/10.1126/science.aal3222>



- Goutman, S. A., Hardiman, O., Al-Chalabi, A., Chió, A., Savelieff, M. G., Kiernan, M. C., & Feldman, E. L. (2022). Emerging insights into the complex genetics and pathophysiology of amyotrophic lateral sclerosis. *The Lancet Neurology*, *21*(5), 465–479. [https://doi.org/10.1016/S1474-4422\(21\)00414-2](https://doi.org/10.1016/S1474-4422(21)00414-2)
- Graffmo, K. S., Forsberg, K., Bergh, J., Birve, A., Zetterström, P., Andersen, P. M., Marklund, S. L., & Brännström, T. (2013). Expression of wild-type human superoxide dismutase-1 in mice causes amyotrophic lateral sclerosis. *Human Molecular Genetics*, *22*(1), 51–60. <https://doi.org/10.1093/hmg/dd3399>
- Gregory, J. M., Fagegaltier, D., Phatnani, H., & Harms, M. B. (2020). Genetics of amyotrophic lateral sclerosis. *Current Genetic Medicine Reports*, *8*, 121–131. <https://doi.org/10.1007/s40142-020-00194-8>/Published
- Gurney, M. E., Pu, H., Chiu, A. Y., Dal Canto, M. C., Polchow, C. Y., Alexander, D. D., Caliendo, J., Hentati, A., Kwon, Y. W., Deng, H.-X., Chen, W., Zhai, P., Sufit, R. L., Siddique, T., Gurney, M. E., Pu, H., Alexander, D. D., Kwon, Y. W., Zhai, P., ... Chen, W. (1994). Motor neuron degeneration in mice that express a human Cu,Zn superoxide dismutase mutation. *Science*, *264*(5166), 1772–1775. <https://doi.org/10.1126/science.8209258>
- Gustafson, M. P., Staff, N. P., Bornschlegl, S., Butler, G. W., Maas, M. L., Kazamel, M., Zubair, A., Gastineau, D. A., Windebank, A. J., & Dietz, A. B. (2017). Comprehensive immune profiling reveals substantial immune system alterations in a subset of patients with amyotrophic lateral sclerosis. *PLoS One*, *12*(7), e0182002. <https://doi.org/10.1371/journal.pone.0182002>
- Guttikonda, S. R., Sikkema, L., Tchieu, J., Saurat, N., Walsh, R. M., Harschnitz, O., Ciceri, G., Sneeboer, M., Mazutis, L., Setty, M., Zumbo, P., Betel, D., de Witte, L. D., Pe'er, D., & Studer, L. (2021). Fully defined human pluripotent stem cell-derived microglia and tri-culture system model C3 production in Alzheimer's disease. *Nature Neuroscience*, *24*(3), 343–354. <https://doi.org/10.1038/s41593-020-00796-z>
- Guzmán-Lenis, M.-S., Navarro, X., & Casas, C. (2009). Drug screening of neuroprotective agents on an organotypic-based model of spinal cord excitotoxic damage. *Restorative Neurology and Neuroscience*, *27*, 335–349. <https://doi.org/10.3233/RNN-2009-0482>
- Haenseler, W., Sansom, S. N., Buchrieser, J., Newey, S. E., Moore, C. S., Nicholls, F. J., Chintawar, S., Schnell, C., Antel, J. P., Allen, N. D., Cader, M. Z., Wade-Martins, R., James, W. S., & Cowley, S. A. (2017). A highly efficient human pluripotent stem cell microglia model displays a neuronal-co-culture-specific expression profile and inflammatory response. *Stem Cell Reports*, *8*(6), 1727–1742. <https://doi.org/10.1016/j.stemcr.2017.05.017>
- Haidet-Phillips, A. M., Hester, M. E., Miranda, C. J., Meyer, K., Braun, L., Frakes, A., Song, S., Likhite, S., Murtha, M. J., Foust, K. D., Rao, M., Eagle, A., Kammesheidt, A., Christensen, A., Mendell, J. R., M Burghes, A. H., & Kaspar, B. K. (2011). Astrocytes from familial and sporadic ALS patients are toxic to motor neurons. *Nature Biotechnology*, *29*(9), 824–828. <https://doi.org/10.1038/nbt1957>
- Hardiman, O., Al-Chalabi, A., Chio, A., Corr, E. M., Logroscino, G., Robberecht, W., Shaw, P. J., Simmons, Z., & van den Berg, L. H. (2017). Amyotrophic lateral sclerosis. *Nature Reviews Disease Primers*, *3*, 17071. <https://doi.org/10.1038/nrdp.2017.71>
- Hasselmann, J., & Blurton-Jones, M. (2020). Human iPSC-derived microglia: A growing toolset to study the brain's innate immune cells. *Glia*, *68*(4), 721–739. <https://doi.org/10.1002/glia.23781>
- Hasselmann, J., Coburn, M. A., England, W., Figueroa Velez, D. X., Kiani Shabestari, S., Tu, C. H., McQuade, A., Kolahdouzan, M., Echeverria, K., Claes, C., Nakayama, T., Azevedo, R., Coufal,

- N. G., Han, C. Z., Cummings, B. J., Davtyan, H., Glass, C. K., Healy, L. M., Gandhi, S. P., ... Blurton-Jones, M. (2019). Development of a chimeric model to study and manipulate human microglia in vivo. *Neuron*, *103*(6), 1016-1033.e10. <https://doi.org/10.1016/j.neuron.2019.07.002>
- Haukedal, H., & Freude, K. (2019). Implications of Microglia in Amyotrophic Lateral Sclerosis and Frontotemporal Dementia. In *Journal of Molecular Biology* (Vol. 431, Issue 9, pp. 1818–1829). Academic Press. <https://doi.org/10.1016/j.jmb.2019.02.004>
- Henkel, J. S., Beers, D. R., Wen, S., Rivera, A. L., Toennis, K. M., Appel, J. E., Zhao, W., Moore, D. H., Powell, S. Z., & Appel, S. H. (2013). Regulatory T-lymphocytes mediate amyotrophic lateral sclerosis progression and survival. *EMBO Molecular Medicine*, *5*(1), 64–79. <https://doi.org/10.1002/EMMM.201201544>
- Herranz-Martin, S., Chandran, J., Lewis, K., Mulcahy, P., Higginbottom, A., Walker, C., Valenzuela, I. M. P. Y., Jones, R. A., Coldicott, I., Iannitti, T., Akaaboune, M., El-Khamisy, S. F., Gillingwater, T. H., Shaw, P. J., & Azzouz, M. (2017). Viral delivery of C9orf72 hexanucleotide repeat expansions in mice leads to repeat-length-dependent neuropathology and behavioural deficits. *Disease Models and Mechanisms*, *10*(7), 859–868. <https://doi.org/10.1242/dmm.029892>
- Hewitt, C., Kirby, J., Highley, J. R., Hartley, J. A., Hibberd, R., Hollinger, H. C., Williams, T. L., Ince, P. G., McDermott, C. J., & Shaw, P. J. (2010). Novel FUS/TLS mutations and pathology in familial and sporadic amyotrophic lateral sclerosis. *Archives of Neurology*, *67*(4), 455–461. <https://doi.org/10.1001/ARCHNEUROL.2010.52>
- Hickman, S., Izzy, S., Sen, P., Morsett, L., & El Khoury, J. (2018). Microglia in neurodegeneration. *Nature Neuroscience*, *21*(10), 1359–1369. <https://doi.org/10.1038/s41593-018-0242-x>
- Hirano, A., Donnenfeld, H., Sasaki, S., & Nakano, I. (1984). Fine structural observations of neurofilamentous changes in amyotrophic lateral sclerosis. *Journal of Neuropathology & Experimental Neurology*, *43*(5), 461–470. <https://doi.org/10.1097/00005072-198409000-00001>
- Hor, J. H., Santosa, M. M., Lim, V. J. W., Ho, B. X., Taylor, A., Khong, Z. J., Ravits, J., Fan, Y., Liou, Y. C., Soh, B. S., & Ng, S. Y. (2021). ALS motor neurons exhibit hallmark metabolic defects that are rescued by SIRT3 activation. *Cell Death and Differentiation*, *28*(4), 1379–1397. <https://doi.org/10.1038/s41418-020-00664-0>
- Hounoum, B. M., Vourc'h, P., Felix, R., Corcia, P., Patin, F., Guéguinou, M., Potier-Cartereau, M., Vandier, C., Raoul, C., Andres, C. R., Mavel, S., Blasco, H., Jaiswal, M. K., Tauskela, J., & Nistri, A. (2016). NSC-34 motor neuron-like cells are unsuitable as experimental model for glutamate-mediated excitotoxicity. *Frontiers in Cellular Neuroscience*, *10*, 118. <https://doi.org/10.3389/fncel.2016.00118>
- Hsu, H. Y., & Wen, M. H. (2002). Lipopolysaccharide-mediated reactive oxygen species and signal transduction in the regulation of interleukin-1 gene expression. *Journal of Biological Chemistry*, *277*(25), 22131–22139. <https://doi.org/10.1074/JBC.M111883200>
- Hu, Y., Cao, C., Qin, X. Y., Yu, Y., Yuan, J., Zhao, Y., & Cheng, Y. (2017). Increased peripheral blood inflammatory cytokine levels in amyotrophic lateral sclerosis: a meta-analysis study. *Scientific Reports*, *7*(1), 9094. <https://doi.org/10.1038/S41598-017-09097-1>
- Huang, S. L., Wu, L. S., Lee, M., Chang, C. W., Cheng, W. C., Fang, Y. S., Chen, Y. R., Cheng, P. L., & Shen, C. K. J. (2020). A robust TDP-43 knock-in mouse model of ALS. *Acta Neuropathologica Communications*, *8*(1), 3. <https://doi.org/10.1186/s40478-020-0881-5>

- Igaz, L. M., Kwong, L. K., Lee, E. B., Chen-Plotkin, A., Swanson, E., Unger, T., Malunda, J., Xu, Y., Winton, M. J., Trojanowski, J. Q., & Lee, V. M. Y. (2011). Dysregulation of the ALS-associated gene TDP-43 leads to neuronal death and degeneration in mice. *Journal of Clinical Investigation*, *121*(2), 726–738. <https://doi.org/10.1172/JCI44867>
- Igoudjil, A., Magrane´, J., Fischer, L. R., Kim, H. J., Hervias, I., Dumont, M., Cortez, C., Glass, J. D., Starkov, A. A., & Manfredi, G. (2011). In vivo pathogenic role of mutant SOD1 localized in the mitochondrial intermembrane space. *The Journal of Neuroscience*, *31*(44), 15826–15837. <https://doi.org/10.1523/JNEUROSCI.1965-11.2011>
- Ince, P., Stout, N., Shaw, P., Slade, J., Hunziker, W., Heizmann, C. W., & Baimbridge, K. G. (1993). Parvalbumin and calbindin D-28k in the human motor system and in motor neuron disease. *Neuropathology and Applied Neurobiology*, *19*(4), 291–299. <https://doi.org/10.1111/J.1365-2990.1993.TB00443.X>
- Irvin, C. W., Kim, R. B., & Mitchell, C. S. (2015). Seeking homeostasis: Temporal trends in respiration, oxidation, and calcium in SOD1 G93A amyotrophic lateral sclerosis mice. *Frontiers in Cellular Neuroscience*, *9*, 248. <https://doi.org/10.3389/fncel.2015.00248>
- Irwin, K. E., Sheth, U., Wong, P. C., & Gendron, T. F. (2024). Fluid biomarkers for amyotrophic lateral sclerosis: a review. *Molecular Neurodegeneration*, *19*(1), 9. <https://doi.org/10.1186/S13024-023-00685-6>
- Ito, Y., Yamada, M., Tanaka, H., Aida, K., Tsuruma, K., Shimazawa, M., Hozumi, I., Inuzuka, T., Takahashi, H., & Hara, H. (2009). Involvement of CHOP, an ER-stress apoptotic mediator, in both human sporadic ALS and ALS model mice. *Neurobiology of Disease*, *36*(3), 470–476. <https://doi.org/10.1016/j.nbd.2009.08.013>
- Jaarsma, D., Rognoni, F., Van Duijn, W., Verspaget, H. W., Haasdijk, E. D., & Holstege, J. C. (2001). CuZn superoxide dismutase (SOD1) accumulates in vacuolated mitochondria in transgenic mice expressing amyotrophic lateral sclerosis-linked SOD1 mutations. *Acta Neuropathologica*, *102*(4), 293–305. <https://doi.org/10.1007/S004010100399/>
- Jauregui, C., Blanco-Luquin, I., Macías, M., Roldan, M., Caballero, C., Pagola, I., Mendioroz, M., & Jericó, I. (2023). Exploring the disease-associated microglia state in amyotrophic lateral sclerosis. *Biomedicines*, *11*(11), 2994. <https://doi.org/10.3390/biomedicines11112994>
- Jeon, Y. M., Kwon, Y., Lee, S., & Kim, H. J. (2023). Potential roles of the endoplasmic reticulum stress pathway in amyotrophic lateral sclerosis. *Frontiers in Aging Neuroscience*, *15*, 1047897. <https://doi.org/10.3389/fnagi.2023.1047897>
- Jiang, J., Zhu, Q., Gendron, T. F., Saberi, S., McAlonis-Downes, M., Seelman, A., Stauffer, J. E., Jafar-nejad, P., Drenner, K., Schulte, D., Chun, S., Sun, S., Ling, S. C., Myers, B., Engelhardt, J., Katz, M., Baughn, M., Platoshyn, O., Marsala, M., ... Lagier-Tourenne, C. (2016). Gain of toxicity from ALS/FTD-linked repeat expansions in C9ORF72 is alleviated by antisense oligonucleotides targeting GGGGCC-containing RNAs. *Neuron*, *90*(3), 535–550. <https://doi.org/10.1016/j.neuron.2016.04.006>
- Jiménez-Villegas, J., Ferraiuolo, L., Mead, R. J., Shaw, P. J., Cuadrado, A., & Rojo, A. I. (2021). NRF2 as a therapeutic opportunity to impact in the molecular roadmap of ALS. *Free Radical Biology and Medicine*, *173*, 125–141. <https://doi.org/10.1016/J.FREERADBIOMED.2021.07.022>
- Jin, M., Günther, R., Akgün, K., Hermann, A., & Ziemssen, T. (2020). Peripheral proinflammatory Th1/Th17 immune cell shift is linked to disease severity in amyotrophic lateral sclerosis. *Scientific Reports*, *10*(1), 5941. <https://doi.org/10.1038/s41598-020-62756-8>

- Jonsson, P. A., Graffmo, K. S., Andersen, P. M., Brännström, T., Lindberg, M., Oliveberg, M., & Marklund, S. L. (2006). Disulphide-reduced superoxide dismutase-1 in CNS of transgenic amyotrophic lateral sclerosis models. *Brain*, *129*(2), 451–464. <https://doi.org/10.1093/brain/awh704>
- Joyce, P. I., Mcgoldrick, P., Saccon, R. A., Weber, W., Fratta, P., West, S. J., Zhu, N., Carter, S., Phatak, V., Stewart, M., Simon, M., Kumar, S., Heise, I., Bros-Facer, V., Dick, J., Corrochano, S., Stanford, M. J., Luong, T. V., Nolan, P. M., ... Acevedo-Arozena, A. (2014). A novel SOD1-ALS mutation separates central and peripheral effects of mutant SOD1 toxicity. *Human Molecular Genetics*, *24*(7), 1883–1897. <https://doi.org/10.1093/hmg/ddu605>
- Kapeli, K., Martinez, F. J., & Yeo, G. W. (2017). Genetic mutations in RNA-binding proteins and their roles in ALS. *Human Genetics*, *136*(9), 1193–1214. <https://doi.org/10.1007/s00439-017-1830-7>
- Kawahara, Y., & Mieda-Sato, A. (2012). TDP-43 promotes microRNA biogenesis as a component of the Drosha and Dicer complexes. *Proceedings of the National Academy of Sciences*, *109*(9), 3347–3352. <https://doi.org/10.1073/pnas.1112427109>
- Kawamata, H., & Manfredi, G. (2017). Proteinopathies and OXPHOS dysfunction in neurodegenerative diseases. *The Journal of Cell Biology*, *216*(12), 3917–3929. <https://doi.org/10.1083/JCB.201709172>
- Kawamata, T., Akiyama, H., Yamada, T., & Mcgeer, P. L. (1992). Immunologic reactions in amyotrophic lateral sclerosis brain and spinal cord tissue. *American Journal of Pathology*, *140*(3), 691–707.
- Kawanokuchi, J., Shimizu, K., Nitta, A., Yamada, K., Mizuno, T., Takeuchi, H., & Suzumura, A. (2008). Production and functions of IL-17 in microglia. *Journal of Neuroimmunology*, *194*(1–2), 54–61. <https://doi.org/10.1016/j.jneuroim.2007.11.006>
- Keren-Shaul, H., Spinrad, A., Weiner, A., Matcovitch-Natan, O., Dvir-Szternfeld, R., Ulland, T. K., David, E., Baruch, K., Lara-Astaiso, D., Toth, B., Itzkovitz, S., Colonna, M., Schwartz, M., & Amit, I. (2017). A unique microglia type associated with restricting development of Alzheimer's disease. *Cell*, *169*(7), 1276–1290. <https://doi.org/10.1016/j.cell.2017.05.018>
- Kerk, S. Y., Bai, Y., Smith, J., Lalgudi, P., Hunt, C., Kuno, J., Nuara, J., Yang, T., Lanza, K., Chan, N., Coppola, A., Tang, Q., Espert, J., Jones, H., Fannell, C., Zambrowicz, B., & Chiao, E. (2022). Homozygous ALS-linked FUS P525L mutations cell-autonomously perturb transcriptome profile and chemoreceptor signaling in human iPSC microglia. *Stem Cell Reports*, *17*(3), 678–692. <https://doi.org/10.1016/j.stemcr.2022.01.004>
- Kierdorf, K., Erny, D., Goldmann, T., Sander, V., Schulz, C., Perdiguero, E. G., Wieghofer, P., Heinrich, A., Riemke, P., Hölscher, C., Müller, D. N., Luckow, B., Brouwer, T., Debowski, K., Fritz, G., Opdenakker, G., Diefenbach, A., Biber, K., Heikenwalder, M., ... Prinz, M. (2013). Microglia emerge from erythromyeloid precursors via Pu.1- and Irf8-dependent pathways. *Nature Neuroscience*, *16*(3), 273–280. <https://doi.org/10.1038/nn.3318>
- Kim, B. W., Ryu, J., Jeong, Y. E., Kim, J., & Martin, L. J. (2020). Human motor neurons with SOD1-G93A mutation generated from CRISPR/Cas9 gene-edited iPSCs develop pathological features of amyotrophic lateral sclerosis. *Frontiers in Cellular Neuroscience*, *14*, 604171. <https://doi.org/10.3389/fncel.2020.604171>
- Kim, E., White, M. A., Phillips, B. U., Lopez-Cruz, L., Kim, H., Heath, C. J., Lee, J. E., Saksida, L. M., Sreedharan, J., & Bussey, T. J. (2020). Coexistence of perseveration and apathy in the TDP-43Q331K knock-in mouse model of ALS-FTD. *Translational Psychiatry*, *10*(1), 377. <https://doi.org/10.1038/s41398-020-01078-9>

- Kirkinezos, I. G., Bacman, S. R., Hernandez, D., Oca-Cossio, J., Arias, L. J., Perez-Pinzon, M. A., Bradley, W. G., & Moraes, C. T. (2005). Cytochrome c Association with the Inner Mitochondrial Membrane Is Impaired in the CNS of G93A-SOD1 Mice. *The Journal of Neuroscience*, *25*(1), 164. <https://doi.org/10.1523/jneurosci.3829-04.2005>
- Kiyong, K. (2021). Glutathione in the nervous system as a potential therapeutic target to control the development and progression of amyotrophic lateral sclerosis. *Antioxidants*, *10*(7), 1011. <https://doi.org/10.3390/antiox10071011>
- Kojak, N., Kuno, J., Fittipaldi, K. E., Khan, A., Wenger, D., Glasser, M., Donnianni, R. A., Tang, Y., Zhang, J., Huling, K., Ally, R., Mujica, A. O., Turner, T., Magardino, G., Huang, P. Y., Kerk, S. Y., Droguett, G., Prissette, M., Rojas, J., ... Kajimura, D. (2024). Somatic and intergenerational G4C2 hexanucleotide repeat instability in a human C9orf72 knock-in mouse model. *Nucleic Acids Research*, *52*(10), 5732–5755. <https://doi.org/10.1093/nar/gkae250>
- Konttinen, H., Cabral-da-Silva, M. e. C., Ohtonen, S., Wojciechowski, S., Shakirzyanova, A., Caligola, S., Giugno, R., Ishchenko, Y., Hernández, D., Fazaludeen, M. F., Eamen, S., Budia, M. G., Fagerlund, I., Scoyni, F., Korhonen, P., Huber, N., Haapasalo, A., Hewitt, A. W., Vickers, J., ... Malm, T. (2019). PSEN1ΔE9, APP<sup>swe</sup>, and APOE4 confer disparate phenotypes in human iPSC-derived microglia. *Stem Cell Reports*, *13*(4), 669–683. <https://doi.org/10.1016/j.stemcr.2019.08.004>
- Koppers, M., Blokhuis, A. M., Westeneng, H. J., Terpstra, M. L., Zundel, C. A. C., Vieira De Sá, R., Schellevis, R. D., Waite, A. J., Blake, D. J., Veldink, J. H., Van Den Berg, L. H., & Pasterkamp, R. J. (2015). C9orf72 ablation in mice does not cause motor neuron degeneration or motor deficits. *Annals of Neurology*, *78*(3), 426–438. <https://doi.org/10.1002/ANA.24453>
- Koss, D. J., Robinson, L., Drever, B. D., Plucińska, K., Stoppelkamp, S., Veselcic, P., Riedel, G., & Platt, B. (2016). Mutant Tau knock-in mice display frontotemporal dementia relevant behaviour and histopathology. *Neurobiology of Disease*, *91*, 105–123. <https://doi.org/10.1016/j.NBD.2016.03.002>
- Krasemann, S., Madore, C., Cialic, R., Ochando, J., Haass, C., & Correspondence, O. B. (2017). The TREM2-APOE pathway drives the transcriptional phenotype of dysfunctional microglia in neurodegenerative diseases. *Immunity*, *47*(3), 566–581.e9. <https://doi.org/10.1016/j.immuni.2017.08.008>
- Lacomblez, L., Bensimon, G., Leigh, N. P., Guillet, P., Meininger, V., & ALS/Riluzole Study Group II. (1996). Dose-ranging study of riluzole in amyotrophic lateral sclerosis muscle-strength deterioration in ALS patients. *The Lancet*, *347*(9013), 1425–1431.
- Lago, N., Kaufmann, F. N., Negro-Demontel, M. L., Alí-Ruiz, D., Ghisleni, G., Rego, N., Arcas-García, A., Vitureira, N., Jansen, K., Souza, L. M., Silva, R. A., Lara, D. R., Pannunzio, B., Andrés Abin-Carriquiry, J., Amo-Aparicio, J., Martin-Otal, C., Naya, H., MCGavern, D. B., Sayós, J., ... Peluffo, H. (2020). CD300f immunoreceptor is associated with major depressive disorder and decreased microglial metabolic fitness. *Proceedings of the National Academy of Sciences*, *117*(12), 6651–6662. <https://doi.org/10.1073/pnas.1911816117>
- Lall, D., Lorenzini, I., Mota, T. A., Bell, S., Mahan, T. E., Ulrich, J. D., Davtyan, H., Rexach, J. E., Muhammad, A. K. M. G., Shelest, O., Landeros, J., Vazquez, M., Kim, J., Ghaffari, L., O'Rourke, J. G., Geschwind, D. H., Blurton-Jones, M., Holtzman, D. M., Sattler, R., & Baloh, R. H. (2021). C9orf72 deficiency promotes microglial-mediated synaptic loss in aging and amyloid accumulation. *Neuron*, *109*(14), 2275–2291.e8. <https://doi.org/10.1016/j.neuron.2021.05.020>
- Lambert-Smith, I. A., Saunders, D. N., & Yerbury, J. J. (2022). Proteostasis impairment and ALS. *Progress in Biophysics and Molecular Biology*, *174*, 3–27. <https://doi.org/10.1016/j.pbiomolbio.2022.06.001>

- Lanfer, J., Kaindl, J., Krumm, L., Acera, M. G., Neurath, M., Regensburger, M., Krach, F., & Winner, B. (2022). Efficient and easy conversion of human iPSCs into functional induced microglia-like cells. *International Journal of Molecular Sciences*, *23*(9), 4526. <https://doi.org/10.3390/ijms23094526>
- Leclerc, N., Ribera, F., Zoll, J., Warter, J. M., Poindron, P., Lampert, E., & Borg, J. (2001). Selective changes in mitochondria respiratory properties in oxidative or glycolytic muscle fibers isolated from G93A human SOD1 transgenic mice. *Neuromuscular Disorders*, *11*(8), 722–727. [https://doi.org/10.1016/S0960-8966\(01\)00240-1](https://doi.org/10.1016/S0960-8966(01)00240-1)
- Lee, K. H., Zhang, P., Kim, H. J., Mitrea, D. M., Sarkar, M., Freibaum, B. D., Cika, J., Coughlin, M., Messing, J., Mollieux, A., Maxwell, B. A., Kim, N. C., Temirov, J., Moore, J., Kolaitis, R. M., Shaw, T. I., Bai, B., Peng, J., Kriwacki, R. W., & Taylor, J. P. (2016). C9orf72 dipeptide repeats impair the assembly, dynamics, and function of membrane-less organelles. *Cell*, *167*(3), 774–788.e17. <https://doi.org/10.1016/j.cell.2016.10.002>
- Leigh, P. N., Whitwell, H., Garofalo, O., Buller, J., Swash, M., Martin, J. E., Gallo, J. M., Weller, R. O., & Anderton, B. H. (1991). Ubiquitin-immunoreactive intraneuronal inclusions in amyotrophic lateral sclerosis: Morphology, distribution, and specificity. *Brain*, *114*(2), 775–788. <https://doi.org/10.1093/brain/114.2.775>
- Lepore, A. C., Rauck, B., Dejea, C., Pardo, A. C., Rao, M. S., Rothstein, J. D., & Maragakis, N. J. (2008). Focal transplantation-based astrocyte replacement is neuroprotective in a model of motor neuron disease. *Nature Neuroscience*, *11*(11), 1294–1301. <https://doi.org/10.1038/nn.2210>
- Li, Q., & Barres, B. A. (2018). Microglia and macrophages in brain homeostasis and disease. *Nature Reviews Immunology*, *18*(4), 225–242. <https://doi.org/10.1038/nri.2017.125>
- Liao, B., Zhao, W., Beers, D. R., Henkel, J. S., & Appel, S. H. (2012). Transformation from a neuroprotective to a neurotoxic microglial phenotype in a mouse model of ALS. *Experimental Neurology*, *237*(1), 147–152. <https://doi.org/10.1016/j.expneurol.2012.06.011>
- Liddel, S. A., Guttenplan, K. A., Clarke, L. E., Bennett, F. C., Bohlen, C. J., Schirmer, L., Bennett, M. L., Münch, A. E., Chung, W. S., Peterson, T. C., Wilton, D. K., Frouin, A., Napier, B. A., Panicker, N., Kumar, M., Buckwalter, M. S., Rowitch, D. H., Dawson, V. L., Dawson, T. M., ... Barres, B. A. (2017). Neurotoxic reactive astrocytes are induced by activated microglia. *Nature*, *541*(7638), 481–487. <https://doi.org/10.1038/nature21029>
- Limone, F., Mordes, D. A., Couto, A., Joseph, B. J., Mitchell, J. M., Therrien, M., Dia Ghosh, S., Meyer, D., Zhang, Y., Goldman, M., Cobos, I., Kadiu, I., McCarroll, S. A., Stevens, B., Pietiläinen, O., Eggan, K., & Mordes, D. (2023). Single-nucleus sequencing reveals enriched expression of genetic risk factors in Extratelencephalic Neurons sensitive to degeneration in ALS. *BioRxiv*. <https://doi.org/10.1101/2021.07.12.452054>
- Lino, M. M., Schneider, C., & Caroni, P. (2002). Accumulation of SOD1 mutants in postnatal motoneurons does not cause motoneuron pathology or motoneuron disease. *The Journal of Neuroscience*, *22*(12), 4825–4832. <https://doi.org/10.1523/jneurosci.22-12-04825.2002>
- Liu, E., Karpf, L., & Bohl, D. (2021). Neuroinflammation in amyotrophic lateral sclerosis and frontotemporal dementia and the interest of induced pluripotent stem cells to study immune cells interactions with neurons. *Frontiers in Molecular Neuroscience*, *14*, 767041. <https://doi.org/10.3389/fnmol.2021.767041>
- Liu, G., Fiala, M., Mizwicki, M. T., Sayre, J., Magpantay, L., Siani, A., Mahanian, M., Chattopadhyay, M., La Cava, A., & Wiedau-Pazos, M. (2012). Neuronal phagocytosis by

- inflammatory macrophages in ALS spinal cord: inhibition of inflammation by resolvin D1. *American Journal of Neurodegenerative Diseases*, 1(1), 60–74.
- Liu, J., & Wang, F. (2017). Role of neuroinflammation in amyotrophic lateral sclerosis: Cellular mechanisms and therapeutic implications. In *Frontiers in Immunology* (Vol. 8, Issue AUG). Frontiers Media S.A. <https://doi.org/10.3389/fimmu.2017.01005>
- Liu, X., & Quan, N. (2018). Microglia and CNS interleukin-1: Beyond immunological concepts. *Frontiers in Neurology*, 9, 8. <https://doi.org/10.3389/fneur.2018.00008>
- Liu, Y., Hao, W., Dawson, A., Liu, S., & Fassbender, K. (2009). Expression of amyotrophic lateral sclerosis-linked SOD1 mutant increases the neurotoxic potential of microglia via TLR2. *Journal of Biological Chemistry*, 284(6), 3691–3699. <https://doi.org/10.1074/jbc.M804446200>
- Liu, Y., Pattamatta, A., Zu, T., Reid, T., Bardhi, O., Borchelt, D. R., Yachnis, A. T., & Ranum, L. P. W. (2016). C9orf72 BAC mouse model with motor deficits and neurodegenerative features of ALS/FTD. *Neuron*, 90(3), 521–534. <https://doi.org/10.1016/j.neuron.2016.04.005>
- Lloyd, A. F., Martinez-Muriana, A., Davis, E., Daniels, M. J., Hou, P., Mancuso, R., Brenes, A. J., Geric, I., Snellinx, A., Craessaerts, K., Theys, T., Fiers, M., De Strooper, B., & Howden, A. J. (2024). Deep proteomic analysis of microglia reveals fundamental biological differences between model systems. *BioRxiv*. <https://doi.org/10.1101/2022.07.07.498804>
- Longinetti, E., & Fang, F. (2019). Epidemiology of amyotrophic lateral sclerosis: An update of recent literature. *Current Opinion in Neurology*, 32(5), 771–776. <https://doi.org/10.1097/WCO.0000000000000730>
- López-Erauskin, J., Tadokoro, T., Baughn, M. W., Lagier-Tourenne, C., Cleveland, D. W., & Da Cruz, S. (2018). ALS/FTD-linked mutation in FUS suppresses intra-axonal protein synthesis and drives disease without nuclear loss-of-function of FUS. *Neuron*, 100(4), 816–830.e7. <https://doi.org/10.1016/j.neuron.2018.09.044>
- Lopez-Gonzalez, R., Lu, Y., Gendron, T. F., Karydas, A., Tran, H., Yang, D., Petrucelli, L., Miller, B. L., Almeida, S., & Gao, F. B. (2016). Poly(GR) in C9ORF72-related ALS/FTD compromises mitochondrial function and increases oxidative stress and DNA damage in iPSC-derived motor neurons. *Neuron*, 92(2), 383–391. <https://doi.org/10.1016/J.NEURON.2016.09.015>
- Lopez-Herdoiza, M.-B., Bauché, S., Wilmet, B., Le Duigou, C., Roussel, D., Frah, M., Béal, J., Devely, G., Boluda, S., Frick, P., Bouteiller, D., Dussaud, S., Guillabert, P., Dalle, C., Dumont, M., Camuzat, A., Saracino, D., Barbier, M., Bruneteau, G., ... Latouche, M. (2023). C9ORF72 knockdown triggers FTD-like symptoms and cell pathology in mice. *Frontiers in Cellular Neuroscience*, 17, 1155929. <https://doi.org/10.3389/fncel.2023.1155929>
- Lorenzini, I., Alsop, E., Levy, J., Gittings, L. M., Lall, D., Rabichow, B. E., Moore, S., Pevey, R., Bustos, L. M., Burciu, C., Bhatia, D., Singer, M., Saul, J., McQuade, A., Tzioras, M., Mota, T. A., Logemann, A., Rose, J., Almeida, S., ... Sattler, R. (2023). Moderate intrinsic phenotypic alterations in C9orf72 ALS/FTD iPSC-microglia despite the presence of C9orf72 pathological features. *Frontiers in Cellular Neuroscience*, 17, 1179796. <https://doi.org/10.3389/fncel.2023.1179796>
- Lu, C.-H., Allen, K., Oei, F., Leoni, E., Kuhle, J., Tree, T., Fratta, P., Sharma, N., Sidle, K., Howard, R., Orrell, R., Fish, M., Greensmith, L., Pearce, N., Gallo, V., & Malaspina, A. (2016). Systemic inflammatory response and neuromuscular involvement in amyotrophic lateral sclerosis. *Neurology Neuroimmunology & Neuroinflammation*, 3(4), e244. <https://doi.org/10.1212/nxi.0000000000000244>

- Lueptow, L. M. (2017). Novel object recognition test for the investigation of learning and memory in mice. *Journal of Visualized Experiments*, *126*, 55718. <https://doi.org/10.3791/55718>
- Lutz, C. (2018). Mouse models of ALS: Past, present and future. *Brain Research*, *1693*(Pt A), 1–10. <https://doi.org/10.1016/j.brainres.2018.03.024>
- Lynch, M. A. (2020). Can the emerging field of immunometabolism provide insights into neuroinflammation? *Progress in Neurobiology*, *184*, 101719. <https://doi.org/10.1016/j.pneurobio.2019.101719>
- Mackenzie, I. R. A., Bigio, E. H., Ince, P. G., Geser, F., Neumann, M., Cairns, N. J., Kwong, L. K., Forman, M. S., Ravits, J., Stewart, H., Eisen, A., McClusky, L., Kretzschmar, H. A., Monoranu, C. M., Highley, J. R., Kirby, J., Siddique, T., Shaw, P. J., Lee, V. M. Y., & Trojanowski, J. Q. (2007). Pathological TDP-43 distinguishes sporadic amyotrophic lateral sclerosis from amyotrophic lateral sclerosis with SOD1 mutations. *Annals of Neurology*, *61*(5), 427–434. <https://doi.org/10.1002/ANA.21147>
- Mackenzie, I. R., Arzberger, T., Kremmer, E., Troost, D., Lorenzl, S., Mori, K., Weng, S. M., Haass, C., Kretzschmar, H. A., Edbauer, D., & Neumann, M. (2013). Dipeptide repeat protein pathology in C9ORF72 mutation cases: Clinico-pathological correlations. *Acta Neuropathologica*, *126*(6), 859–879. <https://doi.org/10.1007/s00401-013-1181-y>
- Magrané, J., Cortez, C., Gan, W. B., & Manfredi, G. (2014). Abnormal mitochondrial transport and morphology are common pathological denominators in SOD1 and TDP43 ALS mouse models. *Human Molecular Genetics*, *23*(6), 1413. <https://doi.org/10.1093/HMG/DDT528>
- Mancuso, R., Fattorelli, N., Martinez-Muriana, A., Davis, E., Wolfs, L., Van Den Daele, J., Geric, I., Premereur, J., Polanco, P., Bijmens, B., Preman, P., Serneels, L., Poovathingal, S., Balusu, S., Verfaillie, C., Fiers, M., & De Strooper, B. (2024). Xenografted human microglia display diverse transcriptomic states in response to Alzheimer's disease-related amyloid- $\beta$  pathology. *Nature Neuroscience*, *27*(5), 886–900. <https://doi.org/10.1038/s41593-024-01600-y>
- Mancuso, R., & Navarro, X. (2015). Amyotrophic lateral sclerosis: Current perspectives from basic research to the clinic. *Progress in Neurobiology*, *133*, 1–26. <https://doi.org/10.1016/j.pneurobio.2015.07.004>
- Mancuso, R., Santos-Nogueira, E., Osta, R., & Navarro, X. (2011). Electrophysiological analysis of a murine model of motoneuron disease. *Clinical Neurophysiology*, *122*(8), 1660–1670. <https://doi.org/10.1016/j.CLINPH.2011.01.045>
- Mancuso, R., Van Den Daele, J., Fattorelli, N., Wolfs, L., Balusu, S., Burton, O., Liston, A., Sierksma, A., Fourne, Y., Poovathingal, S., Arranz-Mendiguren, A., Sala Frigerio, C., Claes, C., Serneels, L., Theys, T., Perry, V. H., Verfaillie, C., Fiers, M., & De Strooper, B. (2019). Stem-cell-derived human microglia transplanted in mouse brain to study human disease. *Nature Neuroscience*, *22*(12), 2111–2116. <https://doi.org/10.1038/s41593-019-0525-x>
- Mantovani, S., Garbelli, S., Pasini, A., Alimonti, D., Perotti, C., Melazzini, M., Bendotti, C., & Mora, G. (2009). Immune system alterations in sporadic amyotrophic lateral sclerosis patients suggest an ongoing neuroinflammatory process. *Journal of Neuroimmunology*, *210*(1–2), 73–79. <https://doi.org/10.1016/j.jneuroim.2009.02.012>
- Marschallinger, J., Iram, T., Zardeneta, M., Lee, S. E., Lehallier, B., Haney, M. S., Pluinage, J. V., Mathur, V., Hahn, O., Morgens, D. W., Kim, J., Tevini, J., Felder, T. K., Wolinski, H., Bertozzi, C. R., Bassik, M. C., Aigner, L., & Wyss-Coray, T. (2020). Lipid-droplet-accumulating microglia represent a dysfunctional and proinflammatory state in the aging brain. *Nature Neuroscience*, *23*(2), 194–208. <https://doi.org/10.1038/s41593-019-0566-1>



- Martínez-Muriana, A., Mancuso, R., Francos-Quijorna, I., Olmos-Alonso, A., Osta, R., Perry, V. H., Navarro, X., Gomez-Nicola, D., & López-Vales, R. (2016). CSF1R blockade slows the progression of amyotrophic lateral sclerosis by reducing microgliosis and invasion of macrophages into peripheral nerves. *Scientific Reports*, 6, 25663. <https://doi.org/10.1038/srep25663>
- Masrori, P., Bijmens, B., Davie, K., Poovathingal, S. K., Storm, A., Hersmus, N., Fumagalli, L., Van Den Bosch, L., Fiers, M., Thal, D., Mancuzo, R., & Van Damme, P. (2023). Hexanucleotide repeat expansions in C9orf72 alter microglial responses and prevent a coordinated glial reaction in ALS. *Neurology*, 100(17\_supplement\_2), 3839. <https://doi.org/10.1212/WNL.0000000000203562>
- Massenzio, F., Peña-Altamira, E., Petralla, S., Virgili, M., Zuccheri, G., Miti, A., Polazzi, E., Mengoni, I., Piffaretti, D., & Monti, B. (2018). Microglial overexpression of fALS-linked mutant SOD1 induces SOD1 processing impairment, activation and neurotoxicity and is counteracted by the autophagy inducer trehalose. *Biochimica et Biophysica Acta. Molecular Basis of Disease*, 1864(12), 3771–3785. <https://doi.org/10.1016/j.BBADIS.2018.10.013>
- Masuda, T., Sankowski, R., Staszewski, O., Böttcher, C., Amann, L., Sagar, Scheiwe, C., Nessler, S., Kunz, P., van Loo, G., Coenen, V. A., Reinacher, P. C., Michel, A., Sure, U., Gold, R., Grün, D., Priller, J., Stadelmann, C., & Prinz, M. (2019). Spatial and temporal heterogeneity of mouse and human microglia at single-cell resolution. *Nature*, 566(7744), 388–392. <https://doi.org/10.1038/s41586-019-0924-x>
- Mathews, S., Branch Woods, A., Katano, I., Makarov, E., Thomas, M. B., Gendelman, H. E., Poluektova, L. Y., Ito, M., & Gorantla, S. (2019). Human interleukin-34 facilitates microglia-like cell differentiation and persistent HIV-1 infection in humanized mice. *Molecular Neurodegeneration*, 14(1), 12. <https://doi.org/10.1186/S13024-019-0311-Y>
- Mattiazzi, M., D'Aurelio, M., Gajewski, C. D., Martushova, K., Kiaei, M., Flint Beal, M., & Manfredi, G. (2002). Mutated human SOD1 causes dysfunction of oxidative phosphorylation in mitochondria of transgenic mice. *Journal of Biological Chemistry*, 277(33), 29626–29633. <https://doi.org/10.1074/jbc.M203065200>
- McEachin, Z. T., Parameswaran, J., Raj, N., Bassell, G. J., & Jiang, J. (2020). RNA-mediated toxicity in C9orf72 ALS and FTD. *Neurobiology of Disease*, 145, 105055. <https://doi.org/10.1016/j.nbd.2020.105055>
- McQuade, A., Coburn, M., Tu, C. H., Hasselmann, J., Davtyan, H., & Blurton-Jones, M. (2018). Development and validation of a simplified method to generate human microglia from pluripotent stem cells. *Molecular Neurodegeneration*, 13(1), 1–13. <https://doi.org/10.1186/s13024-018-0297-x>
- Mead, R. J., Shan, N., Reiser, H. J., Marshall, F., & Shaw, P. J. (2023). Amyotrophic lateral sclerosis: a neurodegenerative disorder poised for successful therapeutic translation. *Nature Reviews Drug Discovery*, 22(3), 185–212. <https://doi.org/10.1038/s41573-022-00612-2>
- Meissner, F., Molawi, K., & Zychlinsky, A. (2010). Mutant superoxide dismutase 1-induced IL-1 $\beta$  accelerates ALS pathogenesis. *Proceedings of the National Academy of Sciences*, 107(29), 13046–13050. <https://doi.org/10.1073/pnas.1002396107>
- Melief, J., Sneeboer, M. A. M., Litjens, M., Ormel, P. R., Palmén, S. J. M. C., Huitinga, I., Kahn, R. S., Hol, E. M., & de Witte, L. D. (2016). Characterizing primary human microglia: A comparative study with myeloid subsets and culture models. *Glia*, 64(11), 1857–1868. <https://doi.org/10.1002/glia.23023>

- Menassa, D. A., & Gomez-Nicola, D. (2018). Microglial dynamics during human brain development. *Frontiers in Immunology*, 9, 1014. <https://doi.org/10.3389/fimmu.2018.01014>
- Menzies, F. M., Cookson, M. R., Taylor, R. W., Turnbull, D. M., Chrzanowska-Lightowlers, Z. M. A., Dong, L., Figlewicz, D. A., & Shaw, P. J. (2002). Mitochondrial dysfunction in a cell culture model of familial amyotrophic lateral sclerosis. *Brain*, 125(Pt A), 1522–1533. <https://doi.org/10.1093/brain/awf167>
- Metawi, S. A., Abbas, D., Kamal, M. M., & Ibrahim, M. K. (2011). Serum and synovial fluid levels of interleukin-17 in correlation with disease activity in patients with RA. *Clinical Rheumatology*, 30(9), 1201–1207. <https://doi.org/10.1007/S10067-011-1737-Y/FIGURES/6>
- Mifflin, L., Hu, Z., Dufort, C., Hession, C. C., Walker, A. J., Niu, K., Zhu, H., Liu, N., Liu, J. S., Levin, J. Z., Stevens, B., Yuan, J., & Zou, C. (2021). A RIPK1-regulated inflammatory microglial state in amyotrophic lateral sclerosis. *Proceedings of the National Academy of Sciences*, 118(13), e2025102118. <https://doi.org/10.1073/pnas.2025102118/-/DCSupplemental>
- Milioto, C., Carcolé, M., Giblin, A., Coneys, R., Attrebi, O., Ahmed, M., Harris, S. S., Lee, B. II, Yang, M., Ellingford, R. A., Nirujogi, R. S., Biggs, D., Salomonsson, S., Zanovello, M., De Oliveira, P., Katona, E., Glaria, I., Mikheenko, A., Geary, B., ... Isaacs, A. M. (2024). PolyGR and polyPR knock-in mice reveal a conserved neuroprotective extracellular matrix signature in C9orf72 ALS/FTD neurons. *Nature Neuroscience*, 27(4), 643–655. <https://doi.org/10.1038/s41593-024-01589-4>
- Miller, T., Cudkowicz, M. E., Genge, A., Shaw, P. J., Sobue, G., Bucelli, R. C., Chiò, A., Van Damme, P., Ludolph, A. C., Glass, J. D., Andrews, J. A., Babu, S., Benatar, M., McDermott, C. J., Cochrane, T., Chary, S., Chew, S., Zhu, H., Wu, F., ... Fradette, S. (2022). Trial of antisense oligonucleotide Tofersen for SOD1 ALS. *New England Journal of Medicine*, 387(12), 1099–1110. <https://doi.org/10.1056/nejmoa2204705>
- Miller, T., Cudkowicz, M., Shaw, P. J., Andersen, P. M., Atassi, N., Bucelli, R. C., Genge, A., Glass, J., Ladha, S., Ludolph, A. L., Maragakis, N. J., McDermott, C. J., Pestronk, A., Ravits, J., Salachas, F., Trudell, R., Van Damme, P., Zinman, L., Bennett, C. F., ... Ferguson, T. A. (2020). Phase 1–2 trial of antisense oligonucleotide Tofersen for SOD1 ALS. *New England Journal of Medicine*, 383(2), 109–119. <https://doi.org/10.1056/nejmoa2003715>
- Miquel, E., Cassina, A., Martínez-Palma, L., Bolatto, C., Trías, E., Gandelman, M., Radi, R., Barbeito, L., & Cassina, P. (2012). Modulation of astrocytic mitochondrial function by dichloroacetate improves survival and motor performance in inherited amyotrophic lateral sclerosis. *PLoS One*, 7(4), e34776. <https://doi.org/10.1371/JOURNAL.PONE.0034776>
- Mizielinska, S., Grönke, S., Niccoli, T., Ridler, C. E., Clayton, E. L., Devoy, A., Moens, T., Norona, F. E., Woollacott, I. O. C., Pietrzyk, J., Cleverley, K., Nicoll, A. J., Pickering-Brown, S., Dols, J., Cabecinha, M., Hendrich, O., Fratta, P., Fisher, E. M. C., Partridge, L., & Isaacs, A. M. (2014). C9orf72 repeat expansions cause neurodegeneration in *Drosophila* through arginine-rich proteins. *Science*, 345(6201), 1192–1194. <https://doi.org/10.1126/science.1256800>
- Moens, T. G., Niccoli, T., Wilson, K. M., Atilano, M. L., Birsa, N., Gittings, L. M., Benedikt, , Holbling, V., Dyson, M. C., Thoeng, A., Neeves, J., Glaria, I., Yu, L., Bussmann, J., Storkebaum, , Erik, Pardo, M., Choudhary, J. S., Fratta, P., Partridge, , Linda, & Isaacs, A. M. (2019). C9orf72 arginine-rich dipeptide proteins interact with ribosomal proteins in vivo to induce a toxic translational arrest that is rescued by eIF1A. *Acta Neuropathologica*, 137(3), 487–500. <https://doi.org/10.1007/s00401-018-1946-4>
- Mordes, D. A., Morrison, B. M., Ament, X. H., Cantrell, C., Mok, J., Eggan, P., Xue, C., Wang, J. Y., Eggan, K., & Rothstein, J. D. (2020). Absence of survival and motor deficits in 500 repeat

## References

- C9ORF72 BAC mice. *Neuron*, 108(4), 775-783.e4. <https://doi.org/10.1016/j.neuron.2020.08.009>
- Moreno-Martinez, L., Calvo, A. C., Muñoz, M. J., & Osta, R. (2019). Are circulating cytokines reliable biomarkers for amyotrophic lateral sclerosis? *International Journal of Molecular Sciences*, 20(11), 2759. <https://doi.org/10.3390/ijms20112759>
- Motataianu, A., Barcutean, L., & Balasa, R. (2020). Neuroimmunity in amyotrophic lateral sclerosis: focus on microglia. *Amyotrophic Lateral Sclerosis and Frontotemporal Degeneration*, 21(3-4), 159-166. <https://doi.org/10.1080/21678421.2019.1708949>
- Muffat, J., Li, Y., Yuan, B., Mitalipova, M., Omer, A., Corcoran, S., Bakiasi, G., Tsai, L. H., Aubourg, P., Ransohoff, R. M., & Jaenisch, R. (2016). Efficient derivation of microglia-like cells from human pluripotent stem cells. *Nature Medicine*, 22(11), 1358-1367. <https://doi.org/10.1038/nm.4189>
- Murdock, B. J., Zhou, T., Kashlan, S. R., Little, R. J., Goutman, S. A., & Feldman, E. L. (2017). Correlation of peripheral immunity with rapid amyotrophic lateral sclerosis progression. *JAMA Neurology*, 74(12), 1446-1454. <https://doi.org/10.1001/jamaneurol.2017.2255>
- Murphy, N. A., Arthur, K. C., Tienari, P. J., Houlden, H., Chiò, A., & Traynor, B. J. (2017). Age-related penetrance of the C9orf72 repeat expansion. *Scientific Reports*, 7, 2116. <https://doi.org/10.1038/s41598-017-02364-1>
- Nagai, M., Re, D. B., Nagata, T., Ne Chalazonitis, A., Jessell, T. M., Wichterle, H., & Przedborski, S. (2007). Astrocytes expressing ALS-linked mutated SOD1 release factors selectively toxic to motor neurons. *Nature Neuroscience*, 10(5), 615-622. <https://doi.org/10.1038/nn1876>
- Nardo, G., Trolese, M. C., de Vito, G., Cecchi, R., Riva, N., Dina, G., Heath, P. R., Quattrini, A., Shaw, P. J., Piazza, V., & Bendotti, C. (2016). Immune response in peripheral axons delays disease progression in SOD1G93A mice. *Journal of Neuroinflammation*, 13(1), 261. <https://doi.org/10.1186/S12974-016-0732-2>
- Nardo, G., Trolese, M. C., Verderio, M., Mariani, A., De Paola, M., Riva, N., Dina, G., Panini, N., Erba, E., Quattrini, A., & Bendotti, C. (2018). Counteracting roles of MHCI and CD8+ T cells in the peripheral and central nervous system of ALS SOD1G93A mice. *Molecular Neurodegeneration*, 13(1), 42. <https://doi.org/10.1186/S13024-018-0271-7/>
- Navarro, X., & Udina, E. (2009). Chapter 6: Methods and Protocols in Peripheral Nerve Regeneration Experimental Research: Part III—Electrophysiological Evaluation. *International Review of Neurobiology*, 87, 105-126. [https://doi.org/10.1016/S0074-7742\(09\)87006-2](https://doi.org/10.1016/S0074-7742(09)87006-2)
- Neumann, M., Sampathu, D. M., Kwong, L. K., Truax, A. C., Micsenyi, M. C., Chou, T. T., Bruce, J., Schuck, T., Grossman, M., Clark, C. M., McCluskey, L. F., Miller, B. L., Masliah, E., Mackenzie, I. R., Feldman, H., Feiden, W., Kretzschmar, H. A., Trojanowski, J. Q., & M-Y Lee, V. (2006). Ubiquitinated TDP-43 in frontotemporal lobar degeneration and amyotrophic lateral sclerosis. *Science*, 314(5796), 130-133. <https://doi.org/10.1126/science.1134108>
- Ng, W., & Ng, S. Y. (2022). Remodeling of astrocyte secretome in amyotrophic lateral sclerosis: uncovering novel targets to combat astrocyte-mediated toxicity. *Translational Neurodegeneration*, 11(1), 54. <https://doi.org/10.1186/s40035-022-00332-y>
- Nguyen, L., Laboissonniere, L. A., Guo, S., Pilotto, F., Scheidegger, O., Oestmann, A., Hammond, J. W., Li, H., Hyysalo, A., Peltola, R., Pattamatta, A., Zu, T., Voutilainen, M. H., Gelbard, H. A., Saxena, S., & Ranum, L. P. W. (2020). Survival and motor phenotypes in FVB C9-500 ALS/FTD BAC transgenic mice reproduced by multiple labs. *Neuron*, 108(4), 784-796.e3. <https://doi.org/10.1016/j.neuron.2020.09.009>

- Noh, M. Y., Kwon, M. S., Oh, K. W., Nahm, M., Park, J., Kim, Y. E., Ki, C. S., Jin, H. K., Bae, J. sung, & Kim, S. H. (2023). Role of NCKAP1 in the defective phagocytic function of microglia-like cells derived from rapidly progressing sporadic ALS. *Molecular Neurobiology*, *60*(8), 4761–4777. <https://doi.org/10.1007/s12035-023-03339-2>
- Nordin, A., Akimoto, C., Wuolikainen, A., Alstermark, H., Jonsson, P., Birve, A., Marklund, S. L., Graffmo, K. S., Forsberg, K., Brännström, T., & Andersen, P. M. (2014). Extensive size variability of the GGGCC expansion in C9orf72 in both neuronal and non-neuronal tissues in 18 patients with ALS or FTD. *Human Molecular Genetics*, *24*(11), 3133–3142. <https://doi.org/10.1093/hmg/ddv064>
- Olesen, M. N., Wuolikainen, A., Nilsson, A. C., Wirenfeltd, M., Forsberg, K., Madsen, J. S., Lillevang, S. T., Brandslund, I., Andersen, P. M., & Asgari, N. (2020). Inflammatory profiles relate to survival in subtypes of amyotrophic lateral sclerosis. *Neurology Neuroimmunology and NeuroInflammation*, *7*(3), e697. <https://doi.org/10.1212/NXI.0000000000000697>
- Olszewska, D. A., Lonergan, R., Fallon, E. M., & Lynch, T. (2016). Genetics of frontotemporal dementia. *Current Neurology and Neuroscience Reports*, *16*(12), 107. <https://doi.org/10.1007/s11910-016-0707-9>
- Onyike, C. U., & Diehl-Schmid, J. (2013). The epidemiology of frontotemporal dementia. *International Review of Psychiatry*, *25*(2), 130–137. <https://doi.org/10.3109/09540261.2013.776523>
- O'Rourke, J. G., Bogdanik, L., Muhammad, A. K. M. G., Gendron, T. F., Kim, K. J., Austin, A., Cady, J., Liu, E. Y., Zarrow, J., Grant, S., Ho, R., Bell, S., Carmona, S., Simpkinson, M., Lall, D., Wu, K., Daugherty, L., Dickson, D. W., Harms, M. B., ... Baloh, R. H. (2015). C9orf72 BAC transgenic mice display typical pathologic features of ALS/FTD. *Neuron*, *88*(5), 892–901. <https://doi.org/10.1016/j.neuron.2015.10.027>
- O'rourke, J. G., Bogdanik, L., Yáñez, A., Lall, D., Wolf, A. J., Muhammad, A. K. M. G., Ho, R., Carmona, S., Vit, J. P., Zarrow, J., Kim, K. J., Bell, S., Harms, M. B., Miller, T. M., Dangler, C. A., Underhill, D. M., Goodridge, H. S., Lutz, C. M., & Baloh, R. H. (2016). C9orf72 is required for proper macrophage and microglial function in mice. *Science*, *351*(6279), 1324–1329. <https://doi.org/10.1126/science.aaf1064>
- Paganoni, S., Hendrix, S., Dickson, S. P., Knowlton, N., Macklin, E. A., Berry, J. D., Elliott, M. A., Maiser, S., Karam, C., Caress, J. B., Owegi, M. A., Quick, A., Wymer, J., Goutman, S. A., Heitzman, D., Heiman-Patterson, T. D., Jackson, C. E., Quinn, C., Rothstein, J. D., ... Cudkowicz, M. E. (2021). Long-term survival of participants in the CENTAUR trial of sodium phenylbutyrate-taurursodiol in amyotrophic lateral sclerosis. *Muscle and Nerve*, *63*(1), 31–39. <https://doi.org/10.1002/mus.27091>
- Paganoni, S., Macklin, E. A., Hendrix, S., Berry, J. D., Elliott, M. A., Maiser, S., Karam, C., Caress, J. B., Owegi, M. A., Quick, A., Wymer, J., Goutman, S. A., Heitzman, D., Heiman-Patterson, T., Jackson, C. E., Quinn, C., Rothstein, J. D., Kasarskis, E. J., Katz, J., ... Cudkowicz, M. E. (2020). Trial of sodium phenylbutyrate–Taurursodiol for amyotrophic lateral sclerosis. *New England Journal of Medicine*, *383*(10), 919–930. <https://doi.org/10.1056/nejmoa1916945>
- Pandya, H., Shen, M. J., Ichikawa, D. M., Sedlock, A. B., Choi, Y., Johnson, K. R., Kim, G., Brown, M. A., Elkahoun, A. G., Maric, D., Sweeney, C. L., Gossa, S., Malech, H. L., McGavern, D. B., & Park, J. K. (2017). Differentiation of human and murine induced pluripotent stem cells to microglia-like cells. *Nature Neuroscience*, *20*(5), 753–759. <https://doi.org/10.1038/nn.4534>
- Panov, A., Kubalik, N., Zinchenko, N., Hemendinger, R., Dikalov, S., & Bonkovsky, H. L. (2011). Respiration and ROS production in brain and spinal cord mitochondria of transgenic rats

- with mutant G93A Cu/Zn-superoxide dismutase gene. *Neurobiology of Disease*, 44(1), 53–62. <https://doi.org/10.1016/j.NBD.2011.06.003>
- Paolicelli, R. C., Bolasco, G., Pagani, F., Maggi, L., Scianni, M., Panzanelli, P., Giustetto, M., Ferreira, T. A., Guiducci, E., Dumas, L., Ragozzino, D., & Gross, C. T. (2011). Synaptic pruning by microglia is necessary for normal brain development. *Science*, 333(6048), 1456–1458. <https://doi.org/10.1126/science.1202529>
- Paolicelli, R. C., Sierra, A., Stevens, B., Bennett, M., Bennett, F., Bessis, A., Biber, K., Bilbo, S., Blurton-Jones, M., Boddeke, E., Brites, D., Brône, B., Brown, G. C., Butovsky, O., Carson, M. J., Castellano, B., Colonna, M., & Cowley, S. A. (2022). Microglia states and nomenclature: A field at its crossroads. *Neuron*, 110(21), 3458–3483.
- Parajuli, B., Saito, H., Shinozaki, Y., Shigetomi, E., Miwa, H., Yoneda, S., Tanimura, M., Omachi, S., Asaki, T., Takahashi, K., Fujita, M., Nakashima, K., & Koizumi, S. (2021). Transnasal transplantation of human induced pluripotent stem cell-derived microglia to the brain of immunocompetent mice. *Glia*, 69(10), 2332–2348. <https://doi.org/10.1002/glia.23985>
- Park, H. R., & Yang, E. J. (2021). Oxidative stress as a therapeutic target in amyotrophic lateral sclerosis: Opportunities and limitations. *Diagnostics*, 11(9), 1546. <https://doi.org/10.3390/diagnostics11091546>
- Pattamatta, A., Nguyen, L., Olafson, H. R., Scotti, M. M., Laboissonniere, L. A., Richardson, J., Berglund, J. A., Zu, T., Wang, E. T., & Ranum, L. P. W. (2020). Repeat length increases disease penetrance and severity in C9orf72 ALS/FTD BAC transgenic mice. *Human Molecular Genetics*, 29(24), 3900–3918. <https://doi.org/10.1093/HMG/DDAA279>
- Pedrini, S., Sau, D., Guareschi, S., Bogush, M., Brown, R. H., Nanche, N., Kia, A., Trotti, D., & Pasinelli, P. (2010). ALS-linked mutant SOD1 damages mitochondria by promoting conformational changes in Bcl-2. *Human Molecular Genetics*, 19(15), 2974–2986. <https://doi.org/10.1093/HMG/DDQ202>
- Pehar, M., Harlan, B. A., Killoy, K. M., & Vargas, M. R. (2017). Role and therapeutic potential of astrocytes in amyotrophic lateral sclerosis. *Current Pharmaceutical Design*, 23(33), 5010–5021. <https://doi.org/10.2174/1381612823666170622095802>
- Perry, T. L., Krieger, C., Hansen, S., & Eisen, A. (1990). Amyotrophic lateral sclerosis: Amino acid levels in plasma and cerebrospinal fluid. *Annals of Neurology*, 28(1), 12–17. <https://doi.org/10.1002/ANA.410280105>
- Peruzzotti-Jametti, L., Willis, C. M., Krzak, G., Hamel, R., Pirvan, L., Ionescu, R. B., Reisz, J. A., Prag, H. A., Garcia-Segura, M. E., Wu, V., Xiang, Y., Barlas, B., Casey, A. M., van den Bosch, A. M. R., Nicaise, A. M., Roth, L., Bates, G. R., Huang, H., Prasad, P., ... Pluchino, S. (2024). Mitochondrial complex I activity in microglia sustains neuroinflammation. *Nature*, 628(8006), 195–203. <https://doi.org/10.1038/s41586-024-07167-9>
- Peters, O. M., Cabrera, G. T., Tran, H., Gendron, T. F., McKeon, J. E., Metterville, J., Weiss, A., Wightman, N., Salameh, J., Kim, J., Sun, H., Boylan, K. B., Dickson, D., Kennedy, Z., Lin, Z., Zhang, Y. J., Daugherty, L., Jung, C., Gao, F. B., ... Brown, R. H. (2015). Human C9ORF72 hexanucleotide expansion reproduces RNA foci and dipeptide repeat proteins but not neurodegeneration in BAC transgenic mice. *Neuron*, 88(5), 902–909. <https://doi.org/10.1016/j.neuron.2015.11.018>
- Petrozziello, T., Secondo, A., Tedeschi, V., Esposito, A., Sisalli, M., Scorziello, A., Renzo, G. Di, & Annunziato, L. (2017). ApoSOD1 lacking dismutase activity neuroprotects motor neurons exposed to beta-methylamino-L-alanine through the Ca<sup>2+</sup>/Akt/ERK1/2 prosurvival pathway. *Cell Death and Differentiation*, 24(2), 511–522. <https://doi.org/10.1038/cdd.2016.154>

- Philips, T., & Robberecht, W. (2011). Neuroinflammation in amyotrophic lateral sclerosis: Role of glial activation in motor neuron disease. *The Lancet Neurology*, *10*(3), 253–263. [https://doi.org/10.1016/S1474-4422\(11\)70015-1](https://doi.org/10.1016/S1474-4422(11)70015-1)
- Pick, M., Azzola, L., Mossman, A., Stanley, E. G., & Elefanty, A. G. (2007). Differentiation of human embryonic stem cells in serum-free medium reveals distinct roles for bone morphogenetic protein 4, vascular endothelial growth factor, stem cell factor, and fibroblast growth factor 2 in hematopoiesis. *Stem Cells*, *25*(9), 2206–2214. <https://doi.org/10.1634/stemcells.2006-0713>
- Polymenidou, M., Lagier-Tourenne, C., Hutt, K. R., Huelga, S. C., Moran, J., Liang, T. Y., Ling, S. C., Sun, E., Wancewicz, E., Mazur, C., Kordasiewicz, H., Sedaghat, Y., Donohue, J. P., Shiue, L., Bennett, C. F., Yeo, G. W., & Cleveland, D. W. (2011). Long pre-mRNA depletion and RNA missplicing contribute to neuronal vulnerability from loss of TDP-43. *Nature Neuroscience*, *14*(4), 459–468. <https://doi.org/10.1038/nn.2779>
- Pramatarova, A., Laganière, J., Roussel, J., Brisebois, K., & Rouleau, G. A. (2001). Neuron-specific expression of mutant superoxide dismutase 1 in transgenic mice does not lead to motor impairment. *The Journal of Neuroscience*, *21*(10), 3369–3374. <https://doi.org/10.1523/jneurosci.21-10-03369.2001>
- Qiu, H., Lee, S., Shang, Y., Wang, W. Y., Au, K. F., Kamiya, S., Barmada, S. J., Finkbeiner, S., Lui, H., Carlton, C. E., Tang, A. A., Oldham, M. C., Wang, H., Shorter, J., Filiano, A. J., Roberson, E. D., Tourtellotte, W. G., Chen, B., Tsai, L. H., & Huang, E. J. (2014). ALS-associated mutation FUS-R521C causes DNA damage and RNA splicing defects. *Journal of Clinical Investigation*, *124*(3), 981–999. <https://doi.org/10.1172/JCI72723>
- Quek, H., Cuní-López, C., Stewart, R., Colletti, T., Notaro, A., Nguyen, T. H., Sun, Y., Guo, C. C., Lupton, M. K., Roberts, T. L., Lim, Y. C., Oikari, L. E., La Bella, V., & White, A. R. (2022). ALS monocyte-derived microglia-like cells reveal cytoplasmic TDP-43 accumulation, DNA damage, and cell-specific impairment of phagocytosis associated with disease progression. *Journal of Neuroinflammation*, *19*(1), 58. <https://doi.org/10.1186/s12974-022-02421-1>
- Ransohoff, R. M. (2016). A polarizing question: do M1 and M2 microglia exist? *Nature Neuroscience*, *19*(8), 987–991. <https://doi.org/10.1038/nn.4338>
- Rathinam, C., Poueymirou, W. T., Rojas, J., Murphy, A. J., Valenzuela, D. M., Yancopoulos, G. D., Rongvaux, A., Eynon, E. E., Manz, M. G., & Flavell, R. A. (2011). Efficient differentiation and function of human macrophages in humanized CSF-1 mice. *Blood*, *118*(11), 3119–3128. <https://doi.org/10.1182/blood-2010-12-326926>
- Reich, M., Paris, I., Ebeling, M., Dahm, N., Schweitzer, C., Reinhardt, D., Schmucki, R., Prasad, M., Köchl, F., Leist, M., Cowley, S. A., Zhang, J. D., Patsch, C., Gutbier, S., & Britschgi, M. (2021). Alzheimer's risk gene TREM2 determines functional properties of new type of human iPSC-derived microglia. *Frontiers in Immunology*, *11*, 617860. <https://doi.org/10.3389/fimmu.2020.617860>
- Ren, K., & Torres, R. (2009). Role of interleukin-1 $\beta$  during pain and inflammation. *Brain Research Reviews*, *60*(1), 57–64. <https://doi.org/10.1016/j.brainresrev.2008.12.020>
- Renton, A. E., Majounie, E., Waite, A., Simón-Sánchez, J., Rollinson, S., Gibbs, J. R., Schymick, J. C., Laaksovirta, H., van Swieten, J. C., Myllykangas, L., Kalimo, H., Paetau, A., Abramzon, Y., Remes, A. M., Kaganovich, A., Scholz, S. W., Duckworth, J., Ding, J., Harmer, D. W., ... Traynor, B. J. (2011). A hexanucleotide repeat expansion in C9ORF72 is the cause of chromosome 9p21-linked ALS-FTD. *Neuron*, *72*(2), 257–268. <https://doi.org/10.1016/j.neuron.2011.09.010>

- Rentzos, M., Evangelopoulos, E., Sereti, E., Zouvelou, V., Marmara, S., Alexakis, T., & Evdokimidis, I. (2012). Alterations of T cell subsets in ALS: a systemic immune activation? *Acta Neurologica Scandinavica*, *125*(4), 260–264. <https://doi.org/10.1111/J.1600-0404.2011.01528.X>
- Rizzu, P., Blauwendraat, C., Heetveld, S., Lynes, E. M., Castillo-Lizardo, M., Dhingra, A., Pyz, E., Hobert, M., Synofzik, M., Simón-Sánchez, J., Francescatti, M., & Heutink, P. (2016). C9orf72 is differentially expressed in the central nervous system and myeloid cells and consistently reduced in C9orf72, MAPT and GRN mutation carriers. *Acta Neuropathologica Communications*, *4*(1), 37. <https://doi.org/10.1186/s40478-016-0306-7>
- Roggenbuck, J., Quick, A., & Kolb, S. J. (2017). Genetic testing and genetic counseling for amyotrophic lateral sclerosis: An update for clinicians. *Genetics in Medicine*, *19*(3), 267–274. <https://doi.org/10.1038/gim.2016.107>
- Romero-Molina, C., Neuner, S. M., Ryszawiec, M., Pébay, A., Marcora, E., & Goate, A. (2024). Autosomal dominant Alzheimer's disease mutations in human microglia are not sufficient to trigger amyloid pathology in WT mice but might affect pathology in 5XFAD mice. *International Journal of Molecular Sciences*, *25*(5), 2565. <https://doi.org/10.3390/IJMS25052565/S1>
- Rosen, D. R., Siddiquet, T., Patterson, D., Figlewicz, D. A., Sapp, P., Hentatit, A., Donaldson, D., Goto, J., O, J. P., Deng, H.-X., Rahmanit, Z., Krizus, A., McKenna-Yasek, D., Cayabyab, A., Gaston, S. M., Bergert, R., Tanzi, R. E., Halperin, J. J., Herzfeldt, B., ... Brown Jr, R. H. (1993). Mutations in Cu/Zn superoxide dismutase gene are associated with familial amyotrophic lateral sclerosis. *Nature*, *362*(6415), 59–62. <https://doi.org/10.1038/362059a0>
- Saberi, S., Stauffer, J. E., Jiang, J., Diaz Garcia, S., Taylor, A. E., Schulte, D., Ohkubo, T., Schloffman, C. L., Maldonado, M., Baughn, M., Rodriguez, M. J., Pizzo, D., Cleveland, D., & Ravits, J. (2018). Sense-encoded poly-GR dipeptide repeat proteins correlate to neurodegeneration and uniquely co-localize with TDP-43 in dendrites of repeat-expanded C9orf72 amyotrophic lateral sclerosis. *Acta Neuropathologica*, *135*(3), 459–474. <https://doi.org/10.1007/s00401-017-1793-8>
- Sabogal-Guáqueta, A. M., Marmolejo-Garza, A., Passos De Pádua, V., Eggen, B., Boddeke, E., & Dolga, A. M. (2020). Microglia alterations in neurodegenerative diseases and their modeling with human induced pluripotent stem cell and other platforms. *Progress in Neurobiology*, *190*, 101805. <https://doi.org/10.1016/j.pneurobio.2020.101805>
- Sabogal-Guáqueta, A. M., Marmolejo-Garza, A., Trombetta-Lima, M., Oun, A., Hunneman, J., Chen, T., Koistinaho, J., Lehtonen, S., Kortholt, A., Wolters, J. C., Bakker, B. M., Eggen, B. J. L., Boddeke, E., & Dolga, A. (2023). Species-specific metabolic reprogramming in human and mouse microglia during inflammatory pathway induction. *Nature Communications*, *14*, 6454. <https://doi.org/10.1038/s41467-023-42096-7>
- Saccon, R. A., Bunton-Stasyshyn, R. K. A., Fisher, E. M. C., & Fratta, P. (2013). Is SOD1 loss of function involved in amyotrophic lateral sclerosis? *Brain*, *136*(8), 2342–2358. <https://doi.org/10.1093/BRAIN/AWT097>
- Saez-Atienzar, S., Bandres-Ciga, S., Langston, R. G., Kim, J. J., Wan Choi, S., Reynolds, R. H., Abramzon, Y., Dewan, R., Ahmed, S., Landers, J. E., Chia, R., Ryten, M., Cookson, M. R., Nalls, M. A., Chiò, A., & Traynor, B. J. (2021). Genetic analysis of amyotrophic lateral sclerosis identifies contributing pathways and cell types. *Science Advances*, *7*(3), eabd9036. <https://doi.org/10.1126/sciadv.abd9036>
- Sakae, N., Bieniek, K. F., Zhang, Y.-J., Ross, K., Gendron, T. F., Murray, M. E., Rademakers, R., Petrucelli, L., & Dickson, D. W. (2018). Poly-GR dipeptide repeat polymers correlate with neurodegeneration and clinicopathological subtypes in C9ORF72-related brain disease.

- Acta Neuropathologica Communications*, 6, 63. <https://doi.org/10.1186/s40478-018-0564-7>
- Salter, M. W., & Stevens, B. (2017). Microglia emerge as central players in brain disease. *Nature Medicine*, 23(9), 1018–1027. <https://doi.org/10.1038/nm.4397>
- Sanchis, P., Fernández-Gayol, O., Comes, G., Aguilar, K., Escrig, A., Giral, M., Palmiter, R. D., & Hidalgo, J. (2020). A new mouse model to study restoration of interleukin-6 (IL-6) expression in a Cre-dependent manner: microglial IL-6 regulation of experimental autoimmune encephalomyelitis. *Journal of Neuroinflammation*, 17(1), 304. <https://doi.org/10.1186/s12974-020-01969-0>
- Sanginetto, M., Ciarnelli, M., Cassano, T., Radesco, A., Moola, A., Bukke, V. N., Romano, A., Villani, R., Kanwal, H., Capitano, N., Duda, L., Avolio, C., & Serviddio, G. (2023). Metabolic reprogramming in inflammatory microglia indicates a potential way of targeting inflammation in Alzheimer's disease. *Redox Biology*, 66, 102846. <https://doi.org/10.1016/j.redox.2023.102846>
- Saresella, M., Piancone, F., Tortorella, P., Marventano, I., Gatti, A., Caputo, D., Lunetta, C., Corbo, M., Rovaris, M., & Clerici, M. (2013). T helper-17 activation dominates the immunologic milieu of both amyotrophic lateral sclerosis and progressive multiple sclerosis. *Clinical Immunology*, 148(1), 79–88. <https://doi.org/10.1016/j.clim.2013.04.010>
- Sargsyan, S. A., Blackburn, D. J., Barber, S. C., Grosskreutz, J., De Vos, K. J., Monk, P. N., & Shaw, P. J. (2011). A comparison of in vitro properties of resting SOD1 transgenic microglia reveals evidence of reduced neuroprotective function. *BMC Neuroscience*, 12, 91. <https://doi.org/10.1186/1471-2202-12-91>
- Sasaki, S., & Iwata, M. (2007). Mitochondrial alterations in the spinal cord of patients with sporadic amyotrophic lateral sclerosis. *Journal of Neuropathology & Experimental Neurology*, 66(1), 10–16. <https://doi.org/10.1097/nen.0b013e31802c396b>
- Saxena, S., Cabuy, E., & Caroni, P. (2009). A role for motoneuron subtype-selective ER stress in disease manifestations of FALS mice. *Nature Neuroscience*, 12(5), 627–636. <https://doi.org/10.1038/nn.2297>
- Schiffer, D., Cordera, S., Cavalla, P., & Migheli, A. (1996). Reactive astrogliosis of the spinal cord in amyotrophic lateral sclerosis. *Journal of the Neurological Sciences*, 139(Suppl.), 27–33. [https://doi.org/10.1016/0022-510X\(96\)00073-1](https://doi.org/10.1016/0022-510X(96)00073-1)
- Schipper, L. J., Raaphorst, J., Aronica, E., Baas, F., de Haan, R., de Visser, M., & Troost, D. (2016). Prevalence of brain and spinal cord inclusions, including dipeptide repeat proteins, in patients with the C9ORF72 hexanucleotide repeat expansion: a systematic neuropathological review. *Neuropathology and Applied Neurobiology*, 42(6), 547–560. <https://doi.org/10.1111/nan.12284>
- Schmidt, M. L., Carden, M. J., Lee, V. M., & Trojanowski, J. Q. (1987). Phosphate dependent and independent neurofilament epitopes in the axonal swellings of patients with motor neuron disease and controls. *Laboratory Investigation; a Journal of Technical Methods and Pathology*, 56(3), 282–294.
- Schmitz, A., Pinheiro Marques, J., Oertig, I., Maharjan, N., & Saxena, S. (2021). Emerging perspectives on dipeptide repeat proteins in C9ORF72 ALS/FTD. *Frontiers in Cellular Neuroscience*, 15, 637548. <https://doi.org/10.3389/fncel.2021.637548>
- Schwenk, B. M., Hartmann, H., Serdaroglu, A., Schludi, M. H., Hornburg, D., Meissner, F., Orozco, D., Colombo, A., Tahirovic, S., Michaelsen, M., Schreiber, F., Haupt, S., Peitz, M., Brüstle, O., Küpper, C., Klopstock, T., Otto, M., Ludolph, A. C., Arzberger, T., ... Edbauer, D.



## References

- (2016). TDP-43 loss of function inhibits endosomal trafficking and alters trophic signaling in neurons. *The EMBO Journal*, 35(21), 2350–2370. <https://doi.org/10.15252/embj.201694221>
- Seibenhener, M. L., & Wooten, M. C. (2015). Use of the open field maze to measure locomotor and anxiety-like behavior in mice. *Journal of Visualized Experiments*, 96, e52434. <https://doi.org/10.3791/52434>
- Sellier, C., Campanari, M., Julie Corbier, C., Gaucherot, A., Kolb-Cheynel, I., Oulad-Abdelghani, M., Ruffenach, F., Page, A., Ciura, S., Kabashi, E., & Charlet-Berguerand, N. (2016). Loss of C9ORF72 impairs autophagy and synergizes with polyQ Ataxin-2 to induce motor neuron dysfunction and cell death. *The EMBO Journal*, 35(12), 1276–1297. <https://doi.org/10.15252/embj.201593350>
- Sephton, C. F., Cenik, C., Kucukural, A., Dammer, E. B., Cenik, B., Han, Y. H., Dewey, C. M., Roth, F. P., Herz, J., Peng, J., Moore, M. J., & Yu, G. (2011). Identification of neuronal RNA targets of TDP-43-containing ribonucleoprotein complexes. *Journal of Biological Chemistry*, 286(2), 1204–1215. <https://doi.org/10.1074/jbc.M110.190884>
- Shao, Q., Liang, C., Chang, Q., Zhang, W., Yang, M., & Chen, J.-F. (2019). C9orf72 deficiency promotes motor deficits of a C9ALS/FTD mouse model in a dose-dependent manner. *Acta Neuropathologica Communications*, 7(1), 32. <https://doi.org/10.1186/s40478-019-0685-7>
- Shi, Y., Lin, S., Staats, K. A., Li, Y., Chang, W. H., Hung, S. T., Hendricks, E., Linares, G. R., Wang, Y., Son, E. Y., Wen, X., Kisler, K., Wilkinson, B., Menendez, L., Sugawara, T., Woolwine, P., Huang, M., Cowan, M. J., Ge, B., ... Ichida, J. K. (2018). Haploinsufficiency leads to neurodegeneration in C9ORF72 ALS/FTD human induced motor neurons. *Nature Medicine*, 24(3), 313–325. <https://doi.org/10.1038/nm.4490>
- Shibata, N. (2001). Transgenic mouse model for familial amyotrophic lateral sclerosis with superoxide dismutase-1 mutation. *Neuropathology*, 21(1), 82–92. <https://doi.org/10.1046/j.1440-1789.2001.00361.x>
- Shibata, N., Hirano, A., Kobayashi, M., Sasaki, S., Takeo, K., Matsumoto, S., Shiozawa, Z., Komori, T., Ikemoto, A., Umahara, T., & Asayama, K. (1994). CuZn superoxide dismutase-like immunoreactivity in Lewy body-like inclusions of sporadic amyotrophic lateral sclerosis. *Neuroscience Letters*, 179(1–2), 149–152. [https://doi.org/10.1016/0304-3940\(94\)90956-3](https://doi.org/10.1016/0304-3940(94)90956-3)
- Sierra, A., Paolicelli, R. C., & Kettenmann, H. (2019). Cien años de microglía: milestones in a century of microglial research. *Trends in Neurosciences*, 42(11), 778–792. <https://doi.org/10.1016/j.tins.2019.09.004>
- Singh, T., Jiao, Y., Ferrando, L. M., Yablonska, S., Li, F., Horoszko, E. C., Lacomis, D., Friedlander, R. M., & Carlisle, D. L. (2021). Neuronal mitochondrial dysfunction in sporadic amyotrophic lateral sclerosis is developmentally regulated. *Scientific Reports*, 11(1), 18916. <https://doi.org/10.1038/s41598-021-97928-7>
- Smeyers, J., Banchi, E. G., & Latouche, M. (2021). C9ORF72: What it is, what it does, and why it matters. *Frontiers in Cellular Neuroscience*, 15, 661447. <https://doi.org/10.3389/fncel.2021.661447>
- Smith, E. F., Shaw, P. J., & De Vos, K. J. (2019). The role of mitochondria in amyotrophic lateral sclerosis. *Neuroscience Letters*, 710, 132933. <https://doi.org/10.1016/j.neulet.2017.06.052>
- Soubannier, V., Chaineau, M., Gursu, L., Lépine, S., Kalaydjian, D., Sirois, J., Haggi, G., Rouleau, G., Durcan, T. M., & Stifani, S. (2024). Early nuclear phenotypes and reactive transformation

- in human iPSC-derived astrocytes from ALS patients with SOD1 mutations. *Glia*. <https://doi.org/10.1002/GLIA.24598>
- Spiller, K. J., Restrepo, C. R., Khan, T., Dominique, M. A., Fang, T. C., Canter, R. G., Roberts, C. J., Miller, K. R., Ransohoff, R. M., Trojanowski, J. Q., & Lee, V. M. Y. (2018). Microglia-mediated recovery from ALS-relevant motor neuron degeneration in a mouse model of TDP-43 proteinopathy. *Nature Neuroscience*, *21*(3), 329–340. <https://doi.org/10.1038/s41593-018-0083-7>
- Spreux-Varoquaux, O., Bensimon, G., Lacomblez, L., Salachas, F., Pradat, P. F., Le Forestier, N., Marouan, A., Dib, M., & Meininger, V. (2002). Glutamate levels in cerebrospinal fluid in amyotrophic lateral sclerosis: A reappraisal using a new HPLC method with coulometric detection in a large cohort of patients. *Journal of the Neurological Sciences*, *193*(2), 73–78. [https://doi.org/10.1016/S0022-510X\(01\)00661-X](https://doi.org/10.1016/S0022-510X(01)00661-X)
- Srinivasan, K., Friedman, B. A., Etxeberria, A., Beach, T. G., Serrano, G. E., & Hansen Correspondence, D. V. (2020). Alzheimer's patient microglia exhibit enhanced aging and unique transcriptional activation. *Cell Reports*, *31*(13), 107843. <https://doi.org/10.1016/j.celrep.2020.107843>
- Strogulski, N. R., Portela, L. V., Polster, B. M., & Loane, D. J. (2023). Fundamental neurochemistry review: Microglial immunometabolism in traumatic brain injury. *Journal of Neurochemistry*, *167*(2), 129–153. <https://doi.org/10.1111/jnc.15959>
- Sullivan, P. M., Zhou, X., Robins, A. M., Paushter, D. H., Kim, D., Smolka, M. B., & Hu, F. (2016). The ALS/FTLD associated protein C9orf72 associates with SMCR8 and WDR41 to regulate the autophagy-lysosome pathway. *Acta Neuropathologica Communications*, *4*(1), 51. <https://doi.org/10.1186/s40478-016-0324-5>
- Sun, Y., Eshov, A., Zhou, J., Isiktas, A. U., & Guo, J. U. (2020). C9orf72 arginine-rich dipeptide repeats inhibit UPF1-mediated RNA decay via translational repression. *Nature Communications*, *11*(1), 3354. <https://doi.org/10.1038/s41467-020-17129-0>
- Svoboda, D. S., Barrasa, M. I., Shu, J., Rietjens, R., Zhang, S., Mitalipova, M., Berube, P., Fu, D., Shultz, L. D., Bell, G. W., & Jaenisch, R. (2019). Human iPSC-derived microglia assume a primary microglia-like state after transplantation into the neonatal mouse brain. *Proceedings of the National Academy of Sciences*, *116*(50), 25293–25303. <https://doi.org/10.1073/pnas.1913541116>
- Takahashi, K., & Yamanaka, S. (2006). Induction of pluripotent stem cells from mouse embryonic and adult fibroblast cultures by defined factors. *Cell*, *126*(4), 663–676. <https://doi.org/10.1016/j.cell.2006.07.024>
- Takata, K., Kozaki, T., Lee, C. Z. W., Thion, M. S., Otsuka, M., Lim, S., Utami, K. H., Fidan, K., Park, D. S., Malleret, B., Chakarov, S., See, P., Low, D., Low, G., Garcia-Mirallas, M., Zeng, R., Zhang, J., Goh, C. C., Gul, A., ... Ginhoux, F. (2017). Induced-Pluripotent-Stem-Cell-Derived Primitive Macrophages Provide a Platform for Modeling Tissue-Resident Macrophage Differentiation and Function. *Immunity*, *47*(1), 183–198.e6. <https://doi.org/10.1016/j.immuni.2017.06.017>
- Tan, Y. L., Yuan, Y., & Tian, L. (2020). Microglial regional heterogeneity and its role in the brain. *Molecular Psychiatry*, *25*(2), 351–367. <https://doi.org/10.1038/S41380-019-0609-8>
- Therrien, M., Rouleau, G. A., Dion, P. A., & Parker, J. A. (2013). Deletion of C9ORF72 results in motor neuron degeneration and stress sensitivity in *C. elegans*. *PLoS One*, *8*(12), e83450. <https://doi.org/10.1371/journal.pone.0083450>

## References

- Thornton, P., Pinteaux, E., Gibson, R. M., Allan, S. M., & Rothwell, N. J. (2006). Interleukin-1-induced neurotoxicity is mediated by glia and requires caspase activation and free radical release. *Journal of Neurochemistry*, *98*(1), 258–266. <https://doi.org/10.1111/J.1471-4159.2006.03872.X>
- Timmerman, R., Burm, S. M., & Bajramovic, J. J. (2018). An overview of in vitro methods to study microglia. *Frontiers in Cellular Neuroscience*, *12*, 242. <https://doi.org/10.3389/fncel.2018.00242>
- Todd, T. W., & Petrucelli, L. (2022). Modelling amyotrophic lateral sclerosis in rodents. *Nature Reviews Neuroscience*, *23*(4), 231–251. <https://doi.org/10.1038/s41583-022-00564-x>
- Tondo, G., Iaccarino, L., Cerami, C., Vanoli, G. E., Presotto, L., Masiello, V., Coliva, A., Salvi, F., Bartolomei, I., Mosca, L., Lunetta, C., & Perani, D. (2020). 11C-PK11195 PET-based molecular study of microglia activation in SOD1 amyotrophic lateral sclerosis. *Annals of Clinical and Translational Neurology*, *7*(9), 1513–1523. <https://doi.org/10.1002/acn3.51112>
- Tortelli, R., Zecca, C., Piccininni, M., Benmahamed, S., Dell'Abate, M. T., Barulli, M. R., Capozzo, R., Battista, P., & Logroscino, G. (2020). Plasma Inflammatory Cytokines Are Elevated in ALS. *Frontiers in Neurology*, *11*, 552295. <https://doi.org/10.3389/fneur.2020.552295>
- Trojtsi, F., Siciliano, M., Femiano, C., Santangelo, G., Lunetta, C., Calvo, A., Moglia, C., Marinou, K., Ticozzi, N., Ferro, C., Scialò, C., Sorarù, G., Conte, A., Falzone, Y. M., Tortelli, R., Russo, M., Sansone, V. A., Chiò, A., Mora, G., ... Mandrioli, J. (2019). Comparative analysis of C9orf72 and sporadic disease in a large multicenter ALS population: The effect of male sex on survival of C9orf72 positive patients. *Frontiers in Neuroscience*, *13*, 485. <https://doi.org/10.3389/fnins.2019.00485>
- Trotti, D., Rolfs, A., Danbolt, N. C., Brown, R. H., & Hediger, M. A. (1999). SOD1 mutants linked to amyotrophic lateral sclerosis selectively inactivate a glial glutamate transporter. *Nature Neuroscience*, *2*(5), 427–433. <https://doi.org/10.1038/8091>
- Turner, B. J., Atkin, J. D., Farg, M. A., Da, W. Z., Rembach, A., Lopes, E. C., Patch, J. D., Hill, A. F., & Cheema, S. S. (2005). Impaired extracellular secretion of mutant superoxide dismutase 1 associates with neurotoxicity in familial amyotrophic lateral sclerosis. *The Journal of Neuroscience*, *25*(1), 108–117. <https://doi.org/10.1523/jneurosci.4253-04.2005>
- Turner, M. R., Al-Chalabi, A., Chio, A., Hardiman, O., Kiernan, M. C., Rohrer, J. D., Rowe, J., Seeley, W., & Talbot, K. (2017). Genetic screening in sporadic ALS and FTD. *Journal of Neurology, Neurosurgery and Psychiatry*, *88*(12), 1042–1044. <https://doi.org/10.1136/jnnp-2017-315995>
- Turner, M. R., Cagnin, A., Turkheimer, F. E., Miller, C. C. J., Shaw, C. E., Brooks, D. J., Leigh, P. N., & Banati, R. B. (2004). Evidence of widespread cerebral microglial activation in amyotrophic lateral sclerosis: An [11C](R)-PK11195 positron emission tomography study. *Neurobiology of Disease*, *15*(3), 601–609. <https://doi.org/10.1016/j.nbd.2003.12.012>
- Tzartos, J. S., Friese, M. A., Craner, M. J., Palace, J., Newcombe, J., Esiri, M. M., & Fugger, L. (2008). Interleukin-17 production in central nervous system-infiltrating T cells and glial cells is associated with active disease in multiple sclerosis. *The American Journal of Pathology*, *172*(1), 146–155. <https://doi.org/10.2353/AJPATH.2008.070690>
- Uribe-Querol, E., & Rosales, C. (2020). Phagocytosis: Our current understanding of a universal biological process. *Frontiers in Immunology*, *11*, 1066. <https://doi.org/10.3389/fimmu.2020.01066>

- Vahsen, B. F., Nalluru, S., Morgan, G. R., Farrimond, L., Carroll, E., Xu, Y., Cramb, K. M. L., Amein, B., Scaber, J., Katsikoudi, A., Candalija, A., Carcolé, M., Dafinca, R., Isaacs, A. M., Wade-Martins, R., Gray, E., Turner, M. R., Cowley, S. A., & Talbot, K. (2023). C9orf72-ALS human iPSC microglia are pro-inflammatory and toxic to co-cultured motor neurons via MMP9. *Nature Communications*, *14*(1), 5898. <https://doi.org/10.1038/s41467-023-41603-0>
- van Blitterswijk, M., DeJesus-Hernandez, M., Niemantsverdriet, E., Murray, M. E., Heckman, M. G., Diehl, N. N., Brown, P. H., Baker, M. C., Finch, N. C. A., Bauer, P. O., Serrano, G., Beach, T. G., Josephs, K. A., Knopman, D. S., Petersen, R. C., Boeve, B. F., Graff-Radford, N. R., Boylan, K. B., Petrucelli, L., ... Rademakers, R. (2013). Association between repeat sizes and clinical and pathological characteristics in carriers of C9ORF72 repeat expansions (Xpansize-72): A cross-sectional cohort study. *The Lancet Neurology*, *12*(10), 978–988. [https://doi.org/10.1016/S1474-4422\(13\)70210-2](https://doi.org/10.1016/S1474-4422(13)70210-2)
- Van Der Ende, E. L., Jackson, J. L., White, A., Seelaar, H., Van Blitterswijk, M., & Van Swieten, J. C. (2021). Unravelling the clinical spectrum and the role of repeat length in C9ORF72 repeat expansions. *Journal of Neurology, Neurosurgery and Psychiatry*, *92*(5), 502–509. <https://doi.org/10.1136/jnnp-2020-325377>
- Van Wilgenburg, B., Browne, C., Vowles, J., & Cowley, S. A. (2013). Efficient, long term production of monocyte-derived macrophages from human pluripotent stem cells under partly-defined and fully-defined conditions. *PLoS One*, *8*(8), e71098. <https://doi.org/10.1371/journal.pone.0071098>
- Vandoorne, T., De Bock, K., Ludo, -, & Bosch, V. Den. (2018). Energy metabolism in ALS: an underappreciated opportunity? *Acta Neuropathologica*, *135*(4), 489–509. <https://doi.org/10.1007/s00401-018-1835-x>
- Vatsavayai, S. C., Jin Yoon, S., Gardner, R. C., Gendron, T. F., Norberto Vargas, J. S., Trujillo, A., Pribadi, M., Phillips, J. J., Gaus, S. E., Hixson, J. D., Garcia, P. A., Rabinovici, G. D., Coppola, G., Geschwind, D. H., Petrucelli, L., Miller, B. L., & Seeley, W. W. (2016). Timing and significance of pathological features in C9orf72 expansion-associated frontotemporal dementia. *Brain*, *139*(Pt 12), 3202–3216. <https://doi.org/10.1093/aww264>
- Vaz, A. R., Pinto, S., Ezequiel, C., Cunha, C., Carvalho, L. A., Moreira, R., & Brites, D. (2019). Phenotypic effects of wild-type and mutant SOD1 expression in N9 murine microglia at steady state, inflammatory and immunomodulatory conditions. *Frontiers in Cellular Neuroscience*, *13*, 109. <https://doi.org/10.3389/FNCEL.2019.00109>
- Verdone, B. M., Cicardi, M. E., Wen, X., Sriramoji, S., Russell, K., Markandaiah, S. S., Jensen, B. K., Krishnamurthy, K., Haeusler, A. R., Pasinelli, P., & Trotti, D. (2022). A mouse model with widespread expression of the C9orf72-linked glycine–arginine dipeptide displays non-lethal ALS/FTD-like phenotypes. *Scientific Reports*, *12*(1), 5644. <https://doi.org/10.1038/s41598-022-09593-z>
- Vielhaber, S., Kunz, D., Winkler, K., Wiedemann, F. R., Kirches, E., Feistner, H., Heinze, H. J., Elger, C. E., Schubert, W., & Kunz, W. S. (2000). Mitochondrial DNA abnormalities in skeletal muscle of patients with sporadic amyotrophic lateral sclerosis. *Brain*, *123*(7), 1339–1348. <https://doi.org/10.1093/brain/123.7.1339>
- Vijayan, V., Pradhan, P., Braud, L., Fuchs, H. R., Gueler, F., Motterlini, R., Foresti, R., & Immenschuh, S. (2019). Human and murine macrophages exhibit differential metabolic responses to lipopolysaccharide - A divergent role for glycolysis. *Redox Biology*, *22*, 101147. <https://doi.org/10.1016/j.redox.2019.101147>
- Waite, A. J., Bäumer, D., East, S., Neal, J., Morris, H. R., Ansorge, O., & Blake, D. J. (2014). Reduced C9orf72 protein levels in frontal cortex of amyotrophic lateral sclerosis and frontotemporal degeneration brain with the C9ORF72 hexanucleotide repeat expansion.

- Neurobiology of Aging*, 35(7), 1779.e5-1779.e13. <https://doi.org/10.1016/j.neurobiolaging.2014.01.016>
- Walker, A. K., Spiller, K. J., Ge, G., Zheng, A., Xu, Y., Zhou, M., Tripathy, K., Kwong, L. K., Trojanowski, J. Q., & Lee, V. M. Y. (2015). Functional recovery in new mouse models of ALS/FTLD after clearance of pathological cytoplasmic TDP-43. *Acta Neuropathologica*, 130(5), 643–660. <https://doi.org/10.1007/s00401-015-1460-x>
- Wang, L., Gutmann, D. H., & Roos, R. P. (2011). Astrocyte loss of mutant SOD1 delays ALS disease onset and progression in G85R transgenic mice. *Human Molecular Genetics*, 20(2), 286–293. <https://doi.org/10.1093/HMG/DDQ463>
- Wang, Q., Lu, M., Zhu, X., Gu, X., Zhang, T., Xia, C., Yang, L., Xu, Y., & Zhou, M. (2022). The role of microglia immunometabolism in neurodegeneration: Focus on molecular determinants and metabolic intermediates of metabolic reprogramming. *Biomedicine and Pharmacotherapy*, 153, 113412. <https://doi.org/10.1016/j.biopha.2022.113412>
- Wang, W., Li, L., Lin, W. L., Dickson, D. W., Petrucelli, L., Zhang, T., & Wang, X. (2013). The ALS disease-associated mutant TDP-43 impairs mitochondrial dynamics and function in motor neurons. *Human Molecular Genetics*, 22(23), 4706–4719. <https://doi.org/10.1093/HMG/DDT319>
- Wang, Y., Szretter, K. J., Vermi, W., Gilfillan, S., Rossini, C., Cella, M., Barrow, A. D., Diamond, M. S., & Colonna, M. (2012). IL-34 is a tissue-restricted ligand of CSF1R required for the development of Langerhans cells and microglia. *Nature Immunology*, 13(8), 753–760. <https://doi.org/10.1038/NI.2360>
- Wang, Y., Yu, P., Li, Y., Zhao, Z., Wu, X., Zhang, L., Feng, J., & Hong, J. S. (2021). Early-released interleukin-10 significantly inhibits lipopolysaccharide-elicited neuroinflammation in vitro. *Cells*, 10(9), 2173. <https://doi.org/10.3390/cells10092173>
- Washer, S. J., Perez-Alcantara, M., Chen, Y., Steer, J., James, W. S., Trynka, G., Bassett, A. R., & Cowley, S. A. (2022). Single-cell transcriptomics defines an improved, validated monoculture protocol for differentiation of human iPSC to microglia. *Scientific Reports*, 12(1), 19454. <https://doi.org/10.1038/s41598-022-23477-2>
- Webster, C. P., Smith, E. F., Bauer, C. S., Moller, A., Hautbergue, G. M., Ferraiuolo, L., Myszczyńska, M. A., Higginbottom, A., Walsh, M. J., Whitworth, A. J., Kaspar, B. K., Meyer, K., Shaw, P. J., Grierson, A. J., & De Vos, K. J. (2016). The C9orf72 protein interacts with Rab1a and the ULK 1 complex to regulate initiation of autophagy. *The EMBO Journal*, 35(15), 1656–1676. <https://doi.org/10.15252/embj.201694401>
- Wendt, S., Dedeoglu, A., Speer, O., Wallimann, T., Beal, M. F., & Andreassen, O. A. (2002). Reduced creatine kinase activity in transgenic amyotrophic lateral sclerosis mice. *Free Radical Biology and Medicine*, 32(9), 920–926. [https://doi.org/10.1016/S0891-5849\(02\)00784-0](https://doi.org/10.1016/S0891-5849(02)00784-0)
- Weydt, P., Yuen, E. C., Ransom, B. R., & Möller, T. (2004). Increased cytotoxic potential of microglia from ALS-transgenic mice. *Glia*, 48(2), 179–182. <https://doi.org/10.1002/glia.20062>
- White, M. A., Kim, E., Duffy, A., Adalbert, R., Phillips, B. U., Peters, O. M., Stephenson, J., Yang, S., Massenzio, F., Lin, Z., Andrews, S., Segonds-Pichon, A., Metterville, J., Saksida, L. M., Mead, R., Ribchester, R. R., Barhomi, Y., Serre, T., Coleman, M. P., ... Sreedharan, J. (2018). TDP-43 gains function due to perturbed autoregulation in a Tardbp knock-in mouse model of ALS-FTD. *Nature Neuroscience*, 21(4), 552–563. <https://doi.org/10.1038/s41593-018-0113-5>

- Wiedemann, F. R., Manfredi, G., Mawrin, C., Flint Beal, M., & Schon, E. A. (2002). Mitochondrial DNA and respiratory chain function in spinal cords of ALS patients. *Journal of Neurochemistry*, *80*(4), 616–625. <https://doi.org/10.1046/J.0022-3042.2001.00731.X>
- Wiedemann, F. R., Winkler, K., Kuznetsov, A. V., Bartels, C., Vielhaber, S., Feistner, H., & Kunz, W. S. (1998). Impairment of mitochondrial function in skeletal muscle of patients with amyotrophic lateral sclerosis. *Journal of the Neurological Sciences*, *156*(1), 65–72. [https://doi.org/10.1016/S0022-510X\(98\)00008-2](https://doi.org/10.1016/S0022-510X(98)00008-2)
- Williams, T. L., Day, N. C., Ince, P. G., Kamboj, R. K., & Shaw, P. J. (1997). Calcium-permeable  $\alpha$ -amino-3-hydroxy-5-methyl-4-isoxazole propionic acid receptors: A molecular determinant of selective vulnerability in amyotrophic lateral sclerosis. *Annals of Neurology*, *42*(2), 200–207. <https://doi.org/10.1002/ANA.410420211>
- Workman, M. J., Lim, R. G., Wu, J., Frank, A., Ornelas, L., Panther, L., Galvez, E., Perez, D., Meepe, I., Lei, S., Valencia, V., Gomez, E., Liu, C., Moran, R., Pinedo, L., Tsitkov, S., Ho, R., Kaye, J. A., Thompson, T., ... Svendsen, C. N. (2023). Large-scale differentiation of iPSC-derived motor neurons from ALS and control subjects. *Neuron*, *111*(8), 1191-1204.e5. <https://doi.org/10.1016/j.neuron.2023.01.010>
- Xi, Z., Zhang, M., Bruni, A. C., Maletta, R. G., Colao, R., Fratta, P., Polke, J. M., Sweeney, M. G., Mudanohwo, E., Nacmias, B., Sorbi, S., Tartaglia, M. C., Rainero, I., Rubino, E., Pinessi, L., Galimberti, D., Surace, E. I., McGoldrick, P., McKeever, P., ... Rogava, E. (2015). The C9orf72 repeat expansion itself is methylated in ALS and FTLD patients. *Acta Neuropathologica*, *129*(5), 715–727. <https://doi.org/10.1007/s00401-015-1401-8>
- Xiao, Q., Zhao, W., Beers, D. R., Yen, A. A., Xie, W., Henkel, J. S., & Appel, S. H. (2007). Mutant SOD1G93A microglia are more neurotoxic relative to wild-type microglia. *Journal of Neurochemistry*, *102*(6), 2008–2019. <https://doi.org/10.1111/j.1471-4159.2007.04677.x>
- Xiao, S., MacNair, L., McGoldrick, P., McKeever, P. M., McLean, J. R., Zhang, M., Keith, J., Zinman, L., Rogava, E., & Robertson, J. (2015). Isoform-specific antibodies reveal distinct subcellular localizations of C9orf72 in amyotrophic lateral sclerosis. *Annals of Neurology*, *78*(4), 568–583. <https://doi.org/10.1002/ANA.24469>
- Xu, R., Li, X., Boreland, A. J., Posyton, A., Kwan, K., Hart, R. P., & Jiang, P. (2020). Human iPSC-derived mature microglia retain their identity and functionally integrate in the chimeric mouse brain. *Nature Communications*, *11*(1), 1577. <https://doi.org/10.1038/s41467-020-15411-9>
- Xu, Y. F., Gendron, T. F., Zhang, Y. J., Lin, W. L., D'Alton, S., Sheng, H., Casey, M. C., Tong, J., Knight, J., Yu, X., Rademakers, R., Boylan, K., Hutton, M., McGowan, E., Dickson, D. W., Lewis, J., & Petrucelli, L. (2010). Wild-type human TDP-43 expression causes TDP-43 phosphorylation, mitochondrial aggregation, motor deficits, and early mortality in transgenic mice. *The Journal of Neuroscience*, *30*(32), 10851–10859. <https://doi.org/10.1523/JNEUROSCI.1630-10.2010>
- Xu, Z., Rao, Y., Huang, Y., Zhou, T., Feng, R., Xiong, S., Yuan, T. F., Qin, S., Lu, Y., Zhou, X., Li, X., Qin, B., Mao, Y., & Peng, B. (2020). Efficient strategies for microglia replacement in the central nervous system. *Cell Reports*, *32*(6), 108041. <https://doi.org/10.1016/j.celrep.2020.108041>
- Yamanaka, K., Chun, S. J., Boillee, S., Fujimori-Tonou, N., Yamashita, H., Gutmann, D. H., Takahashi, R., Misawa, H., & Cleveland, D. W. (2008). Astrocytes as determinants of disease progression in inherited amyotrophic lateral sclerosis. *Nature Neuroscience*, *11*(3), 251–253. <https://doi.org/10.1038/nn2047>

- Yanagimachi, M. D., Niwa, A., Tanaka, T., Honda-Ozaki, F., & Nishimoto, S. (2013). Robust and highly-efficient differentiation of functional monocytic cells from human pluripotent stem cells under serum- and feeder cell-free conditions. *PLoS One*, *8*(4), e59243. <https://doi.org/10.1371/journal.pone.0059243>
- Yin, F., Dumont, M., Banerjee, R., Ma, Y., Li, H., Lin, M. T., Beal, M. F., Nathan, C., Thomas, B., & Ding, A. (2010). Behavioral deficits and progressive neuropathology in progranulin-deficient mice: a mouse model of frontotemporal dementia. *The FASEB Journal*, *24*(12), 4639–4647. <https://doi.org/10.1096/FJ.10-161471>
- You, J., Youssef, M. M. M., Santos, J. R., Lee, J., & Park, J. (2023). Microglia and astrocytes in amyotrophic lateral sclerosis: Disease-associated states, pathological roles, and therapeutic potential. *Biology*, *12*(10), 1307. <https://doi.org/10.3390/biology12101307>
- Zampatti, S., Peconi, C., Campopiano, R., Gambardella, S., Caltagirone, C., & Giardina, E. (2022). C9orf72-related neurodegenerative diseases: From clinical diagnosis to therapeutic strategies. *Frontiers in Aging Neuroscience*, *14*, 907122. <https://doi.org/10.3389/fnagi.2022.907122>
- Zhang, X., Wang, F., Hu, Y., Chen, R., Meng, D., Guo, L., Lv, H., Guan, J., & Jia, Y. (2020). In vivo stress granule misprocessing evidenced in a FUS knock-in ALS mouse model. *Brain*, *143*(5), 1350–1367. <https://doi.org/10.1093/BRAIN/AWAA076>
- Zhang, Y. M., Qi, Y. B., Gao, Y. N., Chen, W. G., Zhou, T., Zang, Y., & Li, J. (2023). Astrocyte metabolism and signaling pathways in the CNS. *Frontiers in Neuroscience*, *17*, 1217451. <https://doi.org/10.3389/fnins.2023.1217451>
- Zhao, C., Devlin, A. C., Chouhan, A. K., Selvaraj, B. T., Stavrou, M., Burr, K., Brivio, V., He, X., Mehta, A. R., Story, D., Shaw, C. E., Dando, O., Hardingham, G. E., Miles, G. B., & Chandran, S. (2020). Mutant C9orf72 human iPSC-derived astrocytes cause non-cell autonomous motor neuron pathophysiology. *Glia*, *68*(5), 1046–1064. <https://doi.org/10.1002/GLIA.23761>
- Zhao, J., Wang, X., Huo, Z., Chen, Y., Liu, J., Zhao, Z., Meng, F., Su, Q., Bao, W., Zhang, L., Wen, S., Wang, X., Liu, H., & Zhou, S. (2022). The impact of mitochondrial dysfunction in amyotrophic lateral sclerosis. *Cells*, *11*(13), 2049. <https://doi.org/10.3390/CELLS11132049>
- Zhao, W., Beers, D. R., & Appel, S. H. (2013). Immune-mediated mechanisms in the pathoprosession of amyotrophic lateral sclerosis. *Journal of Neuroimmune Pharmacology*, *8*(4), 888–899. <https://doi.org/10.1007/s11481-013-9489-x>
- Zhao, W., Beers, D. R., Hooten, K. G., Sieglaff, D. H., Zhang, A., Kalyana-Sundaram, S., Traini, C. M., Halsey, W. S., Hughes, A. M., Sathe, G. M., Livi, G. P., Fan, G. H., & Appel, S. H. (2017). Characterization of gene expression phenotype in amyotrophic lateral sclerosis monocytes. *JAMA Neurology*, *74*(6), 677–685. <https://doi.org/10.1001/JAMANEUROL.2017.0357>
- Zhao, W., Beers, D. R., Liao, B., Henkel, J. S., & Appel, S. H. (2012). Regulatory T lymphocytes from ALS mice suppress microglia and effector T lymphocytes through different cytokine-mediated mechanisms. *Neurobiology of Disease*, *48*(3), 418–428. <https://doi.org/10.1016/j.NBD.2012.07.008>
- Zhao, W., Varghese, M., Vempati, P., Dzhun, A., Cheng, A., Wang, J., Lange, D., Bilski, A., Faravelli, I., & Pasinetti, G. M. (2012). Caprylic triglyceride as a novel therapeutic approach to effectively improve the performance and attenuate the symptoms due to the motor neuron loss in ALS disease. *PLoS One*, *7*(11), e49191. <https://doi.org/10.1371/journal.pone.0049191>
- Zhu, Q., Jiang, J., Gendron, T. F., McAlonis-Downes, M., Jiang, L., Taylor, A., Diaz Garcia, S., Ghosh Dastidar, S., Rodriguez, M. J., King, P., Zhang, Y., La Spada, A. R., Xu, H., Petrucelli, L.,

Ravits, J., Da Cruz, S., Lagier-Tourenne, C., & Cleveland, D. W. (2020). Reduced C9ORF72 function exacerbates gain of toxicity from ALS/FTD-causing repeat expansion in C9orf72. *Nature Neuroscience*, 23(5), 615–624. <https://doi.org/10.1038/s41593-020-0619-5>

Ziff, O. J., Clarke, B. E., Taha, D. M., Crerar, H., Luscombe, N. M., & Patani, R. (2022). Meta-analysis of human and mouse ALS astrocytes reveals multi-omic signatures of inflammatory reactive states. *Genome Research*, 32(1), 71–84. <https://doi.org/10.1101/GR.275939.121>

Zöller, T., Schneider, A., Kleimeyer, C., Masuda, T., Potru, P. S., Pfeifer, D., Blank, T., Prinz, M., & Spittau, B. (2018). Silencing of TGF $\beta$  signalling in microglia results in impaired homeostasis. *Nature Communications*, 9, 4011. <https://doi.org/10.1038/s41467-018-06224-y>

Zondler, L., Müller, K., Khalaji, S., Bliedehäuser, C., Ruf, W. P., Grozdanov, V., Thiemann, M., Fundel-Clemes, K., Freischmidt, A., Holzmann, K., Strobel, B., Weydt, P., Witting, A., Thal, D. R., Helferich, A. M., Hengerer, B., Gottschalk, K.-E., Hill, O., Kluge, M., ... Weishaupt, J. H. (2016). Peripheral monocytes are functionally altered and invade the CNS in ALS patients. *Acta Neuropathologica*, 132(3), 391–411. <https://doi.org/10.1007/s00401-016-1548-y>